Examining the influence of pyramidal neuron progenitor type on cortical subnetworks



Gemma Gothard

Supervisor: Prof Colin Akerman

Thesis submitted for the degree of Doctor of Philosophy

St. John's College

University of Oxford

Michaelmas Term 2023

Declaration of Authorship

I, Gemma Gothard, declare that the work presented in this thesis are wholly my own, aside from parts that were completed in collaboration:

- Dr Sarah Newey constructed the following plasmids listed in Section 2.2: Ta1-Flpo, fDIO-tdTom/GFP, Tbr2-Flpo and pCAG-fDIO-TdTom.
- Sasha Tinelli, working under my supervision as an MSc student, assisted in the collection and analysis of the data in Figure 3.3.

Abstract

The precise synaptic connectivity between cortical neurons determines how information is integrated and processed by the mammalian cortex. In somatosensory cortex, for example, excitatory and inhibitory cell types form fine-scale synaptic circuits, which integrate feedforward sensory information with feedback contextual information. The principles by which excitatory and inhibitory neurons are arranged into functional circuits, however, remain unknown. Recent evidence suggests that an excitatory cortical neuron's synaptic connectivity and functional properties can reflect the progenitor type from which the neuron is derived during embryonic development. By combining longitudinal *in utero* lineage labelling techniques with patch-clamp electrophysiology in mature cortex, I test whether progenitor type influences the local synaptic inhibition and cortical feedback received by excitatory pyramidal neurons in layer 2/3 (L2/3) of mouse somatosensory cortex. Firstly, I find that progenitor type predicts a L2/3 pyramidal neuron's inhibitory synaptic activity *in vivo*. Secondly, I find that L2/3 pyramidal neuron progenitor type is not associated with different amounts of inhibition from interneuron subtypes. Rather, progenitor type defines how much inhibitory synaptic input a L2/3 pyramidal neuron shares with its neighbours. Consistent with this, interneurons target neighbouring pyramidal neurons based on the post-synaptic neuron's progenitor type. Finally, I find that progenitor type predicts the degree to which L2/3 pyramidal neurons are recruited by long-range excitatory feedback from primary motor cortex. These observations reveal new significance for progenitor diversity and identify ontogenetic mechanisms underlying fine-scale inhibitory subnetworks and long-range feedback circuits in cortex.

Acknowledgements

I must first thank my supervisor, Colin, whose guidance has not only benefited my understanding of science but has also taught me a great deal about mentorship. It has been an absolute pleasure to discuss science with you over these past few years. I always come out of our meetings feeling optimistic and excited to get on with the next round of experiments. Thank you for your unwavering kindness, patience and for creating a lab that has allowed me, alongside so many others, to flourish and develop as a scientist.

I would like to thank my secondary supervisor, Kashif - an incredible master of ephys - for teaching me most things I know with a level of patience that is rare to find. Thank you for never tiring of my many questions.

Thank you to all the Akerman lab members who I have overlapped with during my DPhil for providing such a positive and enjoyable environment to do science in. The basement is a bright and wonderful place with you lot in it. I would specifically like to thank those who kindly took the time to teach me things throughout my time in the lab: Matt, for always providing a helpful perspective on whatever analysis problem I was currently having; Joram, for taking on the challenging task of teaching me to code; Richard, for showing me the ropes of *in vivo* patching, and emphasising the importance of labelling everything in sight; Alex and Atreyi, for the sharing of various troubleshooting expertise in each of our respective lab equipment speciality domains; Sarah, for being the ultimate teacher of molecular biology; Alex Mathy, for introducing me to the world of 3D printing; and Paul, for never resisting the opportunity to improve my code.

I would like to extend my thanks to the support staff at the Department of Pharmacology and the staff at the BMS for all of their hard work that made the experiments in this thesis possible.

My time in Oxford has been defined by an incredibly special group of friends who have provided a support network that is second to none. I simply could not have done this without any of you.

To Adam, Bruno and Pol: thank you for every single coffee, lunch, brunch, pint, Friday night dinner and Drag Race episode we have shared together over the past 5 years, and especially during the darker pandemic days. You guys kept me going when I couldn't see the finish line. It has been an absolute privilege to spend Oxford with you three.

To my Wallingford friends: I am so grateful to have grown up with such amazing people. Thank you for bringing just the right amount of good chaos into my life and providing much needed distractions from work. In particular, I must mention Tilly, Sarah and Masse, who were never more than a text message away at any given time, being my biggest cheerleaders and forcing me to believe in myself.

To Kaitlyn and Sasha: it is challenging to express just how much your friendships have meant to me in this past year. Thank you for all of the VNs, for keeping me sane in the midsts of broken ankle gate, and for supporting me day in day out during the write up of this thesis.

Lastly, I would like to thank my family. I feel extremely lucky to have such amazing parents that have supported me throughout every academic pursuit of my life so far - it therefore seemed rather fitting that a broken ankle brought me back home to their company to write the majority of this thesis. Thank you for the unconditional care, kindness and support for the past 27 years, and especially during the more challenging moments of the last 6 weeks.

And finally, my grandparents. Thank you for inspiring science in me from a young age, for being excellent role models, A level tutors, friends and never failing to provide hilarious and surprising anecdotes from the equivalent time in your own lives. This thesis is for both of you.

Contents

List of Figures **9**

List of Tables **11**

1 Introduction **13**

1.1 The general organisation of cortex 14

1.1.1 The laminar and columnar organisation of cortical circuits . . 14

1.1.2 The mouse somatosensory whisker system as a model of cortical circuitry 19

1.1.3 The fine-scale organisation of local excitatory circuits 22

1.1.4 The input circuitry of L2/3 pyramidal neurons and its significance for sensory processing 25

1.2 Synaptic inhibition in cortex 28

1.2.1 Cortical inhibitory cell types 29

1.2.2 Inhibitory synaptic circuits in L2/3 31

1.3 Developmental origins of cortical subnetworks 36

1.3.1 Excitatory neurogenesis 37

1.3.2 Inhibitory neurogenesis 41

1.3.3 Circuit assembly of excitatory and inhibitory neurons 43

1.4 Lineage-dependent contributions to fine-scale cortical circuits 45

1.4.1 Lineage-dependent circuit assembly 45

1.4.2 Role of progenitor heterogeneity in fine-scale circuit assembly . 49

1.5 Thesis aims 52

2 Materials and Methods **54**

2.1 Experimental animals 54

2.2 *In utero* electroporation 54

2.3 Postnatal viral injections 57

2.4 *In vivo* patch-clamp electrophysiology . . . 58
2.5 *In vitro* patch-clamp electrophysiology . . . 61
2.6 Histology . . . 63
2.7 Statistical analysis . . . 64

3 Progenitor type predicts a L2/3 pyramidal neuron's inhibitory synaptic activity *in vivo* 66
3.1 Introduction . . . 66
3.2 Results . . . 69
3.2.1 Labelling strategy to target neurons derived from intermediate progenitors . . . 69
3.2.2 Establishing methods for relating a L2/3 pyramidal neuron's synaptic inhibition to local network activity . . . 69
3.2.3 LFP reflects local network activity and can be used as a coupling measure . . . 74
3.2.4 Progenitor type predicts a L2/3 pyramidal neuron's inhibitory synaptic activity *in vivo* . . . 77
3.2.5 Progenitor type predicts the correlation between a neuron's synaptic inhibition and the local network . . . 78
3.3 Discussion . . . 81

4 Cortical inhibitory subnetworks are shaped by pyramidal neuron progenitor type 84
4.1 Introduction . . . 84
4.2 Results . . . 87
4.2.1 Dual colour labelling strategy to target neurons derived from intermediate progenitors . . . 87
4.2.2 Labelled IPs include basal and apical intermediate progenitors 88
4.2.3 L2/3 pyramidal neurons derived from different progenitor types receive similar overall levels of synaptic inhibition from PV, SST and VIP interneurons . . . 92

4.2.4 L2/3 pyramidal neurons derived from different progenitor types receive similar levels of spontaneous action-potential-evoked synaptic inhibition . . . 95
4.2.5 A L2/3 pyramidal neuron's inhibitory subnetwork reflects the progenitor type from which it is derived . . . 96
4.2.6 PV interneurons differentially target L2/3 pyramidal neurons based on post-synaptic progenitor type . . . 100
4.3 Discussion . . . 105

5 Cortical feedback onto progenitor-defined L2/3 pyramidal neurons 109
5.1 Introduction . . . 109
5.2 Results . . . 112
5.2.1 The recruitment of progenitor-defined L2/3 pyramidal populations by local layer 5 feedback . . . 112
5.2.2 The recruitment of progenitor-defined L2/3 pyramidal populations by secondary somatosensory cortex . . . 115
5.2.3 The recruitment of progenitor-defined L2/3 pyramidal populations by primary motor cortex . . . 118
5.3 Discussion . . . 121

6 General Discussion 124
6.1 Experimental findings . . . 124
6.2 Methodological considerations . . . 125
6.2.1 *In utero* electroporation and the longitudinal labelling of progenitor-defined populations . . . 126
6.2.2 *In vivo* electrophysiology in anaesthetised preparations to measure synaptic inhibition . . . 128
6.2.3 Measuring synaptic inhibition with optogenetic and spontaneous *in vitro* electrophysiological recordings . . . 131
6.2.4 Long-range circuit mapping using optogenetics . . . 134
6.3 Implication of findings . . . 135
6.3.1 L2/3 pyramidal neuron progenitor type shapes local inhibitory inputs and long-range feedback . . . 135

6.3.2 Reconciling evidence for blanket versus specific inhibition in cortical circuits . . . 137
6.3.3 The establishment of progenitor-dependent inhibitory subnetworks . . . 141
6.3.4 Implications for the preferential recruitment of IP-derived L2/3 neurons by primary motor cortex . . . 146
6.3.5 Functional implications for cortical excitatory and inhibitory subnetworks specified by progenitor type . . . 148
6.3.6 Progenitor type as a general mechanism for specifying cortical circuitry . . . 152
6.4 Concluding remarks . . . 155

Bibliography **156**

List of Figures

1.1 **Canonical cortical microcircuit in relation to L2/3 pyramidal neurons.** . . . 17
1.2 **Inhibitory circuit motifs in L2/3.** . . . 33
1.3 **Neurogenic niches of excitatory and inhibitory cortical neurons.** . . . 37
1.4 **Excitatory neuron progenitor types in the embryonic mouse brain.** . . . 40
1.5 **Lineage-dependent circuit assembly.** . . . 47

3.1 **Labelling strategy to target neurons derived from intermediate progenitors.** . . . 70
3.2 **Synaptic input detection method for accurately measuring synaptic inhibition.** . . . 71
3.3 **LFP reflects local synaptic activity and can be used as a coupling measure.** . . . 75
3.4 **LFP activity does not differ between unlabeled and IP-derived recordings.** . . . 77
3.5 **Progenitor type predicts a L2/3 pyramidal neuron's inhibitory synaptic activity *in vivo*.** . . . 79
3.6 **Progenitor type predicts the correlation between a L2/3 pyramidal neuron's inhibitory synaptic events and local network events in vivo.** . . . 81

4.1 **Dual colour labelling system to target neurons derived from intermediate progenitors** . . . 88
4.2 **Intermediate progenitors labelled by Tα1 promoter activity comprise a population of apical IPs and basal IPs** . . . 91

4.3 **L2/3 pyramidal neurons derived from different progenitor types receive similar overall levels of synaptic inhibition from PV, SST and VIP interneurons** 94
4.4 **L2/3 pyramidal neurons from different progenitor types receive similar levels of spontaneous action-potential-evoked synaptic inhibition.** 96
4.5 **A L2/3 pyramidal neuron's inhibitory subnetwork reflects the progenitor type from which it is derived.** 98
4.6 **Pairs of IP-derived and OP-derived neurons differ in the amount of inhibitory inputs they share with each other.** . . 101
4.7 **Interneurons differentially target L2/3 pyramidal neurons based on post-synaptic progenitor type.** 103

5.1 **Investigating the recruitment of progenitor-defined L2/3 pyramidal populations by local layer 5 feedback.** 113
5.2 **Feedback from layer 5 does not differ depending upon a L2/3 pyramidal neuron's progenitor type.** 114
5.3 **Investigating the recruitment of progenitor-defined L2/3 pyramidal populations by feedback from S2.** 116
5.4 **Feedback from S2 does not differ depending upon a S1 L2/3 pyramidal neuron's progenitor type.** 117
5.5 **Investigating the recruitment of progenitor-defined L2/3 pyramidal populations by M1.** 119
5.6 **Feedback from M1 differs depending upon a S1 L2/3 pyramidal neuron's progenitor type.** 120

6.1 **Proposed interlaminar excitatory-inhibitory subnetworks.** . 144
6.2 **IP-derived cortical circuits.** 149

List of Tables

2.1 **Distribution of cells collected across animals** 65

For my grandparents, Mary and John Cozens

1 | Introduction

As the evolutionarily 'newest' brain structure, the cerebral cortex plays a fundamental role in a series of higher cognitive functions such as attention, perception and decision-making. Given the complexity of tasks performed by this brain structure, understanding the range of cell types within the cortex and their organising principles has motivated neuroscience research for decades. Comprising a mosaic of highly heterogeneous excitatory and inhibitory cell types, the cortex forms precise fine-scale circuits that shape this brain region's computational capabilities (Shepherd et al., 2015; Jiang et al., 2015; Brown and Hestrin, 2009; Lim et al., 2018a). One area where the organisation of cortical circuitry has been intensively studied is the rodent somatosensory system, where feedforward information from the sensory periphery is passed through increasingly higher order cortical areas in a manner that allows the animal to respond to its environment in the form of perception, learning and movement. In turn, higher order cortical areas send feedback projections to earlier stages of sensory processing, providing contextual information. A key challenge in neuroscience is understanding the organising principles that arrange the vast degree of cell types, along with their local and long-range synaptic inputs, into functional circuits.

One way to understand cortical circuitry is through its assembly during embryonic development. Cortical excitatory neurons are born from a heterogeneous pool of progenitor cells, such that neighbouring excitatory neurons in mature cortex can originate from diverse developmental trajectories (Hippenmeyer, 2023; Huilgol et al., 2023b). Emerging evidence suggest that contemporaneous progenitor heterogeneity prescribes functional properties to neuronal progeny, thereby diversifying the cell types and connectivity patterns across cortical circuits (Tyler et al., 2015; Guillamon-Vivancos et al., 2019; Ellender et al., 2019; Buchan et al., 2022; Matho et al., 2021; Huilgol et al., 2023a). However, it is unclear the extent to which progenitor types can influence the synaptic circuitry of their progeny. This thesis

aims to investigate whether cortical excitatory neuron progenitor type shapes the inhibitory inputs received by excitatory neurons. I will also test whether progenitor type influences the degree of cortical feedback received by excitatory cortical neurons. To provide the necessary context for this work, I will first introduce the organisation of cortical excitatory and inhibitory neurons into functional circuits. I will then focus on the assembly of cortical circuits during development, including emerging evidence for the role of lineage-dependent circuit assembly.

1.1 The general organisation of cortex

The complex circuitry of the cortex is thought to underpin the cognitive capabilities of mammals. A primary focus has therefore been in exploring the organising principles of the connections between cortical neurons, in order to understand how this brain structure implements its computations. The discovery that the cortex is built from modules of stereotyped patterns of connectivity has prompted questions into the functional significance of this circuit and motivated a further dissection of its constituent neuronal subtypes and input-output circuitry. This section will introduce the general organisation of cortical circuitry. Given the focus of this thesis on layer 2/3 (L2/3) pyramidal neurons, I will then explore in depth the fine-scale connections within L2/3 and the synaptic inputs to this cortical layer.

1.1.1 The laminar and columnar organisation of cortical circuits

The mammalian cortex is perhaps most recognisable by its six layered cytoarchitecture. Each layer is identified by a distinct size and distribution of neuronal subtypes (Meynert, 1872; Cajal, 1999; Lund, 1988). Whilst the layers of the cortex were first recognised using purely anatomical studies, their distinction is highly suggestive of functional relevance. As such, the cortical layers have provided a framework upon which to understand cortical connectivity and function, leading to an extensive body of literature exploring the circuits and cell types within and between cortical layers (Douglas and Martin, 2004; Harris and Mrsic-Flogel, 2013; Harris and Shepherd, 2015; Thomson and Lamy, 2007; Feldmeyer, 2012).

The cell types of the cortex can be broadly categorised into excitatory and inhibitory neurons, which form distinct layer-specific local and long-range synaptic connections. Excitatory neurons, often thought of as the principal cells, constitute around 80 % of cortical neurons, use the transmitter glutamate, and form both local and long-range synaptic connections. Inhibitory interneurons comprise the remaining 20 % of cortical neurons, and use gamma-aminobutyric acid (GABA) as their transmitter. Inhibitory interneurons predominantly make local synaptic connections and control the activity of surrounding excitatory neurons (Isaacson and Scanziani, 2011; Galarreta and Hestrin, 2001; Cardin, 2018). It is important to recognise that the distinction between excitatory and inhibitory neurons represents the most rudimentary classification between neuron subtypes. Cortical circuits are now best understood from a perspective of extensive cell-type classification on the basis of morphology, connectivity, developmental origins, molecular identity and electrophysiology (Harris and Shepherd, 2015; Greig et al., 2013; Jiang et al., 2015; Tasic et al., 2018; Gouwens et al., 2020; Molyneaux et al., 2007). Indeed, an integrated approach using multiple methods is likely to produce the most unified and comprehensive cell-type classification system, which identifies neurons according to their phenotype and function (Zeng, 2022; Zeng and Sanes, 2017).

The cortical layers comprise distinct distributions of excitatory and inhibitory cell types. Layer 1 (L1) is the most superficial layer, which borders with the pial mater. This layer is devoid of most cell types but contains long-range axonal inputs from other cortical areas that synapse onto the apical dendrites of pyramidal neurons. The cell bodies found in L1 comprise specific types of inhibitory interneurons, which are thought to gate activity in pyramidal neuron dendrites (Jiang et al., 2015; Mitchell and Cauller, 2001; Pardi et al., 2023; Hartung et al., 2023). L2/3 contains medium sized excitatory pyramidal neurons as well as an array of inhibitory neuron types. Whilst distinctions between layers 2 and 3 have been recognised (Meyer et al., 2011; Lefort et al., 2009; Bureau et al., 2006; Shepherd and Svoboda, 2005; Petreanu et al., 2009; Weiler et al., 2023; Petersen and Crochet, 2013), they are usually referred to as a single layer. Layer 4 (L4) is categorised by a relatively high density of cells, comprising a mixture of morphological excitatory neuron subtypes, such as spiny stellate, star-pyramidal and pyramidal, as well as inhibitory interneurons primarily

of the parvalbumin-expressing (PV) subtype (Beaulieu, 1993; Tremblay et al., 2016; Oberlaender et al., 2012; Brecht and Sakmann, 2002). Layers 5 and 6 (L5, L6) represent the deep cortical layers, containing large pyramidal neurons and a mixture of inhibitory interneuron subtypes (Tremblay et al., 2016). These deeper layers are often divided into sublayers which distinguish neurons by their morphology, electrophysiology and axonal projection targets (Briggs, 2010; Marx and Feldmeyer, 2013; Morishima et al., 2011; Mercier et al., 1990; Hattox and Nelson, 2007; Hoerder-Suabedissen et al., 2018; Chevée et al., 2018).

The mammalian cortex has not only been defined horizontally by the categorisation of cortical layers, but also vertically by the discovery of radially aligned cortical columns. Cortical columns constitute preferentially connected neurons spanning the cortical layers, which are thought to represent the basic processing unit of the cortex. Cortical columns were first described by Vernon Mountcastle in 1955, who discovered that vertically aligned neurons were more likely to share sensory response properties than horizontally aligned neurons (Mountcastle et al., 1955). This was later supported by similar observations across cortical areas and species (Hubel and Wiesel, 1962; Fujita et al., 1992; Kanold et al., 2014; Hooks et al., 2011; Shepherd and Svoboda, 2005; Bureau et al., 2004). Within each cortical column exists stereotyped patterns of excitatory connectivity between layers, known as the canonical cortical microcircuit (Douglas and Martin, 2004). Whilst the validity and applicability of the canonical microcircuit has been widely debated (Guy and Staiger, 2017), it has proven a useful foundation to conceptualise the flow of information through cortical circuits (Feldmeyer, 2012; Harris and Shepherd, 2015; Lefort et al., 2009; Harris and Mrsic-Flogel, 2013).

According to the canonical cortical microcircuit, sensory information from the periphery arrives via thalamocortical afferents that synapse onto L4 excitatory neurons (Sherman and Guillery, 1996; Viaene et al., 2011b,a), and constitute the primary input layer to the cortex. L4 neurons receive comparatively little excitatory input from elsewhere within the column, but exhibit strong recurrent connectivity with one another, which acts to amplify thalamic inputs (Lefort et al., 2009; Binzegger et al., 2004). The cytoarchitecture of L4 varies across cortical areas, which is reflective of the fact that this layer is most malleable to the modality of the thalamic afferents

that it receives (Callaway and Borrell, 2011; Narboux-Nême et al., 2012; Jabaudon et al., 2012). L4 neurons form excitatory synapses onto the basal dendrites of L2/3 pyramidal neurons, representing the next stage of processing in the canonical circuit (Lefort et al., 2009; Feldmeyer, 2012). L2/3 neurons receive sensory-related inputs from L4 neurons, but also contextual inputs from long-range cortical areas that synapse onto the apical dendrites of the L2/3 pyramidal neuron. This makes the L2/3 pyramidal neuron a key stage of cortical processing for integrating different types of information (**Figure 1.1**). However, L2/3 neurons are strongly inhibited by local interneurons (Xue et al., 2014; Packer and Yuste, 2011; Crochet et al., 2011), meaning their firing rates are some of the lowest in cortex (Crochet et al., 2011; Jacob et al., 2017; Sakata and Harris, 2009; Niell and Stryker, 2008; de Kock et al., 2007). Consequently, their response properties are sparse and challenging to interpret (Ranjbar-Slamloo and Arabzadeh, 2019; Crochet et al., 2011; de Kock et al., 2007; Niell and Stryker, 2008; O'Connor et al., 2010).

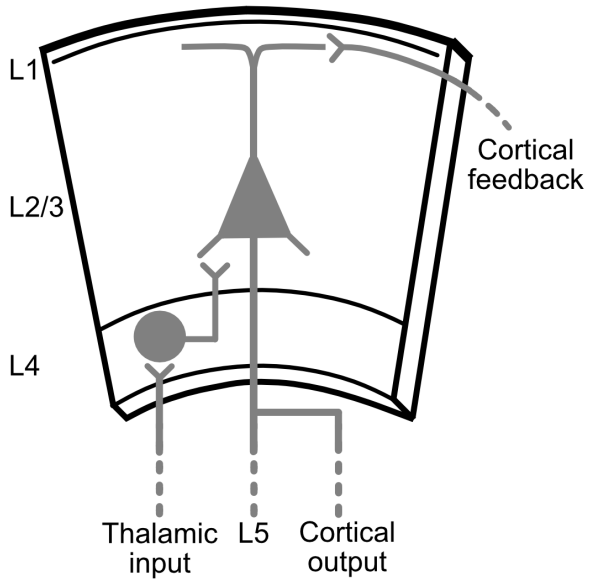


Figure 1.1: Canonical cortical microcircuit in relation to L2/3 pyramidal neurons. L4 neurons receive input from the sensory periphery via the thalamus. L2/3 pyramidal neurons receive feedforward input from L4 neurons on their basal dendrites and integrate this with contextual, feedback inputs arriving on their apical dendrites. L2/3 pyramidal neurons send projections to L5 in addition to sending long-range cortico-cortical outputs. Importantly, many recurrent connections exist within the canonical circuit, which are not depicted here (Lefort et al., 2009; Harris and Shepherd, 2015).

L2/3 neurons output locally to L5 as well as sending long-range projections to a variety of cortical areas and the striatum (Thomson and Lamy, 2007; Petreanu

et al., 2007; Hooks et al., 2011; Yamashita et al., 2013; Kim et al., 2018; Adesnik and Scanziani, 2010; Lefort et al., 2009; Harris and Shepherd, 2015) (**Figure 1.1**). L5 is considered the main output layer of the canonical circuit, and can be subdivided into L5a and L5b. Pyramidal neurons in these sublayers can be distinguished based on their morphological and electrophysiological profiles in addition to differences in their local and long range connectivity (Hattox and Nelson, 2007; Lefort et al., 2009; Petreanu et al., 2007; Morishima et al., 2011; Mercier et al., 1990; Baker et al., 2018; Reiner et al., 2003). L5a neurons are intra-telencephalic (IT), projecting to downstream cortical areas and the striatum (Shepherd, 2013; Alloway, 2008; Aronoff et al., 2010; Oswald et al., 2013). Conversely, L5b neurons are mostly extra-telencephalic (ET), projecting to sub-cortical regions such as the thalamus, pons and superior colliculus (Morishima et al., 2011; Baker et al., 2018; Guo et al., 2017; Rojas-Piloni et al., 2017). Therefore, the two L5 sublayers can be thought of as two distinct output streams of the cortical column. For example, activity in L5a IT neurons drives activity across higher-order cortical areas leading to more complex processing of the sensory environment. Meanwhile, L5b ET neurons may orchestrate subcortically-controlled behavioural outputs, such as sensory-guided movement (Moberg and Takahashi, 2022). Importantly, L5 neurons send axonal collaterals back throughout the cortical column, which recruit both excitatory and inhibitory neurons. This represents a mechanism by which the information that is being sent to long-range targets is simultaneously relayed back to the cortical column, which may be an important source of cortical feedback to orchestrate learning and plasticity (Vecchia et al., 2020; von Klemperer, 2021; Beltramo et al., 2013; Shepherd et al., 2015). Finally, L6 neurons also represent an output of the cortical column, which can be classified by their projection targets to thalamus or cortex (Briggs, 2010). Cortical-projecting L6 neurons receive strong excitatory input from L5, whereas thalamic-projecting L6 neurons are mainly driven by long-range cortical targets (Zliang and Deschênes, 1998; Vélez-Fort et al., 2014; Hooks et al., 2011; Lefort et al., 2009).

Whilst the canonical cortical microcircuit describes the main direction of information flow through cortex, the increasingly recognised diversity of cell types within each layer adds further complexity to how information is routed through these cir-

cuits (Harris and Shepherd, 2015). Therefore, whilst the general connection patterns described here are useful for conceptualising cortical function, it is important to appreciate the many non-canonical connection patterns that are likely to be just as relevant for cortical computation (Harris and Shepherd, 2015; Shepherd and Svoboda, 2005; Hooks et al., 2011; Naka, 2015; Adesnik, 2018). Furthermore, despite the stereotyped nature of the canonical circuit that has been proposed across cortical areas and species (Hubel and Wiesel, 1962; Fujita et al., 1992; Kanold et al., 2014; Hooks et al., 2011; Shepherd and Svoboda, 2005; Bureau et al., 2004), there are significant regional variations in circuitry that underlie functional specialisations of specific cortical areas (Brodmann, 1909; Hooks et al., 2011; Harris and Shepherd, 2015). Taken together, the cortex can be thought of as a modular structure with general organising principles, from which additional functional specialisations and vast neuronal diversity contribute towards its processing capabilities.

1.1.2 The mouse somatosensory whisker system as a model of cortical circuitry

Since it was first described over half a century ago, the mouse whisker system has become one of the most well-established models to study cortical circuitry. In 1970, Woosley and Van der Loos discovered clusters of L4 neurons in the whisker somatosensory cortex of mice that adopted a one-to-one correspondence with each whisker (Woolsey and der Loos, 1970). They named these clusters of neurons 'barrels' and proceeded to show that removal of the whiskers in new-born mice prevented barrel formation, demonstrating that signals from the whiskers instruct barrel formation (Van der Loos and Woolsey, 1973). In the years since, barrel cortex has become an invaluable model to study the processing of sensory information. Indeed, mice are far more dependent on their tactile sensing than their vision, using their whiskers to detect objects and navigate their environment.

The flow of sensory information from the whisker pad arrives in cortex via several distinct pathways, each of which contributes different aspects to sensory processing. Information about single whiskers is delivered via the lemniscal pathway, which adheres to strict somatotopic representation of the whisker pad from the periphery

to cortex. Sensory afferents within the whisker follicle detect tactile movements and project to 'barrelettes' within the principal nucleus of the trigeminal ganglion, which inherit a one-to-one correspondence with each whisker (Ma, 1991). Sensory information is then relayed to the ventral posteriomedial nucleus (VPM) of the thalamus. Neurons within the VPM are arranged into 'barreloids', exhibiting a somatotopic representation of the whisker pad (Pierret et al., 2000). VPM neurons then project thalamocortical axons to barrel cortex, which cluster within the barrel hollows of L4, where they synapse onto the dendrites of L4 neurons (Woolsey and der Loos, 1970). The information from a single whisker is represented by a single cortical column that corresponds to the cortical area centered around each of the barrels within L4.

Whiskers do not act in isolation, however, and in order to decipher information about the sensory environment, the whisker system must convey multi-whisker information to the cortex. This is done via the paralemniscal pathway, which begins with multiwhisker neurons within the caudal part of the interpolaris spinal nuclei of the trigeminal ganglion. These neurons project to the higher-order posteriomedial nucleus of the thalamus (POm) (Jacquin et al., 1989; Williams et al., 1994; Veinante et al., 2000). POm sends thalamocortical axons to barrel cortex that densely innervate L1, L5a and the septa, which represent the regions between the barrels within L4 (Petersen, 2007). In contrast to the lemniscal pathway, the paralemniscal pathway lacks any somatotopic organisation from the peripheral nuclei to barrel cortex (Veinante and Deschênes, 1999; Erzurumlu et al., 1980). In addition to receiving multi-whisker inputs from the trigeminal nuclei, POm also receives input from a range of cortical areas such as primary somatosensory cortex (S1), primary motor cortex (M1) and secondary somatosensory cortex (S2) (Groh et al., 2014; Lohse et al., 2018; Miller-Hansen and Sherman, 2022; Mo and Sherman, 2019; Sampathkumar et al., 2021; Deschênes et al., 1998; Chmielowska et al., 1989). Therefore, POm neurons are embedded within higher-order cortico-thalamo-cortical loops, whereby the relay of higher-order contextual signals to lower-order cortical areas can modulate ongoing sensory processing in a manner that is necessary for learning and plasticity (Williams and Holtmaat, 2019; Gambino et al., 2014; Audette et al., 2019).

Understanding the sensory environment depends on the complex and ongoing inter-

actions between multiple cortical areas and thalamic nuclei. Consequently, sensory processing is not 'complete' once information about the environment reaches the output of the canonical circuit in S1. Rather, signals continue to transcend a hierarchy of cortical areas, deriving progressively more complex representations of the environment in order to guide movement and behaviour. Importantly, higher-order cortical areas send extensive feedback connections to S1, where they engage diverse cell types (Kinnischtzke et al., 2014; Naskar et al., 2021; Petreanu et al., 2009). Two of the main targets of projection neurons in S1 are S2 and M1 (Aronoff et al., 2010; Chen et al., 2013; Condylis et al., 2020; Gilbert and Sigman, 2007; Kinnischtzke et al., 2014; Kwon et al., 2016; Minamisawa et al., 2018; Miyashita et al., 1994; Porter and White, 1983; White and DeAmicis, 1977; Yang et al., 2015). These two areas are targeted by largely non-overlapping groups of L2/3 pyramidal neurons, which display distinct response properties during sensorimotor tasks (Chen et al., 2013; Yamashita et al., 2013, 2018; Yamashita and Petersen, 2016; Sato and Svoboda, 2010; Vavladeli et al., 2020). In return, M1 and S2 send feedback projections that recruit L2/3 pyramidal neurons and inhibitory interneurons in S1 (Aronoff et al., 2010; Denardo et al., 2015; Kinnischtzke et al., 2014; Mao et al., 2011; Naskar et al., 2021; Yang and Sun, 2018).

Whilst the exact role of these feedback connections is still debated, it is clear that they play a crucial role in sensory processing in S1. For example, behavioural performance on sensory-dependent tasks is degraded upon inhibition of feedback connections (Ryan et al., 2023; Manita et al., 2015; Zhang and Zagha, 2023). Furthermore, a range of studies investigating the responses of L2/3 pyramidal neurons to sensory stimuli shows that these neurons exhibit incredibly sparse responses, rarely eliciting action potentials (Ranjbar-Slamloo and Arabzadeh, 2019; Crochet et al., 2011; Ramirez et al., 2014; Barth and Poulet, 2012; O'Connor et al., 2010). One explanation for this sparsity is that L2/3 pyramidal neurons exhibit complex receptive fields that incorporate strong feedback inputs, such that action potential generation only occurs when bottom-up and top-down inputs combine (Zhang and Bruno, 2019; Jordan and Keller, 2020; Zmarz and Keller, 2016; Keller et al., 2020). Whilst the ways in which feedback inputs engage local circuits in barrel cortex is still unclear, these studies demonstrate the active contribution of feedback inputs to sensory pro-

cessing in lower-order cortical areas. Importantly, it should be emphasised that a purely feedforward view of sensory processing is insufficient to explain activity in primary sensory areas and any description of sensory processing must incorporate the interactions between feedforward and feedback circuitry.

1.1.3 The fine-scale organisation of local excitatory circuits

In pursuit of the principles that govern synaptic connectivity, it has become evident that a finer degree of synaptic specification is achieved between cortical neurons, beyond that prescribed by the canonical microcircuit. The probability of a synaptic connection between two pyramidal neurons varies according to cortical layer, but is typically between 10 - 20 % (Harris and Shepherd, 2015; Seeman et al., 2018; Lefort et al., 2009). Indeed, pyramidal neurons only form around 10 - 30 % of potential synapses, given the density of their axons and dendrites (Stepanyants et al., 2002a,b). Furthermore, the topology of synaptic connections within a population of pyramidal neurons has also been shown to be highly non-random (Perin et al., 2011; Song et al., 2005; Ashby and Isaac, 2011). Thus, connectivity is precise at a fine-scale, such that a neuron will form connections with only a subset of potential synaptic partners. This has led to the concept of cortical 'subnetworks', in which groups of preferentially connected neurons operate as functional assemblies for encoding different types of information (Kim et al., 2020; Znamenskiy et al., 2018; Najafi et al., 2020; Kampa et al., 2006; Palagina et al., 2019).

It is generally recognised that the specification of such subnetworks is achieved through a combination of genetically prescribed and activity-dependent mechanisms. However, the exact balance between determinism and freedom in developing circuits is still widely debated (Jabaudon, 2017). On the one hand, molecular mechanisms are known to specify neuronal connectivity on a gross scale, with the domain-specific expression of transcription factors creating a 'protomap' that guides axons across brain areas to their correct destination (Crossley et al., 2001; Grove et al., 1998; Fukuchi-Shimogori and Grove, 2001; Bishop et al., 2000). The molecular mechanisms underlying the protomap have been elegantly demonstrated through the ectopic expression of certain genes, resulting in shifted cortical areas (Fukuchi-Shimogori and Grove, 2001). On a finer scale, it is also evident that molecular mechanisms specify

synaptic connections. Neurons express a wide range of cell adhesion molecules, such as cadherins, which can specify synaptic connections between molecularly defined cell types (Basu et al., 2015; Takeichi, 2006; Jézéquel et al., 2023). However, it is unlikely that a genetic code is sufficient to specify one-to-one connections between all neurons (Zador, 2019). Furthermore, various activity-dependent mechanisms are known to play important roles in specifying neuronal connections on a fine-scale (Markram et al., 1997; Song et al., 2000; Le Bé and Markram, 2006). For example, Hebbian plasticity mechanisms encourage synapse formation between neurons with similar inputs, leading to preferential connectivity in functionally similar neurons (Ko et al., 2011). Specifically, L2/3 pyramidal neurons are more likely to be connected if they receive input from the same L4 neuron (Yoshimura et al., 2005) and the connection probability between L2/3 pyramidal neurons is higher if they have similar orientation tuning (Ko et al., 2011). Further evidence shows that these patterns of connectivity are absent prior to sensory experience, demonstrating the instructive role of sensory input in specifying fine-scale synaptic circuits (Ko et al., 2014, 2013).

An important question therefore is the extent to which activity freely molds synaptic circuits from a tabula rasa, or if there are predetermined organising principles under which activity-dependent mechanisms are constrained (Ashby and Isaac, 2011). Multi patch clamp studies reveal highly non-random synaptic connectivity networks in L5 pyramidal neurons from postnatal day 14 (P14), whereby the connection probability between two neurons depends heavily on other connections within the network (Song et al., 2005; Perin et al., 2011). Additional studies have reported highly specific interlaminar subnetworks, such as Kampa et al. (2006) who investigated the connectivity between L2/3 and L5 pyramidal neurons. It was found that pairs of connected L5 neurons were more likely to receive common input from a single L2/3 neuron. Furthermore, the inputs from unconnected L2/3 pyramidal neurons were more likely to converge onto single L5 neurons, than the inputs from connected L2/3 neurons. These results present a mechanism for the convergence and divergence of distinct information streams through the canonical circuit. Whilst some aspects of these subnetworks could form through Hebbian plasticity (Letzkus et al., 2006), their highly specific nature and early developmental expression suggests that some

level of fine-scale connectivity is genetically prescribed.

Notably, these studies were agnostic towards the heterogeneity amongst L2/3 and L5 pyramidal neurons, which may be a key aspect in the formation of highly specific synaptic subnetworks. Extensive efforts in combining methods such as single-cell RNA sequencing, patch clamp electrophysiology, viral transsynaptic tracing and functional *in vivo* recordings have helped uncover a multitude of cell types that have greatly advanced our understanding of synaptic circuits (Gouwens et al., 2020; Condylis et al., 2020; Bugeon et al., 2022; Sun et al., 2021; Scala et al., 2021; Tasic et al., 2018; Schwarz and Remy, 2019; Gerfen et al., 2018). Whilst the exact definitions of what constitutes a cell type can be debated (Zeng, 2022), not least because at some level most neuronal attributes lie along a continuum, it is generally accepted that there is a level of concordance between key neuronal attributes such as morphology, connectivity and transcriptomics (Gouwens et al., 2020; Hattox and Nelson, 2007; Liu et al., 2023; Kasper et al., 1994). Therefore, it may be that activity-dependent mechanisms are only free to act within the constraints of predetermined synaptic connection probabilities between different cell types.

Defining neuronal cell types according to their long-range projection targets has proven informative in explaining connectivity amongst neighbouring pyramidal neurons. For example, multiple lines of evidence suggests that the connections between L5 pyramidal neurons depends on their long-range projection target (Brown and Hestrin, 2009; Morishima et al., 2011; Bé et al., 2007; Morishima and Kawaguchi, 2006; Kiritani et al., 2012). In some cases, preferential synaptic connections were observed between neurons projecting to the same target, suggesting the amplification of responses to the same downstream circuits. Conversely, in several instances preferential connectivity was observed between neurons with different projection targets, but only in one direction (Brown and Hestrin, 2009; Kiritani et al., 2012). This suggests that cortical circuits are designed to integrate information across subnetworks in a manner that allows one subnetwork to partially control another. Whilst different cortical projection targets are often grouped together within the broad IT class, evidence from L2/3 of visual cortex suggests that differences in long-range cortical targets specify local connections (Kim et al., 2018; Hagihara et al., 2021). Therefore, further dissection of cortical projection target may continue to explain

synaptic connections between neighbouring pyramidal neurons. Indeed, L2/3 neurons projecting to M1 or S2 exhibit differences in the stimulus features that they encode (Chen et al., 2013; Yamashita et al., 2013; Yamashita and Petersen, 2016; Sato and Svoboda, 2010; Vavladeli et al., 2020), meaning that excitatory subnetworks allow the routing of functionally distinct information to separate downstream targets. Taken together, these studies support the idea that fine-scale excitatory circuits are specified through a combination of activity-dependent and cell-type-specific processes, which dictate how information flows through cortical networks.

1.1.4 The input circuitry of L2/3 pyramidal neurons and its significance for sensory processing

The experiments conducted in this thesis examine the synaptic inputs targeting L2/3 pyramidal neurons in S1. While **Chapter 1.1.1** introduces the canonical circuit that describes the trajectory of feedforward information through cortex, the complex involvement of L2/3 neurons in diverse local and long-range circuits are not covered by the canonical cortical microcircuit. This section aims to expand on what is known about the input-output connections within L2/3, and to elucidate the pivotal role that these connections play in the representation and transformation of sensory inputs.

The synaptic inputs to L2/3 pyramidal neurons define how these neurons respond to sensory stimuli. It is perhaps easiest to understand the inputs to L2/3 pyramidal neurons by first considering how L2/3 pyramidal neurons represent sensory stimuli differently to L4 neurons. L2/3 neurons have broader receptive fields, such that they exhibit more multi-whisker responses than neurons in L4 (Voelcker et al., 2022). This results from a convergence of inputs from multiple recurrent horizontal L2/3 connections across neighbouring columns (Petersen, 2007; Petersen and Sakmann, 2001; Petersen et al., 2003; Feldmeyer et al., 2006). Information about sensory stimuli in L2/3 is believed to be represented by a sparse yet reliable code (Voelcker et al., 2022; Harris and Mrsic-Flogel, 2013; O'Connor et al., 2010). This is where a small fraction of highly active neurons produces most of the action potential (spiking) output, displaying high discriminatory power for behavioural choices

(O'Connor et al., 2010). Strong inhibitory input from PV interneurons underlies sparse action potential firing in L2/3 (Crochet et al., 2011; Brecht et al., 2003). This is supported by evidence from *in vivo* patch-clamp recordings reporting that the membrane potential response of L2/3 pyramidal neurons to whisker stimulation is primarily hyperpolarizing, meaning that sensory-evoked responses are typically dominated by inhibition (Crochet et al., 2011). Therefore, it is likely that the functional output of L2/3 relies upon the integration of feedforward sensory inputs with other inputs to this layer.

Interlaminar inputs to L2/3 that are not described by the canonical circuit also make significant contributions to sensory processing. For example, L2/3 neurons receive input from L5. Whilst some reports suggest that connections from L5 to L2/3 are negligible (Lefort et al., 2009), L2/3 neurons residing above septa receive input from L5 that is as strong as input from L4 (Shepherd and Svoboda, 2005). Additionally, L2/3 neurons exhibit strong responses from optogenetically stimulating L5 (Vecchia et al., 2020; von Klemperer, 2021). This connection represents a way for the output of the cortical circuit to be reported back to previous layers, possibly to update predictions about stimuli or alter synaptic weights. Activation of L5 neurons produces both monosynaptic excitatory and disynaptic inhibitory responses in L2/3 pyramidal neurons (von Klemperer, 2021; Vecchia et al., 2020). L5 input to L2/3 is thought to sharpen the temporal response properties of L2/3 pyramidal neurons to incoming stimuli (Vecchia et al., 2020) and has also been implicated in sensory-evoked plasticity mediated by POm inputs (Audette et al., 2019). Taken together, whilst the functional contribution of L5 inputs to L2/3 neurons is not fully elucidated, this pathway is likely to provide important feedback signals to L2/3 neurons and influences their response properties during sensory processing.

The sparse spiking observed amongst L2/3 pyramidal neurons is perplexing, and probes the question of how sensory input can be effectively represented when the majority of neurons are silent? Some evidence suggests that high dimensional receptive field properties of L2/3 pyramidal neurons underlie their sparseness (Ranjbar-Slamloo and Arabzadeh, 2019; Nogueira et al., 2023). For instance, Ranjbar-Slamloo and Arabzadeh (2019) found that the majority of L2/3 neurons did evoke action potentials in response to complex stimulation of the whiskers, such as specific changes

in whisker velocity or curvature. Furthermore, given the complexity of receptive fields and the inability of feedforward inputs to drive spiking in L2/3, it is likely that feedforward inputs need to be integrated with other sources of input in order to elicit spikes. L2/3 pyramidal neurons receive feedback input from a range of higher order areas (Petreanu et al., 2007; Naskar et al., 2021; Jouhanneau et al., 2014; Mao et al., 2011; Minamisawa et al., 2018; Petreanu et al., 2012; Helmchen et al., 2018; Kwon et al., 2016; Denardo et al., 2015). These feedback inputs synapse onto the apical dendrites of L2/3 neurons, where NMDA-dependent dendritic spikes enhance action potential generation (Palmer et al., 2014) and contribute to stimulus selectivity and experience-dependent plasticity (Smith et al., 2013; Zhang and Bruno, 2019; Pagès et al., 2021). Inputs from higher order brain areas are believed to be relevant for contextualising incoming sensory inputs, containing information such as whisker movements and predictions based on what the animals knows about its sensory environment.

Feedback input to L2/3 pyramidal neurons in S1 can originate from other cortical areas or from higher order thalamic nuclei such as POm. Inputs from POm to L2/3 pyramidal neurons may contribute to multi-whisker response properties (Jouhanneau et al., 2014) and encode salient, behaviourally relevant features of sensory input (Gambino et al., 2014; Williams and Holtmaat, 2019; Audette et al., 2019; Zhang and Bruno, 2019; Pagès et al., 2021). Meanwhile, feedback input from cortical areas include those from S2 and M1 (Mao et al., 2011; Aronoff et al., 2010). S2 inputs are important for perceptual learning during sensory-driven behaviour (Kwon et al., 2016). M1 inputs may provide an efference copy of whisker phase during whisking (Hill et al., 2011). For example, in L5, evidence suggests that M1 feedback enables the coincident detection of tactile stimuli at specific points in the whisking cycle to facilitate object localization (Xu et al., 2012). Importantly, feedback inputs also engage a variety of inhibitory interneurons. For example, Yang and Sun (2018) demonstrate that M1 input recruits both monosynaptic excitation and disynaptic inhibition to differing extents across the subcellular compartments of L2/3 pyramidal neurons. Furthermore, strong recruitment of VIP interneurons by M1 input disinhibits L2/3 pyramidal neurons (Lee et al., 2013; Naskar et al., 2021). As such, L2/3 pyramidal neurons may only be able to respond to sensory stimuli

under disinhibitory periods in specific contexts or behavioural states, which may facilitate plasticity and learning (Williams and Holtmaat, 2019; Lee et al., 2013). Taken together, the evidence presented suggests that sensory processing in L2/3 represents a key point of integration between feedforward and feedback signals. This is in accordance with evidence that activity in primary sensory cortices does not only represent sensory information but is also an important site for contextual learning (Chen et al., 2015; Poort et al., 2015; Makino and Komiyama, 2015; David et al., 2012; Audette et al., 2019; Rabinovich et al., 2022; Lacefield et al., 2019; Rodgers et al., 2021).

These studies outline the ways in which inputs to L2/3 pyramidal neurons are relevant for sensory processing. A range of evidence has demonstrated heterogeneity in the sensory features that individual L2/3 neurons can represent, including whisker touches, movements, saliency and texture information (Petreanu et al., 2012; Jouhanneau et al., 2014; Minamisawa et al., 2018; Kwon et al., 2016). Therefore, this diversity is presumably implemented by specific recruitment of L2/3 neuron populations by various local and long-range inputs. Previous reports have supported the specific recruitment of some subpopulations of L2/3 pyramidal neurons by POm (Yassin et al., 2010; Jouhanneau et al., 2014), however, it is unknown whether similar mechanisms underlie the recruitment of L2/3 neurons by S2 or M1.

1.2 Synaptic inhibition in cortex

Inhibitory interneurons constitute 20 % of cortical neurons. Despite being in the minority, interneurons exert strong and diverse control over the activity of pyramidal neurons (Isaacson and Scanziani, 2011). This is in part due to the extensive heterogeneity of interneurons, which is recognised at the molecular, morphological, electrophysiological and functional level (Tremblay et al., 2016; Markram et al., 2004; Rudy et al., 2011; Lourenço et al., 2020). Interneurons mediate important local control of excitatory populations within dense recurrent networks. Without these important 'brakes', network activity would quickly result in uncontrolled, epileptogenic excitation. Furthermore, the specific connectivity patterns between excitatory and inhibitory neurons define the computations performed by cortical circuits. This

section will introduce the different types of cortical inhibitory interneurons and describe their organisation into functional circuits within L2/3.

1.2.1 Cortical inhibitory cell types

A continuing challenge in neuroscience is to categorise and understand the diverse range of cell types that exist throughout the brain. An excellent example of how this has facilitated an understanding of brain circuits is the classification of inhibitory interneurons. Defined as GABAergic cell types, inhibitory interneurons exhibit diverse yet clear patterns of molecular, morphological, electrophysiological and functional characteristics. However, due to their extensive heterogeneity, a consensus of interneuron subtypes is rarely agreed upon, as finer grain distinctions can continually be made (Ascoli et al., 2008; Tremblay et al., 2016). The discovery that almost all interneurons express one of 3 proteins has led this to be the most popular classification system used across neuroscience research (Pfeffer et al., 2013). This section will therefore describe the properties of interneurons expressing PV, somatostatin (SST) or the ionotropic serotonin receptor 5HT3a (5HT3aR) (Tremblay et al., 2016; Lee et al., 2010; Tasic et al., 2016; Zeisel et al., 2015).

Approximately 40 % of cortical interneurons express PV. Within the PV class there are two main subtypes: basket cells and chandelier cells, named after their distinct morphological characteristics (Kawaguchi and Kubota, 1997). PV basket cells form dense synapses around the post-synaptic neuron's soma and proximal dendrites, in a manner that resembles a basket. PV basket cells are found throughout the cortical layers and exhibit a diverse range of dendritic and axonal targeting patterns (Helmstaedter et al., 2009b,a; Wang et al., 2002; Runyan and Sur, 2013). Therefore, these cells can implement various types of intralaminar, translaminar and intercolumnar inhibition (Helmstaedter et al., 2009b; Tremblay et al., 2016; Bortone et al., 2014; Buchanan et al., 2012). PV interneurons possess very distinctive electrophysiological properties that make them specialised for providing fast, temporally precise synaptic inhibition. These include rapid EPSP kinetics (Hu et al., 2010), short-latency spike generation in response to single excitatory inputs (Jouhanneau et al., 2018), sustained, high frequency action potential firing (McCormick et al., 1985; Rudy and McBain, 2001; Hu and Jonas, 2014) and high neurotransmitter release probability at

their output synapses (Zaitsev et al., 2007). These characteristics allow PV basket cells to tightly control pyramidal neuron activity in cortical circuits, with functional relevance for the generation of synchronicity and oscillatory activity (Cardin et al., 2009; Sohal et al., 2009; Lourenço et al., 2020).

Chandelier cells target the axon initial segment of pyramidal neurons. They received their name because their axon terminals are vertically aligned, resembling candlesticks on a chandelier. Whilst their targeting of the axon initial segment suggests strong control over pyramidal neuron spike generation, their function in cortical circuits has been comparatively less explored than that of basket cells (Howard et al., 2005). Recent work suggests chandelier cells are biased to target specific pyramidal neuron subtypes (Lu et al., 2017) and their mode of inhibition varies, including shunting mechanisms (Lipkin and Bender, 2023).

Around one third of interneurons express SST. These interneurons are found throughout the cortical layers and preferentially form synapses onto the dendritic compartment of pyramidal neurons (Kawaguchi and Kubota, 1997; Wang et al., 2004). In contrast to PV interneurons, SST interneurons are recruited by facilitatory excitatory synapses, meaning they are typically activated by bursts of action potentials in presynaptic excitatory neurons (Silberberg and Markram, 2007; Reyes et al., 1998). SST interneurons are typically classified into two morphological subtypes. Martinotti SST interneurons target the apical tufts of pyramidal neuron dendrites within L1, whereas non-Martinotti SST interneurons lack this feature (Chiu et al., 2013; Xu et al., 2013; Silberberg and Markram, 2007). Non-Martinotti SST interneurons preferentially reside in L4 and L5 with their axonal projections remaining within these layers, or targeting L2/3 (Xu et al., 2013; Nigro et al., 2018; Ma et al., 2006; Naka et al., 2019). SST interneurons display a range of spiking patterns in response to current injection, such as low-threshold, regular or burst spiking (Tremblay et al., 2016). The differing features of SST interneurons compared to those of PV interneurons reflect the distinct functional contributions that these interneuron types make within cortical circuits.

The remaining 30 % of cortical interneurons can be categorised by expression of 5HT3aR. These represent a diverse group that are primarily found in the upper cor-

tical layers and can be further subdivided based on the expression of vasointestinal peptide (VIP). VIP interneurons are enriched in L2/3 and receive inputs from across cortical layers, as well as being targeted by long-range axonal projections, particularly those from M1 (Naskar et al., 2021). Perhaps the most distinguishing feature of VIP interneurons is their preference for targeting other interneurons (primarily SST interneurons) over excitatory neurons (Lee et al., 2010; Naskar et al., 2021; Pfeffer et al., 2013). Non-VIP 5HT3aR interneurons comprise many L1 interneuron subtypes, such as neurogliaform cells (Jiang et al., 2015). Neurogliaform interneurons are thought to modulate large populations of neurons via GABAergic volume transmission (Oláh et al., 2009). Recently, the identification of neuron-derived neurotrophic factor (NDNF) as a genetic marker for the majority of L1 interneurons has enabled the functional contribution of these cell types to be explored (Hartung et al., 2023; Hartung and Letzkus, 2021; Ibrahim et al., 2021; Abs et al., 2018; Schuman et al., 2019). NDNF-expressing interneurons are targeted by long-range inputs and thought to be involved in mediating arousal-dependent changes in neural activity (Malina et al., 2021).

In summary, these studies demonstrate the extensive efforts that have been made to classify interneurons as well as the substantial heterogeneity that is still left to explore. Importantly, this morphological and genetic diversity correlates with the vast functional diversity exhibited by interneurons within cortical circuits. The next section will expand upon how the function of these interneuron types described above contributes to sensory processing within L2/3.

1.2.2 Inhibitory synaptic circuits in L2/3

The inhibitory effects of GABAergic synaptic inputs are mediated by the opening of ionotropic $GABA_A$ receptors, which are primarily permeable to chloride ion (Cl^-) flux into the postsynaptic neuron, and therefore tend to move the postsynaptic neuron's membrane potential away from action potential threshold. The degree of inhibition therefore depends on the Cl^- reversal potential compared to the resting membrane potential. For example, in certain cases where intracellular Cl^- is relatively high, GABAergic inputs can be depolarizing (Alfonsa et al., 2023; Ellender et al., 2014). Alternatively, if the Cl^- reversal potential and membrane

potential are similar, this results in 'shunting' inhibition, whereby decreases in the membrane's input resistance temporally 'clamps' the membrane potential at the Cl^- reversal (Burman et al., 2023; Staley and Mody, 1992; Borg-Graham et al., 1998). Whether GABAergic inputs are hyperpolarizing, shunting or depolarizing has important implications for the temporal integration of excitatory and inhibitory inputs and determines the computations that neurons perform (Burman et al., 2023; Mitchell and Silver, 2003).

Interneurons protect cortical networks from runaway excitation by interacting with excitatory neurons through particular circuit motifs. Feedforward motifs are where a presynaptic excitatory axon synapses with an excitatory neuron and an inhibitory neuron. The inhibitory neuron then provides inhibition onto the excitatory neuron (**Figure 1.2**). Therefore, upon stimulation of this circuit, the post-synaptic excitatory neuron will receive a monosynaptic excitatory response closely followed by disynaptic inhibition. This generates a very strict temporal window for synaptic integration of excitatory inputs (Pouille and Scanziani, 2001). An example of this circuit motif is the connection from L4 to L2/3, as demonstrated by Xu et al. (2014). Optogenetic stimulation of L4 neurons produces a monosynaptic excitatory response in L2/3 pyramidal neurons, which is matched in size by a subsequent disynaptic inhibitory response via PV interneurons (Xue et al., 2014). SST interneurons also partake in feedforward motifs in L2/3, whereby excitation of a single L2/3 pyramidal neuron leads to inhibition in surrounding pyramidal neurons (Kapfer et al., 2007). This circuit operates on longer timescales than those mediated by PV interneurons because SST interneuron recruitment is facilitatory, resulting in frequency-dependent disynaptic inhibition (FDDI) (Silberberg and Markram, 2007; Kapfer et al., 2007; Berger et al., 2010). SST interneurons residing in both L2/3 and L5 participate in FDDI circuits that result in the widespread inhibition of L2/3 pyramidal neurons (Kapfer et al., 2007). Taken together, these studies represent how the same circuit motif can differentially control L2/3 pyramidal neurons depending on the synaptic properties of the interneurons involved.

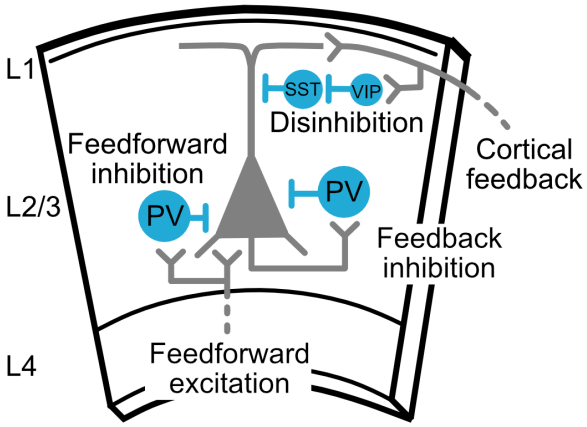


Figure 1.2: Inhibitory circuit motifs in L2/3. L2/3 pyramidal neurons (grey) receive feedforward and feedback synaptic inhibition that is primarily mediated by PV interneurons (blue). Feedforward inhibitory circuits comprise PV interneurons and L2/3 pyramidal neurons that are both recruited by the same excitatory input. PV interneurons then provide feedforward inhibition onto the pyramidal neurons, creating a short temporal window for excitation. Conversely, feedback inhibitory circuits involve PV interneurons that are excited by the same pyramidal neurons that they inhibit. Cortical feedback inputs to L1 activate L2/3 pyramidal neuron dendrites in addition to VIP interneurons. VIP interneurons inhibit SST interneurons, resulting in disinhibition of the L2/3 pyramidal neuron dendrites. Some inhibitory motifs are not included for simplicity, such as feedforward and feedback inhibition mediated by SST interneurons.

Another type of inhibitory circuit motif is feedback inhibition. This involves a reciprocal connection between a population of pyramidal neurons and interneurons, such that excitation of the pyramidal neurons will excite the inhibitory population, which then leads to the subsequent inhibition of the pyramidal population (Miles, 1990; Isaacson and Scanziani, 2011) (**Figure 1.2**). Such circuits are found throughout L2/3 and can involve both PV and SST interneurons, which make frequent reciprocal connections with nearby pyramidal neurons (Packer and Yuste, 2011; Fino and Yuste, 2011; Avermann et al., 2012). Specifically, feedback inhibition between PV interneurons and pyramidal neurons is necessary for the generation of cortical gamma oscillations, which are thought to improve information transfer between cortical circuits (Sohal et al., 2009). Both feedforward and feedback inhibition ensure that excitation in cortical networks is always closely followed by inhibition. The resulting 'balance' of excitation and inhibition is a general feature throughout cortical networks. In order for action potential generation and the propagation of information, brief temporal imbalances that favour excitation are generated through synchronous excitatory inputs (Roux and Buzsáki, 2015).

Inhibitory interneurons also inhibit one another, giving rise to disinhibitory circuits in L2/3 (Pfeffer et al., 2013; Avermann et al., 2012). PV interneurons primarily inhibit one another and SST interneurons, whereas SST interneurons inhibit both PV and VIP interneuron types, but avoid inhibiting other SST interneurons (Pfeffer et al., 2013). One of the most widely studied inhibitory-inhibitory connections is the strong preference for VIP interneurons to inhibit SST interneurons (Pfeffer et al., 2013) (**Figure 1.2**). This leads to the disinhibition of L2/3 pyramidal neuron dendrites during periods of VIP interneuron activity. VIP interneurons are recruited by long-range cortical inputs, thereby implicating this disinhibitory circuit in a range of cortical computations such as gain modulation, reward modulation, motor integration and plasticity (Letzkus et al., 2015; Williams and Holtmaat, 2019; Lee et al., 2013; Keller et al., 2020; Karnani et al., 2016; Fu et al., 2014; Lourenço et al., 2020; Ramamurthy et al., 2023). To summarise, the inhibitory synaptic motifs described here can be thought of as the canonical microcircuits for inhibition in L2/3 of cortex. Interneurons target their post-synaptic neurons with extremely high sub-cellular and cell-type specificity, leading to inhibitory microcircuits that can dynamically control the excitation delivered to pyramidal neurons along their entire somato-dendritic axis.

In contrast to their targeting of subcellular domains of postsynaptic pyramidal neurons, it has been proposed that PV and SST interneurons are not selective in terms of which particular pyramidal neurons they connect with. This has been referred to as 'blanket inhibition' (Packer and Yuste, 2011; Fino and Yuste, 2011). Connection rates from PV or SST interneurons onto pyramidal neurons vary from 50-100 % across different studies (Packer and Yuste, 2011; Fino and Yuste, 2011; Jouhanneau et al., 2018; Xue et al., 2014; Safari et al., 2017; Holmgren et al., 2003; Hofer et al., 2011). It is likely that these discrepancies depend on inter-somatic distances between the cell types and reflect the variety of cortical areas examined (Packer and Yuste, 2011). However, it is increasingly clear that whilst connectivity rates between excitatory and inhibitory neurons are far higher than those between excitatory neurons, there still exists a level of selectivity in terms of which pyramidal neurons an individual interneuron targets (Krook-Magnuson et al., 2012). This generates inhibitory subnetworks, which refers to the pool of individual interneurons

from which any given pyramidal neuron receives input from and is a useful term for describing how inhibition is shared between excitatory neurons. By definition, two pyramidal neurons within the same inhibitory subnetwork will receive more shared inhibition from common presynaptic interneurons, than pyramidal neurons that are in separate inhibitory subnetworks. Indeed, there may exist different degrees of overlap between separate subnetworks, for example, whilst the majority of neurons exhibit preferential control by a primary subnetwork, other neurons may coordinate and control communication between subnetworks (Palagina et al., 2019).

Evidence suggests that a pyramidal neuron's inhibitory subnetwork can reflect the pyramidal neuron's receptive field properties, long-range output, or long-range input (Palagina et al., 2019; Znamenskiy et al., 2018; Wu et al., 2023; Jézéquel et al., 2023; D'Souza et al., 2019). This supports the idea that separate excitatory subnetworks are in turn controlled by different pools of inhibitory interneurons (Negrón et al., 2023). Recent work suggests that in L5 of S1, pyramidal neurons with distinct projection targets are innervated by separate transcriptomic subnetworks of PV and SST interneurons (Jézéquel et al., 2023; Wu et al., 2023). This is reflective of previous studies in other brain regions such as frontal cortex and hippocampus, which show that inhibition is specified by pyramidal neuron subtype (Lee et al., 2014a; Varga et al., 2010; Valero et al., 2015; Lee et al., 2014b; Lu et al., 2017). Given that L2/3 pyramidal neurons exhibit a range of projection targets, it is unknown whether a similar mechanism shapes inhibition in this layer. Interestingly, evidence from L2/3 of V1 demonstrates that inhibitory subnetworks are arranged by the strength of feedback from higher order cortical areas (D'Souza et al., 2019). Taken together, these studies suggest that functional heterogeneity amongst pyramidal neurons may be reflected through their inhibitory subnetworks and the preferential sampling of certain interneuron subtypes over others. This would allow separate modulation of distinct information processing streams by a diverse range of inhibitory interneurons, however, the organising principles underlying inhibitory subnetwork generation in L2/3 remain largely unexplored.

1.3 Developmental origins of cortical subnetworks

Sections 1.1 and **1.2** have described how excitatory and inhibitory neurons interact to form cortical subnetworks in the mature rodent brain. An essential question that emerges is how these subnetworks are established during development. Indeed, this question motivates the experimental work in this thesis and I will therefore consider evidence for some of the relevant developmental processes that could contribute to subnetwork assembly. While it is evident that both activity-dependent and genetically-specified mechanisms determine final neuronal fates, an emerging consensus suggests that diverse neuronal types are produced through distinct developmental origins. A poignant example of this is demonstrated by the neurogenesis of excitatory versus inhibitory cortical neurons, which derive from distinct developmental trajectories in separate proliferative zones of the embryonic brain (**Figure 1.3**). This section will describe the origins of circuit assembly during development, including the neurogenesis of excitatory and inhibitory neurons.

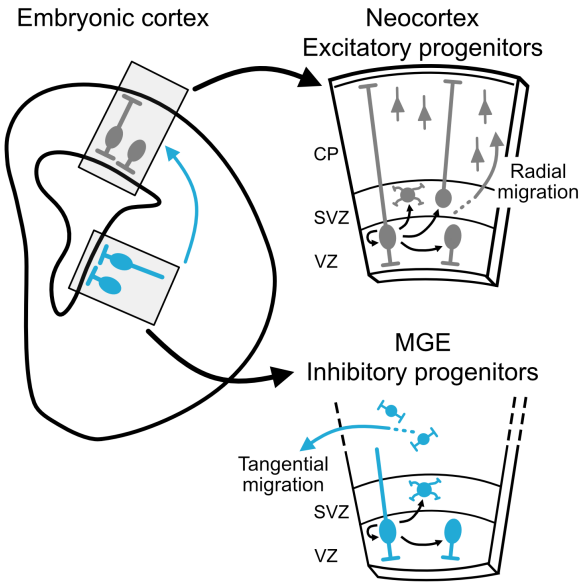


Figure 1.3: Neurogenic niches of excitatory and inhibitory cortical neurons. Excitatory and inhibitory neurons are born between embryonic days 10-18 in the mouse. Excitatory neurons are born from progenitor cells in the dorsal telencephalon (pallium). Excitatory neurons are born from one of several types of progenitor cell in the ventricular zone (VZ) or subventricular zone (SVZ), from which they migrate radially to populate the cortical plate (CP). PV and SST inhibitory interneurons are born from one of several types of progenitor cell in a region of the ventral telencephalon (subpallium) known as the medial ganglionic eminence (MGE). After birth, inhibitory interneurons migrate tangentially towards the CP, where they integrate into functional circuits with excitatory neurons over the course of development.

1.3.1 Excitatory neurogenesis

Between embryonic days 10 and 18 (E10-18) in the mouse, all excitatory cortical neurons are born from progenitor cells within the neurogenic zones of the dorsal telencephalon (**Figure 1.3**). This process is tightly orchestrated by the strict temporal and spatial expression patterns of transcription factors that guide progenitor cells to produce the correct number and type of excitatory neurons (Greig et al., 2013; Telley et al., 2016, 2019). The onset of neurogenesis is marked by the birth of radial glial cells (RGCs) from neuroepithelial cells around E10 within the ventricular zone (VZ) (Tan and Shi, 2013). RGCs are viewed as the principal neurogenic cell type, from which all subsequent progenitor types, post-mitotic neurons and glia are born (Hippenmeyer, 2023; Tamamaki et al., 2001; Freeman and Rowitch, 2013; Wang et al., 2011). RGCs firstly undergo symmetric divisions, producing 2 daughter RGCs in order to amplify the RGC pool. At around E12, RGCs switch to

self-renewing asymmetric divisions, which produce one RGC and either a neuron or an intermediate progenitor (IP), which can further divide to produce two daughter neurons (Noctor et al., 2001, 2004).

Once born, daughter neurons migrate to the cortical plate (CP) via one of several distinct types of radial migration (Nadarajah et al., 2001; Tabata et al., 2003; O'Rourke et al., 1992; Rakic, 1972; Miyata et al., 2004). These include using the radial fibres of RGCs as a scaffold (Nadarajah et al., 2001), somal-translocation, whereby the neuron moves its nucleus along a leading process towards the pia (Miyata et al., 2001), and multipolar migration, which involves the dynamic extension and retraction of multiple processes as the neuron ascends to the cortical plate (Tabata et al., 2003). It is thought that glutamatergic signalling between newly born excitatory neurons and subplate neurons facilitates a transition of migration from multipolar to radial (Ohtaka-Maruyama et al., 2018). Cortical neurons are born in an inside-out manner, such that neurons occupying the deep cortical layers are born first, followed by neurons that go on to occupy progressively more superficial layers (Sidman and Rakic, 1973; Caviness Jr, 1982). As such, a single RGC gives rise to a group of neurons that span the cortical layers, often termed as a 'radial unit' (Rakic, 1988). Multiple studies have attempted to label neurons born from single RGCs to determine their unitary output, which is estimated to be approximately 60 neurons in early neurogenesis versus 10 neurons in later neurogenesis (Gao et al., 2014). The variation in this number is because labelling of RGCs earlier in neurogenesis will encompass the progeny of RGCs subsequently produced from the same lineage.

The observation that deep and superficial layer neurons are produced at separate times during neurogenesis has generated several possible models of neurogenesis, involving varying degrees of progenitor fate restriction versus multipotency (Greig et al., 2013; Franco and Müller, 2013; Huilgol et al., 2023b). On the one hand, it is possible that multiple pools of progenitors co-exist and differ in their competency to generate specific cortical neuron subtypes (Franco et al., 2012; Huilgol et al., 2023a; Matho et al., 2021; Arlotta et al., 2005; Hirata et al., 2009; Molyneaux et al., 2005; Nieto et al., 2004; Shohayeb et al., 2021). Conversely, multipotent progenitors may undergo progressive fate restriction determined by temporally programmed transcriptional waves to produce distinct neuron subtypes (Magrinelli et al., 2022;

Telley et al., 2016, 2019; Oberst et al., 2019; Bella et al., 2021; Ruan et al., 2021). This question is central to how cell type diversity is generated in cortex and there is evidence that supports both possibilities. For example, progenitors expressing the superficial layer gene cut-like homeobox 2 (Cux2) are present from the onset of neurogenesis and exclusively give rise to superficial layer neurons, arguing that they are a distinct lineage from progenitors that produce deep layer neurons (Franco et al., 2012; Gil-Sanz et al., 2015). On the other hand, single RGCs can produce neurons that occupy all cortical layers (Gao et al., 2014) and transplantation studies have demonstrated the ability of progenitors to be re-programmed to generate different neuron types according to the environment of the host tissue (Oberst et al., 2019; McConnell, 1988; Desai and McConnell, 2000; McConnell and Kaznowski, 1991). Therefore, it is likely that a combination of contemporaneous progenitor heterogeneity with specific fate restrictions in addition to a progressive temporal programming is necessary to generate the full diversity of excitatory neurons that are found both within and across cortical layers (Greig et al., 2013; Huilgol et al., 2023b; Harris and Shepherd, 2015).

Further support for contemporaneous progenitor heterogeneity comes from the fact that several distinct types of progenitor co-exist within the VZ and subventricular zone (SVZ) throughout neurogenesis (Gal et al., 2006; Stancik et al., 2010; Tyler and Haydar, 2013; Huilgol et al., 2023a; Noctor et al., 2004) (**Figure 1.4**). Therefore, simultaneously born excitatory neurons can exhibit diverse developmental lineages despite occupying the same cortical layer (Tyler et al., 2015; Guillamon-Vivancos et al., 2019; Ellender et al., 2019; Matho et al., 2021). The most well-described progenitor types which produce excitatory neurons in the mouse are RGCs, apical IPs (aIPs), basal IPs (bIPs) and basal radial glia (bRGs) (Gal et al., 2006; Stancik et al., 2010; Tyler and Haydar, 2013; Wang et al., 2011; Noctor et al., 2004; Englund et al., 2005). Generally, these progenitor types are distinguished by their morphology, gene expression patterns, cell cycle kinetics, and position within the neurogenic zones (Bedogni and Hevner, 2021; Gal et al., 2006; Stancik et al., 2010; Englund et al., 2005; Wang et al., 2011; Govindan and Jabaudon, 2017). aIPs reside in the VZ, exhibit short radial morphology and express tubulin alpha 1 (Tα1) (Gal et al., 2006; Stancik et al., 2010). bIPs, on the other hand, are multipolar cells that

express T-box brain protein 2 (Tbr2) and undergo one or few neurogenic divisions within the SVZ (Englund et al., 2005; Miyata et al., 2004). Finally, bRGs undergo self-renewing and neurogenic divisions in the SVZ, although this progenitor type is thought to be much more common in gyrencephalic mammals (Shitamukai et al., 2011; Wang et al., 2011; Tyler and Haydar, 2010). It is also worth noting that whilst RGCs are typically classified as one progenitor type, extensive heterogeneity exists within this group (Ruan et al., 2021; Huilgol et al., 2023b; Li et al., 2020). Interestingly, recent genetic dissection of RGCs has found further evidence that separate RGC lineages give rise to excitatory neurons with distinct projection patterns (Matho et al., 2021; Huilgol et al., 2023b). Further exploration of progenitor heterogeneity in combination with lineage-labelling techniques such as genetic barcoding will hopefully reveal the specific fate restriction of RGCs during neurogenesis (Ratz et al., 2022; Bandler et al., 2021).

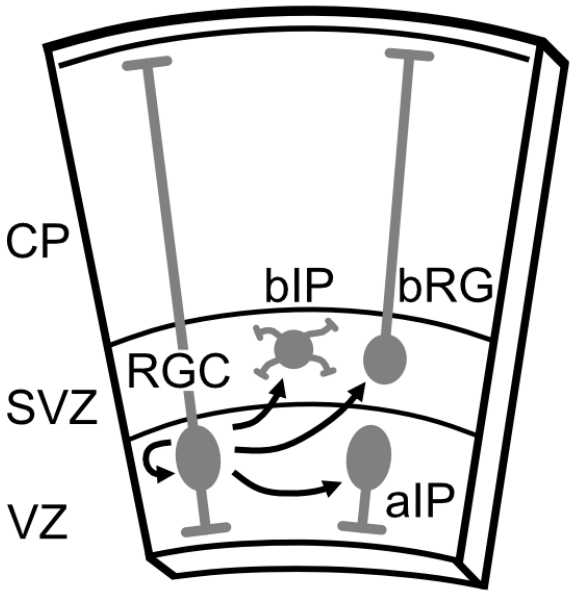


Figure 1.4: Excitatory neuron progenitor types in the embryonic mouse brain. Radial glial cells (RGCs) are generated from neuroepithelial cells around E10 and constitute the primary cortical progenitor type. RGCs directly produce neurons as well as giving rise to other progenitor types, namely basal intermediate progenitors (bIPs), apical intermediate progenitors (aIPs) and basal radial glial (bRGs). aIPs exhibit short radial morphology, reside in the VZ, are thought to divide symmetrically to produce two daughter neurons. bIPs and bRGs reside in the SVZ. Whilst bIPs exhibit multipolar morphology and symmetrically divide to produce two daughter neurons, bRGs extend a radial process to the pia and undergo self-renewing divisions.

The evolutionary expansion of the cortex has been mirrored by an expansion of

progenitor types during neurogenesis (Martinez-Cerdeno et al., 2006). The presence of multiple progenitor types begs the question of the functional relevance of progenitor heterogeneity. The generation of multiple progenitor types may exist to simply amplify the number of neurons that can be produced during corticogenesis (Martinez-Cerdeno et al., 2006; Florio and Huttner, 2014). Alternatively, each progenitor type may exhibit biases for certain cell types, thereby contributing to the diversity of excitatory neurons (Greig et al., 2013; Huilgol et al., 2023b). Evidence for these possibilities will be explored in **Section 1.4.2**.

1.3.2 Inhibitory neurogenesis

In contrast to excitatory neurons, cortical inhibitory interneurons are born from progenitor cells within the ganglionic eminences and preoptic area (POA) of the subpallium over embryonic days E10 - E18 (Lim et al., 2018a; Wonders and Anderson, 2006; Gelman et al., 2011; Bartolini et al., 2013) (**Figure 1.3**). The ganglionic eminences can be divided into distinct proliferative zones that produce different types of interneurons (Butt et al., 2008; Flames et al., 2007). These include the medial ganglionic eminence (MGE), which produces PV and SST interneurons, and the cadual ganglionic eminence (CGE), which produces VIP and cholecystokinin (CCK) interneurons (Lim et al., 2018a). Neurogliaform cells and several other types of L1 interneurons are born from the POA (Niquille et al., 2018; Gelman et al., 2009; Torigoe et al., 2016). The spatiotemporal patterning of specific transcription factors within these regions determines the specific interneuron types that are produced (Butt et al., 2008; Kanatani et al., 2008; Flames et al., 2007; Tyson et al., 2015; Hu et al., 2017).

In parallel to excitatory neurogenesis, the proliferative zones that produce inhibitory interneurons contain heterogeneous progenitor types, each displaying biases in their generation of different interneuron types (Pilz et al., 2013; Hu et al., 2017; Petros et al., 2015). There is evidence to support the idea that both contemporaneous progenitor heterogeneity and progressive evolution of progenitor types are involved in the specification of interneuron identity (Wamsley and Fishell, 2017; Lim et al., 2018a). For example, progenitors in the dorsal MGE primarily produce SST interneurons whereas PV interneurons originate from progenitors in the ventrocaudal

MGE (Flames et al., 2007; Fogarty et al., 2007; He et al., 2016; Inan et al., 2012; Wonders et al., 2008). Furthermore, it is thought that SST interneurons are produced mainly from apical progenitors in the VZ of the MGE, while PV interneurons are produced via indirect neurogenesis from IPs in the SVZ of the MGE (Petros et al., 2015). At the same time, it is thought that interneuron identity and laminar position are encoded by the time course of neurogenesis, whereby interneurons generated in early neurogenesis populate deeper cortical layers and are biased towards an SST interneuron fate (Inan et al., 2012; Miyoshi et al., 2007; Rymar and Sadikot, 2007; Valcanis and Tan, 2003; Butt et al., 2005). This temporal pattern aligns with the laminar 'inside-out' trajectory observed in the generation of excitatory neurons. Nevertheless, exceptions to this paradigm exist, such as the generation of chandelier cells during late neurogenesis (Inan et al., 2012; Taniguchi et al., 2013).

Following their birth, cortical interneurons migrate to the pallium to reach the developing CP. This is achieved through chemoattractive and chemorepulsive signalling by the pallium and striatum, respectively (Marín et al., 2003; Wichterle et al., 2003; Flames et al., 2004). Migration of interneurons into the cortical plate occurs in a non-random manner, whereby interneuron subtypes choose specific migratory routes (Lim et al., 2018b; Antypa et al., 2011; Zimmer et al., 2011). Migratory paths form either through the marginal zone (MZ) or through the SVZ (Tanaka and Nakajima, 2012). Lim et al. (2018b) found that the MZ migration route is preferred by translaminar PV interneurons and Martinotti SST interneurons. Notably, interference with the MZ migration of Martinotti SST interneurons disrupts their characteristic axonal arborization in L1, highlighting the instructive role of interneuron migration in the specification of interneuron subtypes.

These migratory routes also involve signalling with excitatory progenitors and postmitotic excitatory neurons. For example, interneurons migrating along the MZ path have been shown to interact with the basal end feet of RGCs (D'Arcy et al., 2023) and interneurons migrating along the SVZ are thought to partake in chemokine signalling with bIPs (Sessa et al., 2010; Tiveron et al., 2006; López-Bendito et al., 2008). Furthermore, the final laminar destination of migratory interneurons is thought to be influenced by postmitotic excitatory neurons already in the CP (Pla et al., 2006). The migration of interneurons is switched from tangential to radial through neureg-

ulin signalling by pyramidal neurons (Bartolini et al., 2017) and their laminar position is regulated by specific types of projection neurons (Lodato et al., 2011). These studies demonstrate the interplay between inhibitory and excitatory neurons, and the important role of these interactions in shaping circuit assembly at the earliest time points following neurogenesis. Interneuron migration into the cortical layers is largely complete by P0, following which interneurons and excitatory neurons undergo circuit assembly and refinement.

1.3.3 Circuit assembly of excitatory and inhibitory neurons

Once excitatory and inhibitory neurons have reached their laminar destinations within cortex, a combination of intrinsic genetic programs and activity-dependent mechanisms influence how these neurons interact with one another to generate mature circuits (Foeller and Feldman, 2004). During the late embryonic period and first few weeks of postnatal life, spontaneous and sensory-evoked activity refine neuronal circuits in a manner that establishes strict topography and prepares the barrel cortex for sensory processing (Hanganu-Opatz et al., 2021; Lim et al., 2018b; Ashby and Isaac, 2011; Bender et al., 2003; Jiao et al., 2006). Spontaneous activity occurs in the absence of sensory input and can be either cortical or thalamic in origin (Dupont et al., 2005; Anton-Bolanos et al., 2019). Beginning from as early as E17, thalamic activity can result in highly synchronized waves of activity that propagate across S1, recruiting pyramidal neurons and primarily PV and SST (MGE-derived) interneurons (Duan et al., 2020; Modol et al., 2020; Anton-Bolanos et al., 2019; Alléne et al., 2008). Both depolarizing and shunting responses to GABAergic inputs contribute to the spread and limitation of network activity during this period, respectively (Alléne et al., 2008; Khalilov et al., 2015; Duan et al., 2020). By the end of the first postnatal week, highly synchronous spontaneous activity forms functional excitatory-inhibitory neuron ensembles (Duan et al., 2020).

Following this period of highly synchronous network activity, interneurons become integrated into spatially segregated assemblies of co-active excitatory and inhibitory neurons. The integration of interneurons is affected by a significant wave of apoptosis that occurs around P7-P9 in the mouse, when up to 30 % of cortical interneurons are removed (Southwell et al., 2012). Apoptosis of interneurons is thought to be

intrinsically programmed and their recruitment into active synaptic networks effectively 'rescues' interneurons from cell death (Priya et al., 2018; Southwell et al., 2012; Wong et al., 2018). This is supported by work that has manipulated excitation levels during this developmental window, resulting in lower levels of apoptosis (Denaxa et al., 2018; Priya et al., 2018; Wong et al., 2018; Duan et al., 2020).

Into the second post-natal week, local network activity begins to decorrelate as functional assemblies consisting of excitatory pyramidal neurons and primarily PV interneurons begin to respond to sensory input independently from one another (Modol et al., 2020). During this time, L2/3 circuits are particularly responsive to manipulations in sensory input, which is often referred to as the 'critical period' (Hensch, 2005; Erzurumlu and Gaspar, 2012; Sun and Zhang, 2011). Indeed, sensory deprivation through whisker trimming dramatically alters the dynamics of both excitatory and inhibitory circuits during this period (Modol et al., 2020). For example, whisker deprivation interrupts the formation of recurrent connections between excitatory cortical neurons (Ashby and Isaac, 2011). Furthermore, the critical period is thought to be tightly regulated by inhibition from PV interneurons, whereby the maturation of these circuits via peri-neuronal net formation reduces the potential for plasticity (Pizzorusso et al., 2002). There are also birth-date-dependent effects upon critical period plasticity, suggesting that early-born, deeper layer circuits mature before later-born superficial circuits (Fox, 1992; Wen and Barth, 2011; Stern et al., 2001; Erzurumlu and Gaspar, 2012; Lee et al., 2009; Maravall et al., 2004). By the onset of active whisking at the end of the second post-natal week, these circuits are ready to respond appropriately to the sensory environment (Baruchin et al., 2022).

Whilst the majority of circuit motifs assembled during development continue to be expressed and refined throughout an animal's lifetime, some circuits are expressed transiently only during development. For example, L4 excitatory neurons first receive feedforward inhibition from a transient thalamocortical circuit that recruits L5 SST interneurons, in contrast to the PV interneuron-mediated feedforward inhibition that serves this function in later life (Marques-Smith et al., 2016). Furthermore, L4 PV interneurons initially receive their excitatory input from L2/3 pyramidal neurons, before L4 excitatory neurons take on this role towards the end of the second

postnatal week (Anastasiades et al., 2016). Finally, transient thalamic innervation of L1 neurogliaform cells during the first post-natal week controls the formation of L2/3 sensory maps in an activity-dependent manner (Garcia et al., 2015; Che et al., 2018). Thus, although these circuits are only transiently expressed, they serve a crucial role in the correct development of thalamocortical circuits and responses to sensory inputs.

1.4 Lineage-dependent contributions to fine-scale cortical circuits

The previous section provided an overview of the generation of excitatory and inhibitory neuron types and how these neurons begin to form organised circuits during development. These studies illustrate how a combination of genetically-specified and activity-dependent mechanisms give rise to mature cortical circuits. However, it is unclear how developmental mechanisms orchestrate both the generation of a diverse array of excitatory cell types and the fine-scale synaptic connections between individual neurons. The following section will explore evidence supporting the role of neuronal lineage in the formation of fine-scale cortical circuits. Furthermore, this will be placed in the context of emerging evidence for the role of contemporaneous progenitor heterogeneity in generating diverse cortical excitatory neuron types.

1.4.1 Lineage-dependent circuit assembly

The observation that a single RGC gives rise to a limited number of radially aligned excitatory neurons that span the cortical layers led to the proposal of the radial unit hypothesis by Rakic (1988). The radial unit hypothesis predicts that ontogenetic columns, comprising clonally related neurons derived from a common RGC, constitute a developmental foundation for building the cortical column. Accordingly, these clonally related neurons are predicted to exhibit preferred connectivity and function. The first direct evidence supporting this hypothesis came from a series of studies from the lab of Song-Hai Shi. These studies used a retroviral labelling strategy to identify excitatory neurons derived from an individual RGC. Yu et al. (2009) found that sister neurons from the same ontogenetic clone exhibited prefer-

ential synaptic connectivity. Preferential synapses formed between sister neurons in a layer-dependent manner that matched the flow of excitatory information through the canonical cortical circuit (Yu et al., 2009) (**Figure 1.5a**).

Further studies found that sister neurons go on to develop preferential orientation tuning in visual cortex, thereby demonstrating Rakic's prediction that ontogenetic columns serve a functional role in cortical circuits (Li et al., 2012). Notably, the establishment of lineage-dependent synaptic connectivity and orientation tuning was found to depend on favoured gap junction formation between sister neurons during early post-natal development (Yu et al., 2012; Li et al., 2012). The formation of gap junctions enabled electrical coupling between sister neurons, thereby facilitating synchronous action potential generation in response to spontaneous synaptic input and promoting chemical synapse formation through Hebbian plasticity mechanisms (Yu et al., 2012). Collectively, these studies highlight the significance of lineage-dependent mechanisms in the construction of fine-scale cortical circuits.

Whilst the work of Song-Hai Shi and colleagues used retroviral labelling to identify clonal neurons generated from one RGC, further studies have since used alternative methods to label much larger RGC clones that encompass more distally related neurons (Ohtsuki et al., 2012; Cadwell et al., 2020). These studies have confirmed the findings that clonally related neurons exhibit preferential response properties (Ohtsuki et al., 2012) and radial connectivity (Cadwell et al., 2020), although the influence of clonality was less strong amongst clones comprising more distally related neurons.

This suggests that whilst clonality is a strong determinant of synaptic connectivity between two neurons originating from the same RGC, lineage-dependent mechanisms have limited influence on the functional connections amongst hundreds or thousands of neurons (Smith and Fitzpatrick, 2012). Interestingly, recent research from Song-Hai Shi's lab suggest that more complex lineage mechanisms regulate the synaptic connections amongst larger groups of neurons (Lin et al., 2023). For example, whilst radially aligned sister neurons exhibit preferential synaptic connectivity, horizontally aligned 'cousin' neurons, which are derived from separate RGCs, avoid forming synaptic connections with one another and have less similar orienta-

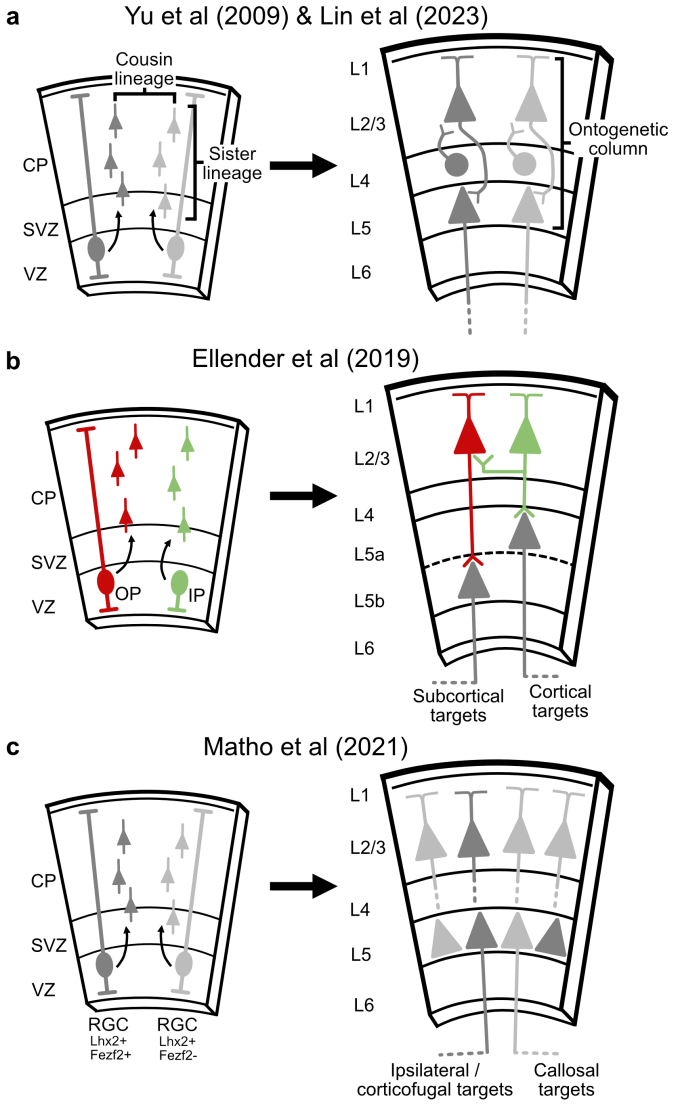


Figure 1.5: Lineage-dependent circuit assembly. (**a**) Radially aligned sister neurons generated from the same RGC form an ontogenetic column go on to develop preferential synaptic connectivity in mature cortex (Yu et al., 2009; Li et al., 2012). Horizontally aligned cousin neurons generated from separate RGCs avoid forming synaptic connections with one another in mature cortex (Lin et al., 2023). (**b**) Neurons derived from intermediate progenitors (IP-derived) prefer to connect to neurons derived from other progenitors (OP-derived) and send translaminar projections to L5a neurons, whereas OP-derived neurons prefer to send translaminar projections to L5b neurons (Ellender et al., 2019). (**c**) Two intermixed radial glia cell (RGC) populations give rise to cortical projection neurons throughout the cortical layers. Neurons derived from RGCs expressing Lhx2 and Fezf2 send ipsilateral or corticofugal projections. Neurons derived from RGCs expressing Lhx2 but not Fezf2 send callosal projections (Matho et al., 2021).

tion tuning preferences than would be expected by chance (Lin et al., 2023). The relationship between sister versus cousin neurons could be predicted by the expression of clustered-protocadherins (cPCDH), which are a group of cadherin proteins involved in cell-surface identity and dendritic self-avoidance (Yagi, 2012; Kostadinov and Sanes, 2015; Lefebvre et al., 2012; Lin et al., 2023; Lv et al., 2022). Therefore, the effects of clonality may be 'diluted' in studies that label large clones early in development, due to the inclusion of cousin lineages within the clonal population. Nevertheless, these studies support the role of progenitor-dependent mechanisms in the construction of fine-scale cortical circuits. In this sense, lineage can both encourage synapse formation to aid the construction of functional cortical columns, whilst also discouraging synapse formation between horizontally aligned neurons, thereby contributing towards the highly heterogeneous response properties of neighbouring L2/3 neurons and tiling of the stimulus space in sensory cortices.

Lineage-dependent circuit assembly has been observed in other brain areas (Xu et al., 2014) and even other species (Muldal et al., 2014), therefore making it an attractive mechanism for the implementation of evolutionarily conserved patterns of fine-scale connectivity amongst neurons. Indeed, one study in hippocampus has extended these ideas to excitatory-inhibitory connectivity, reporting that two clonally related excitatory neurons from the same individual progenitor are more likely to receive common inhibitory inputs from the same fast-spiking interneuron than pairs of non-clonally related neurons (Xu et al., 2014). This suggests that lineage-dependent mechanisms not only influence the synaptic connections between excitatory neurons but can also impact the integration of neurons into functional inhibitory subnetworks. However, it is so far unknown whether similar mechanisms influence inhibitory subnetwork formation in cortical circuits.

Taken together, these studies demonstrate the potential for lineage to affect cortical circuit assembly, offering compelling evidence that relationships between clonally related neurons can generate precise, fine-scale synaptic connectivity in cortical circuits. It is important to recognise, however, that the extent of cortical circuitry that lineage relationships can explain is limited (Smith and Fitzpatrick, 2012; Ohtsuki et al., 2012). Numerically, a typical cortical neuron receives inputs from hundreds or thousands of pre-synaptic partners, and therefore the inputs from its clonal sisters

would represent a small fraction of this total input (Rancz et al., 2011; Vélez-Fort et al., 2014). Furthermore, clonal studies have so far overlooked the nuances of progenitor heterogeneity and the functional implications of clonal neurons originating from distinct progenitor types. For example, if an individual progenitor is biased to produce certain neuron types and those neuron types are more likely to synapse with one another, then the observed effect of clonality could in fact be an effect of cell type. Indeed, growing evidence supports the influence of progenitor type on the transcriptomic cell type identity and the synaptic connectivity patterns exhibited by its progeny (Huilgol et al., 2023a; Matho et al., 2021; Buchan et al., 2022; Ellender et al., 2019). The implications of these findings will be discussed in the following section.

1.4.2 Role of progenitor heterogeneity in fine-scale circuit assembly

Given the evidence of lineage-dependent connectivity and the fact that excitatory neurons arise from a heterogeneous pool of progenitors, one hypothesis posits that the functional properties of excitatory neurons reflect the progenitor type from which they were born (Hippenmeyer, 2023; Huilgol et al., 2023b). This would suggest that progenitor heterogeneity represents a mechanism to generate neuronal diversity in the cortex, as opposed to simply amplifying neuronal numbers. Contemporaneous progenitor heterogeneity would therefore enable neighbouring excitatory neurons to be born from diverse developmental trajectories, creating a mosaic of neuronal diversity throughout cortical circuits.

Multiple lines of evidence support the hypothesis that different progenitor types exhibit varying competency for different excitatory neuron types. For example, both L4 and L2/3 excitatory neurons derived from bIPs exhibit specific morphological and electrophysiological properties when compared to neurons derived from a non-bIP lineage (Tyler et al., 2015; Guillamon-Vivancos et al., 2019). bIP-derived neurons in L4 and L2/3 exhibit a more depolarized membrane potential and higher action potential firing rates in response to current injections compared to their neighbouring non-bIP-derived neurons. These results suggest that bIP-derived neurons have a

higher output gain in response to the same input. Furthermore, bIP-derived neurons exhibit differences in the complexity of their dendritic morphology in L2/3 and dendritic polarization in L4 (Tyler et al., 2015; Guillamon-Vivancos et al., 2019). These results suggest that progenitor type influences the functional identity of neuronal progeny in a layer-specific manner.

Further evidence supporting the idea that progenitor type influences neuronal identity comes from Ellender et al. (2019). This study found connectivity biases in the intra and interlaminar excitatory synaptic connectivity of neurons derived from IPs compared to those derived from other progenitors (OP-derived). Specifically, IP-derived neurons in L2/3 and L4 exhibited an 'out-of-class' connectivity bias, whereby they avoided connections with other IP-derived neurons in the same layer, preferring to synapse with OP-derived neurons. Therefore, it is possible that connectivity biases between neurons derived from different progenitor types contribute to some of the 'cousin' lineage-dependent connectivity patterns observed in Lin et al. (2023). Furthermore, L2/3 IP-derived neurons exert translaminar connectivity differences in their synaptic output to L5. While IP-derived neurons preferentially connect to neurons in L5a, OP-derived neurons preferentially connect to neurons in L5b (Ellender et al., 2019) (**Figure 1.5b**). Some of these biases in connectivity may be explained by the fact that transcriptomic differences were found between IP-derived and OP-derived L2/3 populations, suggesting that progenitor type can restrict the cell types of their neuronal progeny (Ellender et al., 2019).

Additional studies suggest that progenitor type can also influence the selective connectivity of long range axonal projections. Buchan et al. (2022) found that L4 IP-derived neurons receive preferential input from the thalamic nucleus POm, whereas OP-derived neurons receive preferential input from VPM. The differential sampling of these two thalamic nuclei by IP-derived and OP-derived neurons was responsible for their preferential response properties for multiple or single whisker stimulation, respectively (Buchan et al., 2022). As a result of these thalamic biases, IP-derived and OP-derived L4 neurons were found to be differentially implicated in sensory-evoked plasticity (Buchan et al., 2022). This demonstrates that progenitor type, in addition to clonal relationship, influences the functional response properties of cortical neurons.

Recent findings also propose that the combinatorial expression of few key transcription factors identifies RGC lineages that generate neurons with distinct axonal projection patterns (Matho et al., 2021; Huilgol et al., 2023b). For example, RGCs expressing the transcription factors Lhx2 and Fezf2 can be found intermingled within the dorsal VZ throughout neurogenesis, giving rise to excitatory projection neurons across the cortical layers (Matho et al., 2021). Whereas $Lhx2^{+}/Fezf2^{-}$ RGCs give rise to neurons with callosal projections, $Lhx2^{+}/Fezf2^{+}$ RGCs give rise to neurons with corticofugal projection patterns and a small proportion of upper-layer neurons with non-callosal projection patterns (Matho et al., 2021; Huilgol et al., 2023b) (**Figure 1.5c**). Indeed, it would be interesting to explore whether these RGC subtypes give rise to different types of IPs, which are further specified to generate neurons with distinct projection patterns. Consistent with this possibility, Huilgol et al. (2023a) found that neurons generated from direct neurogenesis via RGCs and indirect neurogenesis via IPs differentially contribute to different projection neuron classes.

Collectively, these studies demonstrate that the specification of diverse cortical excitatory neuron subtypes begins during neurogenesis through mechanisms of progenitor heterogeneity and fate-restriction. This aids the generation of a mosaic of excitatory neuron types exhibiting diverse projection patterns and functional properties. More generally, these studies support the idea that the evolutionarily expansion of progenitor types diversifies excitatory neuron subtypes.

1.5 Thesis aims

The studies outlined above support the idea that excitatory neuron progenitor type can influence the functional properties of its neuronal progeny, including morphology, electrophysiology and excitatory synaptic connectivity. This thesis aims to build upon these findings by investigating whether progenitor type can influence how L2/3 pyramidal neurons receive their local inhibitory inputs and their long-range cortical feedback. To achieve this, I have used a combination of *in utero* lineage labelling techniques, *in vitro* and *in vivo* patch-clamp electrophysiology, plus optogenetic circuit mapping. My findings are presented in three results chapters:

- **Chapter 3** aimed to establish an embryonic labelling method to identify IP-derived L2/3 pyramidal neurons such that they could be subsequently targeted by two-photon *in vivo* patch clamp recordings in S1 of mature mice. This would enable me to record the synaptic inhibitory inputs received by IP-derived L2/3 pyramidal neurons, with the aim of determining how these relate to local network activity in the intact brain.

- **Chapter 4** aimed to explore how IP-derived and OP-derived L2/3 pyramidal neurons sample synaptic inputs from local interneurons . Firstly, this would require me to establish a novel dual-colour labelling method to target both IP-derived and OP-derived L2/3 neurons in transgenic mice. I would then be able to test whether IP-derived and OP-derived neurons receive different amounts of synaptic inhibition from PV, SST and VIP interneurons by performing dual patch-clamp recordings. Finally, I aimed to examine the degree to which IP-derived and OP-derived L2/3 neurons receive common inhibitory synaptic inputs, through a combination of spontaneous recordings and minimal stimulation optogenetic experiments.

- **Chapter 5** aimed to explore whether IP-derived and OP-derived L2/3 neurons receive differential feedback from L5 of S1, from S2 or from M1. This would be achieved by performing dual patch-clamp recordings from IP-derived and OP-derived L2/3 neurons and using optogenetic circuit mapping techniques to determine the monosynaptic excitatory and disynaptic inhibitory feedback

from different cortical areas.

2 | Materials and Methods

2.1 Experimental animals

Experiments were performed using both male and female mice, which were bred, housed, and used in accordance with the UK animals (Scientific Procedures) Act (1986). Animals were reared in a dedicated facility with a 12-hour light/dark cycle with access to food and water ad libitum. Unless stated, experiments were conducted in C57BL/6 wildtype mice. For optogenetic experiments, mice were the result of breeding crosses between a homozygous floxed ChR2 mouse (B6;129S-Gt(ROSA)26Sor$^{tm32(CAG-COP4*H134R/EYFP)Hze}$/J) and either a homozygous PV-Cre mouse (B6;129P2-Pvalb$^{tm1(cre)Arbr}$/J), a homozygous SST-Cre mouse (Sst$^{tm2.1(cre)Zjh}$/J), or a homozygous VIP-Cre mouse (Vip$^{tm1(cre)Zjh}$/J). Mice were purchased from The Jackson Laboratory (USA).

2.2 *In utero* electroporation

Females were paired for timed matings and checked daily for vaginal plugs. Embryonic day 0.5 (E0.5) was defined as midday on the day that the vaginal plug was detected. *In utero* electroporation was performed at E15.5 using standard procedures. Dams were induced and maintained under anaesthesia with isofluorane (Zoetis). Depth of anaesthesia was assessed by monitoring the animal's respiration rate and righting reflex. Surgery was performed under sterile conditions and dams were operated on a heating map to prevent loss of body temperature. Viscotears (Bausch and Lomb) was applied to protect the corneas during surgery. Meloxicam (5 mg/kg) (Boehringer Ingelheim Vetmedica Gmbh) and Buprenorphine (0.1 mg/kg) (Vetergesic Multidose, Alstoe Animal Health) analgesics were administered by subcutaneous injection. The abdomen was shaved and sterilized using Hibiscrub (Regent Medical). A midline laparotomy was performed and the uterine horns were

exposed. A mixture of plasmid DNA ($\sim$ 1 μg/μl) and 0.03 % fast green dye (Sigma-Aldrich) was injected intraventricularly in each embryo through the uterine wall and amniotic sac, with a glass micropipette (World Precision Instruments; outer diameter (OD): 1.5 mm, inner diameter (ID): 1.12 mm) that had been pulled using a Flaming/Brown Micropipette Puller (Sutter Instrument Company). Plasmids were prepared using an EndoFree plasmid kit (Qiagen). The total volume injected per embryo was $\sim$1.5 μL. All plasmids were injected as a 1:1 ratio.

Plasmid DNA included:

(i) "Tα1-Cre", in which Cre recombinase is under the control of a portion of the Tubulin alpha-1 (Tα1-Cre) promoter (Tα1-Cre was a gift from Tarik Haydar).

(ii) "Tα1-Flpo", in which codon optimized Flp recombinase is under the control of a portion of the Tubulin alpha-1 (Tα1-Cre) promoter. To generate Tα1-Flpo, Cre recombinase and its associated 3' poly(A) sequences were removed from Tα1-Cre using XhoI/SacI and replaced with Flpo recombinase and its associated poly(A) sequences from pCAG-Flpo (a gift from Massimo Scanziani Addgene plasmid 60662; http://n2t.net/addgene:60662; RRID;Addgene 60662). The Flpo sequence was amplified using Phusion DNA polymerase (New England Biolabs) and the primers "Flpo-XhoI-Fwr" (gagaagctcgaggccgccaccatggctcctaaga) and "Flpe-pATerm-SacI-Rev" (ctgaatgagctcgggctgcaggtcgagggatct). The PCR product was digested and ligated into the Tα1 backbone.

(iii) "FLEX-GFP", a single colour Cre-dependent reporter that uses the chicken β-actin (CAG) promoter to control a flexible excision (FLEx) cassette, whereby Cre recombination permanently turns on expression of enhanced green fluorescent protein (GFP). FLEX-GFP was a gift from Edward Boyden (Addgene plasmid 28304; http://n2t.net/addgene:28304; RRID:Addgene-28304).

(iv) "fDIO-tdTom/GFP", a dual colour Flp-dependent reporter that uses the human elongation factor-1a promoter (Ef1a) to express tandem Tomato (tdTomato), until Flp recombination permanently switches expression to GFP. To generate fDIO-tdTom/EGFP, Channelrhodopsin enahnced yellow fluorescent protein (ChR2-EYFP) was removed from the backbone vector pAAV-Ef1a-fDIO hChR2(H134R)-EYFP using AscI/NheI and replaced with tdTomato/EGFP from pAAV-Ef1a-DO-DIO-

TdTomato-EGFP-WPRE-pA digested using the same restriction enzymes. pAAV-Ef1a-fDIO hChR2(H134R)-EYFP was a gift from Karl Deisseroth (Addgene plasmid 55639, http://n2t.net/addgene:55639, RRID:Addgene55639). pAAV-Ef1a-DO-DIO-TdTomato-EGFP-WPRE-pA was a gift from Bernardo Sabatini (Addgene plasmid 37120; http://n2t.net/addgene:37120; RRID:Addgene37120).

(v) "Tbr2-Flpo", in which Flp recombinase is under the control of a portion of the T-box brain protein 2 (Tbr2) promoter. To generate Tbr2-Flpo, first pRV mTBr2(s)-GFP was generated in the retroviral backbone CAG-GFP. CAG-GFP was a gift from from Fred Gage (Addgene plasmid 16664; http://n2t.net/addgene:16664; RRID:Addgene16664). The CAG promoter was removed using restriction enzymes SalI/ AgeI and replaced with a 2.5kb fragment of the mouse Tbr2 promoter (Tyler et al., 2015). The promoter region was amplified from mouse cerebellum genomic DNA using Phusion High Fidelity DNA Polymerase (New England Biolabs) and the following primers: MuTbr2FwrS-Sal1: CTGCAGAAGTCGACTTTACTGAGGTGGGGTTCCAG, MuTbr2Rev-AgeI: TTCTGCAGACCGGTGCTTTAGCGAATCGCAGACG. The PCR product was gel purified, digested with the relevant enzymes and ligated into the vector backbone using the Mighty Mix Ligation Kit (Takara). Ligations were transformed into Max Efficiency Stb2 competent cells (Invitrogen). Confirmation of cloning was performed by restriction digest and sequencing of plasmid DNA. The GFP sequence was subsequently removed and replaced with a small multiple cloning site (MCS) containing sites AgeI, HindIII, StuI and BamHI inserted between the Tbr2 promoter and the improved Cre recombinase sequence (iCre) to generate pRV mTBr2(s)-iCre. iCre was amplified from pAAV-CAG-iCre (Addgene plasmid 51904; http://n2t.net/addgene:51904; RRID:Addgene51904). Subsequently, pRV mTbr2(s)-Flpo was generated by removing the iCre sequence using a BamHI/PmeI digest and replacing it with the Flpo sequence amplified from pCAG-Flpo (Addgene plasmid 60662) using the primers: BamHI-Flpo-Fwr: CTGCAGAAGGATTCGCCGCCACCATGGCTCCTAAGAAGAAGAGGA PmeI-Flpo-Rev: ATGACGTCGTTTAAACTCAGATCCGCCTGTTGATGTAG.

(vi) "pCAG-fDIO-TdTom", a single-colour Flpo-dependent reporter that uses the CAG promoter to control a flpo-dependent double-floxed inverted open-reading frame (fDIO), whereby Flpo expression permanently switches on the expression of

Tdtomato. pCAG-fDIO-TdTom was derived from pAAV-CAG-fDIO-mNeonGreen (Addgene plasmid 99133; http://n2t.net/addgene:99133; RRID:Addgene99133). The mNeonGreen sequence was removed using a AscI/NheI digest and replaced with a TdTomato sequence that was amplified from pCAG-mNaChBac-T2A-tdTomato (Addgene plasmid 60650; http://n2t.net/addgene:60650; RRID:Addgene60650). Phusion High Fidelity DNA Polymerase (New England Biolabs) and the following primers were used to amplify both fluorescent protein sequences: AscI-eGFPRev-Fwr: GAGAACGGCGCGCCTTACTTGTACAGCTCGTCCATGC, NheI-eGFPFwr-Rev: GAGACCGCTAGCGCCACCATGGTGAGCAAGG. The PCR products were gel purified, digested with the relevant enzymes and ligated into the vector backbone pAAV-CAG-fDIO using the Mighty Mix Ligation Kit (Takara). Ligations were transformed into Max Efficiency Stb2 competent cells (Invitrogen). Confirmation of cloning was performed by restriction digest and sequencing of plasmid DNA.

Electroporation was performed by placing the anode of the platinum Tweezertrodes (Genetronics) over the dorsal telencephalon. Five pulses (50 ms duration separated by 950 ms) at 40 V were delivered with a BTX ECM 830 square pulse generator (Genetronics). All accessible embryos underwent electroporation. The uterus was lavaged with warmed, sterile phosphate-buffered saline (PBS) and replaced into the abdomen. The abdominal muscle and skin incision were closed with Vicryl and Prolene (Ethicon) sutures, respectively. Animals were recovered from anaesthesia in a chamber heated to 38 °C. Meloxicam and Buprenorphine were provided orally during the postoperative window, as appropriate. Dams were allowed to litter down naturally, and the day of birth was recorded as postnatal day 0 (P0).

2.3 Postnatal viral injections

Animals that had undergone IUE were subsequently used for intracerebral injections at P28. Mice were anaesthetised with Isoflurane (Zoetis) and placed on a heating pad (Harvard Apparatus) within a stereotaxic frame (Kopf Instruments). Meloxicam (5 mg/kg) (Boehringer Ingelheim Vetmedica Gmbh), Buprenorphine (0.1 mg/kg) (Vetergesic Multidose, Alstoe Animal Health) and sodium chloride 0.9 % w/v with glucose monohydrate 5.5 % w/v (5 mg/kg) solutions were administered

subcutaneously. Viscotears (Bausch and Lomb) was applied to protect the corneas during surgery. The skin over the cranium was shaved and sterilized using Hibiscrub (Regent Medical). Marcain (0.25%, AstraZeneca) was administered subcutaneously to provide topical analgesia. A small midline incision was made to expose bregma and lambda on the skull. A small craniotomy (< 1 mm^2) was performed using a H.MH-170 pneumatic dentral drill (Foredom) to expose the pial surface. Craniotomies were targeted to either primary motor cortex (M1) (in mm: 1.7 lateral, 1.4 anterior to bregma) or secondary somatosensory cortex (S2) (in mm: 4.7 lateral, 0.8 posterior to bregma). Injection of an adeno-associated virus (AAV) carrying hSyn-ChR2(H134R)-EYFP in which ChR2-EYFP was under the control of the human synapsin promoter. pAAV-hSyn-hChR2(H134R)-EYFP was a gift from Karl Deisseroth (Addgene viral prep 26973-AAV5; http://n2t.net/addgene:26973 ; RRID:Addgene-26973). Injections were made over a period of 8 - 12 minutes at a volume of 132 - 198 nL per animal. Injections were made at 350 and 700 μm below the pial surface using a pulled glass micropipette (Blaubrand intraMARK). The craniotomy was covered and the scalp incision was subsequently closed with Vicryl (Ethicon) sutures. Further analgesia was provided as appropriate. Animals were used for *in vitro* electrophysiology 1 - 2 weeks following the viral injection. Post hoc histology was used to quantify the specificity of the viral injections.

2.4 *In vivo* patch-clamp electrophysiology

Animals (aged 4-6 weeks old) were anaesthetized and maintained with 0.8 - 1.5 % isoflurane for the duration of the recording. Depth of anaesthesia was assessed using breathing rate and toe pinch reflex. Animals were secured into the ear bars (Narishige), placed on a heat pad to maintain body temperature and Viscotears was applied to protect the corneas. The hair over the scalp was shaved and treated with hair removal cream (Veet). Craniotomies were performed under a stereoscope (Olympus) and were targeted over barrel cortex (coordinates: -1 mm AP, +3.5 mm ML, from bregma). An incision was made to expose the cranium and the surrounding skin was fixed with superglue (Loctite). Dental cement (Simplex Rapid) was used to build a chamber around the exposed skull, which could hold 1 - 2

drops of cortex buffer. Successive rounds of drilling were made using a dental drill (Foredom) to gently loosen the cranium, whilst the cranium was kept moist with cortex buffer, containing (in mM): 125 NaCl, 5 KCl, 10 HEPES, 2 $MgSO_4.7H_2O$, 2 $CaCl_2.2H_2O$, 10 Glucose. The skull and underlying dura were carefully removed with a 0.3 mL syringe needle. The brain was submerged with cortex buffer throughout the recording. A silver-chloride ground electrode (Multichannel systems) was placed on the skull anterior to the craniotomy.

The animal was transfered to an upright microscope (Olympus BX51WI) that had been customized for *in vivo* recordings. Pyramidal neurons in L2/3 of S1 were targeted using methods described previously (Jordan, 2021; Wang et al., 2016; Jouhanneau and Poulet, 2019; Margrie et al., 2002). Briefly, a cesium-based internal solution (containing, in mM: 126 $CsOH.H_20$, 126 gluconic acid, 10 HEPES, 5 TEA-Cl, 2 QX-314 Cl, 4 Mg_2ATP, 0.4, NaGTP, 10 Na Phosphocreatine, 2 EGTA, 0.2 % Biocytin, 0.02 Alexa594, pH 7.2 - 7.3, 290 - 295 mOsmol/L) was used to fill micropipettes with a tip resistance of 5-8 MΩ, pulled from borosilicate glass (Harvard Aparatus; OD: 1.5 mm, ID: 0.86 mm) using a vertical puller (Narishige). Positive pressure (800 mbar) was applied whilst the pipette was placed onto the surface of the brain and located using a 4x objective (Olympus PLN; NA: 0.1). Upon entering cortex by 80 μm, the positive pressure was reduced to 70 mbar and the pipette was advanced in 10 μm/s increments (up to a maximum depth of 350 μm) whilst looking for large changes in resistance, as an indicator of the close proximity of a cell membrane. At this point, the positive pressure was released to facilitate gigaseal formation and after approximately 1 minute in gigaseal, the whole-cell configuration was achieved by applying small suction pulses to the pipette. In addition to monitoring electrical signals, GFP-expressing neurons were targeted using a custom-built two-photon microscope, equipped with a 40 x water-immersion objective (Olympus LUMPLFLN, NA: 0.8), modified confocal scan unit (Olympus, FV300) and Ti:Sapphire laser (Newport Spectra-Physics Mai Tai HP; wavelength 850 nm, power 50 mW). The mean cell distance from pia was 111.59 ± 8.60 μm and did not differ between experimental conditions (two-tailed unpaired t-test, unlabeled neuron mean: 123.27 ± 14.11 μm, n = 11 neurons from 5 animals, IP-derived neuron mean: 99.91 ± 9.18 μm, n = 11 neurons from 5 animals, P = 0.18, df = 20, T = 1.39).

Inhibitory post-synaptic currents (IPSCs) were recorded in voltage clamp mode at a holding potential of +20 mV, close to the reversal potential of glutamate receptors. This led to the detection of outward synaptic currents, consistent with a strong driving force on the GABAA receptor (Haider et al., 2016). LFP recordings were made using a glass pipette that had been broken to a resistance of 0.5-1 MΩ. LFP pipettes were slowly inserted into the brain, to be in close proximity to the patch pipette. Electrophysiological data were acquired using a Multiclamp 700B amplifier (Molecular Devices) and digitizer (Digidata 1550, Molecular Devices), controlled by Clampex software (Molecular Devices). The LFP signal was band passed filtered at 0.1 - 200 Hz and then digitized at 10 kHz. Spontaneous IPSCs and LFP activity were recorded for 7.5 minutes. Every 15 s, a 10 mV hyperpolarizing pulse (100 ms duration) was applied to the command voltage of the patch pipette to monitor access resistance. Mean access resistance across all cells was 58.48 ± 4.23 MΩ. To account for the effects of access resistance, offline correction was performed (Traynelis, 1998). This involved multiplying the measured current response with 90 % of the access resistance, and then subtracting this from the command voltage to produce a corrected holding potential. Current traces were converted into inhibitory synaptic conductances by using the driving force calculated from the difference between the estimated chloride equilibrium potential (-73 mV) and the corrected holding potential.

Inhibitory synaptic inputs were detected using the first derivative of the conductance trace from the patched neuron. Firstly, conductance traces were median-subtracted, low-pass filtered at 100 Hz, and down-sampled to 4 kHz. Peaks in the first derivative were identified using a threshold-based method. Input start and input peak were defined as times at which the peak in the first derivative returned to 10 % of its peak value before and after its maximum, respectively. Input amplitudes were then calculated by subtracting the conductance value at the input start time from the conductance value at the input peak time. Input amplitude threshold was set at 40 pA to maximise the detection of action-potential-evoked inhibitory conductances (Safari et al., 2017; Xue et al., 2014; Yoshimura and Callaway, 2005).

LFP traces were median-subtracted and down-sampled to 4 kHz to match the conductance traces. The input-triggered LFP (IT-LFP) was calculated by averaging all

100 ms LFP epochs that were centred on the start time of the defined inhibitory synaptic inputs detected in the patched neuron. The peak of the IT-LFP was defined as the mean IT-LFP during the 10 ms following the onset of the inhibitory input. LFP events were identified by detecting peaks in the LFP recording that were at least 100 μV in amplitude and with a duration of 50 ms at 50 % peak height. An event time tiling coefficient (ETTC) was calculated from the LFP events and the inhibitory synaptic inputs/events using methods described previously (Chini et al., 2022; Cutts and Eglen, 2014; Yang et al., 2021). Briefly, this measure calculates the proportion of coincident events between two traces (traces A and B) that occur above chance level, by calculating the proportion of events in trace A that fall within a short temporal window (± dt) of events in trace B. I used a dt of 25 ms for my analysis. To account for events that are expected to co-occur by chance, the proportion of trace A that occurs within ± dt windows from events in trace A is subtracted. The measure is then calculated reciprocally for trace B with respect to events in trace A. This generates a coefficient that reflects trace A's relationship to trace B, and a coefficient that reflects trace B's relationship to trace A. The mean of the two coefficients is the ETTC, and therefore represents a bi-directional measure of synchrony.

2.5 *In vitro* patch-clamp electrophysiology

Acute cortical slices were prepared from primary somatosensory cortex (S1). Animals (aged 3 - 6 weeks old) were anaesthetized with isoflurane and then decapitated. Coronal 350 μm slices were cut using a vibrating microtome (Microm HM650V). Slices were prepared in artificial cerebrospinal fluid (aCSF) containing (in mM): 65 Sucrose, 85 NaCl, 2.5 KCl, 1.25 NaH_2PO_4, 7 $MgCl_2$, 0.5 $CaCl_2$, 25 $NaHCO_3$ and 10 glucose, pH 7.2 - 7.4, bubbled with carbogen gas (95% O2 / 5% CO2). Slices were immediately transferred to a storage chamber containing aCSF (in mM): 130 NaCl, 3.5 KCl, 1.2 NaH_2PO_4, 2 $MgCl_2$, 2 $CaCl_2$, 24 $NaHCO_3$ and 10 glucose, pH 7.2-7.4 and bubbled with carbogen gas for 1 hour at 35 °C. When required, slices were transferred to the glass coverslip that formed the bottom of the recording chamber, and continuously perfused with aCSF bubbled with carbogen gas (perfusion speed

3 ml/min).

Whole-cell patch-clamp recordings were performed using glass pipettes (4-6 MΩ), pulled from standard wall borosilicate glass capillaries (Harvard Apparatus; OD: 1.2 mm ID: 0.69 mm) and containing (in mM): 126 CsOH.H_20, 126 Gluconic acid, 10 HEPES, 1.5 $MgCl_2.6H_20$, 2 QX-314 Cl, 4 Mg_2ATP, 0.4 NaGTP, 10 Na Phosphocreatine, 2 EGTA, (pH 7.2 - 7.3, osmolarity, 290 - 295 mOsmol/l) and 0.25 mg/ml biocytin. Pairs of neighboring L2/3 pyramidal neurons approximately 40 μm below the surface of the slice were visualized for simultaneous patch-clamp recording under an upright microscope (Olympus BX51WI) equipped with a 20 x water-immersion objective (Olympus XLUMPLFLN; 1.0 NA), dodt gradient contrast, and epifluorescence illumination. IP-derived and OP-derived L2/3 pyramidal neurons were identified using epifluorescence and appropriate filter sets for separating GFP and TdTomato signals.

In vitro electrophysiological data were acquired using a Multiclamp 700A amplifier (Molecular Devices) and digitizer (ITC-18, Instrutech), controlled by WinWCP software (University of Strathclyde, UK, RRID:SCR014713). Access resistance was measured during every sweep on all experimental protocols using a hyperpolarizing pulse (10 mV, 100 ms duration), and only recordings where access resistance was less than 30 MΩ were included. Access resistance did not systemically vary between any of the experimental groups. To detect spontaneous action-potential-evoked IPSCs (sIPSCs), 7.5 minutes of spontaneous activity was recorded whilst holding each neuron at 0 mV, at the reversal potential of glutamate receptors under these recording conditions. sIPSCs were observed as large outward currents and were identified using the same detection method described for *in vivo* inhibitory conductances (see above). Traces were low-pass filtered at 100 Hz and down-sampled to 4 kHz. To maximize the detection of action-potential-evoked IPSCs, an amplitude threshold of 40 pA was applied, which was selected based on reported values of unitary IPSCs (Safari et al., 2017; Xue et al., 2014; Yoshimura and Callaway, 2005).

For widefield optogenetic stimulation of ChR2-expressing interneurons and ChR2-expressing axons from L5, from S2 and from M1, blue light pulses (473 nm, 1 ms or 500 μs duration, 0.05 Hz) were delivered via a high-power light emitting diode (LED;

Luxeon Star, Farnell) positioned below the recording chamber, so as to illuminate the entire brain slice. Light intensity recorded at the tissue surface closest to the LED was 10-40 mW/mm^2. A different optical setup was used to activate putative single ChR2-expressing PV interneurons, which involved delivering a spot of blue light to the upper surface of the brain slice (40 μm diameter at the slice surface, 1 ms duration, 0.05 Hz) from a diode-pumped solid-state laser (473 nm peak wavelength; Shanghai Laser and Optics Century). The laser was coupled to a 200 μm diameter multimode optic fiber via a collimating lens (Thorlabs), the tip of the optic fiber was positioned at an image plane in the center of the microscope's optical axis, and the light was directed into the objective (Olympus XLUMPLFLN; 20 x, 1.0 NA) via a dichroic mirror. In line with previous work that has used minimal optogenetic stimulation to reveal shared connections (Morgenstern et al., 2016), the intensity of the light spot was adjusted (0.3 - 4.2 mW/mm^2) to a regime where we observed post-synaptic IPSC successes and failures, analogous to electrical minimal stimulation conditions. When separate PV interneurons were stimulated for the same pair of pyramidal neurons, the stimulation sites were on average 611.01 $\pm$ 90.62 μm apart. If the axon of the stimulated PV interneuron connected with similar probability and strength to the two post-synaptic pyramidal neurons, the optically-evoked IPSCs would be expected to co-fluctuate across stimulations, exhibiting similar probability and amplitude on a trial-to-trial basis.

2.6 Histology

Following *in vivo* electrophysiology, animals were fixed by cardiac perfusion with 4 % PFA (Sigma Aldrich) in 0.1 M PBS (pH 7.4) and then left in PFA for an additional 24-48 hours. Fixed brains were then sectioned at 100 μm on a vibratome (Microm). Following *in vitro* electrophysiology, slices were fixed in 4 % PFA in 0.1 M PBS (pH 7.4) for 24 hours then transferred to 0.1 M PBS. To visualize biocytin-filled neurons, sections were incubated in streptavidin Alexa Fluor 647 (1:1000, Thermo Fisher) for 2 hours at room temperature. Sections were then stained with 4',6- Diamidino-2-Phenylindole, Dihydrochloride (DAPI, 1:10,000, Thermo Fisher). Three PBS washes were performed in between each step. Sections were then mounted with Vectashield

(Vectorlabs) onto glass slides (Avantor) and sealed. Images were acquired with an LSM 710 confocal microscope using ZEN software (Zeiss).

2.7 Statistical analysis

Data were assessed for normality and appropriate parametric (1 sample t-test, paired t-test or unpaired t-test) or non-parametric (Wilcoxon signed rank test, Mann-Whitney U test) statistical tests were applied. For tests that had more than 2 groups, either a one-way ANOVA (parametric data) or Kruskal Wallis (non-parametric data) was used to test for differences between groups. If differences were detected, Bonferroni's correction was used to adjust P values for multiple comparisons. Statistically significant differences are indicated with asterisks on graphs as * $P < 0.05$, ** $P < 0.01$, *** $P < 0.001$. Analysis was carried out using custom written scripts in Python 3.7. Data are presented as mean ± sem unless otherwise stated.

Statistics were not adjusted for inter-animal variation, however, care was taken to collect each dataset from multiple animals and litters. The distribution of cells collected per animal are displayed in **Table 2.1** below.

Dataset		Number of cells from single animal											Total N
		1	2	3	4	5	6	7	8	9	10	11	
		Frequency											
Fig 3.5	IP-derived		4	1									11
	Unlabelled	3		1		1							11
Fig 4.3	PV	2	3	3									17
	SST	4	5		2								22
	VIP	1		6	1								23
Fig 4.6	IP-OP	3	4	2	1								21
	Unlabelled	10	3	1	2								27
	OP-OP	10	6	3									31
	IP-IP	6	4	1									17
Fig 4.7	IP-OP	1	1		1	1		1				1	30
	Unlabelled	2		2		1							13
Fig 5.2	L5 - EPSC		3	4	1								22
	L5 - IPSC		5		3								22
Fig 5.4	S2 - EPSC	3	1										5
	S2 - IPSC	3	1										5
Fig 5.6	M1 - EPSC	4	1		2								14
	M1 - IPSC	5	1										7

Table 2.1: Distribution of cells collected across animals. The distribution of how data was collected across multiple animals shown for each main dataset in this thesis. Each dataset is shown as a distribution of frequencies. For instance, in Figure 3.5 the IP-derived dataset consisted of 2 cells collected from a single animal on 4 occasions and 3 cells collected from a single animal on 1 occasion.

3 | Progenitor type predicts a L2/3 pyramidal neuron's inhibitory synaptic activity *in vivo*

3.1 Introduction

Cortical circuits are comprised of synaptically connected excitatory pyramidal and inhibitory interneuron cell types. The precise synaptic connectivity within and between these cell types determines how information is integrated and processed by cortical circuits (Douglas and Martin, 2004; Harris and Mrsic-Flogel, 2013; Harris and Shepherd, 2015). A fundamental question in neuroscience is how this precise synaptic circuitry is established during development.

In L2/3 of cortex, sparse connections between excitatory pyramidal neurons form highly specific excitatory subnetworks which shape the information flow through cortical circuits (Brown and Hestrin, 2009; Kim et al., 2018; Otsuka and Kawaguchi, 2011; Lefort et al., 2009; Ko et al., 2011; Yoshimura et al., 2005; Kampa et al., 2006). This excitation is balanced by strong inhibitory input to L2/3 pyramidal neurons, which tends to maintain the membrane potential of the pyramidal neuron below action potential threshold, and therefore generates low firing rates *in vivo* (Haider et al., 2013; Mateo et al., 2011; Ranjbar-Slamloo and Arabzadeh, 2019; O'Connor et al., 2010; de Kock et al., 2007; Crochet et al., 2011). It is estimated that over 90% of monosynaptic inhibition to L2/3 pyramidal neurons is provided through PV and SST interneurons (Safari et al., 2017), with the remaining types of interneurons primarily influencing pyramidal neurons through disinhibitory connections or network-wide changes in excitability (Hioki et al., 2013; Jiang et al., 2013, 2015; Oláh et al., 2009; Pfeffer et al., 2013). PV interneurons primarily provide fast, feedforward inhibition to a neuron's soma, shaping their spatio-temporal response properties to

incoming stimuli (Galarreta and Hestrin, 2001; Hang and Dan, 2011; Jang et al., 2020; Wehr and Zador, 2003; Wilent and Contreras, 2005). SST interneurons, on the other hand, provide feedback inhibition to pyramidal neuron dendrites, having a major role in gating dendritic excitability (Silberberg and Markram, 2007; Urban-Ciecko and Barth, 2016; Wang et al., 2004; Williams and Holtmaat, 2019). Taken together, inhibition plays a crucial role in controlling the timing of action potential generation in L2/3 subnetworks, with implications for the receptive field properties, plasticity and output correlations in cortical networks (Galarreta and Hestrin, 2001; Holmgren et al., 2003; Isaacson and Scanziani, 2011; Jang et al., 2020; Khan et al., 2018; Stringer et al., 2016; Williams and Holtmaat, 2019).

The discovery of very high connection rates between interneurons and nearby pyramidal neurons has led to the theory that, as opposed to specificity in the wiring of excitatory subnetworks, there is a non-specific 'blanket' of synaptic inhibition (Fino and Yuste, 2011; Packer and Yuste, 2011; Pfeffer et al., 2013). One of the pieces of evidence seen as supporting this theory is that the probability of shared inhibitory input from a single PV or SST to a pyramidal neuron pair does not depend on whether the pyramidal neurons are themselves synaptically connected (Fino and Yuste, 2011; Packer and Yuste, 2011; Yoshimura et al., 2005). Interestingly however, a range of evidence now supports the organisation of inhibitory connectivity into functional subnetworks (D'Souza et al., 2019; Jézéquel et al., 2023; Karnani et al., 2016; Kätzel et al., 2010; Najafi et al., 2020; Otsuka and Kawaguchi, 2011; Palagina et al., 2019; Yoshimura and Callaway, 2005; Znamenskiy et al., 2018). Therefore, whilst inhibitory connections may not directly reciprocate the wiring rules of local pyramidal neurons, inhibitory subnetworks act to direct information flow in specific ways through cortical circuits. This means that each pyramidal neuron may receive inhibitory inputs from a specific, or restricted, pool of inhibitory neurons, which will determine the pyramidal neuron's activity within the circuit. The mechanism through which these inhibitory subnetworks are established is unknown.

An expanding body of research has highlighted the contribution of developmental history to a neuron's identity and synaptic connectivity (Buchan et al., 2022; Cadwell et al., 2020; Cavalieri et al., 2021; Ellender et al., 2019; Guillamon-Vivancos et al., 2019; Huilgol et al., 2023a; Li et al., 2012; Ohtsuki et al., 2012; Save et al., 2019; Tyler

et al., 2015; Xu et al., 2014; Yu et al., 2009). For example, cortical L2/3 neurons derived from IPs exhibit biases in their local excitatory connectivity such as preferred synaptic output to L5a over L5b (Ellender et al., 2019). Other evidence has shown that the morphology and intrinsic properties of L2/3 pyramidal neurons can differ based on the progenitor type from which they are derived (Tyler et al., 2015). These studies have exclusively focused on excitatory connectivity and have not explored whether excitatory neurons derived from specific progenitor types receive different inhibitory connectivity. Therefore, the ways in which progenitor type may influence the inhibition received by cortical pyramidal neurons is unknown.

This chapter will characterise the inhibition received by L2/3 pyramidal neurons *in vivo* based upon the progenitor type from which the pyramidal neuron is derived. This chapter has the following three aims:

- To outline a labelling strategy to target L2/3 pyramidal neurons derived from intermediate progenitors
- To validate analysis methods for measuring synaptic inhibition and local field potentials *in vivo*
- To assess whether progenitor type predicts a L2/3 pyramidal neuron's inhibitory synaptic activity *in vivo*

3.2 Results

3.2.1 Labelling strategy to target neurons derived from intermediate progenitors

Mouse cortical excitatory neurons and inhibitory interneurons are born from separate pools of embryonic progenitors in the pallium and subpallium, respectively. Thereafter, they migrate to meet in the cortical plate where they form synaptic circuits over the course of development (Anderson et al., 2002; Anthony et al., 2004; Nery et al., 2002; Rakic, 1988; Wichterle et al., 2001) (**Figure 3.1a-b**). To target pallial progenitor cells that are giving rise to L2/3 pyramidal neurons, excitatory neuron *in utero* electroporation (IUE) was performed in C57BL/6 mice at embryonic day 15.5 (E15.5) (Langevin et al., 2007) (**Figure 3.1c**). Consistent with previous work, the tubulin alpha1 (Tα1) promoter was used to label a subset of L2/3 pyramidal neurons derived from a population of intermediate progenitors (IPs) (Ellender et al., 2019; Gal et al., 2006; Mizutani et al., 2007; Stancik et al., 2010). This labeling strategy used Cre recombinase downstream of the Tα1 promoter to permanently turn on expression of GFP from a reporter construct (**Figure 3.1c**). The region corresponding to barrel cortex (S1) was targeted, such that 24 hours after IUE, GFP-expressing IPs and newly born neurons derived from IPs ('IP-derived') were observed in the germinal zone (**Figure 3.1d**). When the mice reached 4 weeks of age, GFP-expressing IP-derived pyramidal neurons were observed in mature S1 at pial depths corresponding to L2/3 (average pial depth: 233.28 $\pm$ 8.43 μm; **Figure 3.1d**). These results demonstrate an effective labelling strategy, enabling the precise targeting of neurons originating from specific progenitor types within the postnatal brain.

3.2.2 Establishing methods for relating a L2/3 pyramidal neuron's synaptic inhibition to local network activity

In order to investigate the inhibitory synaptic input to IP-derived neurons, it was first necessary to establish a method for measuring synaptic inhibition *in vivo*. Two-photon targeted whole-cell patch-clamp recordings of inhibitory synaptic conduc-

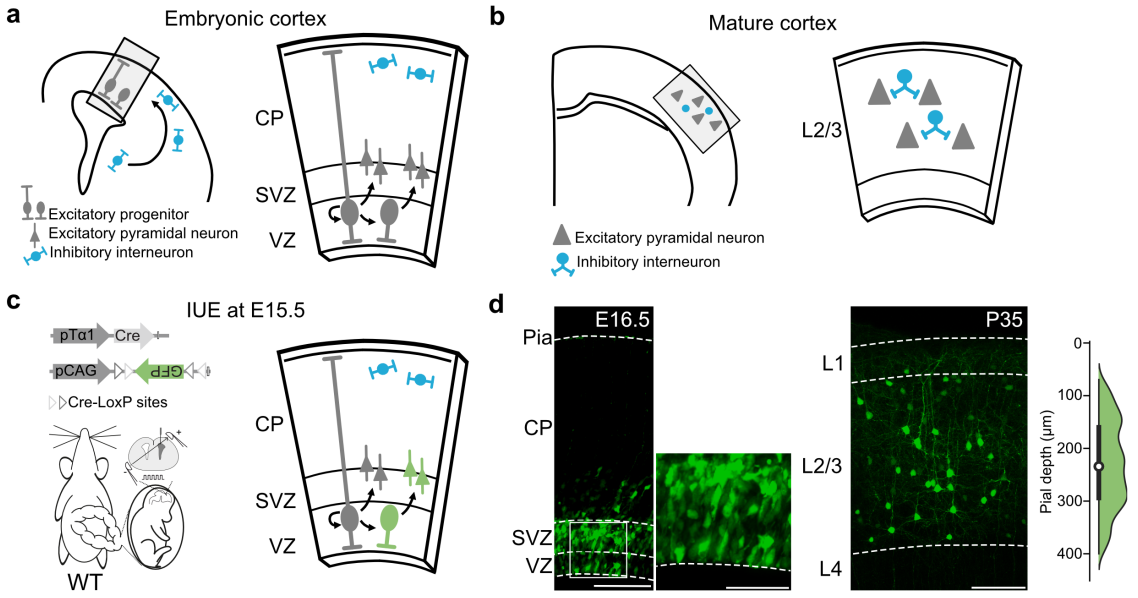


Figure 3.1: Labelling strategy to target neurons derived from intermediate progenitors. (**a**) Schematics of embryonic cortex, showing excitatory neurons (grey) and inhibitory interneurons (blue) born from separate progenitor pools in the pallium and subpallium, respectively, migrating to meet and form synaptic networks in the cortical plate. (**b**) Schematics of mature cortex, where neighboring pyramidal neurons receive inhibitory input from interneurons to generate inhibitory subnetworks. (**c**) Excitatory neuron *in utero* electroporation (IUE) of Tα1-Cre and FLEX-GFP was used to label IP-derived L2/3 pyramidal neurons in S1. (**d**) GFP-expressing IPs and newly born IP-derived neurons were observed 24 hours after IUE (left). Scale bar 100 μm, 50 μm for inset. At P35, IP-derived pyramidal neurons were distributed throughout L2/3 (right). Pial depth is shown as a kernel density estimate alongside mean $\pm$ standard deviation. Scale bar 100 μm.

tances were performed from IP-derived neurons and compared to separate recordings from unlabeled L2/3 pyramidal neurons, which were therefore not derived from a defined progenitor type (**Figure 3.2a-b**). Patch-clamp recordings were performed under light isoflurane anaesthesia and combined with simultaneous local field potential (LFP) recordings to be able to relate the neuron's synaptic inhibition to local network activity (Haider et al., 2016).

To compare the synaptic inhibition received by unlabeled and IP-derived neurons, an accurate input detection method is required to identify individual inhibitory synaptic inputs in an automated manner. Existing methods can suffer from issues relating to the accurate detection of inputs, the correct determination of input times, and difficulties in terms of integrating the methods into existing analysis pipelines. For these reasons, I developed my own input detection method using Python, the

validation for which is outlined in **Figure 3.2**. This input detection method uses the first differential of the synaptic input trace ('d(g_{inh})/dt') to identify where synaptic inputs occur ('Differential method'; **Figure 3.2c**). Peaks in the first differential of the trace were identified using a basic peak detection method in Python. Next, the intersection point where the peak returns to 10 % of its maximum value were identified either side of the peak. These were used to determine the start and maximum of the synaptic input (**Figure 3.2c**). The amplitude of the peak is taken as the difference in conductance between the maximum conductance and the start conductance. This method enables an accurate read-out of both the start time and amplitude of the synaptic input, which is crucial for analysis involving correlations.

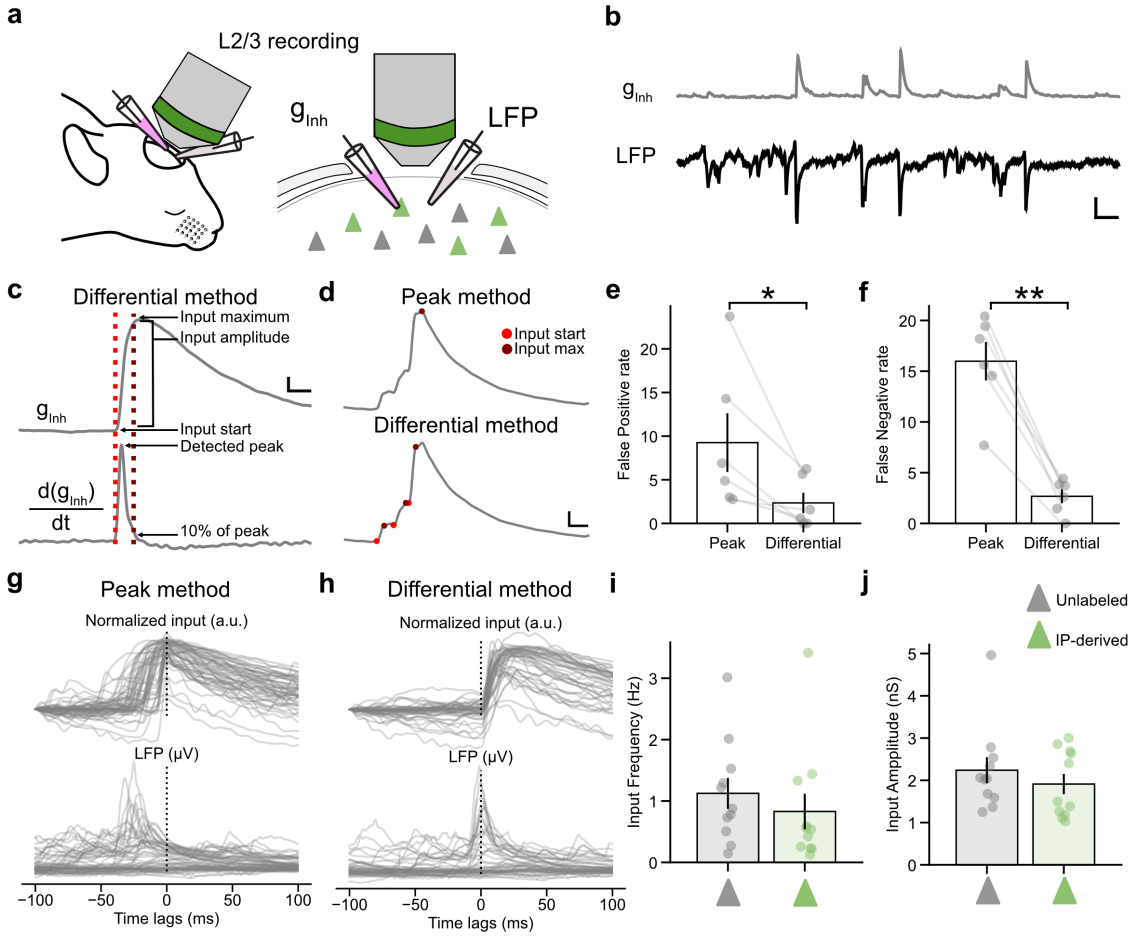


Figure 3.2: Synaptic input detection method for accurately measuring synaptic inhibition (**a**) At P28-42, animals underwent *in vivo* electrophysiology that combined simultaneous whole-cell patch-clamp recordings of inhibitory synaptic conductances (g_{Inh}) and the local field potential (LFP). (**b**) Example simultaneous recordings of inhibitory synaptic inputs and the LFP. Scale bar, 2 nS, 200 μV, 250ms. (**c**) Input detection was performed using the first differential ($d(g_{Inh})/dt$) of the inhibitory synaptic conductance (g_{Inh}). Peaks were detected in the first differential and then each input start time and maximum was inferred from where the peak returned to 10 % of its value either side of the peak. Scale bar 2 nS, 25 ms. (**d**) Example input demonstrating how a standard peak detection method fails to identify multiple synaptic inputs in rapid succession (top). In contrast, the differential method correctly identifies each separate peak (bottom). Scale bar 2 nS, 25 ms. (**e**) False positive detection rates were significantly reduced when using the Differential method compared to the Peak method (two-tailed paired t-test, n = 6 neurons from 4 animals, P = 0.038, T = 2.80).(**f**) False negative rate was significantly reduced when using the Differential method compared to the Peak method (two-tailed paired t-test, n = 6 neurons from 4 animals, P = 0.00035, T = 8.58). (**g**) Example of a neuron's synaptic inputs detected via the Peak method, aligned by their peak max (top). The corresponding LFP trace for these synaptic inputs is shown below. (**h**) Example of a neuron's synaptic inputs detected via the Differential method, aligned by the input start time (top). The corresponding LFP trace for these synaptic inputs is shown below. (**i**) Inhibitory input frequency did not differ between unlabeled and IP-derived neurons (two-tailed Mann-Whitney U test, unlabeled n = 11 neurons from 5 animals, IP-derived n = 11 neurons from 5 animals, P = 0.21, U = 80). (**j**) Inhibitory input amplitude did not differ between unlabeled and IP-derived neurons (two-tailed Mann-Whitney U test, unlabeled n = 11 neurons from 5 animals, IP-derived n = 11 neurons from 5 animals, P = 0.55, U = 70).

This Differential detection method can be compared to a more basic approach, such as simply finding peaks in the synaptic input trace ('Peak method'; **Figure 3.2d**). Inhibitory synaptic inputs often occur in quick succession and their relatively slow decay times means that it is common to see temporally overlapping inputs. In the example in **Figure 3.2d**, the simpler Peak method only identifies these as one synaptic input, and therefore incorrectly assigns the amplitude to be the sum of all 3 inputs. The Differential method, however, identifies 3 separate synaptic inputs with accurate start and maximum times, giving the correct amplitude of each synaptic input.

Accordingly, to quantify the effectiveness of the Differential method compared to the Peak method, manual validation was performed on a total of approximately 600 seconds of inhibitory conductance recording time from 6 different neurons. False positive and false negative rates were taken as a fraction of the total number of true inputs detected. The Differential method detected significantly less false positives (two-tailed paired t-test, Peak method mean: 9.25 $\pm$ 3.69 %, Differential method

mean: 2.35 ± 1.28 %, n = 6 neurons from 4 animals, P = 0.038, T = 2.80; **Figure 3.2e**) and false negatives (two-tailed paired t-test, Peak method mean: 15.98 ± 2.07 %, Differential method mean: 2.67 ± 0.75 %, n = 6 neurons from 4 animals, P = 0.00035, T = 8.58; **Figure 3.2f**) than the Peak method. This demonstrates that the Differential method is significantly more accurate at detecting synaptic inputs.

Another important point of comparison between the Differential and Peak detection methods is their accuracy in determining the timing of synaptic inputs. In the Peak method, inputs are detected by their maximum (**Figure 3.2g**, top). The presence of false positives and varying rise-times in these detected inputs creates a large amount of jitter in the input start times when the inputs are aligned by their peak, as seen in **Figure 3.2g** (top). This impacts measures of correlation with the LFP (or any other simultaneously recorded trace), as it creates variability in the alignment of the input-triggered LFP (IT-LFP) (**Figure 3.2g**, bottom). Alternatively, using the Differential method on the same example trace accurately detects and aligns inputs by their start times, which removes the majority of this jitter (**Figure 3.2h**, top). Consequently, the jitter in the IT-LFP is considerably reduced (**Figure 3.2h**, bottom).

Given the effectiveness of the Differential input detection method, this method was used for inhibitory input detection in unlabeled and IP-derived neurons. Inhibitory synaptic inputs were measured and compared in unlabeled and IP-derived neurons. Consistent with previous evidence that L2/3 pyramidal neurons are under strong inhibitory synaptic control *in vivo*, robust inhibitory synaptic conductances were identified in all of the recorded neurons (Haider et al., 2016). No differences in mean inhibitory input frequency or amplitude were found between unlabeled and IP-derived neurons (two-tailed Mann-Whitney U test, unlabeled frequency mean: 1.13 ± 0.25 Hz, IP-derived frequency mean: 0.83 ± 0.29 Hz, P = 0.21, U = 80, **Figure 3.2i**) (two-tailed Mann-Whitney U test, unlabeled amplitude mean: 2.24 ± 0.31 nS, IP-derived amplitude mean: 1.91 ± 0.24 nS, P = 0.55, U = 70; **Figure 3.2j**). Taken together, these results demonstrate an effective method for accurately detecting synaptic inputs and show that unlabeled and IP-derived L2/3 pyramidal neurons receive comparable levels of spontaneous synaptic inhibition *in vivo*.

3.2.3 LFP reflects local network activity and can be used as a coupling measure

The LFP represents a widely used tool for sampling local network activity (Buzsáki et al., 2012; Deweese and Zador, 2004; Katzner et al., 2009; Okun et al., 2010; Okun and Lampl, 2008; Poulet and Petersen, 2008; Taub et al., 2015). Indeed, the LFP is a relatively easy and accessible recording method and has previously been used when examining the relationship between synaptic inhibition and local network activity (Atallah and Scanziani, 2009; Haider et al., 2006; Hasenstaub et al., 2005; Haider et al., 2016). Specifically, research supports that activity in the LFP primarily reflects local excitatory synaptic potentials, more so than action potentials or intrinsic membrane currents (Buzsáki and Wang, 2012; Einevoll et al., 2013; Taub et al., 2015).

To ensure the LFP was an effective and appropriate method to measure synaptic coupling, I performed a series of experiments to validate the LFP as a coupling measure for my analysis. Firstly, I tested whether my LFP recordings reflected local synaptic activity. LFP recordings were performed *in vivo* before and after an injection of the AMPA receptor blocker, NBQX (**Figure 3.3a-b**). Sharp deflections in the LFP, reflecting local synaptic potentials, were blocked following a local NBQX injection (see example traces in **Figure 3.3b**). A simple event detection was performed on these synaptic potentials, such that events that were 100 μV in amplitude and less than 100 ms in duration were detected. The frequency of these events was significantly reduced following NBQX injection (two-tailed Wilcoxon test, pre-NBQX mean: 1.22 $\pm$ 0.41 Hz, post-NBQX mean: 0.04 $\pm$ 0.01 Hz, n = 7 recordings from 7 animals, P = 0.016, W = 0; **Figure 3.3c**). This demonstrates that the LFP can be used to sample local synaptic activity, and a simple event detection method can be used to measure the activity of the local network.

Secondly, to validate the LFP as a genuine readout of local network activity, it was important to establish that the degree to which the LFP and synaptic inputs are coupled to one another is affected by distance. I therefore performed simultaneous LFP and whole-cell patch clamp recordings at different distances of separation. Initially, the LFP and whole-cell patch clamp recordings were performed from the

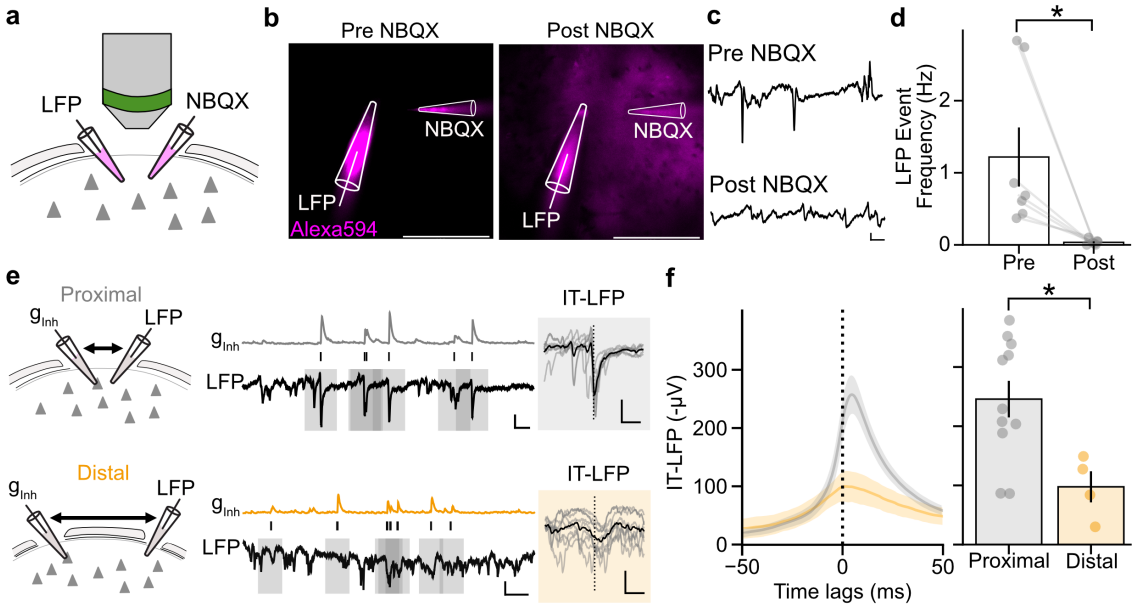


Figure 3.3: LFP reflects local synaptic activity and can be used as a coupling measure. (**a**) LFP was recorded before and after a local injection of the AMPA receptor antagonist NBQX *in vivo*. (**b**) Alexa594 was added to the NBQX pipette such that successful NBQX injection was confirmed through visualisation of Alexa594 in the extracellular space. Image scale bar 50 μm. (**c**) Example traces showing sharp deflections in LFP activity, reflecting nearby synaptic potentials that were blocked by NBQX. Scale bar 50 μV, 250ms. (**d**) LFP event frequency was significantly reduced following NBQX injection (two-tailed Wilcoxon test, n = 7 recordings from 7 animals, P = 0.016, W = 0). (**e**) Simultaneous LFP and whole-cell patch clamp recordings were performed proximally to one another, under 500 μm apart. LFP and g_{Inh} were tightly correlated on a millisecond timescale, reflected in the large input-triggered LFP (IT-LFP) (top). Scale bar 2 nS, 200 μV, 250 ms, IT-LFP scale bar 200 μV, 100 ms. Recordings were also performed distally, where the LFP and patch pipette were in separate craniotomies separated by more than 1 mm. LFP and g_{Inh} were less tightly coupled, reflected in the smaller IT-LFP (bottom). Scale bar 2 nS, 200 μV, 250 ms, IT-LFP scale bar 200 μV, 100 ms. (**f**) IT-LFP was significantly larger in proximal recordings than distal recordings (two-tailed unpaired t-test, proximal n = 11 neurons from 5 animals, distal n = 4 neurons from 3 animals, P = 0.017, T = 2.73).

same craniotomy and therefore with minimal separation (**Figure 3.3d**). Under these conditions the inhibitory synaptic inputs were typically associated with events in the LFP, consistent with periods of local network activity (Haider et al., 2016; Okun et al., 2010, 2015). To capture this relationship, I applied a measure of population coupling that has previously been used to relate an individual neuron's activity to the LFP (Okun et al., 2010, 2015). For each neuron, the onset times of every inhibitory synaptic input was identified via automated detection and these onset times were used to extract the periods of LFP trace which surround each inhibitory input. By averaging these LFP windows across all of the inhibitory inputs, it was possible to define an input-triggered LFP (IT-LFP; **Figure 3.3e-f**), which reflected the average local network activity during any given inhibitory synaptic input received by the recorded neuron. The peak IT-LFP was defined as the mean of the IT-LFP during the 10 ms following the onset of the inhibitory input. The IT-LFP measure can be used to quantify the degree of coupling between the inhibitory synaptic inputs of the neuron and the LFP. This measure reflects the synchrony of individual synaptics inputs with the local population of neurons (Okun et al., 2010, 2015; Shepherd et al., 2015). To validate the IT-LFP as a coupling measure, I conducted a separate set of simultaneous recordings that had a much greater separation distance, where the LFP and patch pipette were performed from separate craniotomies that were over 1 mm apart (**Figure 3.3e**). Consistent with the coupling reflecting distance, the IT-LFP for the proximal recordings was significantly larger than that for the distal recordings (two-tailed unpaired t-test, proximal mean: 246.27 ± 31.00 μV, n = 11 neurons from 5 animals, distal mean: 97.79 ± 26.30 μV, n = 4 neurons from 3 animals, P = 0.017, T = 2.73; **Figure 3.3f**). This confirms that the LFP is more strongly correlated with proximal synaptic activity and therefore validates IT-LFP as a measure of local coupling.

Finally, to be able to compare IT-LFP between unlabeled and IP-derived neurons, the LFP recordings should be comparable between the two conditions, such that any differences detected could be attributed to the identity of the neurons, not to any differences in LFP activity. In support of this, there were no differences in the distribution of LFP values, measured by their inter-quartile range (IQR), between unlabeled and IP-derived recordings (two-tailed Mann-Whitney U test, unlabeled

mean: 78.11 ± 6.2, n = 11 recordings from 5 animals, IP-derived mean: 70.77 ± 4.63, n = 11 recordings from 5 animals, P = 0.36, U = 75; **Figure 3.4a-b**). Additionally, LFP event frequency and amplitude did not differ between unlabeled and IP-derived recordings (two-tailed unpaired t-test, unlabeled mean frequency: 1.57 ± 0.24 Hz, n = 11 neurons from 5 animals, IP-derived mean frequency: 1.58 ± 0.22 Hz, n = 11 neurons from 5 animals, P = 0.95, T = -0.045; **Figure 3.4c**) (two-tailed unpaired t-test, unlabeled mean amplitude: 319.30 ± 16.41 μV, n = 11 neurons from 5 animals, IP-derived mean amplitude: 305.17 ± 14.80 μV, n = 11 neurons from 5 animals, P = 0.53, T = 0.64; **Figure 3.4d**). These results ensure that the LFP recordings were comparable across conditions.

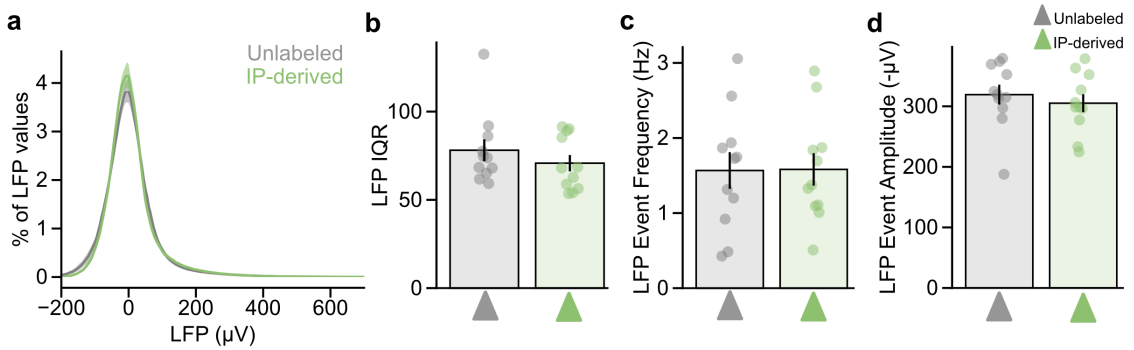


Figure 3.4: LFP activity does not differ between unlabeled and IP-derived recordings. (**a**) Distribution of LFP values for unlabeled and IP-derived recordings. (**b**) The interquartile range (IQR) for LFP values did not differ between unlabeled and IP-derived recordings (two-tailed Mann-Whitney U test, n = 11 unlabeled recordings from 5 animals, n = 11 IP-derived recordings from 5 animals, P = 0.36, U = 75). (**c**) LFP event frequency did not differ between unlabeled and IP-derived recordings (two-tailed unpaired t-test, n = 11 unlabeled recordings from 5 animals, n = 11 IP-derived recordings from 5 animals, P = 0.95, T = -0.045). (**d**) LFP event amplitude did not differ between unlabeled and IP-derived recordings (two-tailed unpaired t-test, n = 11 unlabeled recordings from 5 animals, n = 11 IP-derived recordings from 5 animals, P = 0.53, T = 0.64).

3.2.4 Progenitor type predicts a L2/3 pyramidal neuron's inhibitory synaptic activity *in vivo*

To investigate whether progenitor type influences a L2/3 pyramidal neuron's synaptic inhibition, *in vivo* two-photon targeted whole-cell patch-clamp recordings of inhibitory synaptic conductances were performed from IP-derived neurons (**Figure 3.5a**). GFP-expressing IP-derived L2/3 neurons were targeted for whole-cell patch-clamp recordings under two-photon microscopy and compared to separate record-

ings from unlabeled L2/3 pyramidal neurons. In a subset of recordings, neurons were filled with biocytin and visualised post-hoc to confirm their pyramidal identity (**Figure 3.5b**). Patch-clamp recordings were performed with simultaneous local field potential (LFP) and the coupling of the inhibitory synaptic inputs with the LFP was measured using the IT-LFP (described in **3.2.3**). In unlabeled neurons, inhibitory synaptic inputs were frequently coupled with large events in the LFP (**Figure 3.5c**). In contrast, inhibitory synaptic inputs in IP-derived neurons and activity in the LFP were often less strongly coupled to one another (**Figure 3.5c**). This was reflected in the peak of the IT-LFP, which was significantly smaller in IP-derived neurons than unlabeled neurons, revealing that synaptic inhibition in IP-derived neurons was more weakly coupled to local network activity (two-tailed unpaired t-test, unlabeled IT-LFP: -245.35 ± 30.62 μV, n = 11 unlabeled neurons from 5 animals, IP-derived IT-LFP: -170.09 ± 16.27 μV, n = 11 IP-derived neurons from 5 animals, P = 0.042, T = 2.17; **Figure 3.5d**). Taken together, these data suggest the inhibition received by an IP-derived L2/3 pyramidal neuron is more weakly coupled to local network activity.

3.2.5 Progenitor type predicts the correlation between a neuron's synaptic inhibition and the local network

To support the observation that IP-derived neurons have a lower IT-LFP than unlabeled neurons, a separate event-based analysis was performed that used automated methods to detect inhibitory synaptic events (described in **3.2.2**) and local network events in the LFP (described in **3.2.3**). The temporal relationship between local network events and inhibitory synaptic events was captured using a method previously used to quantify spike time correlations (Chini et al., 2022; Cutts and Eglen, 2014; Yang et al., 2021). The event time tiling coefficient (ETTC) was calculated, which measures the synchrony of local network events and synaptic events over short timescales (**Figure 3.6a**). This timescale was set at 25 ms, meaning the ETTC increases each time inhibitory synaptic events and LFP events occur within ± 25 ms of one another. The measured ETTC was stable over the course of a single recording (**Figure 3.6b**; first half of recording versus second half of recording: r^2 = 0.94). When this analysis was used to compare the different neuronal populations,

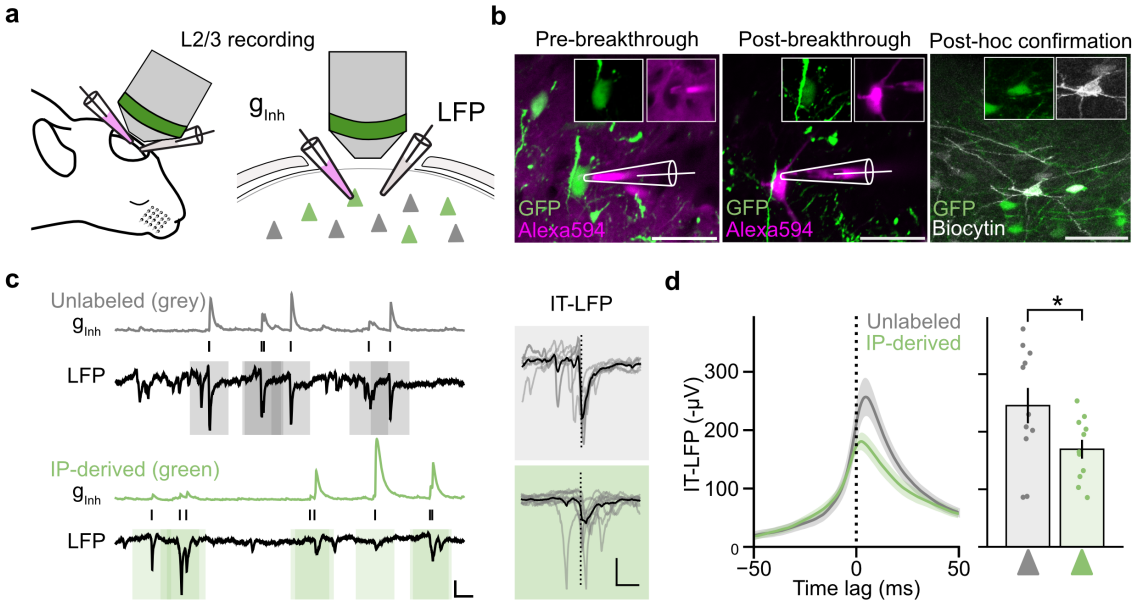


Figure 3.5: Progenitor type predicts a L2/3 pyramidal neuron's inhibitory synaptic activity *in vivo*. (**a**) At P28-42, animals underwent *in vivo* electrophysiology that combined simultaneous whole-cell patch-clamp recordings of inhibitory synaptic conductances (g_{Inh}) and the local field potential (LFP). (**b**) Images from an example two-photon targeted whole-cell patch-clamp recording from a GFP-expressing IP-derived L2/3 pyramidal neuron with post-hoc confirmation. Scale bar, 50 μm. (**c**) Example simultaneous recordings of inhibitory synaptic inputs and the LFP for an unlabeled (top) and IP-derived (bottom) L2/3 pyramidal neuron. The onset of individual inhibitory inputs were identified via automated detection (vertical ticks) and the surrounding 500 ms of LFP was extracted (shaded areas), such that an input-triggered LFP (IT-LFP) was generated for each neuron (right). Scale bar, 2 nS, 200 μV, 250 ms. IT-LFP inset scale bar, 200 μV and 100 ms. (**d**) IT-LFP averaged across all neurons within each group plotted for the 50 ms surrounding inhibitory input onset (left). IP-derived neurons exhibited a lower peak IT-LFP than unlabeled neurons (right) (two-tailed unpaired t-test n = 11 unlabeled neurons from 5 animals, n = 11 IP-derived neurons from 5 animals, P = 0.042, T = 2.17).

it was found that IP-derived neurons had a lower ETTC than unlabeled neurons (two-tailed Mann-Whitney U test, unlabeled ETTC: 0.54 ± 0.05, n = 11 unlabeled neurons from 5 animals, IP-derived ETTC: 0.38 ± 0.05, n = 11 IP-derived neurons from 5 animals, P = 0.021, U = 97; **Figure 3.6c-d**), revealing that local network events are less likely to co-occur with synaptic inhibition in IP-derived neurons. This supports the conclusion that progenitor type can define how strongly coupled a L2/3 pyramidal neuron's synaptic inhibition is to local network activity.

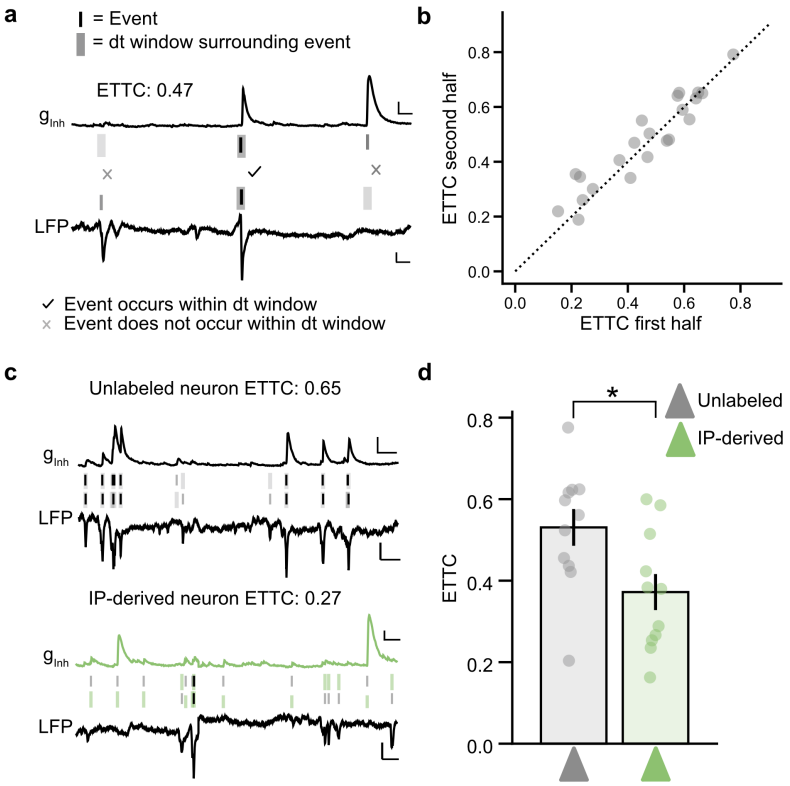


Figure 3.6: Progenitor type predicts the correlation between a L2/3 pyramidal neuron's inhibitory synaptic events and local network events in vivo. (**a**) Example traces depicting detection of inhibitory synaptic events (top) and local network events (bottom). A 25 ms ± dt window was used to determine the event time tiling coefficient (ETTC) - a bidirectional correlation measure of the synaptic events and local network events. ETTC increases when inhibitory synaptic events and LFP events occur close to one another in time (see example with tick) and decreases when inhibitory synaptic events and LFP events occur independently of one another (see examples with crosses). Vertical lines indicate a detected event in the synaptic recording or the LFP. Shaded areas represent the ± 25 ms dt window, which was then used to search for an event in the other trace. Darker vertical lines and shaded areas indicate where inhibitory events and network events co-occur within ± 25 ms of one another. Scale bar, 1 nS, 100 μV, 125 ms. (**b**) ETTC values for individual neurons were comparable between the first and second half of the recording (n = 22 neurons from 10 animals, r^2 = 0.93). (**c**) Example trace for an unlabeled (top, grey) and an IP-derived (bottom, green) L2/3 pyramidal neuron with their respective ETTC values. Scale bar, 1 nS, 100 μV, 250 ms. (**d**) ETTC was lower for IP-derived neurons than unlabeled neurons (two-tailed Mann-Whitney U test, n = 11 unlabeled neurons from 5 animals, n = 11 IP-derived neurons from 5 animals, P = 0.021, U = 97).

3.3 Discussion

In this chapter I have used a combination of *in utero* labelling techniques and *in vivo* whole-cell patch clamp recordings to assess whether progenitor type predicts a L2/3 pyramidal neuron's inhibitory synaptic activity *in vivo*. Firstly, I described

an *in utero* labelling method that can be used to label IP-derived neurons, so that they can be subsequently targeted by two-photon *in vivo* patch clamp in the mature brain. Next, I validated several aspects of my analysis pipeline in order to develop an experimental paradigm for measuring inhibitory synaptic coupling to LFP. Lastly, I measured the synaptic inhibition spontaneously received by IP-derived and unlabeled L2/3 neurons *in vivo* whilst simultaneously recording LFP. The results from this chapter support the conclusion that whilst IP-derived and unlabeled L2/3 pyramidal neurons receive similar overall levels of synaptic inhibition, the correlation between this synaptic inhibition and local network activity is weaker for IP-derived neurons compared to randomly selected unlabeled neurons.

LFP recordings were used to measure local network activity, similar to methods described previously (Haider et al., 2016; Okun et al., 2010, 2015; Okun and Lampl, 2008; Pala and Petersen, 2015). In agreement with earlier studies, the LFP was found to be predictive of inhibitory synaptic inputs (Haider et al., 2016). Further, there was significant diversity across neurons in how strongly their inhibitory inputs coupled to the local network. This was similar to prior reports that found the spiking activity of cortical pyramidal neurons diversely couples to population activity (Okun et al., 2015). Some neurons were described as 'soloists', because their spiking activity was largely independent of the population. Whereas other neurons were described as 'choristers', because their spiking activity was more strongly coupled to the rest of the network. Whilst this previous study focuses on the coupling of a neuron's action potentials to LFP, my work advances these observations by extending the applications of population coupling to inhibitory synaptic inputs. Intuitively, one may predict that the population coupling of a neuron's synaptic input would reflect that of its spiking output. Interestingly, Okun et al. (2015) found that strongly coupled neurons have higher input connectivity from neighbouring pyramidal neurons. Therefore, differential inhibitory connectivity to IP-derived neurons may underlie the coupling effects seen in this chapter. One possibility is that IP-derived neurons receive preferential input from a particular subtype of interneuron. This is an attractive theory as different interneurons have been shown to vary in how much their output correlates with population activity (Khan et al., 2018; Knoblich et al., 2019). Therefore, one could imagine a mechanism whereby IP-derived neurons

receive preferential input from a type of interneuron which has low population coupling. Alternatively, IP-derived neurons may differ in their inhibitory connections within a particular subtype of interneuron, similar to the lineage and birth-date dependent inhibitory connectivity described in the hippocampus (Cavalieri et al., 2021; Huszár et al., 2022; Xu et al., 2014).

Recording spontaneous inhibitory inputs makes it possible to sample a neuron's inhibition without manipulating any synapses within the circuit, allowing an unbiased assessment of the inhibitory control the neuron is under *in vivo*. However, it is important to note that the inhibitory inputs recorded could have come from a diverse range of presynaptic inhibitory cell types, and spontaneous recordings alone cannot determine which input came from which interneuron type. PV and SST interneurons provide the majority of functional, hyperpolarizing inhibition to pyramidal neurons (Safari et al., 2017), making these two interneuron types the most likely candidates for providing the synaptic inhibition recorded in my experiments. Beyond this however, recordings from the cell body will primarily detect PV inhibitory inputs that arrive at, or near to, the neuron's soma. In addition, PV interneurons can readily fire action potentials in response to a single or few synaptic inputs under anaesthesia *in vivo* (Jouhanneau et al., 2018), whilst SST interneurons typically require the integration of multiple inputs in rapid succession to reach action potential threshold (Silberberg and Markram, 2007). Taken together, it therefore seems likely that the majority of the synaptic inhibition that I recorded reflected PV interneuron input to the L2/3 pyramidal neurons.

In summary, this chapter has shown that progenitor type can predict the inhibition received by L2/3 pyramidal neurons *in vivo*. A potential explanation for this is that progenitor type biases the inhibitory connections a L2/3 pyramidal neuron receives. This will be explored in **Chapter 4**.

4 | Cortical inhibitory subnetworks are shaped by pyramidal neuron progenitor type

4.1 Introduction

Inhibitory interneurons exhibit an incredible degree of diversity, which has led to an extensive effort to categorise them according to their morphology, electrophysiology, connectivity and transcriptomics (Jiang et al., 2015; Kepecs and Fishell, 2014; Markram et al., 2004; Nigro et al., 2018; Rudy et al., 2011; Tasic et al., 2018; Tremblay et al., 2016). This diversity has led to the exploration of how these interneurons function differently within cortical circuits. Classically, interneurons have been subdivided based on the expression of single genes, although new techniques now use a combinatorial classification approach that can more appropriately segregate interneurons into functional subtypes (Cadwell et al., 2015; Fuzik et al., 2015; Gouwens et al., 2020; Wu et al., 2023). Similar to excitatory neurons, much of interneuron diversity is rooted in embryonic development. Different interneuron subtypes are born at different timepoints, from different neurogenic niches and progenitor types (Butt et al., 2005; Hu et al., 2017; Miyoshi et al., 2007; Petros et al., 2015; Tyson et al., 2015; Wichterle et al., 2001; Wonders and Anderson, 2006; Wonders et al., 2008). For example, SST and PV interneurons are born from apical and basal progenitors in the dorsal and ventral medial ganglionic eminence (MGE), respectively (Flames et al., 2007; Inan et al., 2012; Miyoshi et al., 2007; Petros et al., 2015; Xu et al., 2004). The remaining 30 % of interneurons originate from the cadual ganglionic eminence (CGE), which mainly comprise those expressing the 5-HT3A receptor, including VIP interneurons (Lee et al., 2010; Miyoshi et al., 2010; Nery et al., 2002; Vucurovic et al., 2010). From these locations interneurons migrate tangentially to the cortical plate, where they interact with developing cortical neurons and begin forming synaptic connections (Lim et al., 2018b). These developmental

parallels between excitatory and inhibitory neurons in the specification of neuronal identity through progenitor type highlight the importance of neurogenesis in the construction of cortical circuits.

Differing connectivity motifs and functional properties between interneuron subtypes means that each subtype is well-placed to modulate pyramidal neurons at specific stages of cortical processing. For instance, PV, SST and VIP interneurons differ in terms of their local and long-range input and output connectivity, the spatial location of their innervation domains on pyramidal neurons, their short-term synaptic dynamics, and their activity patterns in active cortical networks (Beierlein et al., 2003; Gentet et al., 2010, 2012; Gupta et al., 2000; Ma et al., 2012; Naskar et al., 2021; Reyes et al., 1998; Silberberg and Markram, 2007; Wall et al., 2016; Wang et al., 2004). This therefore leads to these three interneuron subtypes executing different modes of inhibition. An excellent example of how this division of labour contributes to cortical processing is described in Williams and Holtmaat (2019). The authors of this study demonstrate how co-activation of top-down and bottom-up inputs to cortical circuits differentially engage PV, SST and VIP interneuron subtypes, leading to the disinhibition of L2/3 pyramidal dendrites and the potentiation of L4 to L2/3 synapses. Therefore, the specific connectivity of inhibitory circuits enables the integration of incoming sensory stimuli with contextual signals.

In addition to a diverse range of inhibitory subtypes, pyramidal neurons also differ in how they participate in these inhibitory circuits. For example, neighbouring L2/3 pyramidal neurons in visual cortex differ in how much PV-mediated disynaptic inhibitory input they receive from L4, which is proportional to the level of monosynaptic excitation (Xue et al., 2014). Furthermore, inhibitory inputs received by L2/3 pyramidal neurons depend on their receptive field properties (Palagina et al., 2019; Znamenskiy et al., 2018), are known to vary across cortical layers (Kätzel et al., 2010) and create subnetworks that reflect long-range inputs (D'Souza et al., 2019). At the level of individual neurons, the probability and strength of inhibitory connections from a fast spiking interneuron to a pyramidal neuron strongly depends on whether there is a reciprocal excitatory connection (Yoshimura and Callaway, 2005). In cases of reciprocity, these neuron pairs are more likely to receive shared excitatory inputs from other cortical layers (Yoshimura and Callaway, 2005). Furthermore, a

range of evidence suggests that neighbouring pyramidal neurons vary substantially in how they share inhibition from common presynaptic interneurons (Jézéquel et al., 2023; Krook-Magnuson et al., 2012; Lee et al., 2014a,b; Lu et al., 2017; Packer and Yuste, 2011; Sippy and Yuste, 2013; Valero et al., 2015; Varga et al., 2010). Taken together, these principles of inhibitory connectivity create diverse inhibitory cortical subnetworks. Given that the synaptic inhibition received by IP-derived L2/3 pyramidal neurons is less strongly coupled to local network activity (**Chapter 3**), one hypothesis is that these neurons have differential inhibitory connectivity. This could be in the form of more or less inhibitory input from a particular inhibitory subtype, or differences in how synaptic inhibition is shared with other pyramidal neurons.

This chapter will use a combination of *in utero* labelling, optogenetics and *in vitro* electrophysiology techniques to test whether neurons receive different inhibitory input based on the progenitor type from which they are derived. The aims of this chapter are as follows:

- To develop a dual-colour strategy for labelling defined progenitor populations in transgenic mice
- To test whether inhibitory synaptic input from PV, SST and VIP interneurons is influenced by pyramidal neuron progenitor type
- To determine whether progenitor type shapes a L2/3 pyramidal neuron's inhibitory subnetwork

4.2 Results

4.2.1 Dual colour labelling strategy to target neurons derived from intermediate progenitors

One potential explanation for the observations in **Chapter 3** is that L2/3 pyramidal neurons receive different amounts of inhibitory synaptic input from interneuron subtypes. To investigate this possibility, an optogenetic approach was adopted in order to determine whether the amount of synaptic input from interneuron subtypes varies depending on the pyramidal neuron's progenitor type. This approach made use of Cre-Lox transgenic mouse technology to express ChR2 in a defined interneuron population (e.g. PV, SST, or VIP interneurons). Consequently, the progenitor labelling strategy had to be independent of the Cre recombinase system and therefore a new dual-colour reporter construct was developed that made use of the Flpo recombinase system (fDIO-tdTom/EGFP, see **Chapter 2**). This enabled two different subpopulations of L2/3 pyramidal neurons to be distinguished based on their progenitor type. Flpo recombinase downstream of the Tα1 promoter was combined with a reporter construct incorporating a flexible excision (FLEx) cassette, in which Flpo recombination permanently switches expression from TdTomato fluorescent protein to GFP (**Figure 4.1a**). With this strategy, the IP-derived pyramidal neurons express GFP, whilst neighboring pyramidal neurons derived from other progenitors ('OP-derived') express TdTomato (Ellender et al., 2019) (**Figure 4.1b-c**). On average, 58.73 % of electroporated L2/3 neurons were OP-derived and 41.27 % of electroporated L2/3 neurons were IP-derived (**Figure 4.1b**). In line with previous work, the soma of IP-derived and OP-derived L2/3 pyramidal neurons showed overlapping distributions in mature cortex, with the average IP-derived neuron located slightly further from pia, consistent with the OP population including progenitors that undergo self-renewing divisions (Ellender et al., 2019; Stancik et al., 2010) (two-tailed paired t-test, OP-derived mean: 215.85 $\pm$ 7.84 μm, IP-derived mean: 254.94 $\pm$ 11.33 μm, n = 14 brains, P = 0.01, T = -3.02; **Figure 4.1c**)

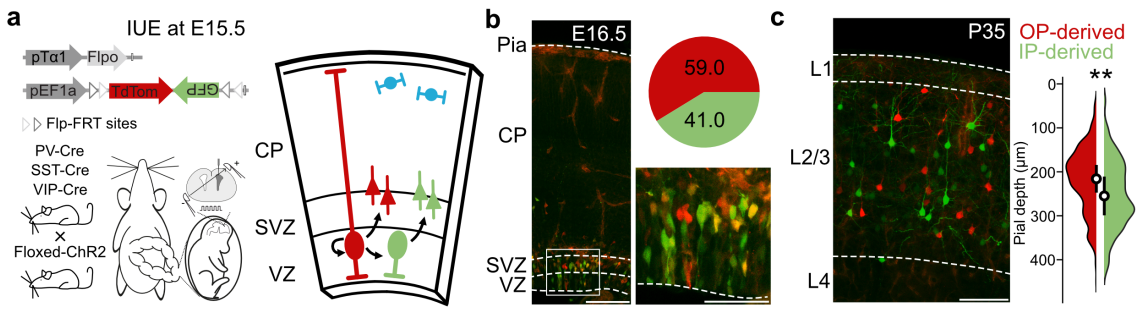


Figure 4.1: Dual colour labelling system to target neurons derived from intermediate progenitors. (**a**) IUE was performed at E15.5 using Tα1-Flpo and fDIO-tdTom/EGFP to label IP-derived and OP-derived neurons in mice expressing ChR2 in either PV, SST or VIP interneurons. (**b**) TdTomato-expressing OPs and GFP-expressing IPs can be seen along with newly born IP-derived and OP-derived neurons 24 hours following IUE. Scale bar, 100 μm, 50 μm for inset. (left, bottom). On average, 58.73 % of electroporated neurons were OP-derived and 41.27 % of electroporated neurons were IP-derived, n = 14 brains (top, right). (**c**) At P35, the L2/3 pyramidal neurons showed overlapping distributions, with the average IP-derived neuron further from pia than the average OP-derived neuron (two-tailed paired t-test, n = 14 brains, P = 0.01, T = -3.02). Pial depth is shown as a kernel density estimate alongside mean ± standard deviation. Scale bar, 100 μm.

4.2.2 Labelled IPs include basal and apical intermediate progenitors

Research has described two different types of intermediate progenitors (Attardo et al., 2008; Ellender et al., 2019; Englund et al., 2005; Gal et al., 2006; Haubensak et al., 2004; Kawaguchi et al., 2008; Kowalczyk et al., 2009; Miyata et al., 2004; Noctor et al., 2004, 2008; Stancik et al., 2010; Tyler and Haydar, 2013). However, there is a lack of consensus upon how these two progenitor types relate to one another. Some studies suggest that aIPs are nascent bIPs (Kawaguchi et al., 2008; Kowalczyk et al., 2009; Noctor et al., 2008), whereas other studies suggest these two types of intermediate progenitors are born separately from RGCs (Stancik et al., 2010; Tyler and Haydar, 2013). These mixed interpretations demonstrate the challenge of distinguishing progenitor lineages using IUE-based methods, which can only provide a single temporal snapshot of a highly dynamic process. Additionally, these methods typically rely on labelling progenitor types with single genes. The Tα1 promoter has been used to label aIPs (Ellender et al., 2019; Gal et al., 2006; Stancik et al., 2010), although some studies suggest it also labels bIPs (Mizutani et al., 2007; Tyler and Haydar, 2013). Meanwhile, the Tbr2 promoter has been used to label bIPs (Englund

et al., 2005; Guillamon-Vivancos et al., 2019; Noctor et al., 2008; Tyler et al., 2015).

Whilst some studies have performed labelling of progenitors using constructs with transient on/off dynamics (Tyler and Haydar, 2013), to my knowledge no study has used longitudinal fluorescent labelling to map the lineage of multiple intermediate progenitor types. Therefore, to better characterise the neurons included in my IP-derived population of interest, I employed a strategy that made use of two recombinase systems (Cre and Flpo recombinases) and "flip-excision" technology for longitudinal labelling (Schnütgen et al., 2003). The Tα1 promoter was used to control expression of a Cre-dependent flip-excision GFP reporter construct, pCAG-FLEx-GFP. Meanwhile, the Tbr2 promoter was used to control expression of a Flpo-dependent flip-excision TdTomato reporter construct, pCAG-fDIO-TdTom (**Figure 4.2a**). This four-plasmid labelling strategy enables me to identify progenitors and their progeny derived from pTα1+ and pTbr2+ lineages within a single brain (**Figure 4.2b**).

When these plasmids were delivered by IUE at E15.5 and the tissue collected 24 hours later at E16.5, TdTomato-pTbr2+ labelling was largely restricted to multipolar cells in the SVZ, where bIPs are known to reside (Haubensak et al., 2004; Kowalczyk et al., 2009; Miyata et al., 2004; Noctor et al., 2004) (**Figure 4.2c-d**). Interestingly, almost all TdTomato-pTbr2+ cells were also GFP-pTa1+, in agreement with studies that have suggested that pTα1 is also expressed in bIPs (Tyler and Haydar, 2013). A second population of cells were labelled by GFP-pTα1 but not by TdTomato-pTbr2, these cells had short radial morphology and resided in the VZ, consistent with an aIP identity (**Figure 4.2d**). Indeed, some of these could be seen dividing at the ventricular wall (**Figure 4.2d**, bottom left example).

To map the progeny of these progenitors, the same plasmids were delivered at E15.5, and then tissue was collected at the later time point of P28, where labelled neurons now occupied mature L2/3 of somatosensory cortex (**Figure 4.2e**). A similar pattern of labelling was observed to the embryonic tissue, whereby the majority of labelled neurons were derived from a pTa1+ pTbr2+ bIP lineage (60.46 ± 4.73 %; **Figure 4.2f**). Most of the remaining labelled neurons were derived from a pTa1+ pTbr2- aIP lineage (36.08 ± 4.66 %). Extremely few neurons were derived from a

pTa1- pTbr2+ lineage (3.46 ± 0.55 %). Neurons derived from the pTa1+ pTbr2+ bIP lineage and the pTa1+ pTbr2- aIP lineage sat at similar distances from pia (two-tailed Wilcoxon signed-rank test, pTα1+ pTbr2- mean: 219.34 ± 18.73 μm, pTα1+ pTbr2+ mean: 211.37 ± 16.31 μm, n = 11 brains, P = 0.24, W = 19; **Figure 4.2g**), suggesting that these two populations of neurons are born simultaneously from a pool of transiently dividing progenitors. Overall, these results suggest that the pTα1 labelling strategy used throughout this thesis labels a population of intermediate progenitors comprising both aIPs and bIPs.

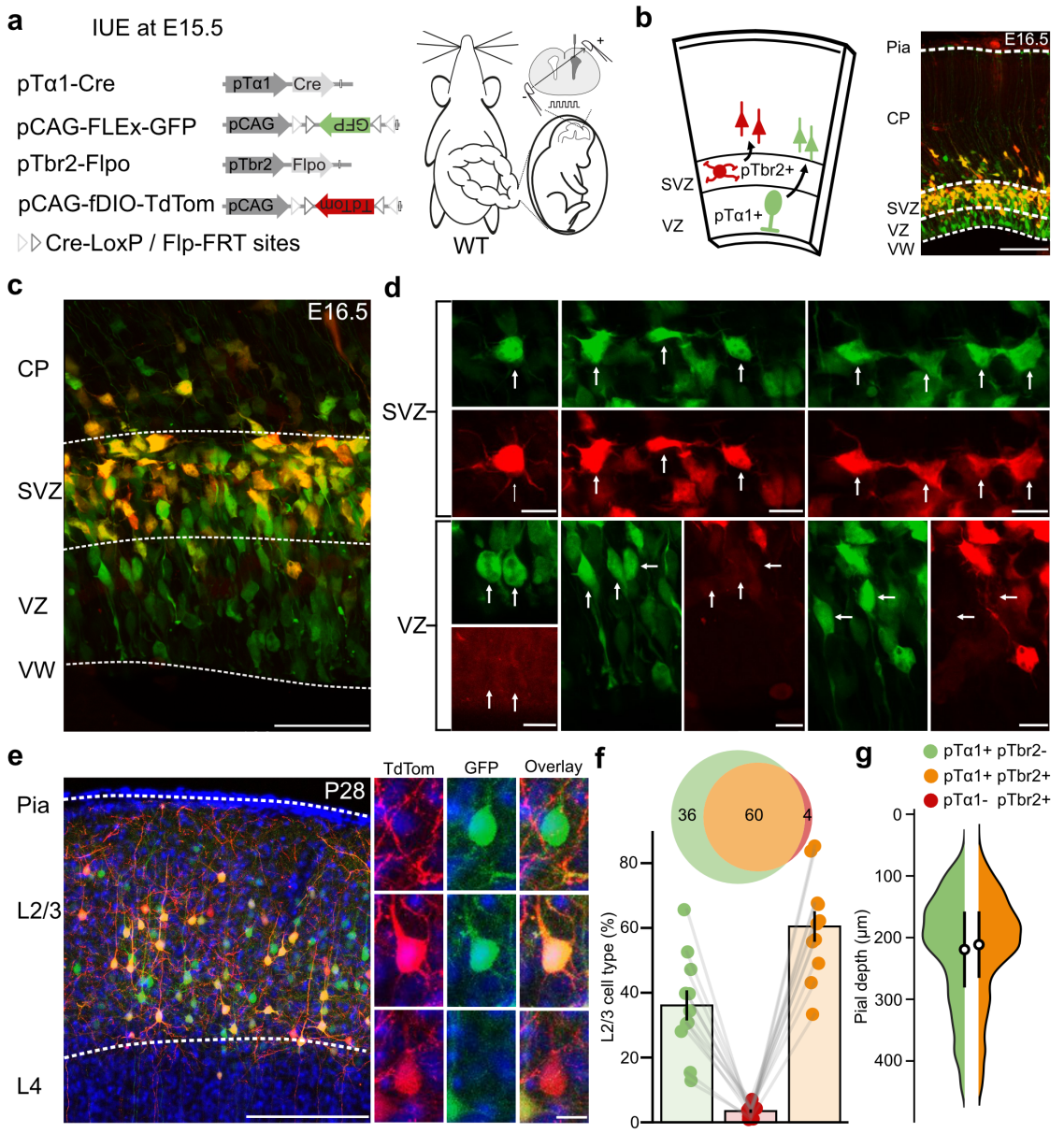


Figure 4.2: Intermediate progenitors labelled by Tα1 promoter activity comprise a population of apical IPs and basal IPs (**a**) Four plasmid IUE of pTα1-Cre, pCAG-FLEx-GFP, pTbr2-Flpo and pCAG-fDIO-TdTom was performed at E15.5 to label intermediate progenitors and their progeny. (**b**) Tissue was collected 24 hours after IUE at E16.5 to visualise IPs and newly born IP-derived neurons in the VZ and SVZ. Scale bar, 100 μm. (**c**) pTα1+ (GFP+ TdTom-) aIP-derived neurons can be seen in the ventricular zone (VZ) and pTα1+ pTbr2+ (GFP+ TdTom+) bIP-derived neurons can be seen in the subventricular zone (SVZ). Scale bar 50 μm. VW = ventricular wall, CP = cortical plate. (**d**) Selected enlarged sections from '**c**'. GFP and TdTom channels for each image are shown separately. The top row shows examples of multipolar pTbr2+ pTα1+ bIPs residing in the SVZ. The bottom row shows examples of pTα1+ pTbr2- aIPs with radial morphology in the VZ, some of which are dividing. Scale bars, 20 μm. (**e**) L2/3 IP-derived neurons at P28 following IUE of the plasmids in '**a**'. Scale bar, 100 μm. Insets (right) show examples of neurons derived from a pTα1+ pTbr2- lineage (top), a pTα1+ pTbr2+ lineage (middle) and a pTα1- pTbr2+ lineage (bottom). Scale bar, 20 μm. (**f**) Percentage of each L2/3 cell type, n = 11 brains. (**g**) pTα1+ pTbr2- and pTα1+ pTbr2+ lineage sat at equal distances from pia (two-tailed Wilcoxon signed-rank test, n = 11 brains, P = 0.24, W = 19). Pial depth is shown as a kernel density estimate alongside mean ± standard deviation.

4.2.3 L2/3 pyramidal neurons derived from different progenitor types receive similar overall levels of synaptic inhibition from PV, SST and VIP interneurons

Having characterised the IP populations targeted by the pTα1 labelling strategy, I returned to the pTα1-Flpo and dual-color reporter construct (**Figure 4.1**) in order to label IP-derived and OP-derived L2/3 pyramidal neurons in transgenic mice expressing ChR2 in a specific interneuron population (PV, SST, or VIP interneurons). This strategy enabled me to use an optogenetic approach to examine the strength of monosynaptic input from each interneuron population. Firstly, the inhibitory input from PV interneurons was examined, which are known to provide strong peri-somatic input to L2/3 pyramidal neurons (Fino et al., 2013; Markram et al., 2004; Safari et al., 2017; Xue et al., 2014) (**Figure 4.3a**). Animals that had undergone IUE were allowed to reach maturity (ages P21-42) and acute slices were prepared from S1 to allow for simultaneous whole-cell patch-clamp recordings from neuronal pairs comprising a GFP-expressing IP-derived L2/3 pyramidal neuron, and a neighboring TdTomato-expressing OP-derived L2/3 pyramidal neuron (mean inter-somatic distance of 67.38 ± 7.21 μm). Brief pulses from a widefield light-emitting diode (LED; 473 nm, 1 ms duration) were used to activate ChR2-expressing PV interneurons throughout the brain slice, whilst the resulting monosynaptic inhibitory post-synaptic currents ($IPSC_{PV}$) were recorded and their amplitude compared between the IP-derived and neighboring OP-derived pyramidal neuron (**Figure 4.3a-c**). Consistent with previous work, this elicited large $IPSC_{PV}$ whose amplitude varied across neurons (Xue et al., 2014). However, there was no systematic difference in the amplitude of the $IPSC_{PV}$ between IP-derived and OP-derived neurons (one sample t-test, OP-derived mean: 462.71 ± 59.32 pA, IP-derived mean: 444.00 ± 69.92 pA, n = 17 pairs from 8 animals, P = 0.80, T = 0.26; **Figure 4.3b**). This suggests that progenitor type is not associated with a different level of PV interneuron input.

Next, the synaptic input from SST interneurons was tested, which are a major source of dendritic input to L2/3 pyramidal neurons (Silberberg and Markram, 2007; Urban-Ciecko and Barth, 2016; Wang et al., 2004). Widefield ChR2 activation of

SST interneurons elicited a large $IPSC_{SST}$ in pairs of neighboring L2/3 pyramidal neurons (**Figure 4.3d**; mean inter-somatic distance of 85.55 ± 10.12 μm), but the $IPSC_{SST}$ amplitude did not exhibit systematic differences between IP-derived and OP-derived L2/3 neurons (one-sample t-test, OP-derived mean: 497.47 ± 42.12 pA, IP-derived mean: 474.43 ± 48.32 pA, n = 22 pairs from 11 animals, P = 0.36, T = -0.94; **Figure 4.3e** and **4.3f**). Finally, I examined the input from VIP interneurons, which provide monosynaptic input to L2/3 pyramidal neurons, in addition to their role in disinhibitory cortical circuits (Naskar et al., 2021; Pfeffer et al., 2013). Widefield ChR2 activation of VIP interneurons tended to elicit somewhat smaller post-synaptic responses (**Figure 4.3g**; mean inter-somatic distance of 67.25 ± 6.90 μm), but again the amplitude of $IPSC_{VIP}$ did not differ between IP-derived and OP-derived neurons (one-sample t-test, OP-derived mean: 182.19 ± 40.313 pA, IP-derived mean: 153.20 ± 18.66 pA n = 23 pairs from 7 animals, P = 0.80, T = 0.26; **Figure 4.3h-i**). These results indicate that the overall amount of synaptic inhibition provided by major interneuron subtypes does not vary according to a L2/3 pyramidal neuron's progenitor type. Therefore, the differences in how synaptic inhibition couples to local network activity is unlikely to reflect different levels of input from interneuron subtypes.

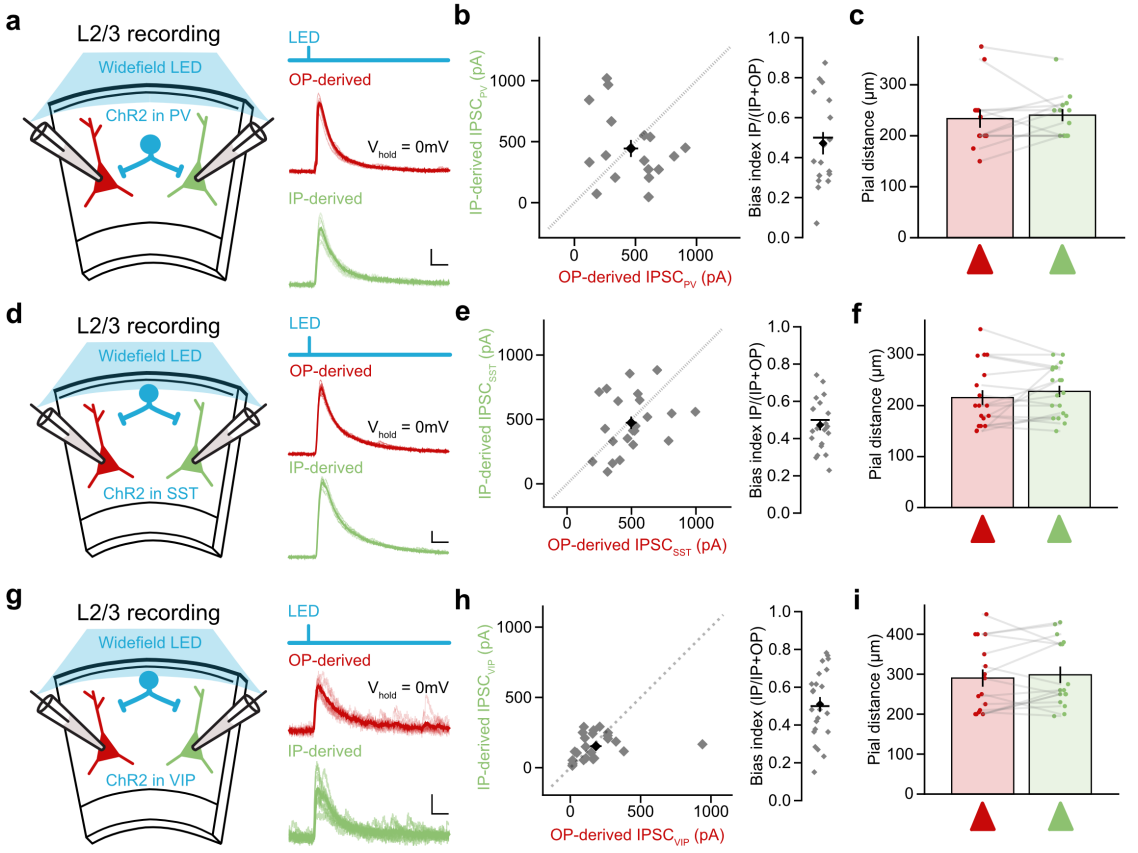


Figure 4.3: L2/3 pyramidal neurons derived from different progenitor types receive similar overall levels of synaptic inhibition from PV, SST and VIP interneurons. (**a**) Acute slices were prepared from S1 and simultaneous recordings were performed from pairs of IP-derived and OP-derived L2/3 pyramidal neurons, whilst brief widefield light pulses from a LED (473 nm, 1 ms duration) were used to activate ChR2-expressing PV interneurons throughout the brain slice (left). Example IPSC$_{PV}$ recorded from an IP-derived and OP-derived neuron pair (right). Scale bar, 100 pA, 25 ms. (**b**) IPSC$_{PV}$ did not differ between IP-derived and OP-derived neurons (one sample t-test, n = 17 pairs from 8 animals, P = 0.80, T = 0.26). (**c**) On average IP-derived and OP-derived neurons sat equidistant from pia (two-tailed Wilcoxon signed-rank test, OP-derived mean: 233.62 ± 17.98 μm, IP-derived mean: 240.46 ± 12.13 μm n = 13 pairs from 7 animals, P = 0.43, W = 51.5). (**d**) Simultaneous patch-clamp recordings were made from IP-derived and OP-derived neurons, whilst activating ChR2-expressing SST interneurons (left). Example IPSC$_{SST}$ recorded from an IP-derived and OP-derived pair (right). Scale bar, 100 pA, 25 ms. (**e**) IPSC$_{SST}$ did not differ between IP-derived and OP-derived neurons (one-sample t-test, n = 22 pairs from 11 animals, P = 0.36, T = -0.94) (**f**) On average IP-derived and OP-derived neurons sat equidistant from pia (two-tailed Wilcoxon signed-rank test, OP-derived mean: 219.06 ± 14.56 μm, IP-derived mean: 226.72 ± 11.76 μm, n = 18 pairs from 11 animals, P = 0.48, W = 54.5). (**g**) Simultaneous patch-clamp recordings were made from IP-derived and OP-derived neurons, whilst activating ChR2-expressing VIP interneurons (left). Example IPSC$_{VIP}$ recorded from an IP-derived and OP-derived pair (right). Scale bar, 50 pA, 25 ms. (**h**) IPSC$_{VIP}$ amplitude did not differ between IP-derived and OP-derived neurons (one-sample t-test, n = 23 pairs from 8 animals, P = 0.80, T = 0.26). (**i**) On average IP-derived and OP-derived neurons sat equidistant from pia (two-tailed Wilcoxon signed-rank test, OP-derived mean: 290.31 ± 21.63 μm, IP-derived mean: 298.44 ± 20.80 μm, n = 16 pairs from 7 animals, P = 0.43, W = 51.5).

4.2.4 L2/3 pyramidal neurons derived from different progenitor types receive similar levels of spontaneous action-potential-evoked synaptic inhibition

The previous experiments suggest that progenitor type does not influence the overall input that a L2/3 pyramidal neuron receives from PV, SST or VIP interneurons. However, differences in a L2/3 pyramidal neuron's fine-scale inhibitory synaptic connectivity could underlie the *in vivo* observations made in **Chapter 3**. For instance, whilst the ChR2 experiments activated interneurons throughout the brain slice simultaneously, an alternative method of characterising synaptic inhibition is to record the spontaneous inhibitory inputs that neurons receive. This provides information on the frequency and amplitude of spontaneous IPSCs, as well as information on their respective timing to one another in two simultaneously recorded neurons. To explore this, IP-derived and OP-derived L2/3 neurons were labelled using IUE at E15.5 and acute slices were prepared from S1 once the animals reached maturity (ages P21-P42). Simultaneous whole-cell patch-clamp recordings were performed from unlabeled, OP-derived or IP-derived L2/3 neurons (**Figure 4.4a**). Spontaneous IPSCs were observed in all recorded neurons and an input threshold was used to maximize the detection of unitary, action potential-evoked IPSCs, rather than miniature events (Safari et al., 2017; Xue et al., 2014) (see **Chapter 2**). The frequency of IPSCs were not different between unlabeled, OP-derived or IP-derived neurons (Kruskal-Wallis one-way analysis of variance, unlabeled mean frequency: 0.50 ± 0.06 Hz, n = 54 neurons from 16 animals, OP-derived mean frequency: 0.57 ± 0.08 Hz, n = 85 neurons from 29 animals, IP-derived mean frequency: 0.71 ± 0.08 Hz, n = 55 neurons from 30 animals, P = 0.05, H = 5.99; **Figure 4.4b**). Additionally, the amplitude of IPSCs did not differ between the neuron types (Kruskal-Wallis one-way analysis of variance, unlabeled amplitude mean: 58.56 ± 2.14 pA, n = 54 neurons from 16 animals, OP-derived amplitude mean: 59.43 ± 1.99 pA, n = 85 neurons from 29 animals, IP-derived amplitude mean: 52.31 ± 1.12 pA, n = 55 neurons from 30 animals, P = 0.08, H = 4.85; **Figure 4.4c**). Therefore, unlabeled, IP-derived and OP-derived L2/3 neurons receive comparable levels of spontaneous synaptic inhibition, which is consistent with the previous *in vivo* and ChR2-evoked

findings (**Figures 3.2** and **4.3**).

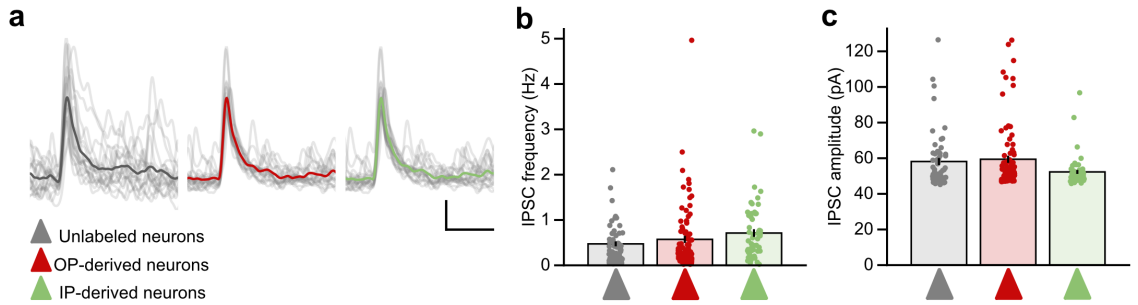


Figure 4.4: L2/3 pyramidal neurons from different progenitor types receive similar levels of spontaneous action-potential-evoked synaptic inhibition. (**a**) Whole-cell patch clamp recordings were made from unlabeled, IP-derived and OP-derived neurons in cortical slices. IPSCs were detected using automated detection. Example traces show 20 detected IPSCs from each neuron type, mean is overlaid in bold. Scale bar 20 pA, 50 ms. (**b**) IPSC frequency did not differ between unlabeled, IP-derived and OP-derived L2/3 pyramidal neurons (Kruskal-Wallis one-way analysis of variance, n = 54 unlabeled neurons from 16 animals, n = 85 OP-derived neurons from 29 animals, n = 55 IP-derived neurons from 30 animals, P = 0.05, H = 5.99). (**c**) IPSC amplitude did not differ between unlabeled, IP-derived and OP-derived L2/3 neurons (Kruskal-Wallis one-way analysis of variance, n = 54 unlabeled neurons from 16 animals, n = 85 OP-derived neurons from 29 animals, n = 55 IP-derived neurons from 30 animals, P = 0.08, H = 4.85).

4.2.5 A L2/3 pyramidal neuron's inhibitory subnetwork reflects the progenitor type from which it is derived

Previous work has established that neighboring pyramidal neurons can vary in how much shared input they receive from common pre-synaptic interneurons (Packer and Yuste, 2011; Salkoff et al., 2015; Sippy and Yuste, 2013; Yoshimura et al., 2005). To account for the observed differences in how a pyramidal neuron's synaptic inhibition couples to local network activity, it is possible that progenitor type influences how pyramidal neurons share input from the same presynaptic interneurons. To explore this, the first approach was to investigate the degree to which spontaneous inhibitory inputs are shared by neighboring L2/3 pyramidal neurons, as this can be used to measure common input from the same individual pre-synaptic interneuron (Sippy and Yuste, 2013; Xu et al., 2014). Simultaneous whole-cell patch-clamp recordings were performed from pairs of neurons comprising either two unlabeled neighboring pyramidal neurons, whose progenitor type was therefore unknown (**Figure 4.5a**), or from pairs comprising an IP-derived and a neighboring OP-derived pyramidal neuron

(**Figure 4.5b**). Spontaneous IPSCs were observed in all recorded neurons and an input threshold was used to maximize the detection of unitary, action potential-evoked IPSCs, rather than miniature events (Safari et al., 2017; Xue et al., 2014) (see **Chapter 2**).

Firstly, I compared how many inputs were shared (received simultaneously between both neurons) or unshared (received by only one neuron) between the recorded pair of neurons. In pairs of unlabeled pyramidal neurons, 22.23 ± 2.73 % of inhibitory inputs were classified as shared. In contrast, shared inhibitory inputs were much less common in pairs comprising IP-derived and OP-derived pyramidal neurons, where the proportion of shared inputs was only 11.51 ± 1.81 % (two-tailed Mann-Whitney U test, P = 0.004, U = 421; **Figure 4.5c**). Secondly, I compared the amplitude and variability of the inputs that were shared between the neurons. The mean amplitude of shared inhibitory inputs was similar across the two pair types (two-tailed Mann-Whitney U test, unlabeled mean: 123.79 ± 8.24 pA, n = 27 pairs from 16 animals, OP-derived and IP derived mean: 135.54 ± 17.91 pA, n = 20 from 10 animals, P = 0.91, U = 276; **Figure 4.5d**). However, the amplitude of shared inputs varied more for IP-derived and OP-derived pairs than for unlabeled pairs (two-tailed Mann-Whitney U test, unlabeled neuron pairs: 88.02 ± 7.28 %, n = 27 pairs from 16 animals, IP-derived and OP-derived neuron pairs: 142.26 ± 18.85 %, n = 21 pairs from 10 animals, P = 0.01, U = 166; **Figure 4.5e**; where the difference in shared input amplitude is expressed as a percentage of the median shared input amplitude). Thus, pyramidal neurons from different progenitor types had fewer shared inhibitory inputs and the shared inputs they did receive were more variable in strength. The inter-somatic distances of the neuronal pairs were comparable (two-tailed Mann-Whitney U test, unlabeled mean: 64.15 ± 3.90 μm, n = 20 pairs of unlabeled neurons from 13 animals, IP-derived and OP-derived mean: 69.21 ± 7.14 μm, n = 19 pairs of from 11 animals, P = 0.48, U = 164.5; **Figure 4.5f**), as were the distances from pia between the two pair types (two-tailed Mann-Whitney U test, unlabeled mean: 261.68 ± 17.45 μm, n = 19 pairs from 13 animals, IP-derived and OP-derived mean: 270.28 ± 17.56 μm, n = 18 pairs from 11 animals, P = 0.48, U = 164.5; Figure 4.5g) and within the IP-derived and OP-derived populations (two-tailed paired t-test, OP-derived neuron mean: 266.94 ± 22.80 μm, IP-derived

neuron mean: 273.61 ± 23.65 μm, n = 18 pairs from 11 animals, P = 0.53, T = 0.64; **Figure 4.5h**). These data therefore indicate that progenitor type can specify the degree to which neighboring pyramidal neurons share their inhibitory synaptic input from presynaptic interneurons.

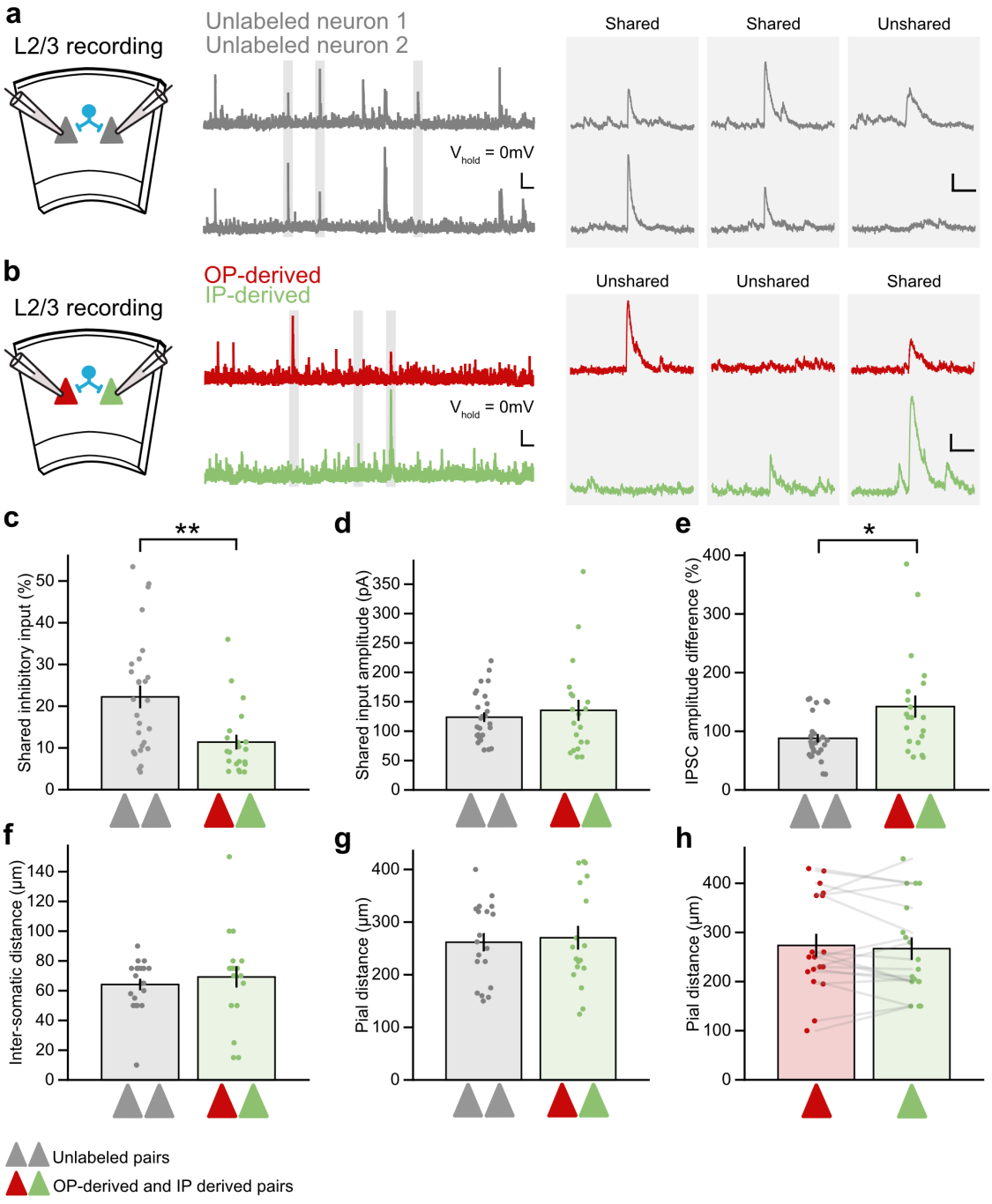


Figure 4.5: A L2/3 pyramidal neuron's inhibitory subnetwork reflects the progenitor type from which it is derived. (**a**) Example traces of spontaneous IPSC recordings from two unlabeled L2/3 pyramidal neurons at P21-42. Scale bar, 50 pA, 1 s. Expanded shaded regions illustrating examples of shared and unshared inhibitory inputs. Scale bar, 50 pA, 100 ms. (**b**) Example traces of spontaneous IPSC recordings from a pair of IP-derived and OP-derived L2/3 pyramidal neurons. Scale bar, 50 pA, 1 s. Expanded shaded regions illustrating examples of shared and unshared inhibitory inputs. Scale bar, 50 pA, 100 ms. (**c**) IP-derived and OP-derived neuron pairs shared less inhibitory inputs than unlabeled neuron pairs (two-tailed Mann-Whitney U test, n = 27 pairs of unlabeled neurons from 16 animals, n = 21 pairs of IP-derived and OP-derived neurons from 10 animals, P = 0.004, U = 421). (**d**) Mean amplitude of shared synaptic inhibition did not differ between unlabeled pairs and IP-derived and OP-derived pairs (two-tailed Mann-Whitney U test, unlabeled n = 27 pairs from 16 animals, OP-derived and IP derived n = 20 from 10 animals, P = 0.91, U = 276). (**e**) The IPSC amplitude difference for shared inhibitory inputs was greater for pairs comprising an IP-derived and OP-derived L2/3 pyramidal neuron, than for pairs comprising two unlabeled L2/3 pyramidal neurons (two-tailed Mann-Whitney U test, unlabeled n = 27 pairs from 16 animals, IP-derived and OP-derived n = 21 pairs from 10 animals, P = 0.01, U = 166). (**f**) Inter-somatic distance was not different between the pair types (two-tailed Mann-Whitney U test, unlabeled n = 20 pairs of unlabeled neurons from 13 animals, IP-derived and OP-derived n = 19 pairs of from 11 animals, P = 0.48, U = 164.5). (**g**) Distance from pia did not differ between unlabeled pairs and IP-derived and OP-derived pairs (two-tailed Mann-Whitney U test, unlabeled n = 19 pairs from 13 animals, IP-derived and OP-derived n = 18 pairs from 11 animals, P = 0.48, U = 164.5). (**h**) Distance from pia was not different between IP-derived and OP-derived neurons (two-tailed paired t-test, n = 18 pairs from 11 animals, P = 0.53, T = 0.64).

To further explore how progenitor type influences the sharing of synaptic inhibition, pairs of L2/3 pyramidal neurons derived from the same type of progenitor were simultaneously recorded and their inhibitory inputs analysed. This included pairs comprising two OP-derived neurons or two IP-derived neurons (**Figure 4.6a-b**). The amount of shared synaptic inhibition between the pair types was then compared to one another and to the pairs comprising either two unlabeled neurons or one OP-derived and one IP-derived neuron (**Figure 4.5**). Interestingly, pairs of two OP-derived neurons shared 27.12 ± 2.79 % of their inhibitory inputs on average, which was similar to pairs of unlabeled neurons. On the other hand, pairs consisting of two IP-derived neurons shared on average 14.03 ± 2.26 % of their inhibitory inputs, which was comparable to pairs of neurons consisting of one OP-derived and one IP-derived neuron (**Figure 4.6c**). Therefore, pairs of two OP-derived neurons shared significantly more inhibitory inputs than either pairs of two IP-derived neurons, or pairs of IP-derived and OP-derived neurons (Kruskal-Wallis one-way analysis of variance, K = 10.55, P = 0.01; **Figure 4.6c**). There were no differences in

the distances between the recorded neurons (Kruskal-Wallis one-way analysis of variance, unlabeled pair mean: 64.15 ± 3.90 μm, IP-derived and OP-derived pair mean: 69.21 ± 7.14 μm, OP-derived pair mean: 66.74 ± 3.68 μm, IP-derived pair mean: 62.65 ± 8.01 μm, K = 1.98, P = 0.37; **Figure 4.6d**) or in their distances from pia (Kruskal-Wallis one-way analysis of variance, unlabeled pair mean: 261.68 ± 17.45 μm, IP-derived and OP-derived pair mean: 270.28 ± 22.64 μm, OP-derived pair mean: 245.50 ± 16.62 μm, IP-derived pair mean: 304.69 ± 18.91 μm, K = 4.47, P = 0.21; **Figure 4.6e**). These results suggest that neurons derived from an IP tend to share less of their synaptic inhibition with other L2/3 pyramidal neuron types, including OP-derived neurons and other IP-derived neurons.

4.2.6 PV interneurons differentially target L2/3 pyramidal neurons based on post-synaptic progenitor type

Given the finding that progenitor type influences the way in which L2/3 pyramidal neurons share inhibitory inputs, one hypothesis is that individual interneurons target L2/3 pyramidal neurons according to progenitor type. To investigate this, I conducted an optogenetic experiment to assess the inhibitory output from putative single PV interneurons onto IP-derived and OP-derived L2/3 neurons. Monosynaptic IPSCs were recorded from simultaneously recorded pairs of neighboring L2/3 pyramidal neurons, except now a laser beam was used to focally activate ChR2-expressing PV interneurons with spatially-restricted pulses of light (**Figure 4.7a-c**). In line with previous ChR2-assisted mapping of local unitary connectivity, the photostimulation conditions were set such that a mixture of successes and failures in post-synaptic responses were observed across trials, consistent with the activation of a single or small number of interneurons (Morgenstern et al., 2016) (see **Chapter 2**). If interneurons connect with similar probability and strength to the two pyramidal neurons, one would expect to observe similar post-synaptic responses on a trial-to-trial basis. In contrast, if interneurons exhibit a biased connectivity to one of the two pyramidal neurons, the expectation is that the post-synaptic responses would exhibit differences on a trial-to-trial basis (**Figure 4.7a-c**). Examining recordings where each of the post-synaptic neurons exhibited at least one response across trials, I first asked what proportion of these trials exhibited responses in both neurons (i.e.

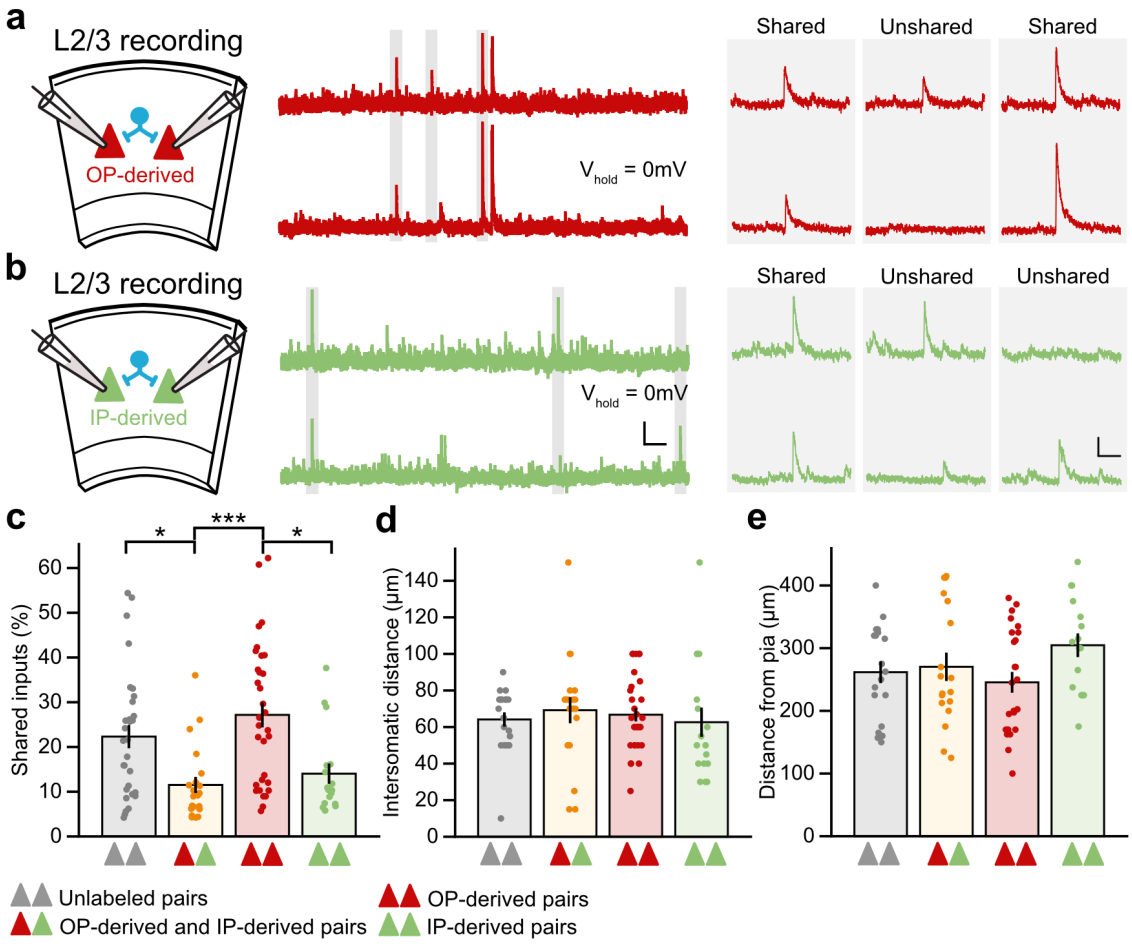


Figure 4.6: Pairs of IP-derived and OP-derived neurons differ in the amount of inhibitory inputs they share with each other. (**a**) Example traces of spontaneous IPSC recordings from pairs of neighbouring OP-derived L2/3 pyramidal neurons. Scale bar, 50 pA, 1 s. Expanded shaded regions illustrating examples of shared and unshared inhibitory inputs. Scale bar, 50 pA, 100 ms. (**b**) Example traces of spontaneous IPSC recordings from pairs of IP-derived L2/3 pyramidal neurons. Scale bar, 50 pA, 1 s. Expanded shaded regions illustrating examples of shared and unshared inhibitory inputs. Scale bar, 50 pA, 100 ms. (**c**) Progenitor type determined how pairs of L2/3 pyramidal neurons shared inhibitory input (Kruskal-Wallis one-way analysis of variance, K = 10.55, P = 0.01, n = 4 groups). Specifically, pairs of two OP-derived neurons shared more inhibitory inputs than pairs of two IP-derived neurons (two-tailed Mann-Whitney post-hoc with Bonferroni correction, n = 31 OP-derived pairs from 19 animals, n = 17 IP-derived pairs from 11 animals, P = 0.03) and pairs of IP-derived and OP-derived neurons (two-tailed Mann-Whitney post-hoc with Bonferroni correction, n = 21 IP-derived and OP-derived pairs from 10 animals, P = 0.0006). (**d**) Inter-somatic distance did not different between the pair types (Kruskal-Wallis one-way analysis of variance, P = 0.37, K = 1.98). (**e**) Distance from pia did not differ between the pair types (Kruskal-Wallis one-way analysis of variance, P = 0.21, K = 4.47).

a shared output). This revealed that the probability of such shared output responses was lower in pairs comprising an IP-derived and a neighboring OP-derived pyramidal neuron, than the probability of shared output responses in pairs of unlabeled L2/3 pyramidal neurons from unknown progenitors (two-tailed Mann-Whitney U test, unlabeled pairs: 0.68 ± 0.07, n = 13 PV interneurons from 8 unlabeled pairs and 5 animals, IP-derived and OP-derived pairs: 0.48 ± 0.05, n = 30 PV interneurons from 10 IP-derived and OP-derived pairs and 6 animals, P = 0.02, U = 278.5; **Figure 4.5d**). Furthermore, similar to the spontaneous measurements (**Figure 4.5e**), progenitor type was associated with greater variability in shared output responses. IP-derived and OP-derived pairs had greater differences in response amplitudes than unlabeled pairs (two-tailed Mann-Whitney U test, unlabeled pairs: 74.13 ± 17.84 %, n = 13 PV interneurons from 8 unlabeled pairs and 5 animals, IP-derived and OP-derived pairs: 130.50 ± 10.68 %, n = 30 PV interneurons from 10 IP-derived and OP-derived pairs and 6 animals, P = 0.01, U = 102; **Figure 4.7e**).

These differences in the output of interneurons were not associated with differences in mean IPSC amplitude between the pair types (two-tailed unpaired t-test, unlabeled mean: 51.59 ± 7.36 pA, n = 8 pairs from 5 animals, IP-derived and OP-derived mean: 68.10 ± 14.76 pA, n = 10 pairs from 6 animals, P = 0.37, T = -0.93; **Figure 4.7f**). Similarly, there was no difference in inter-somatic distances between pair types (two-tailed unpaired t-test, unlabeled pairs: 56.88 ± 6.68 μm, n = 8 pairs of unlabeled neurons from 5 animals, IP-derived and OP-derived neuron pairs: 65.00 ± 6.83 μm, n = 10 pairs of IP-derived and OP-derived neurons from 6 animals, P = 0.41, T = -0.84; **Figure 4.7g**) or the distance to pia (two-tailed unpaired t-test, unlabeled mean: 309.69 ± 22.62 μm, n = 8 pairs from 5 animals, IP-derived and OP-derived mean: 274.25 ± 21.89 μm, n = 10 pairs from 6 animals, P = 0.28, T = 1.12; **Figure 4.7h**) (two-tailed paired t-test, OP-derived neurons: 266.00 ± 22.49 μm, IP-derived neurons: 282.50 ± 22.38 μm, n = 10 pairs from 6 animals, P = 0.61, T = -0.52; **Figure 4.7i**). Thus, PV interneurons exhibit biased connectivity to postsynaptic pyramidal neurons derived from different progenitor types. Taken together, these results suggest that progenitor type specifies a L2/3 pyramidal neuron's local inhibitory subnetwork, by defining the degree to which the pyramidal neuron shares local inhibitory synaptic input with neighbouring pyramidal neurons.

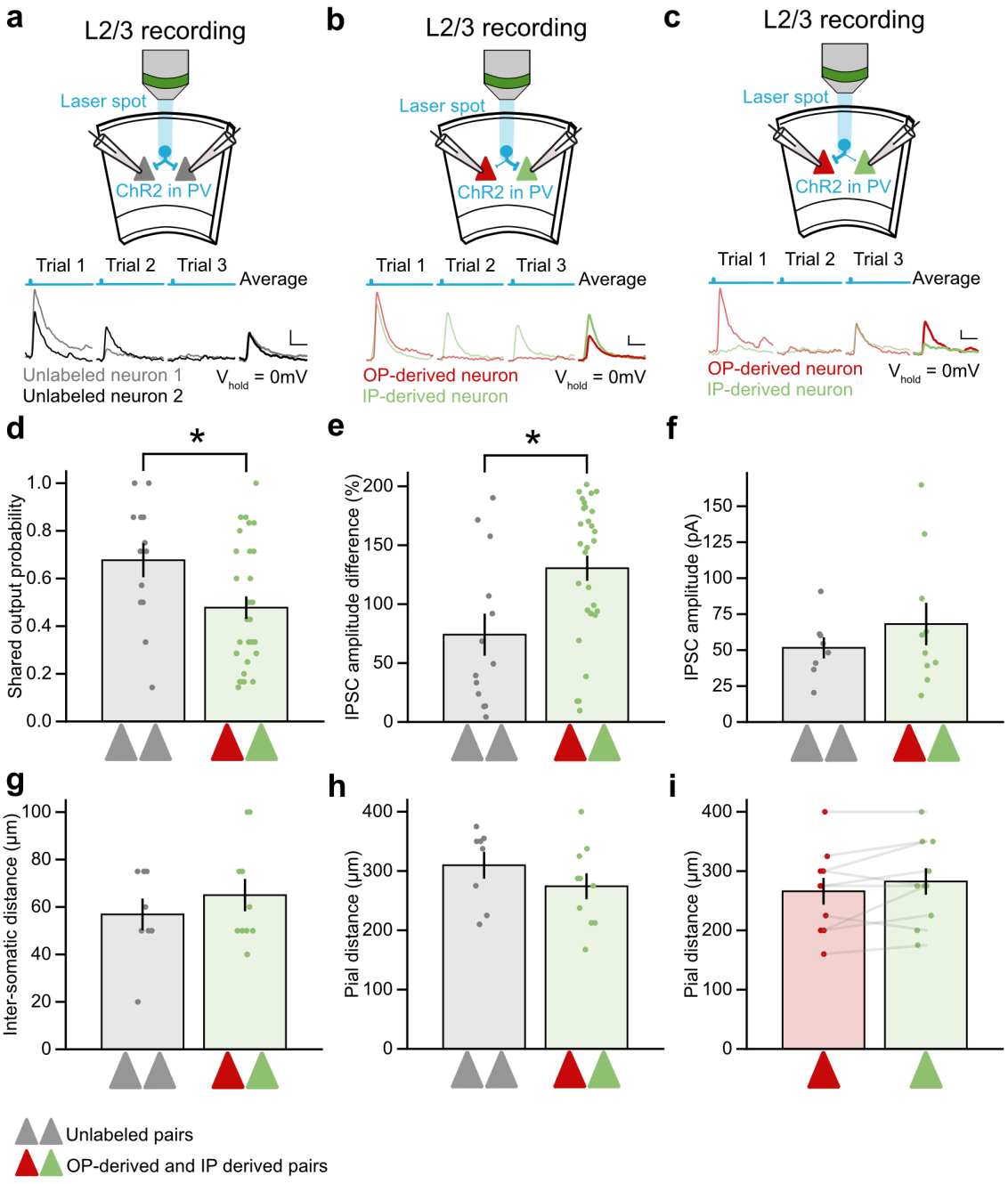

a
L2/3 recording
Laser spot
ChR2 in PV
Trial 1
Trial 2
Trial 3
Average
Unlabeled neuron 1
Unlabeled neuron 2
V hold = 0mV
b
L2/3 recording
Laser spot
ChR2 in PV
Trial 1
Trial 2
Trial 3
Average
OP-derived neuron
IP-derived neuron
V hold = 0mV
c
L2/3 recording
Laser spot
ChR2 in PV
Trial 1
Trial 2
Trial 3
Average
OP-derived neuron
IP-derived neuron
V hold = 0mV
d
Shared output probability
1.0
0.8
0.6
0.4
0.2
0.0
*
e
IPSC amplitude difference (%)
200
150
100
50
0
*
f
IPSC amplitude (pA)
150
125
100
75
50
25
0
g
Inter-somatic distance (µm)
100
80
60
40
20
0
h
Pial distance (µm)
400
300
200
100
0
i
Pial distance (µm)
400
300
200
100
0
Unlabeled pairs
OP-derived and IP derived pairs

Figure 4.7: Interneurons differentially target L2/3 pyramidal neurons based on post-synaptic progenitor type. (**a**) Monosynaptic IPSCs were simultaneously recorded from pairs of unlabeled pyramidal neurons, whilst a laser was used to focally activate pre-synaptic ChR2-expressing PV interneurons (top). PV interneurons were minimally stimulated to produce a mix of successes and failures in post-synaptic responses. Example trials are from a pair of unlabeled L2/3 pyramidal neurons (bottom). Scale bar 50 pA, 25 ms. (**b**) As in 'a', but recordings were performed from a pair comprising an IP-derived and an OP-derived neuron. Example trials are where the IP-derived neuron received biased input. Scale bar, 50 pA, 25 ms. (**c**) As in 'b', but example trials are where the OP-derived neuron received biased input. Scale bar, 50 pA, 25 ms. (**d**) The probability of observing a shared output was lower in IP-derived and OP-derived neuron pairs, than for unlabeled neuron pairs (two-tailed Mann-Whitney U test, n = 13 PV interneurons from 8 unlabeled pairs and 5 animals, n = 30 PV interneurons from 10 IP-derived and OP-derived pairs and 6 animals, P = 0.02, U = 278.5). (**e**) The IPSC amplitude difference for shared inhibitory inputs (expressed as a percentage of the mean response amplitude) was greater for pairs comprising an IP-derived and OP-derived neuron, compared to pairs comprising two unlabeled neurons (two-tailed Mann-Whitney U test, n = 13 PV interneurons from 8 pairs and 5 animals, n = 30 PV interneurons from 10 pairs and 6 animals, P = 0.01, U = 102). (**f**) Mean IPSC amplitude does not differ between unlabeled pairs and IP-derived and OP-derived pairs (two-tailed unpaired t-test, n = 8 unlabeled pairs from 5 animals, n = 10 IP-derived and OP-derived pairs from 6 animals, P = 0.37, T = -0.93). (**g**) Inter-somatic distance was not different between the pair types (two-tailed unpaired t-test, n = 8 unlabeled pairs from 5 animals, n = 10 IP-derived and OP-derived pairs from 6 animals, P = 0.41, T = -0.84). (**h**) Pial distance does not differ between unlabeled pairs and IP-derived and OP-derived pairs (two-tailed unpaired t-test, n = 8 unlabeled pairs from 5 animals, n = 10 IP-derived and OP-derived pairs from 6 animals, P = 0.28, T = 1.12). (**i**) Pial distance was not different between the IP-derived and OP-derived neurons (two-tailed paired t-test, n = 10 pairs from 6 animals, P = 0.61, T = -0.52).

4.3 Discussion

In this chapter, a combination of *in utero* labelling, *in vitro* electrophysiology and optogenetics was used to assess the inhibitory input to progenitor-defined populations of L2/3 pyramidal neurons. The data support the conclusion that progenitor type influences the inhibitory input that a L2/3 pyramidal neuron receives. Whilst progenitor type did not influence the overall level of synaptic inhibition received, it did shape the extent to which L2/3 pyramidal neurons receive common inhibitory input from shared presynaptic PV interneurons.

The finding that IP-derived neurons reside further from the pial surface than simultaneously labelled OP-derived neurons is consistent with previous work, and supports the idea that the OP population comprise self-renewing RGCs (Stancik et al., 2010; Tyler and Haydar, 2013). Despite there being differences on average, these two neuron populations exhibit significant overlap within L2/3 and therefore confirm the idea that neighbouring pyramidal neurons can be derived from different developmental trajectories (Ellender et al., 2019; Guillamon-Vivancos et al., 2019; Tyler et al., 2015). As distance from pia was controlled across all experiments, the observed differences in connectivity are unlikely to be attributed to differences in sub-layer or birth date. Given previous reported differences in connectivity patterns between pyramidal neurons in layers 2 and 3, it is interesting to consider whether such differences could be attributed to different progenitor outputs contributing to each of these sub-layers (Audette et al., 2018; Brecht et al., 2003; Bureau et al., 2006; Karimi et al., 2020; Lefort and Petersen, 2017; Meyer et al., 2011; Shepherd and Svoboda, 2005). Therefore, progenitor type may act as a mechanism that contributes towards the generation of subnetworks in cortex.

The IP-derived progenitor population examined in this study was further characterised in order to better define the progenitors labelled by the Tα1 promoter. It was found that the IP-derived pTα1+ neuronal population can be further subdivided into two lineages based on whether the progenitor also exhibits Tbr2 promoter activity. It is appreciated that given the labelling strategy used, in which Tα1 or Tbr2 promoter activity in a cell permanently switches on the reporter expression in all subsequent progeny, one interpretation of these findings is that pTbr2+ bIPs

are pTα1+ because they are derived from a pTα1+ aIP. However, this outcome is unlikely for several reasons. Firstly, for bIPs to be derived from aIPs they would need to undergo an extra round of division, which would presumably influence the respective distances from pia of the neuronal progeny. It was found that neurons derived from pTα1+ pTbr2+ lineages and pTα1+ pTbr2- lineages resided at similar distances from pia, suggesting these progenitor types undergo a similar number of divisions. Secondly, similar results have been previously reported using constructs which did not use recombination of a constitutive reporter construct (Tyler and Haydar, 2013). In this study the authors used a labelling strategy where the reporter is turned off if the promoter is no longer active in the cell. This therefore suggests that the Tα1 and Tbr2 promoters are simultaneously active in bIPs. Taken together, these results support the conclusion that pTα1+ progenitors comprise a population of progenitors consisting of aIPs and bIPs. In future work it would be interesting to explore how the neuronal output of aIPs and bIPs relate to one another.

Having established a dual-labelling strategy of a defined progenitor population, I tested the inhibitory synaptic input received by IP-derived and OP-derived L2/3 neurons using multiple experimental paradigms. Firstly, the total inhibitory synaptic input from 3 defined interneuron subtypes to IP-derived and OP-derived L2/3 neurons was tested using a widefield optogenetic stimulation strategy. It was found that IP-derived and OP-derived L2/3 neurons received similar overall levels of input from PV, SST and VIP interneurons. This optogenetic method activates all interneurons belonging to the subtype at the same time (Safari et al., 2017; Xue et al., 2014). Importantly, this experiment does not test whether these pyramidal populations are inhibited by the same individual interneurons within a subtype. To measure this, spontaneous inhibitory inputs were simultaneously recorded from pairs of neurons and the amount of shared synaptic inhibition was compared across the neuron types. Pairs of neurons which contained at least one IP-derived neuron shared less of their synaptic inhibition than other pair types, suggesting that IP-derived neurons tend to be inhibited independently of one another within their inhibitory network. This was supported by further optogenetic experiments, which found that PV interneurons exhibited biased targeting of L2/3 postsynaptic pyramidal neurons based on their progenitor type.

Taken together, these findings suggest that the pool of interneurons from which a pyramidal neuron samples its presynaptic input, can be shaped by the pyramidal neuron's progenitor type. Specifically, it seems to be a feature of IP-derived neurons to share less of their synaptic inhibition with neighboring pyramidal neurons. Synaptic inhibition is primarily recruited locally from the home layer, with contributions from other layers in the same cortical area (Helmstaedter et al., 2009b; Kätzel et al., 2010). Interestingly, studies have demonstrated there is considerable variation in how neighbouring pyramidal neurons recruit synaptic inhibition across cortical layers and columns (Kätzel et al., 2010). Consequently, layer-specific distinctions may exist in how IP-derived neurons recruit their inhibitory inputs. Considering that there may be at least 10 transcriptomic subtypes of PV interneurons across the cortical layers (Tasic et al., 2018), one could imagine a mechanism whereby IP-derived neurons preferentially receive inhibitory input from particular PV transcriptomic subtypes. This preference could be orchestrated by the cell-type-specific expression of cadherins (Basu et al., 2015; Duan et al., 2018; Sun et al., 2021; Földy et al., 2016), which are known to reflect the embryonic origin of cortical pyramidal neurons (Lv et al., 2022; Tarusawa et al., 2016). Interestingly, recent evidence points towards a similar mechanism in L5 pyramidal neuron subtypes, which display segregated PV interneuron subnetworks (Jézéquel et al., 2023).

The differential sampling of synaptic inhibition by IP-derived neurons may serve multiple functions. For instance, synaptic inhibition can act to both desynchronise and coordinate the activity of pyramidal neurons (Bush and Sejnowski, 1996; Chini et al., 2022; Hasenstaub et al., 2005; Lytton and Sejnowski, 1991; Sippy and Yuste, 2013; Stringer et al., 2016; Vreeswijk et al., 1994). One theory that reconciles these opposing functions would be that activation across a large number of interneurons would unanimously control pyramidal neuron activity. Conversely, select activation of a single or few PV interneurons would desynchronise activity based upon the specific connection patterns of the interneurons that are activated. Sharing fewer inhibitory inputs with neighboring neurons may therefore enhance this decorrelation effect, increasing the information that can be represented by a population of neurons (Ecker et al., 2011; Panzeri et al., 2022). This may direct information flow through cortical circuits in a subnetwork-specific manner, shaping the response properties of

individual neurons. An interesting idea to consider is that an individual neuron's participation in local circuits reflects their long-range inputs and outputs (Brown and Hestrin, 2009; Kiritani et al., 2012; Morishima et al., 2011; Morishima and Kawaguchi, 2006; Otsuka and Kawaguchi, 2008; Sato and Svoboda, 2010). It is well described that inhibitory interneurons are recruited by feedback projections from higher order cortex (D'Souza et al., 2019; Naskar et al., 2021; Wall et al., 2016). These feedback projections modulate processing in local circuits, gate plasticity, and shape the representation of sensory information (Audette et al., 2018; Bullier et al., 2001; Naskar et al., 2021; Petreanu et al., 2009; Sermet et al., 2019; Williams and Holtmaat, 2019; Zagha et al., 2013). It is so far unknown if IP-derived and OP-derived L2/3 neurons are recruited to a similar extent by such feedback projections.

Overall, this chapter has shown that the extent to which pyramidal neurons share inhibitory synaptic inputs is influenced by the progenitor type from which they are derived. Given the strong recruitment of synaptic inhibition by feedback projections and the relationship between local and long-range connectivity, it is possible that these differences in local inhibitory connections may reflect specific feedback pathways from higher-order cortical areas. This possibility will be explored in the next chapter.

5 | Cortical feedback onto progenitor-defined L2/3 pyramidal neurons

5.1 Introduction

Perhaps the most distinctive feature of the cerebral cortex is its stereotyped columnar structure, which comprises laminar-specific patterns of connectivity between defined excitatory and inhibitory cell types (Harris and Mrsic-Flogel, 2013; Harris and Shepherd, 2015). The conservation of specific connectivity patterns across cortical areas has led to the idea of the canonical cortical microcircuit, which is thought of as the basic processing unit of the cortex (Douglas et al., 1989; Gilbert, 1983; Gilbert and Wiesel, 1983). The canonical circuit performs computations on incoming information, which it then outputs to another brain area via long-range projections. Typically, the main direction of information flow through the cortex is feedforward, beginning at so-called 'lower order' brain areas, such as primary sensory cortices, and progressively ascending towards increasingly 'higher order' brain areas, such as the association cortices. These higher order cortical areas send extensive feedback projections to lower order cortical areas from which they receive input from (Aronoff et al., 2010; Chen et al., 2013; Condylis et al., 2020; Gilbert and Sigman, 2007; Kinnischtzke et al., 2014; Kwon et al., 2016; Minamisawa et al., 2018; Miyashita et al., 1994; Porter and White, 1983; White and DeAmicis, 1977; Yang et al., 2015). Within lower order cortical areas, feedback projections engage a variety of excitatory and inhibitory cell types (Kinnischtzke et al., 2014; Naskar et al., 2021; Petreanu et al., 2009) and modulate ongoing sensory processing in a manner that is thought to be necessary for perception, attention and plasticity (Bastos et al., 2012; Condylis et al., 2020; Gilbert and Li, 2013; Larkum et al., 2004; Yang et al., 2015). Taken together, feedback projections represent a key part of sensory processing, although the specific ways in which these feedback projections engage

different cortical cell types is relatively unexplored.

Two of the main cortical projection targets of L2/3 pyramidal neurons in barrel cortex of S1 are secondary somatosensory cortex (S2) and primary motor cortex (M1) (Alloway et al., 2004; Aronoff et al., 2010; Chakrabarti and Alloway, 2006; Hoffer et al., 2003; Mao et al., 2011). These areas are targeted by largely non-overlapping groups of L2/3 pyramidal neurons that display distinct roles in sensory processing (Chen et al., 2013, 2015; Yamashita et al., 2013). In return, these higher order cortical areas send feedback projections back to S1, recruiting L2/3 pyramidal neurons and local interneurons to varying degrees (Aronoff et al., 2010; Denardo et al., 2015; Kinnischtzke et al., 2014; Mao et al., 2011; Naskar et al., 2021). Several studies have imaged the activity of M1 or S2 projections in S1 during sensory driven behavioural tasks, leading to categorisation of the types of feedback signals that these projections provide to lower-order cortical areas (Chen et al., 2015; Kwon et al., 2016; Minamisawa et al., 2018; Petreanu et al., 2012; Yang et al., 2015). M1 feedback projections to S1 convey contextual information about whisker movements, which is thought to assist object location (Petreanu et al., 2012). S2 feedback projections, on the other hand, encode decision choices to guide perceptual learning and refine receptive field properties (Chen et al., 2015; Condylis et al., 2020; Kwon et al., 2016; Minamisawa et al., 2018; Yang et al., 2015). However, it is unknown how these feedback projections integrate into previously described L2/3 pyramidal subnetworks (Ellender et al., 2019; Kampa et al., 2006; Yoshimura et al., 2005) (**Chapters 3** and **4**).

Connections within a single cortical column can also be thought of as feedforward or feedback. For example, the major feedforward component of the canonical circuit begins with sensory input arriving at thalamocortical afferents in L4, the input layer to the cortical column. L4 neurons primarily synapse onto L2/3 pyramidal neurons, which send cortico-cortical projections as well as feedforward inputs to L5 (Douglas and Martin, 2004; Hooks et al., 2011; Lefort et al., 2009; Shepherd and Svoboda, 2005; Thomson and Lamy, 2007). L5 is typically thought of as the main output layer of the cortex, containing pyramidal neurons that project to cortical and subcortical targets (Douglas and Martin, 2004; Feldmeyer, 2012; Harris and Shepherd, 2015). Importantly, L5 pyramidal neurons also send axon collaterals

superficially within the same cortical column, providing monosynaptic excitation and recruiting local disynaptic inhibition onto L2/3 pyramidal neurons (Hage et al., 2022; Kätzel et al., 2010; Oberlaender et al., 2012; Onodera and Kato, 2022; Shepherd et al., 2005; Shepherd and Svoboda, 2005; Vecchia et al., 2020; von Klemperer, 2021). These feedback connections from L5 to L2/3 are thought to increase the precision of temporal coding by L2/3 pyramidal neurons (Onodera and Kato, 2022; Vecchia et al., 2020), but the full extent of their role in L2/3 sensory processing is not yet understood (von Klemperer, 2021). Whilst feedforward connections from L2/3 to L5 can exhibit fine-scale specificity (Ellender et al., 2019; Kampa et al., 2006), it is unknown if this specificity is reflected in the feedback connections from L5 to L2/3.

In summary, feedback connections represent a major role in sensory processing, allowing the integration of contextual signals into local circuits. The recognised differences in excitatory and inhibitory subnetworks between IP-derived and OP-derived L2/3 neurons could position them to route different information streams through cortical circuits, such as feedforward and feedback information. Therefore, this chapter will use a combination of *in utero* labelling, optogenetics and *in vitro* electrophysiology techniques to test whether IP-derived and OP-derived L2/3 neurons receive different amounts of monosynaptic excitation and disynaptic inhibition from L5 of S1, from S2, or from M1. The aims of this chapter are as follows:

- To investigate whether progenitor type influences the amount of feedback that a L2/3 pyramidal neuron receives from L5 of primary somatosensory cortex
- To investigate whether progenitor type influences the amount of feedback that a L2/3 pyramidal neuron receives from S2
- To investigate whether progenitor type influences the amount of feedback that a L2/3 pyramidal neuron receives from M1

5.2 Results

5.2.1 The recruitment of progenitor-defined L2/3 pyramidal populations by local layer 5 feedback

One potential explanation for the observations from **Chapter 4** is that biases in the local circuitry of L2/3 pyramidal neurons reflect differences in their level of cortical feedback. To investigate this, an optogenetic approach was used to determine whether the level of feedback from L5 to L2/3 depends on the progenitor type from which the L2/3 pyramidal neurons are derived. The dual-colour Flpo recombinase system described in **Chapter 4.2.1** was used to label IP-derived and OP-derived L2/3 pyramidal neurons. This was performed in mice that were a cross between RBP4-Cre and Floxed-ChR2 transgenic mouse lines (**Figure 5.1a**). These mice therefore expressed ChR2 in L5 pyramidal neurons throughout cortical areas (Gerfen et al., 2013) (**Figure 5.1a**). Animals that had undergone IUE were allowed to reach maturity (P28-42) and acute slices were prepared from S1 to allow for simultaneous whole-cell patch-clamp recordings from neuronal pairs comprising a GFP-expressing IP-derived L2/3 pyramidal neuron, and a neighbouring TdTomato-expressing OP-derived L2/3 pyramidal neuron (mean intersomatic distance of 58.95 ± 5.35 μm). In a subset of experiments, neurons were filled with biocytin and visualised post-hoc to confirm their pyramidal identity (**Figure 5.1b**). Activation of L5 pyramidal neurons with brief pulses of a widefield LED (473 ms, 1 ms duration) produced monosynaptic excitation of L2/3 pyramidal neurons via axon collaterals ($EPSC_{L5}$), in addition to disynaptic inhibition ($IPSC_{L5}$) through the recruitment of local inhibitory circuits in L2/3 (Vecchia et al., 2020). To confirm that light-evoked responses were dependent on glutamatergic synaptic transmission, 10 μM NBQX was added to the recording solution, which successfully blocked the monosynaptic $EPSC_{L5}$ and disynaptic $IPSC_{L5}$ (**Figure 5.1b**). Furthermore, the mean $EPSC_{L5}$ latency was 8.70 ± 0.15 ms, which was significantly shorter than mean $IPSC_{L5}$ latency of 11.58 ± 0.33 ms (two-tailed paired t-test, n = 40 pairs of neurons, P = 1.14*e-10, T = 8.77; **Figure 5.1c**), and consistent with the recruitment of dysynaptic inhibition (Pouille and Scanziani, 2001).

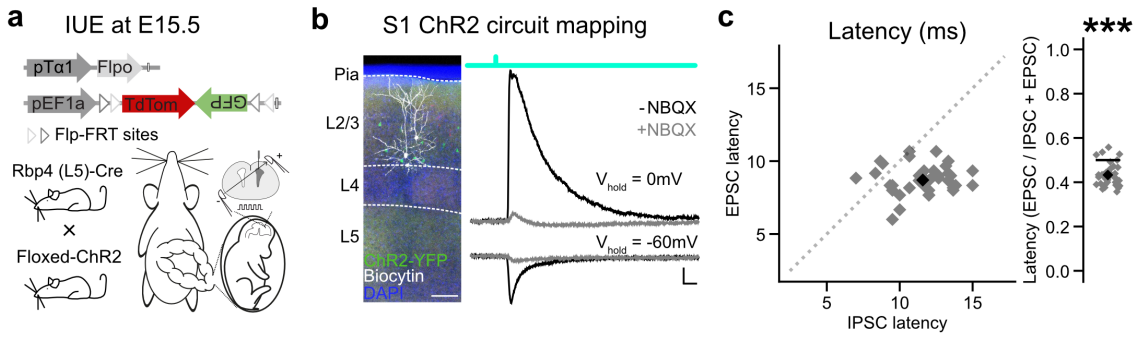


Figure 5.1: Investigating the recruitment of progenitor-defined L2/3 pyramidal populations by local layer 5 feedback. (**a**) Excitatory neuron IUE at E15.5 was used to label IP-derived and OP-derived neurons in transgenic mice expressing ChR2 in L5 pyramidal neurons. (**b**) Simultaneous whole-cell patch-clamp recordings were performed from pairs of neighboring IP-derived and OP-derived L2/3 neurons at P28-42. In a subset of recordings, neurons were filled with biocytin to confirm their pyramidal identity (left). Scale bar, 100 μm. Brief, widefield light pulses from an LED (473 nm, 1ms) were used to activate ChR2-expressing layer 5 pyramidal neurons (right). Blockade of AMPA receptors using 10 μm NBQX abolished the evoked monosynaptic EPSC and disynaptic IPSC almost completely. Scale bar, 100 pA, 25 ms. (**c**) The latency from LED onset to response start time was shorter for EPSCs than for IPSCs, consistent with the recruitment of disynaptic inhibition (two-tailed paired t-test, n = 40 pairs of neurons, P = 1.14*e^{-10}, T = 8.77).

Activation of ChR2 evoked large EPSC$_{L5}$ and IPSC$_{L5}$ responses across neurons, consistent with previous work that feedback projections from L5 recruit L2/3 pyramidal neurons (Bureau et al., 2006; Hage et al., 2022; Shepherd et al., 2005; Shepherd and Svoboda, 2005; Vecchia et al., 2020). To test whether L5 feedback depended on progenitor type, the amplitudes of the responses were compared between simultaneously recorded IP-derived and OP-derived L2/3 neurons. The mean EPSC$_{L5}$ amplitude was comparable in IP-derived and OP-derived L2/3 neurons (two-tailed Wilcoxon signed rank test, IP-derived mean: 150.13 ± 18.43 pA, OP-derived mean: 172.35 ± 19.60 pA, n = 22 pairs from 8 animals, P = 0.39, W = 99; **Figure 5.2a**). In agreement with previous observations (Hage et al., 2022; Onodera and Kato, 2022; Vecchia et al., 2020; von Klemperer, 2021), the IPSC$_{L5}$ was larger than the EPSC$_{L5}$, but again did not differ by progenitor type (two-tailed paired t-test, IP-derived mean: 598.36 ± 71.01 pA, OP-derived mean: 554.47 ± 71.01 pA, n = 22 pairs from 8 animals, P = 0.55, T = -0.61; **Figure 5.2b**). To determine the overall level of excitation recruited relative to inhibition for each neuron type, the excitatory to inhibitory (E/I) ratio was calculated. The E/I ratio did not differ between IP-derived and OP-derived L2/3 neurons (two-tailed paired t-test, IP-derived mean:

0.22 ± 0.02, OP-derived mean: 0.27 ± 0.04, n = 18 pairs from 8 animals, P = 0.28, T = 1.12; **Figure 5.2c**). To confirm that there was no confound associated with soma location of the recorded neurons, their distance from pia was measured and found to not vary between the two conditions (two-tailed paired t-test, IP-derived mean: 283.61 ± 21.88 μm, OP-derived mean: 277.22 ± 24.85 μm, n = 18 pairs from 8 animals, P = 0.40, T = 0.86; **Figure 5.2d**). These results suggest that the progenitor type from which L2/3 pyramidal neurons are derived, does not influence local feedback from L5.

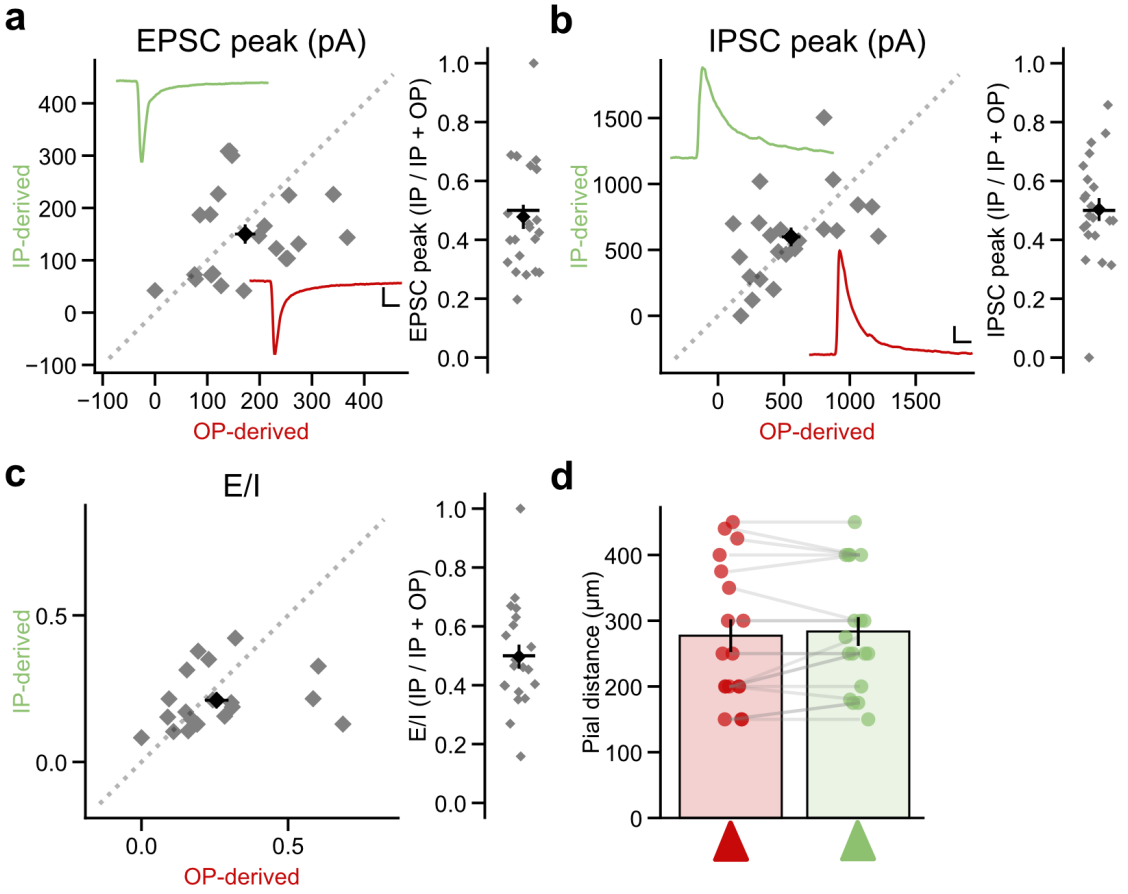


Figure 5.2: Feedback from layer 5 does not differ depending upon a L2/3 pyramidal neuron's progenitor type. (**a**) $EPSC_{L5}$ peak amplitude did not differ between simultaneously recorded IP-derived and OP-derived L2/3 neurons (two-tailed Wilcoxon signed-rank test, n = 22 pairs from 8 animals, P = 0.39, W = 99). Scale bar 50 pA, 25 ms. (**b**) $IPSC_{L5}$ peak amplitude did not differ between simultaneously recorded IP-derived and OP-derived neurons (two-tailed paired t-test, n = 22 pairs from 8 animals, P = 0.55, T = -0.61). Scale bar 50 pA, 25ms. (**c**) The ratio of $EPSC_{L5}$ to $IPSC_{L5}$ peak amplitudes (E/I) did not differ between IP-derived and OP-derived neurons (two-tailed paired t-test, n = 18 pairs from 8 animals, P = 0.28, T = 1.12). (**d**) Distance from pia did not differ between IP-derived and OP-derived neurons (two-tailed paired t-test, n = 18 pairs from 8 animals, P = 0.40, T = 0.86).

5.2.2 The recruitment of progenitor-defined L2/3 pyramidal populations by secondary somatosensory cortex

I next tested whether progenitor type influences the level of feedback that a S1 L2/3 pyramidal neuron receives from S2. To do so, IUE was used at E15.5 to label IP-derived and OP-derived L2/3 neurons using the dual-colour Flpo recombinase system previously described (**Chapter 4.2.1**; **Figure 5.3a**). Once these mice had reached maturity (P28), an intracranial injection was performed to deliver ChR2 (pAAV-hSyn-ChR2(H134R)-EYFP) into S2 (**Figure 5.3b**). Injection specificity (i.e. the percentage of ChR2 expression within S2) was calculated post-hoc and had a mean of 76.80 ± 5.47 % (n = 2 animals). Two weeks following the injection, acute slices were prepared from S1 to allow for simultaneous whole-cell patch-clamp recordings from neuronal pairs comprising an IP-derived L2/3 pyramidal neuron, and a neighbouring OP-derived L2/3 pyramidal neuron (mean intersomatic distance of 71.00 ± 8.12 μm). ChR2-expressing S2 axons were activated using an LED (473 nm, 500 μs duration) and the resulting monosynaptic EPSC ($EPSC_{S2}$) and disynaptic IPSC ($IPSC_{S2}$) were recorded. In a subset of experiments, neurons were filled with biocytin and visualised post-hoc to confirm their pyramidal identity (**Figure 5.3c**). To establish that light-evoked responses were dependent upon glutamatergic synaptic transmission, 10 μM NBQX was added to the recording solution, which successfully blocked the monosynaptic $EPSC_{S2}$ and disynaptic $IPSC_{S2}$ (**Figure 5.3c**). Furthermore, the mean $EPSC_{S2}$ latency was 4.32 ± 0.20 ms, which was significantly shorter than the mean $IPSC_{S2}$ latency of 6.06 ± 0.65 ms (two-tailed paired t-test, n = 10 pairs of neurons, P = 0.006, T = 3.49; **Figure 5.3d**), and consistent with the recruitment of disynaptic inhibition (Pouille and Scanziani, 2001).

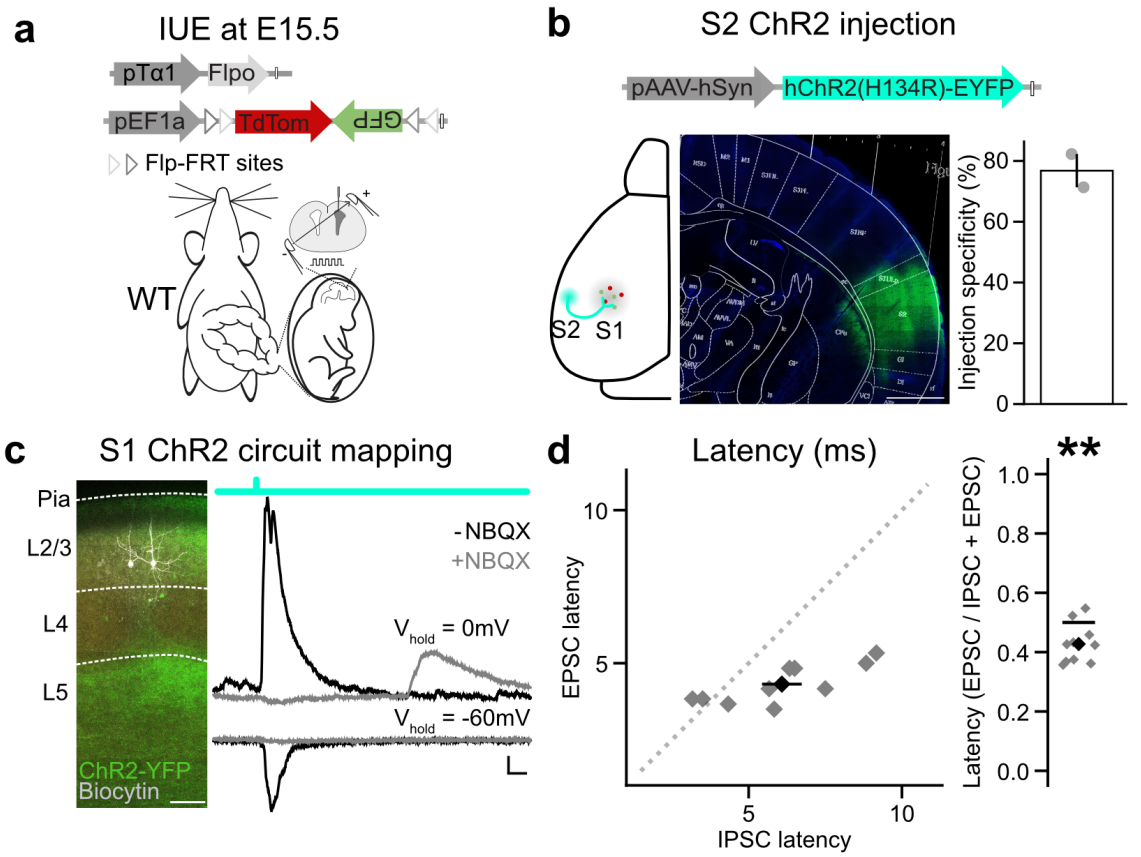


Figure 5.3: Investigating the recruitment of progenitor-defined L2/3 pyramidal populations by feedback from S2. (**a**) Excitatory neuron IUE at E15.5 was used to label IP-derived and OP-derived neurons. (**b**) At P28, animals received an injection of a ChR2 virus (pAAV-hSyn-hChR2(H134R)-EYFP) into S2. Average injection specificity was 76.80 ± 5.47 % (n = 2 animals). Scale bar 1 mm. (**c**) Simultaneous whole-cell patch-clamp recordings were performed from pairs of neighboring IP-derived and OP-derived neurons at P35-42. In a subset of recordings, neurons were filled with biocytin to confirm their pyramidal identity (left). Scale bar, 100 μm. Brief, widefield light pulses from an LED (473 nm, 500 μs) were used to activate ChR2-expressing S2 fibres. Blockade of AMPA receptors using 10 μm NBQX abolished the evoked monosynaptic EPSC and disynaptic IPSC. Scale bar, 50 pA, 25 ms. (**d**) The latency from LED onset to response start time was shorter for EPSCs than for IPSCs (two-tailed paired t-test, n = 10 pairs of neurons, P = 0.006, T = 3.49).

Activation of ChR2-expressing S2 axons evoked responses of varying amplitudes across IP-derived and OP-derived L2/3 neurons. However, there was no systematic bias in $EPSC_{S2}$ according to progenitor type (two-tailed paired t-test, IP-derived mean: 197.69 ± 101.56 pA, OP-derived mean: 157.93 ± 47.58 pA, n = 5 pairs from 4 animals, P = 0.54, T = -0.66; **Figure 5.4a**). Disynaptic $IPSC_{S2}$ responses were larger than the monosynaptic $EPSC_{S2}$ responses and these were also comparable between progenitor types (two-tailed Wilcoxon signed rank test, IP-derived mean: 775.33 ± 315.67 pA, OP-derived mean: 614.88 ± 214.47 pA, n = 5 pairs from 4

animals, W = 5, P = 0.63; **Figure 5.4b**). Furthermore, the E/I ratio was similar across IP-derived and OP-derived L2/3 neurons (two-tailed paired t-test, IP-derived mean: 0.19 ± 0.08, OP-derived mean: 0.21 ± 0.04, n = 5 pairs from 4 animals, T = 0.45, P = 0.67; **Figure 5.4c**) and distance from pia was comparable for each neuron type (two-tailed paired t-test, IP-derived mean: 292.00 ± 46.63 μm, OP-derived mean: 288.00 ± 47.48 μm, n = 5 pairs from 4 animals, P = 0.72, T = 0.39; **Figure 5.4d**). These results suggest that feedback from S2 to S1 L2/3 pyramidal neurons does not depend upon the progenitor from which the L2/3 pyramidal neurons are derived.

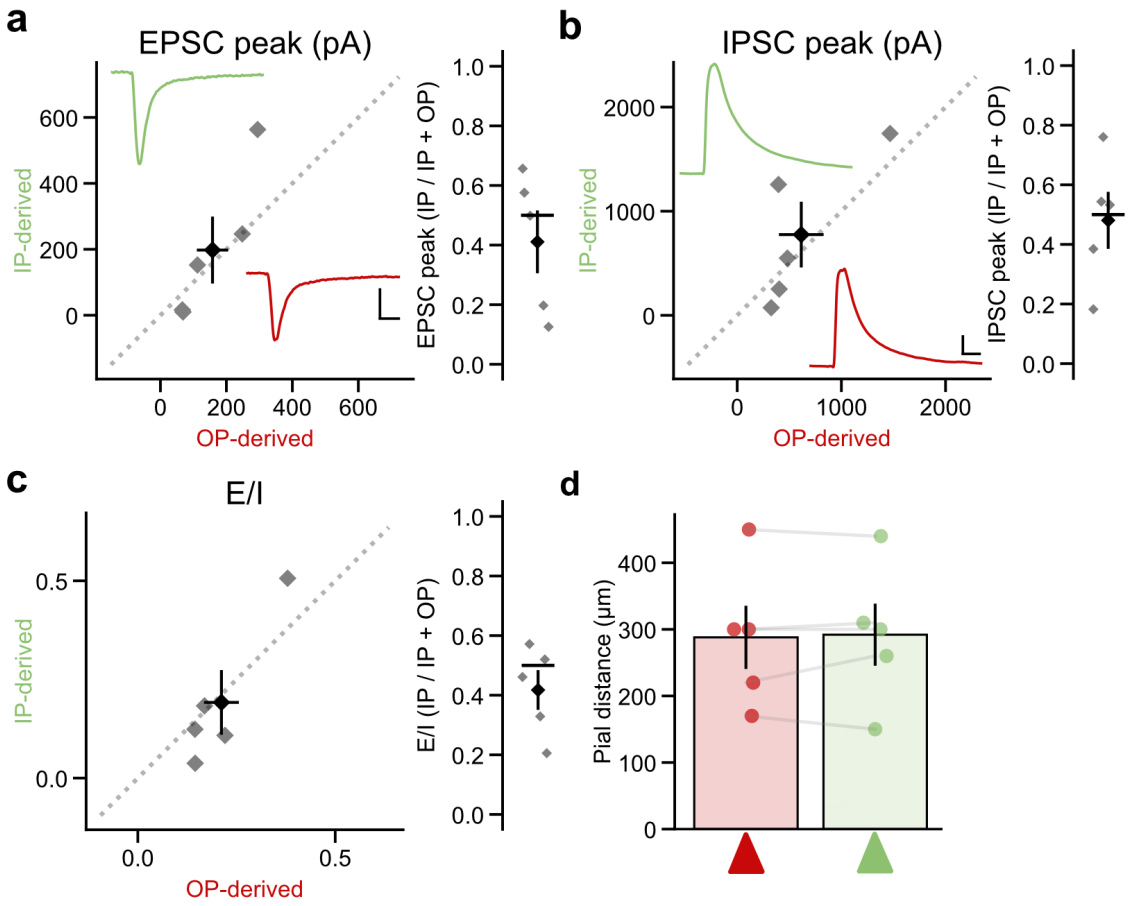


Figure 5.4: Feedback from S2 does not differ depending upon a S1 L2/3 pyramidal neuron's progenitor type. (**a**) $EPSC_{S2}$ peak amplitude did not differ between simultaneously recorded IP-derived and OP-derived neurons (two-tailed paired t-test, n = 5 pairs from 4 animals, P = 0.54, T = -0.66). Scale bar 50 pA, 25 ms. (**b**) $IPSC_{S2}$ peak amplitude did not differ between simultaneously recorded IP-derived and OP-derived neurons (two-tailed Wilcoxon signed-rank test, n = 5 pairs from 4 animals, P = 0.63, W = 5). Scale bar 50 pA, 25ms. (**c**) The ratio of $EPSC_{S2}$ to $IPSC_{S2}$ peak amplitudes (E/I) did not differ between IP-derived and OP-derived neurons (two-tailed paired t-test, n = 5 pairs from 4 animals, P = 0.67, T = 0.45). (**d**) Distance from pia did not differ between IP-derived and OP-derived neurons (two-tailed paired t-test, n = 5 pairs from 4 animals, P = 0.72, T = 0.39).

5.2.3 The recruitment of progenitor-defined L2/3 pyramidal populations by primary motor cortex

Finally, I tested whether progenitor type influences the level of feedback that a S1 L2/3 pyramidal neuron receives from M1. To do so, IUE was used at E15.5 to label IP-derived and OP-derived L2/3 neurons using the dual-colour Flpo recombinase system previously described (**Chapter 4.2.1**; **Figure 5.5a**). Once these mice had reached maturity (P28), an intracranial viral injection was performed in order to express ChR2 (pAAV-hSyn-ChR2(H134R)-EYFP) in M1 (**Figure 5.5b**). Injection specificity (i.e. the percentage of ChR2 expression within M1) was calculated post-hoc and had a mean of 83.55 ± 5.11 % (n = 6 animals). Two weeks following the injection, acute slices were prepared from S1 to allow for simultaneous whole-cell patch-clamp recordings from neuronal pairs comprising an IP-derived L2/3 pyramidal neuron, and a neighbouring OP-derived L2/3 pyramidal neuron (mean intersomatic distance of 68.46 ± 5.11 μm). ChR2-expressing M1 axons were activated using an LED (473 nm, 500 μs duration) and the resulting monosynaptic EPSC ($EPSC_{M1}$) and disynaptic IPSC ($IPSC_{M1}$) were recorded. In a subset of experiments, neurons were filled with biocytin and visualised post-hoc to confirm their pyramidal identity (**Figure 5.5c**). To confirm that light-evoked responses were dependent on glutamatergic synaptic transmission, 10 μM NBQX was added to the recording solution, which successfully blocked the monosynaptic $EPSC_{M1}$ and disynaptic $IPSC_{M1}$ (**Figure 5.5c**). Furthermore, the mean $EPSC_{M1}$ latency was 5.56 ± 0.48 ms, which was significantly shorter than the mean $IPSC_{S2}$ latency of 8.15 ± 0.59 ms (two-tailed paired t-test, n = 9 pairs of neurons, P = 0.0009, T = 5.07; **Figure 5.5d**), and consistent with the recruitment of disynaptic inhibition (Pouille and Scanziani, 2001).

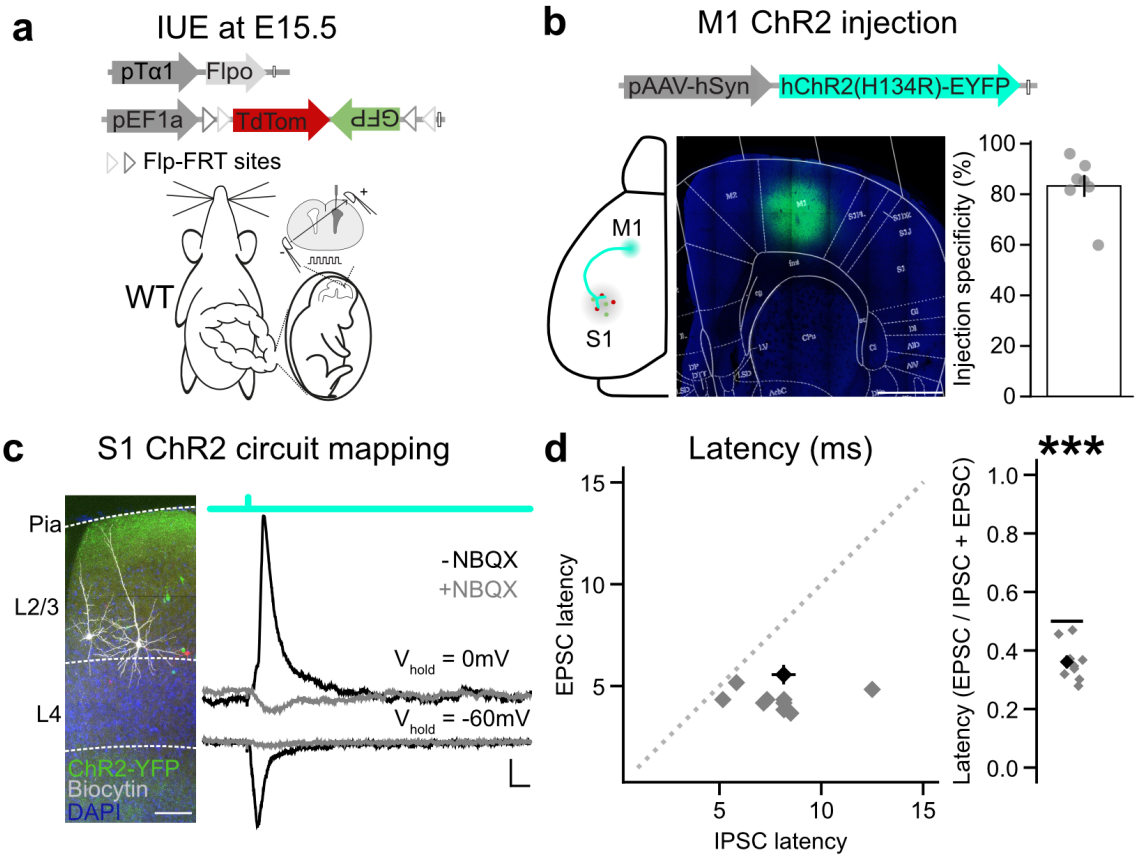


Figure 5.5: Investigating the recruitment of progenitor-defined L2/3 pyramidal populations by M1. (**a**) Excitatory neuron IUE at E15.5 was used to label IP-derived and OP-derived neurons. (**b**) At P28 animals were injected with a ChR2 virus (pAAV-hSyn-hChR2(H134R)-EYFP) into M1. Average injection specificity was 83.55 ± 5.11 % (n = 6 animals). Scale bar 1 mm. (**c**) Simultaneous whole-cell patch-clamp recordings were performed from pairs of neighboring IP-derived and OP-derived neurons at P35-42. In a subset of recordings, neurons were filled with biocytin to confirm their pyramidal identity (left). Scale bar, 100 μm. Brief, widefield light pulses from an LED (473 nm, 500 μs) were used to activate ChR2-expressing M1 fibres. Blockade of AMPA receptors using 10 μM NBQX abolished the evoked monosynaptic EPSC and disynaptic IPSC. Scale bar, 25 pA, 25 ms. (**d**) The latency from LED onset to response start time was shorter for EPSCs than for IPSCs (two-tailed paired t-test, n = 9 pairs of neurons, P = 0.0009, T = 5.07).

Activation of ChR2-expressing M1 axons evoked responses of varying amplitudes across IP-derived and OP-derived L2/3 neurons. Interestingly, mean $EPSC_{M1}$ was larger in IP-derived neurons than in OP-derived neurons (two-tailed Wilcoxon signed rank test, IP-derived mean: 121.66 ± 33.95 pA, OP-derived mean: 66.28 ± 15.25 pA, n = 14 pairs from 7 animals, P = 0.02, W = 16; **Figure 5.6a**). Meanwhile, $IPSC_{M1}$ was comparable between the neuron types (two-tailed Wilcoxon signed rank test, IP-derived mean: 391.12 ± 214.70 pA, OP-derived mean: 203.26 ± 100.66 pA, n = 7 pairs from 6 animals, P = 0.69, W = 11, **Figure 5.6b**). As recordings of both EPSCs

and IPSCs were only obtained in a subset of neuronal pairs, there was no detectable difference in E/I ratio (two-tailed paired t-test, IP-derived mean: 0.37 ± 0.13, OP-derived mean: 0.47 ± 0.22, n = 5 pairs from 5 animals, P = 0.40, T = 0.94; **Figure 5.6c**). Additionally, there were no differences in pial distances between IP-derived and OP-derived L2/3 neurons (two-tailed paired t-test, IP-derived mean: 278.85 ± 29.10 μm, OP-derived mean: 279.62 ± 29.22 μm, n = 13 pairs from 6 animals, P = 0.92, T = -0.10; **Figure 5.6d**). Taken together, excitatory feedback from M1 differentially recruits S1 L2/3 pyramidal neurons based on the L2/3 neuron's progenitor type.

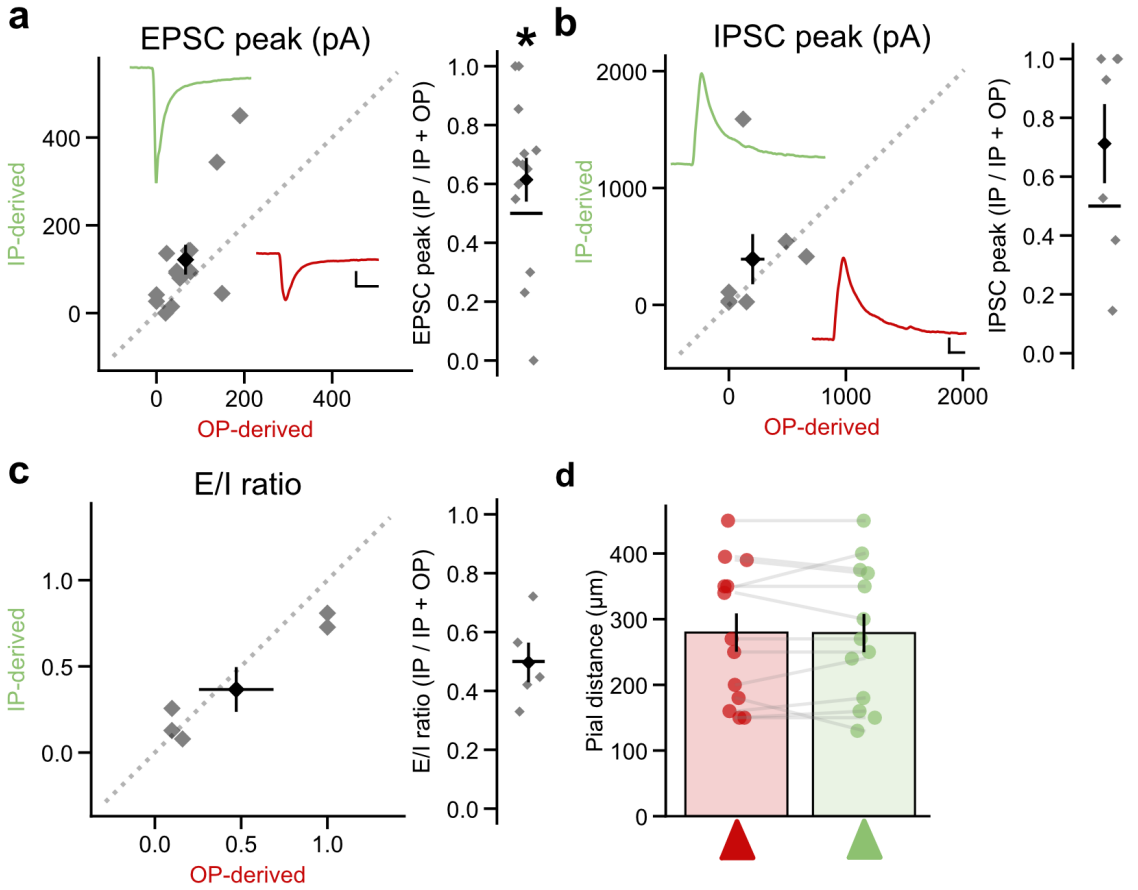


Figure 5.6: Feedback from M1 differs depending upon a S1 L2/3 pyramidal neuron's progenitor type. (**a**) $EPSC_{M1}$ peak amplitude was significantly larger in IP-derived neurons than simultaneously recorded OP-derived neurons (two-tailed Wilcoxon signed-rank test, n = 14 pairs from 7 animals, P = 0.02, W = 16). Scale bar 50 pA, 25 ms. (**b**) $IPSC_{M1}$ peak amplitude did not differ between simultaneously recorded IP-derived and OP-derived neurons (two-tailed Wilcoxon signed-rank test, n = 7 pairs from 6 animals, P = 0.69, W = 11). Scale bar 100 pA, 25ms. (**c**) The ratio of $EPSC_{M1}$ to $IPSC_{M1}$ peak amplitudes (E/I) did not differ between IP-derived and OP-derived neurons (two-tailed paired t-test, n = 5 pairs from 5 animals, P = 0.40, T = 0.94). (**d**) Distance from pia did not differ between IP-derived and OP-derived neurons (two-tailed paired t-test, n = 13 pairs from 7 animals, P = 0.92, T = -0.10).

5.3 Discussion

In this chapter, a combination of *in utero* labelling, *in vitro* electrophysiology and optogenetics was used to investigate the strength of feedback connections to progenitor-defined populations of L2/3 pyramidal neurons in S1. The data support the conclusion that whilst IP-derived and OP-derived L2/3 neurons receive similar levels of monosynaptic excitation and disynaptic inhibition from L5 S1 and from S2, IP-derived neurons receive stronger monosynaptic excitation from M1.

The technical development of ChR2 circuit mapping has greatly advanced the investigation of long-range connectivity between cortical areas, as synaptic strength can still be tested in connections that have been severed due to experimental preparation. Whilst many studies have utilised this technique to map the feedforward and feedback connections of cortical neurons (Kinnischtzke et al., 2014; Mao et al., 2011; Naskar et al., 2021; Petreanu et al., 2009; Young et al., 2021), comparatively few studies have looked at how long-range connection patterns might reflect the developmental history of a neuron (Abe et al., 2023; Ellender et al., 2019; Huilgol et al., 2023a). The results from this chapter therefore build upon this work and extends existing evidence that progenitor type of origin influences local synaptic connections (Ellender et al., 2019). Indeed, many studies have found biases in the local connectivity of neurons that have different long-range connections (Anderson et al., 2010; Brown and Hestrin, 2009; Kim et al., 2018; Kiritani et al., 2012; Morishima et al., 2011; Otsuka and Kawaguchi, 2009; Yamawaki and Shepherd, 2015). Therefore, a holistic approach that relates a neuron's local circuitry to its long-range inputs and outputs is needed in order to fully elucidate how cortical circuits process information. Local circuits do not operate in isolation, as the nature of their computation is defined by their long-range inputs and outputs.

In addition to investigating the feedback strength from higher order cortical areas, this chapter also assessed the strength of local feedback connections within a cortical area. L5 pyramidal neurons are known to provide monosynaptic excitation and recruit disynaptic inhibition within L2/3 (Hage et al., 2022; Onodera and Kato, 2022; Shepherd et al., 2005; Shepherd and Svoboda, 2005; Vecchia et al., 2020; von Klemperer, 2021). It was found that the strength of this feedback is not dependent

on the progenitor type from which the L2/3 neurons were derived. Interestingly, previous work found that OP and IP-derived neurons in L2/3 differentially target neurons in the L5 sublayers (Ellender et al., 2019). Pyramidal neurons in L5a, which mainly consist of cortico-cortical projecting neurons, were preferentially targeted by IP-derived neurons compared to OP-derived neurons. Conversely, pyramidal neurons in L5b, which comprise subcortical-projecting neurons, received preferential input from OP-derived neurons. In the present study a transgenic mouse was used to express ChR2 in pyramidal neurons throughout L5 (Gerfen et al., 2013). Therefore, it is possible that there are differences in the feedback from each of the L5 sublayers to IP-derived and OP-derived L2/3 neurons. Future experiments could test this by injecting a retrograde ChR2 virus into areas targeted by L5a and L5b neurons (Brown and Hestrin, 2009; Kim et al., 2015; Mercier et al., 1990; Moberg and Takahashi, 2022; Young et al., 2021). Whilst L5 is considered the main output of the cortical column, growing evidence suggests that feedback connections to L2/3 play a key role in sensory processing (Onodera and Kato, 2022; Vecchia et al., 2020; von Klemperer, 2021). It is thought that relaying cortical output back to superficial layers may provide an error message to update synaptic weights in superficial layers, leading to learning and plasticity (Keller and Mrsic-Flogel, 2018). Therefore, it would be interesting to investigate the function of feedback connections from L5 pyramidal neurons with different long-range targets, particularly with respect to the inhibition that they recruit (Hage et al., 2022; Kätzel et al., 2010; von Klemperer, 2021).

Previous work has used retrograde tracing in M1 to show that OP-derived and IP derived L2/3 neurons have similar feedforward projections to M1 (Ellender et al., 2019).Therefore, intuitively one might expect there to be no differences in the strength of feedback from M1 to S1 between OP and IP derived neurons (Kim et al., 2020). However, several studies suggest that feedforward and feedback connection strengths are not matched at the single cell level in L2/3 (Mao et al., 2011; Young et al., 2021). Experiments combining retrograde tracing and ChR2 circuit mapping in visual cortex indicate that feedback projections from a higher order cortical area do not discriminate between L2/3 neurons that have feedforward projections to that higher order cortical area and neurons that don't (Young et al., 2021). Therefore,

it is possible that there are no differences between the feedforward connections that IP-derived and OP-derived L2/3 neurons send to M1, but that IP-derived neurons receive preferential feedback connections from this cortical area. Interestingly, evidence suggests that M1 neurons project to S1 in a diffuse manner, in order to broadcast motor signals across a wide population of neurons (Kinnischtzke et al., 2014). L2/3 IP-derived neurons exhibit local excitatory connectivity biases whereby they preferentially connect to OP-derived neurons (Ellender et al., 2019). This might therefore represent a mechanism to more efficiently 'broadcast' signals from M1 across L2/3 pyramidal populations. One advantage of delivering feedback signals to certain populations of pyramidal neurons is to ensure the separation of these inputs from feedforward sensory inputs, allowing for the subsequent integration of sensory and motor related signals at relevant parts of sensory processing.

In summary, this chapter has assessed whether neurons derived from different progenitor types receive different amounts of feedback from three cortical areas. The findings reveal that IP-derived neurons receive preferential input from M1, therefore highlighting the significance of progenitor type in the construction of long-range as well as local cortical circuits. The implications of these findings, and directions for future work will be discussed in **Chapter 6**.

6 | General Discussion

6.1 Experimental findings

In **Chapter 3**, I began by investigating whether the inhibitory input received by L2/3 pyramidal neurons was shaped by their progenitor type of origin. To achieve this, I outlined an *in utero* labelling method that can be used to label IP-derived neurons, so that they can be subsequently targeted by two-photon *in vivo* patch clamp in the mature brain. Next, I validated several aspects of my analysis pipeline in order to develop an experimental paradigm for measuring inhibitory synaptic coupling to a LFP. Lastly, I measured the synaptic inhibition spontaneously received by IP-derived and unlabeled L2/3 neurons *in vivo* whilst simultaneously recording a LFP. These experiments revealed that L2/3 IP-derived neurons receive similar levels of synaptic inhibition to unlabeled L2/3 neurons *in vivo*. However, the correlation between inhibitory inputs and local network activity was weaker for IP-derived neurons. This therefore suggests that progenitor type influences the inhibition received by L2/3 neurons *in vivo*. It was predicted that these differences in correlation with the LFP might reflect connectivity biases from different interneurons depending on the L2/3 neuron's progenitor type.

In **Chapter 4**, I used a combination of *in utero* labelling, *in vitro* electrophysiology and optogenetics to test the prediction that the inhibition received by L2/3 pyramidal neurons depends on the L2/3 neuron's progenitor type. Firstly, I validated a new Flpo-based dual-colour reporter construct to label IP-derived and OP-derived L2/3 neurons in transgenic mice. Secondly, to better characterise the neurons included in my IP-derived population, I developed a labelling strategy that used both Cre and Flpo recombinases to label neurons derived from progenitors with Tα1 and Tbr2 promoter activity. This revealed that the pTα1 labelling strategy used throughout this thesis labels a population of intermediate progenitors comprising both aIPs and bIPs. Thirdly, I tested the overall level of synaptic inhibition received by IP-derived

and OP-derived L2/3 neurons through optogenetic activation of PV, SST and VIP interneurons. This revealed that progenitor type did not influence the overall level of synaptic inhibition received from any of these three interneuron subpopulations. Finally, I measured the spontaneous inhibition received from pairs of neurons comprising IP-derived, OP-derived and unlabelled L2/3 neurons. From this I found that progenitor type influences the degree of common inhibitory synaptic input received by pairs of L2/3 neurons. This was supported by further optogenetic experiments demonstrating that PV interneurons exhibit biased connectivity to postsynaptic pyramidal neurons derived from different progenitor types. Together, these observations suggest that the extent to which pyramidal neurons share inhibitory synaptic input is influenced by their progenitor type of origin.

In **Chapter 5**, I aimed to investigate whether progenitor type influences the amount of monosynaptic excitatory and disynaptic inhibitory feedback L2/3 neurons receive from L5 of S1, from S2 or from M1. To measure feedback from L5, I performed *in utero* labelling in transgenic mice that expressed ChR2 in L5 of cortex. Subsequent simultaneous whole-cell *in vitro* patch-clamp recordings from IP-derived and OP-derived L2/3 neurons revealed that L2/3 neuron progenitor type does not influence feedback received from L5 of S1. To measure feedback from S2 and M1, I performed *in utero* labelling in wildtype mice and subsequent intracranial injections to deliver ChR2 into the cortical area of interest. Subsequent simultaneous whole-cell *in vitro* patch-clamp recordings from IP-derived and OP-derived L2/3 neurons revealed that progenitor type does not influence the feedback received from S2, but monosynaptic excitatory feedback from M1 was stronger to IP-derived neurons. These data therefore support the conclusion that progenitor type influences the level of feedback recruited from M1.

6.2 Methodological considerations

In this section I will consider the strengths and limitations of the methodological techniques that I have used, and how these may impact the findings of this thesis.

6.2.1 *In utero* electroporation and the longitudinal labelling of progenitor-defined populations

The findings of this thesis rely upon the labelling of progenitor-defined populations of neurons achieved through IUE. IUE represents a well-established tool for efficiently delivering DNA plasmids into populations of progenitors and their progeny (Baumgart and Grebe, 2015; Saito and Nakatsuji, 2001; Shimogori and Ogawa, 2008). This method provides advantages over alternative techniques, such as transgenic mouse lines or intracranial injections, in that it allows excellent spatio-temporal control of neuronal labelling and causes minimal damage to neuronal tissue. IUE can be targeted to label proliferating cells in either the dorsal or ventral telencephalon, meaning it can be used to study the development of a wide variety of cell types (Garcia et al., 2015; Ellender et al., 2019; Petros et al., 2015; Tyler et al., 2015; van Heusden et al., 2021). A key advantage of IUE in this regard is that constructs can be designed to allow longitudinal labelling of progenitor-defined populations of neurons, enabling them to be visualised into late postnatal ages (Buchan et al., 2022; Ellender et al., 2019; Guillamon-Vivancos et al., 2019; Saito, 2006; Saito and Nakatsuji, 2001; Tyler et al., 2015). This allowed me to address the central question to this thesis, of whether neuronal progenitor types influence the synaptic connectivity of their progeny in the postnatal brain.

Whilst the timing of IUE determines the temporal cohort of neurons that are labelled, additional control can be exhibited through labelling progenitor types based on the expression patterns of specific genes. Consistent with previous work, this thesis labelled a population of IPs through the expression of the Tα1 promoter (Ellender et al., 2019; Gal et al., 2006; Mizutani et al., 2007; Stancik et al., 2010). However, recent research has highlighted the complexity of progenitor diversity, and as such there may be a limit to the specificity of labelling that can be achieved through single genes (Bella et al., 2021; Greig et al., 2013; Li et al., 2020; Oberst et al., 2019; Ruan et al., 2021; Telley et al., 2016, 2019). For example, as with neuronal types within the adult brain, single-cell transcriptomics has revealed the extent of progenitor diversity in the mouse brain, including 5 types of IPs (Li et al., 2020). One possibility is that the Tα1-promoter labelling strategy identifies a specific subset of

aIPs and bIPs. Interestingly, recent work has identified genes that are differentially expressed in aIPs and bIPs (Bedogni and Hevner, 2021). Therefore, future work could further characterise the Tα1 labelling, by examining Tα1 promoter activity in combination with the aIP and bIP defined genes identified in this study.

There is some evidence to suggest that RGCs can also express Tα1 (Ramos et al., 2020; Tyler and Haydar, 2013). However, it is possible that RGCs begin to express Tα1 prior to, or during, their transition into IPs. Furthermore, it is suggested that Tα1 promoter activity might be an instructive signal that induces the production of IPs from RGCs (Ramos et al., 2020). One explanation might be the sensitivity of DNA constructs to endogenous gene regulation. For example, very low levels of endogenous Tα1 promoter activity may be sufficient to turn on the Tα1 promoter labelling construct following IUE, and the Tα1 promoter may show low levels of activity in RGCs that are committed to an IP fare. This was found to be the case for Tbr2 promoter activity in subsets of RGCs that were committed to producing bIPs (Li et al., 2020).

The differential regulation of Notch genes is arguably the most distinguishing genetic feature that separates RGCs from aIPs and bIPs (Bedogni and Hevner, 2021; Kawaguchi et al., 2008; Mizutani et al., 2007; Yoon et al., 2008). Activation of the Notch signalling pathway in RGCs allows them to maintain a proliferative state, whereas down-regulation of Notch signalling in IPs promotes their differentiation into neurons (Kawaguchi et al., 2008; Yoon et al., 2008). Importantly, Notch signalling between these two progenitor populations regulates the balance between proliferation and differentiation in the ventricular zone (Kageyama et al., 2008; Kawaguchi et al., 2008; Mizutani et al., 2007; Shimojo et al., 2008; Yoon et al., 2008). Therefore, future studies could assess the relationship between Tα1 promoter activity and Notch gene expression levels, in order to better characterise the progenitors labelled by the Tα1 promoter. Overall, these studies demonstrate the highly dynamic process in which progenitor identity is determined. Consequently, a limitation of the IUE method is that it can only provide a single temporal snapshot of this process.

This thesis used IUE to label two cohorts of neurons: those derived from IPs and

those derived from OPs. The OP-derived group is less well defined than the IP-derived group, as OP-derived neurons are labelled by the absence of Tα1 promoter activity (Ellender et al., 2019). In **Chapter 4.2.1**, it was found that OP-derived neurons are located closer to pia than IP-derived neurons on average, in agreement with previous work suggesting that at least some of the OP-derived neuronal population are born from RGCs as direct neurogenic divisions (Ellender et al., 2019; Stancik et al., 2010). Additionally, embryonic studies suggest that the morphology of OPs is consistent with that of RGCs (Ellender et al., 2019). It is also possible that some OP-derived neurons are derived from bRGs. bRGs are poorly categorised in terms of their gene expression patterns compared to other progenitor types, and it is unclear the extent to which they can be labelled using IUE (Wang et al., 2011). However, bRGs are thought to undergo self renewing divisions, consistent with the observation that OP-derived neurons tend to be located closer to pia than IP-derived neurons (Shitamukai et al., 2011). In summary, future work could aim to identify which progenitor populations contribute to the OP-derived neurons. This could be achieved by through labelling RGCs via genes such as GLAST or BLBP (Mizutani et al., 2007; Ramos et al., 2020; Tyler and Haydar, 2013).

6.2.2 *In vivo* electrophysiology in anaesthetised preparations to measure synaptic inhibition

Chapter 3 of this thesis used two-photon targeted *in vivo* whole-cell patch clamp recordings to determine the inhibitory synaptic inputs received by L2/3 pyramidal neurons. *In vivo* electrophysiology constitutes the gold standard for recording neuronal activity. Whilst there are multiple ways to record neuronal activity *in vivo* (Buzsáki, 2004; Kerr and Denk, 2008; Margrie et al., 2002), measuring synaptic inhibition is particularly challenging, necessitating the use of voltage clamp to hold the neuron's membrane potential at the reversal potential for excitatory synaptic inputs (Haider et al., 2016). This technique is subject to several caveats that need to be acknowledged.

Firstly, all whole-cell electrophysiological recordings are subject to errors due to series resistance, which comprises the resistance between the recording electrode and

the inside of the neuron (Sigworth, 1995). Series resistance impacts the ability of the current injected by the amplifier to reach the neuron's membrane. This therefore creates a voltage drop, such that, depending on the size of the series resistance, the neuron's membrane potential is held somewhere between the resting membrane potential and the desired holding voltage. Series resistance is typically higher during *in vivo* patch clamp recordings in comparison to those performed *in vitro* (Jordan, 2021). This is due to the technical challenges of performing *in vivo* patch clamp recordings, including compromised visualisation of the recording pipette and neuron soma. Additionally, in order to record synaptic inhibition, the neuron's membrane potential needs to be held at voltages that are far away from the resting membrane potential, thereby increasing the amount of current that needs to be injected to achieve the desired potential.

A second factor that contributes to voltage clamp errors is that neuronal membrane resistances are typically lower *in vivo* than *in vitro* due to higher levels of synaptic activity (Destexhe et al., 2003; Destexhe and Paré, 1999). This affects the ability to clamp the membrane at the desired voltage. Thirdly, due to the small dendritic compartments of neurons, clamping the neuron's membrane potential at the desired voltage is much less effective at dendritic compartments further from the soma, an issue known as 'space clamp' (Poleg-Polsky and Diamond, 2011; Spruston et al., 1993; To et al., 2022; Williams and Mitchell, 2008). Space clamp is more pronounced *in vivo* because neuronal dendrites are more active (Bar-Yehuda and Korngreen, 2008; Bernander et al., 1991; Destexhe and Paré, 1999; Holmes and Woody, 1989), thus reducing the ability for their voltage to be clamped. Therefore, it is predicted that the inhibitory inputs arriving at the distal dendrites are greatly attenuated and difficult to detect with somatic voltage clamp (Poleg-Polsky and Diamond, 2011). In summary, these issues highlight the limitations of voltage clamp recordings *in vivo*. It is therefore likely that the inhibitory inputs that I have recorded do not fully reflect the inhibitory inputs that a neuron receives throughout its dendritic compartments.

Several measures were taken to address these issues surrounding voltage clamp errors. Firstly, to record synaptic inhibition, I held the neuron's membrane potential at +20 mV. This is 10-20 mV higher than the excitatory reversal potential typi-

cally used to record inhibitory synaptic inputs *in vitro* (Sippy and Yuste, 2013; Xu et al., 2014; Xue et al., 2014), thereby attempting to compensate for the expected voltage drop (Haider et al., 2016). Secondly, I continually measured the series resistance throughout each recording and performed post-hoc quality control measures to ensure series resistance did not systematically vary between experimental groups. Thirdly, I performed an offline correction, which calculated the voltage drop across the series resistance and subsequently approximated the inhibitory synaptic conductance using the estimated driving forces (Traynelis, 1998). The calculated voltage drop values were within the 5-15 mV range, confirming that setting the command voltage to +20 mV appropriately compensated for this voltage drop. Taken together, these measures address some of the issues of using voltage clamp to measure synaptic inhibition *in vivo*.

Whilst recording synaptic inhibition *in vivo*, I simultaneously recorded local network activity using a LFP. These experiments were conducted in animals anaesthetised with isoflurane. Isoflurane was selected because anaesthetic depth can be bi-directionally modulated during recordings to maintain consistent depth, there are no problems with respiratory depression unlike with other anaesthetics, and isoflurane has been used in similar experimental paradigms (Golshani et al., 2009; Haider et al., 2016). However, all anaesthetics affect neuronal activity and the implications this could have upon my findings should be acknowledged (Destexhe et al., 2003; Greenberg et al., 2008; Yin et al., 2016). For example, neuronal activity is often more correlated during anaesthesia, similar to slow wave sleep (Pachitariu et al., 2015). Secondly, further evidence suggests that synaptic inhibition increases during wakefulness compared to anaesthetised states (Haider et al., 2013). This may contribute to the decorrelation of cortical activity during wakefulness, consistent with mechanisms of sparse coding in awake cortex (Chini et al., 2022; Crochet et al., 2011; Greenberg et al., 2008; Haider et al., 2013; Ranjbar-Slamloo and Arabzadeh, 2019). As such, coupling of inhibitory inputs to the LFP has been found to be reduced in awake compared to anaesthetised conditions (Haider et al., 2016). The fact that cortical inhibition and synchronicity vary across different states, means that a limitation of my findings is that it is unclear to what extent they can be applied to awake conditions (Burman et al., 2023; Haider et al., 2013; Poulet and

Crochet, 2019; Poulet and Petersen, 2008). However, avenues for future work could include exploring the coupling of inhibitory inputs to LFP in IP-derived neuron across different cortical states (Haider et al., 2016).

Given the modulation of neuronal activity by anaesthesia, it is possible that variation in anaesthetic depth could influence the coupling of inhibitory synaptic inputs to the LFP (Haider et al., 2013, 2016). For this reason, it was essential that anaesthetic depth was consistently monitored throughout my recordings. This was achieved through continual assessment of the breathing rate of the animal and observation of activity levels in the LFP, which varies with anaesthetic depth (Hu et al., 2023; Yin et al., 2016). Additionally, LFP recordings were compared between experimental groups to ensure that anaesthetic depth did not systematically vary (**Chapter 3.2.3**). In this sense, the LFP was a useful tool for not only measuring the coupling of inhibitory inputs, but also to act as a control for levels of network activity across recordings. Overall, this has enabled me to ensure that conditions were comparable between recordings of IP-derived and unlabeled neurons.

6.2.3 Measuring synaptic inhibition with optogenetic and spontaneous *in vitro* electrophysiological recordings

A major technique used in this thesis is the assessment of synaptic input strength from specific interneuron subpopulations using optogenetics. Optogenetics is a powerful tool to efficiently and selectively activate specific neuronal populations using brief pulses of light (Boyden et al., 2005; Boyden, 2011). I used widefield illumination to activate ChR2 whilst performing dual patch clamp recordings to test synaptic connection strength from PV, SST or VIP interneurons onto L2/3 pyramidal neurons. One concern with this strategy surrounds the specificity of cell labelling, particularly for the SST-Cre mouse line (Müller-Komorowska et al., 2020). Another limitation surrounds the degree to which these three interneuron subpopulations reflect different cell types. For instance, recent research suggests that these three interneuron subpopulations constitute relatively broad classes, and there may be considerable functional diversity within each (Ascoli et al., 2008; Tasic et al., 2018; Tremblay et al., 2016). Therefore, future work may wish to capitalise on combi-

natorial genetic labelling techniques, in order to target interneuron subtypes with greater specificity (Fenno et al., 2014).

In addition to widefield illumination, I also used optogenetics to test the input to IP-derived and OP-derived L2/3 neurons from putative single PV interneurons. This was achieved through the minimal stimulation of PV interneurons, which involved reducing stimulation until synaptic failures were observed, as described in previous work (Morgenstern et al., 2016). However, I cannot conclusively say that only one PV interneuron was activated at each stimulation site, due to the high density of axonal projections from PV interneurons throughout the cortex (Helmstaedter et al., 2009b). Therefore, it is possible that in some cases multiple PV interneurons were stimulated, suggesting that my results may overestimate the shared output from PV interneurons. Despite this, I still found differences in how PV interneurons targeted IP-derived and OP-derived L2/3 neurons, potentially meaning that stronger effects would be seen in an experimental paradigm that ensures single PV interneuron stimulation.

Optogenetic experiments were complimented by *in vitro* recordings of spontaneous inhibitory inputs. One advantage of spontaneous recordings is that they reflect the neuron's endogenous inhibitory network. For example, if a neuron receives preferential input from an interneuron subtype that has a high firing rate, this would be reflected in spontaneous recordings. Conversely, this would not be detected by optogenetic assays, where the experimenter controls the levels of presynaptic activity. However, there are several general limitations to *in vitro* slice electrophysiology that need to be addressed because they could impact the findings from my spontaneous synaptic input measurements. Firstly, the process of slice preparation results in axons being cut, tissue damage and cell death (Khurana and Li, 2013). This leads to deviations in synaptic physiology from those seen *in vivo* (Ivanov and Zilberter, 2011; Medvedeva et al., 2009; Voss, 2020). In the case of my experiments, particular interneuron subtypes may be more susceptible to cell death under these conditions, biasing the interneurons that are active during spontaneous activity. Furthermore, there is a progressive deterioration of slice health throughout the recording session. Consequently, neuronal recordings can only be performed from for approximately 6 hours following slicing (Buskila et al., 2014; Colbert, 2006) and it is possible that

changes in spontaneous activity occur as tissue health deteriorates.

Several aspects of my experiment were designed to control for these limitations. Firstly, by performing simultaneous dual patch clamp recordings, the level of spontaneous activity in the slice is matched between the two neurons. This ensures that recording conditions of the neurons are identical, including the level of oxygenation and the concentration of metabolites and synaptic molecules. In **Chapter 4**, comparisons were made between different pairs of neurons, for example, pairs of two OP-derived neurons and pairs of two IP-derived neurons. Consequently, it is possible that variability between pair types is introduced across experimental days, or by the time of recording within a single day. However, this was addressed by recording interchangeably from different pair types on a single experimental day. Recording different pair types on the same day ensures that any variation across experimental days is minimised, and randomising the order of recordings within a single day addresses the potential confound of the progressive deterioration of slice health. Taken together, these measures attempt to account for some of the limitations associated with *in vitro* slice electrophysiology, such that meaningful conclusions can still be drawn from recordings of spontaneous inhibitory inputs.

Another concern is the extent to which simultaneous inhibitory synaptic inputs reflect common inhibitory synaptic connections between two neurons. For example, it is possible that two interneurons fire an action potential at the same time, perhaps due to being simultaneously excited. In such a case, a coincident inhibitory input in two postsynaptic pyramidal neurons could originate from two separate presynaptic inhibitory connections, instead of a shared connection to both pyramidal neurons. However, previous evidence suggests that synchronous inhibitory inputs are a result of common presynaptic connections, instead of synchronous firing (Sippy and Yuste, 2013). Secondly, it was found that interneurons do not exhibit more synchronous firing than pyramidal neurons in response to thalamic stimulation *in vitro*, suggesting that coincident action potential generation in interneurons is rare (Sippy and Yuste, 2013). Thirdly, the fraction of shared synaptic inputs across neuron types reported in **Chapter 4.2.5** ($\sim$ 20 %) is similar to the probability of shared inhibitory input reported in previous studies using different experimental approaches ($\sim$ 30 % in Packer and Yuste 2011; $\sim$ 25 % in Yoshimura et al. 2005), suggesting that syn-

chronous inhibitory inputs during spontaneous activity represent shared inhibitory connections. The 10 % increase in shared inhibitory connections reported in Packer and Yuste (2011) compared to the results of **Chapter 4.2.5** could reflect differences in the recording techniques used, which may be sensitive to how much of the presynaptic inhibitory subnetwork was sampled. Alternatively, this difference could also reflect the different representation of pyramidal neuron subtypes between the two studies. Taken together, this evidence supports the use of spontaneous recordings of inhibitory synaptic inputs to estimate common inhibitory connections.

6.2.4 Long-range circuit mapping using optogenetics

Chapter 5 of this thesis used optogenetics to map the feedback that L2/3 pyramidal neurons receive from L5 of S1, from S2 or from M1. Whilst the strength of long-range connections can be tested in slice preparations through cutting the brain along specific axes (Rocco and Brumberg, 2007), the assessment of long-range connections has been greatly aided through the use of ChR2, which allows the stimulation of axons that may be severed from their cell body during the slicing process (Petreanu et al., 2007). However, there are several considerations that affect the validity of the optogenetic approach that I have adopted. Firstly, the vast majority of the viral ChR2 injection must be specific to the region of interest in order to draw the conclusion that the synaptic connections tested do indeed originate from the appropriate cortical area. I addressed this concern by calculating the injection specificity for the animals in which I conducted the recordings, by performing post-mortem histological analysis. The injections into M1 and S2 were approximately 70 - 80 % accurate. Therefore, it is reasonable to conclude that the majority of synaptic connections tested were specific to M1 or S2 neurons, and not the surrounding cortical areas.

Another consideration is the potential for variation in the viral ChR2 injection across experimental animals. This variation could include differences in the amount of neurons transfected, or even a different distribution of transfection across cortical layers. This issue is largely addressed by comparing response amplitudes between simultaneously patched neurons within the same slice. However, it is important to consider how this may still impact the interpretation of these experimental results.

For example, there are reported connectivity differences between how the upper and lower layers of M1 send feedback projections to S1 (Hooks et al., 2013; Mao et al., 2011), therefore, further differences in connectivity patterns between IP-derived and OP-derived L2/3 neurons may exist between the upper and lower layers of M1. Additionally, these sources of variation make it difficult to compare absolute response amplitudes across experimental animals, across different injection targets, or with other studies such as Naskar et al. (2021). Whilst these issues do not affect the conclusions drawn in this thesis, they do limit the interpretations that can be made from this type of data.

6.3 Implication of findings

Having explored the technical considerations of my results in the previous section, I will now discuss the implications of the findings reported in this thesis.

6.3.1 L2/3 pyramidal neuron progenitor type shapes local inhibitory inputs and long-range feedback

The results of this thesis contribute to a growing body of literature that has described a number of ways in which excitatory neuron progenitors can influence their progeny (Buchan et al., 2022; Cadwell et al., 2020; Ellender et al., 2019; Guillamon-Vivancos et al., 2019; Huilgol et al., 2023a; Matho et al., 2021; Ohtsuki et al., 2012; Tyler et al., 2015; Yu et al., 2009). To understand the implications of my findings, it is important to explore how my results relate to and extend these current findings.

Previous studies in cortex have primarily focused on the excitatory synaptic connections between neurons derived from separate clones or different progenitor types. These studies have not explored how lineage relationships may also influence synaptic connections with local interneurons. My work therefore extends these findings by revealing how excitatory neuron progenitor type can influence the inhibitory synaptic inputs to L2/3 pyramidal neurons. I demonstrate that excitatory neuron progenitor type shapes how pyramidal neurons share inhibitory inputs and how their inhibitory inputs couple to local network activity. Interestingly, similar findings have been seen in hippocampal circuits. These include the preferential sampling

of inhibition by clonal neurons born from the same progenitor (Xu et al., 2014), as well as the influence of excitatory neuron birthdate upon inhibitory connections (Cavalieri et al., 2021; Huszár et al., 2022). Therefore, my results suggest that progenitor type, as well as clonal relationship and birthdate, can also influence how excitatory neurons sample from inhibitory circuits. The ways in which progenitor type, birth date and clonal relationships relate to one another remains to be determined, but the potential for these lineage trajectories to interact could generate yet further diversity within neuronal circuits. Furthermore, my results suggest that these mechanisms extend beyond hippocampus to cortical circuits. Taken together, these studies demonstrate the importance of mechanisms during neurogenesis on the formation of synaptic circuits between excitatory and inhibitory neurons.

Influential work from the lab of Song-Hai Shi provided the first evidence for a role of ontogeny in the fine-scale organisation of cortical circuits, by demonstrating that clonal neurons produced from the same RGC exhibit preferential synaptic connectivity (Yu et al., 2009). Subsequent studies have shown that clonally related neurons develop more similar sensory response properties than non-clonally related neurons (Li et al., 2012; Ohtsuki et al., 2012). Furthermore, more recent evidence suggests further complexity in lineage relationships, such as 'cousin' neurons born from different RGCs that avoid making synaptic connections with one another (Lin et al., 2023). However, the explanatory power of clonal relationships is limited because clone sizes are small (Gao et al., 2014), and it is evident that the connectivity principles governing circuit assembly are more complex than a binary choice between clone and non-clone. It is therefore important to understand clonal relationships in the context of increasingly recognised progenitor diversity (Hippenmeyer, 2023; Huilgol et al., 2023b; Li et al., 2020; Ruan et al., 2021). For example, it is unclear how the synaptic connectivity between clonally related neurons is influenced by whether neurons are produced by direct asymmetric RGC divisions or via indirect symmetric divisions from an IP. Given that there are multiple transcriptomic subtypes of RGCs and IPs, a comprehensive approach that accounts for progenitor heterogeneity and clonal relationships is required to fully understand the assembly of synaptic circuits. My work advances our understanding in this area by acknowledging progenitor heterogeneity and labelling excitatory pyramidal neurons according

to their progenitor type.

It is generally accepted that an increase in the number of neuronal progenitors underlies the evolutionary expansion of the mammalian neocortex (Cárdenas et al., 2018; Florio and Huttner, 2014; Kriegstein, 2006; Martinez-Cerdeno et al., 2006). However, this expansion in the progenitor pool has occurred alongside increases in the molecular diversity of progenitors and progenitor subtypes, therefore it is important to discuss the influence of progenitor amplification versus diversification upon cortical circuits. On the one hand, the generation of neurons via symmetric IP divisions increases the number of neurons compared to those that would be born through only asymmetric RGC divisions (Cárdenas et al., 2018; Martinez-Cerdeno et al., 2006). Furthermore, in gyrencephalic species such as ferrets and non-human primates, an expansion of the SVZ containing additional progenitor subtypes such as bRGs are thought to contribute to the enlargement of the neocortex (Betizeau et al., 2013; Florio and Huttner, 2014; Pilz et al., 2013). Therefore, an amplification hypothesis would assume that additional progenitor types solely act to increase the neurogenic output over the same neurogenic period. However, a range of studies support a diversification hypothesis, whereby an increase in progenitor diversity produces a broader range of cell types that exhibit specific connectivity patterns in cortex (Buchan et al., 2022; Ellender et al., 2019; Guillamon-Vivancos et al., 2019; Huilgol et al., 2023a; Tyler et al., 2015). My work contributes to existing evidence that IP-derived neurons form differential local and long-range circuits, and therefore IP-derived neurons do not only amplify neuronal output number, but also diversify cortical circuitry. This may offer a mechanism for evolutionarily conserved patterns of synaptic connectivity to be developmentally expressed at the level of cell types, thereby enhancing the computational capabilities of cortical circuits (Zador, 2019).

6.3.2 Reconciling evidence for blanket versus specific inhibition in cortical circuits

The results of this thesis challenge existing evidence that interneurons connect non-specifically to all nearby excitatory neurons, a concept known as 'blanket inhibition' (Fino and Yuste, 2011; Packer and Yuste, 2011). Using a combination of glutamate

uncaging and electrophysiology, these previous studies mapped the monosynaptic connections to a single pyramidal neuron from surrounding PV or SST interneurons. They found that interneurons connected densely to most surrounding pyramidal neurons in a distance-dependent manner. Additionally, they did not find any apparent specificity in how an interneuron connects to multiple nearby pyramidal neurons, such as when two pyramidal neurons were found to be synaptically connected to one another (Fino and Yuste, 2011; Packer and Yuste, 2011; Yoshimura et al., 2005). Supported by other studies across cortical layers, brain areas and using different recording techniques, blanket inhibition has been proposed as a canonical feature of cortical inhibition (Hofer et al., 2011; Holmgren et al., 2003; Isaacson and Scanziani, 2011; Safari et al., 2017; Wang et al., 2002; Xue et al., 2014). In accordance with this, various functions for dense inhibitory connectivity in cortical circuits have been proposed. By pooling inputs from surrounding pyramidal neurons, the receptive field properties of interneurons are broader than those of pyramidal neurons (Bock et al., 2011; Cardin et al., 2007; Hofer et al., 2011). This allows interneurons to approximate the average population activity and thus appropriately control levels of excitation (Kerlin et al., 2010; Pouille et al., 2009). Furthermore, this pooling of activity enables interneurons to sharpen the tuning properties of pyramidal neurons, resulting in a 'winner takes all' competitive strategy for excitatory responses to sensory input (Adesnik, 2018; Adesnik and Scanziani, 2010; hua Liu et al., 2011). Additionally, disinhibitory circuits act to specifically relieve blanket inhibition during certain behavioural states or in response to top-down inputs (Fu et al., 2014; Karnani et al., 2016; Letzkus et al., 2015; Williams and Holtmaat, 2019). In summary, blanket inhibition has provided a useful framework for understanding principles of inhibitory connectivity and function within cortical circuits.

It is important to recognise, however, that studies describing blanket inhibition have not explored inhibitory connectivity from the perspective of pyramidal neuron heterogeneity (Krook-Magnuson et al., 2012). Technical advances in single-cell transcriptomics and viral connectivity tracing over the past decade have led to the subclassification of pyramidal neuron populations that were previously considered homogeneous. Therefore, in addition to the concept of blanket inhibition, there is also growing evidence that interneurons make selective connections with pyramidal

neurons based on their molecular identity or long-range connectivity (Jézéquel et al., 2023; Karimi et al., 2020; Lee et al., 2014a,b; Lu et al., 2017; Valero et al., 2015; Varga et al., 2010; Wu et al., 2017, 2023). These studies highlight how specificity of inhibition would be overlooked unless differences amongst pyramidal populations are recognised. Whilst the majority of these studies have focused on differential inhibitory input to L5 subpopulations with separate projection targets (Jézéquel et al., 2023; Lu et al., 2017; Otsuka and Kawaguchi, 2009; Wu et al., 2017, 2023), my work extends these findings by revealing that a similar precedent exists in L2/3, whereby IP-derived and OP-derived L2/3 neurons receive different inhibitory input. These findings suggest that in addition to projection target, inhibitory interneurons can also discriminate between pyramidal neurons based on their progenitor type. Interestingly, Jézéquel et al. (2023) identified an intriguing molecular mechanism relating the sampling of PV interneuron subnetworks depending upon their transcriptomic subtype. This supports the idea that inhibitory connections can be specific according to the molecular identity and projection target of the inhibitory and excitatory neuron, respectively. Indeed, it is possible that some molecular subtypes of interneuron make specific connections depending on the post-synaptic pyramidal neuron type, whereas other subtypes of interneuron connect non-specifically to all local pyramidal neurons, thereby reconciling evidence for both specific and dense connectivity profiles (Krook-Magnuson et al., 2012).

Synaptic connections between interneurons and pyramidal neurons are dependent upon the distance between the two neurons (Fino and Yuste, 2011; Packer and Yuste, 2011). Whilst this is the case for horizontal distances within the home layer, evidence suggests there might be stereotyped patterns of intralaminar connectivity between interneurons and pyramidal neurons (Dantzker and Callaway, 2000; Denardo et al., 2015; Jézéquel et al., 2023; Kätzel et al., 2010; Yetman et al., 2019). Therefore, another source of specificity in inhibitory input is the extent to which pyramidal neurons sample inhibition across cortical layers. Using a combination of ChR2 circuit mapping and electrophysiological recordings, Kätzel et al. (2010) mapped the columnar distribution of inhibitory connections to L2/3 pyramidal neurons in 3 separate cortical areas. In addition to several area-specific attributes of translaminar inhibition, neighbouring L2/3 pyramidal neurons displayed differences in the

amount of translaminar inhibitory input they received. Whilst this study did not discriminate between interneuron subtypes, similar results were found from L2/3 pyramidal neurons and translaminar PV interneurons using monosynaptic rabies tracing (Yetman et al., 2019). Furthermore, several distinct morphological subtypes of PV interneurons have been identified, including those that are consistent with translaminar inhibition (Helmstaedter et al., 2009b). Taken together, these studies support the idea that L2/3 pyramidal neurons may differ in their laminar sources of PV inhibition. It is important to note that studies using synaptic tracing can identify the full presynaptic inhibitory subnetwork connecting to a pyramidal neuron, whilst uncaging methods may be biased towards testing connections that lie most proximal to the pyramidal neuron, where connection rates are highest. Therefore, one could reconcile evidence for both blanket versus specific inhibition when considering the fraction of the presynaptic inhibitory subnetwork that is being tested.

The findings from **Chapter 3** demonstrate that inhibitory synaptic inputs to IP-derived neurons are less correlated to local network activity than those of unlabeled L2/3 pyramidal neurons. This likely impacts the timing of action potentials amongst IP-derived neurons (Cardin, 2018; Galarreta and Hestrin, 2001; Salkoff et al., 2015; Vreeswijk et al., 1994), and could therefore contribute to the observation that pyramidal neurons exhibit diversity in their pairwise correlations and population coupling (Bartolo et al., 2020; Ecker et al., 2010; Knoblich et al., 2019; Okun et al., 2015). Heterogenous correlations amongst pyramidal neurons is thought to be important for optimal encoding strategies (Ecker et al., 2011; Panzeri et al., 2022; Shamir and Sompolinsky, 2006; Wilke and Eurich, 2002). Therefore, progenitor type may present a mechanism for specifying connectivity patterns that maximise the information that can be represented within cortical circuits. Interestingly, recent evidence from computational models suggests that clustered inhibition reflecting excitatory subnetworks effectively recapitulates correlation structures observed amongst pyramidal neurons (Negrón et al., 2023). It would be interesting to use computational modelling to explore the influence of shared inhibitory inputs on the distribution of spike correlations and the impact this has on encoding capacity. This would help elucidate the functional implications of weak inhibitory coupling of IP-derived neurons within a large population of neurons.

Taken together, the evidence presented supports the idea that whilst synaptic connectivity rates from inhibitory interneurons to pyramidal neurons are substantially higher than those between pyramidal neurons, interneurons can still exhibit selectively in their targeting of post-synaptic pyramidal types. As such, understanding inhibitory inputs as a function of pyramidal neuron heterogeneity has provided additional insight into the principles that govern inhibitory connectivity (Krook-Magnuson et al., 2012). The results of **Chapter 4** demonstrate that the degree to which pyramidal neurons share inhibition varies as a function of pyramidal neuron progenitor type. This builds upon previous work showing that inhibition varies as a function of projection target in L5 (Jézéquel et al., 2023; Lu et al., 2017; Otsuka and Kawaguchi, 2009; Wu et al., 2017, 2023). This is interesting given findings that projection target is biased by progenitor type (Huilgol et al., 2023a), suggesting that separate information processing streams are controlled by different local inhibitory subnetworks. The relation of inhibitory inputs to pyramidal neuron progenitor type suggest that these principles of connectivity are rooted in embryonic development. Therefore, multiple progenitor types may have evolved to diversify the connections between excitatory and inhibitory neurons, in addition to those between excitatory neurons.

6.3.3 The establishment of progenitor-dependent inhibitory subnetworks

A pivotal question arising from the work in this thesis is the potential mechanisms that could underlie the influence of progenitor type on shaping a L2/3 pyramidal neuron's inhibitory subnetwork. Typically, mechanisms explaining the development of neuronal connectivity are divided into either being genetic or activity dependent (Flavell and Greenberg, 2008; Jabaudon, 2017). However, this is an overly reductionist way to interpret the complexity of cortical circuit assembly. Multiple mechanisms, involving interactions between genetic and activity-dependent processes, are more likely to underlie connection biases between neurons derived from different progenitor types. However, at a fundamental level, the mechanism would need to involve the inheritance of a molecular or genetic program from the progenitor type to its neuronal progeny. This could then either act to molecularly specify synap-

tic connections or influence activity patterns in a manner that encourages synaptic connections between certain types of interneuron and pyramidal neuron. In this section I will review potential mechanisms, including those which underlie previously described relationships between progenitors and their neuronal progeny.

Seminal studies found that neurons derived from the same individual progenitor cell exhibit preferential connectivity to one another in mature cortex (Li et al., 2012; Tarusawa et al., 2016; Yu et al., 2009). The mechanism underlying this preferential connectivity has been shown to involve the inheritance of DNA methylation patterns, which regulate the expression of clustered protocadherin (cPcdh) isoforms (Lv et al., 2022; Reik et al., 2001; Tarusawa et al., 2016; Toyoda et al., 2014). cPcdhs represent a large subfamily of the cadherin genes, which encode neuronal molecular identity. cPdchs are transmembrane proteins with intracellular and extracellular domains expressed at neuronal synapses (Basu et al., 2015; Junghans et al., 2008; Kohmura et al., 1998; Phillips et al., 2003; Wu and Maniatis, 1999). Combinatorial expression of cPdch isoforms at synapses enables neurites to differentiate between self and non-self, allowing them to avoid forming synapses onto their own dendrites (Basu et al., 2015; Brasch et al., 2019; Lefebvre et al., 2012; Rubinstein et al., 2015; Schreiner and Weiner, 2010; Thu et al., 2014; Yagi, 2012). A similar mechanism involving cPcdh isoforms is thought to underlie the recognition of neurons born from the same or different progenitor cell (Lv et al., 2022; Tarusawa et al., 2016). The fact that methylation of cPcdh isoform genes in neuronal progeny is inherited from their progenitor makes it an attractive mechanism for underlying progenitor-type-dependent differences in the connectivity of neuronal progeny. As such, knockout of the DNA methyltransferase dnmt3b abolishes preferential reciprocal synaptic connections between clonal neurons (Tarusawa et al., 2016). Furthermore, synaptic connectivity between radial clones was found to reflect differences in cPcdh isoform expression (Lv et al., 2022). Taken together, this evidence suggests that inheritance of cPcdhs are a plausible mechanism for progenitor-type-dependent effects on neuronal connectivity. Indeed, recent work suggests that several genes involved in synapse formation are differentially expressed in IPs relative to RGCs (Bedogni and Hevner, 2021). However, whether inheritance of specific cPcdh isoforms could influence connections between pyramidal neurons and inhibitory interneurons is less

well understood.

cPcdhs are part of a larger family of genes known as cadherins (Basu et al., 2015; Takeichi, 2006). Similar to cPcdhs, cadherin expression is thought to create a molecular identity code across neuronal subtypes, facilitating cell-type-specific connection patterns (Basu et al., 2015; Duan et al., 2014; Price et al., 2002). Interestingly, a recent study has identified the role of two cadherins in the specification of different inhibitory input onto L5 cortical neuron subtypes (Jézéquel et al., 2023). Enriched expression of Cadherin 12 in L5a IT projection neurons was required for preferential input from CCK interneurons. Conversely, expression of Cadherin 13 in L5b ET projection neurons mediated preferential input from PV interneurons. Furthermore, viral rabies tracing revealed that these two L5 pyramidal subtypes received inhibitory input from segregated subnetworks of presynaptic PV interneurons. L5a IT neurons received input from PV interneurons spread across cortical layers, whereas L5b ET neurons received input primarily from PV interneurons within their home layer (Jézéquel et al., 2023). In addition, these segregated PV subnetworks also showed different cadherin expression profiles. Therefore, the findings of this study suggest that differences in cadherin expression may underlie the specification of inhibitory subnetworks. Indeed, these findings are particularly interesting given previous work that has shown that IP-derived L2/3 neurons preferentially connect to L5a IT neurons, whilst OP-derived L2/3 neurons preferentially connect to L5b ET neurons (Ellender et al., 2019). The results from **Chapter 4** found that IP-derived neurons share less of their inhibitory input with OP-derived neurons and other IP-derived neurons. This could result from having a similar inhibitory subnetwork to the L5a IT neurons, whereby their inhibitory inputs come from a wider pool of interneurons which is spread across the cortical layers. OP-derived neurons, on the other hand, may receive more inhibition from their home layer, much like the L5b ET neurons. One hypothesis from these findings would be that IP-derived L2/3 neurons and L5a IT neurons form a preferentially connected excitatory-inhibitory subnetwork, perhaps suggesting participation in different information processing streams or modes of control from inhibitory interneurons (**Figure 6.1**). Further studies could explore this mechanism by examining the expression profile of cadherins in IP-derived and OP-derived L2/3 neurons and performing rabies tracing to uncover the distribution

of PV interneurons connecting to IP-derived and OP-derived L2/3 neurons across cortical layers.

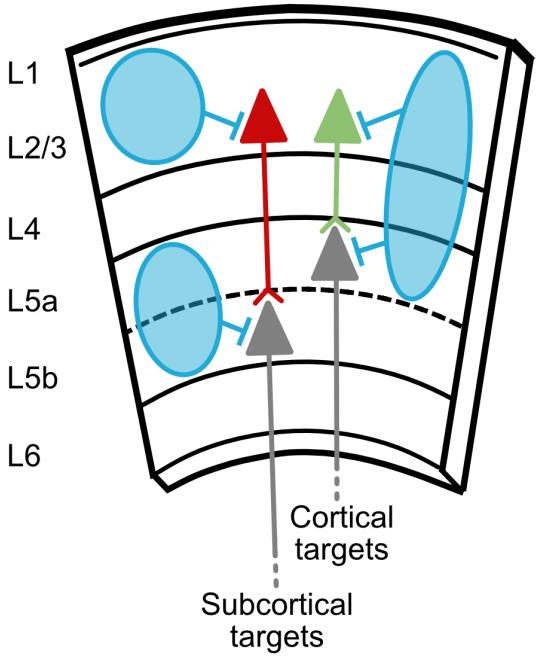


Figure 6.1: Proposed interlaminar excitatory-inhibitory subnetworks. One theory that unites the findings of my thesis, with the results of Ellender et al. (2019) and Jézéquel et al. (2023) is that L2/3 IP-derived neurons form a preferential excitatory-inhibitory subnetwork with L5a pyramidal neurons and translaminar PV interneurons. Specifically, IP-derived neurons (green) preferentially synapse with L5a pyramidal neurons, whereas OP-derived neurons (red) preferentially target those in L5b (Ellender et al., 2019). L5a and L5b pyramidal neurons form separate presynaptic PV inhibitory subnetworks, whereby L5a neurons receive mainly translaminar inhibition and L5b neurons primarily receive inhibition from their home layer (Jézéquel et al., 2023). My results extend these findings by showing that IP-derived L2/3 neurons share less of their inhibition with OP-derived and other IP-derived neurons. One potential explanation for this is their participation in segregated PV subnetworks (represented by blue circles), mirroring those found between L5a and L5b pyramidal neurons.

Whilst the differential expression of cadherin genes is a seemingly likely candidate mechanism that could underlie differences in inhibitory subnetworks, expression differences in single genes are unlikely to constitute a complete mechanism. For instance, Jézéquel et al. (2023) found that overexpression of Cadherin 12 or 13 in L5 ET or IT neurons, respectively, did not produce the reciprocal phenotype, suggesting there are additional differences in the downstream signalling pathways between these neuron types that contribute to their differences in inhibitory input. One possibility is the differential expression of genes between IP-derived and OP-derived L2/3 neu-

rons during early development, when interneurons initially form synaptic circuits with pyramidal neurons (Golshani et al., 2009; Modol et al., 2020; Wong et al., 2018). For example, in L4, IP-derived and OP-derived neurons exhibit differential expression of the transcription factor Lhx2 during the first postnatal week (Buchan et al., 2022). Lhx2 is expressed in early development and regulates the polarization of L4 dendrites in response to thalamocortical afferents (Bulchand et al., 2003; Wang et al., 2017). Interestingly, reduced expression of Lhx2 in IP-derived compared to OP-derived L4 neurons during the first postnatal week regulates differences in the targeting of these cell populations by thalamic nuclei (Buchan et al., 2022). Lhx2 targets the activity-dependent gene Btbd3, such that this genetic pathway regulates the response of L4 dendrites to thalamocortical afferents (Matsui et al., 2013; Shetty et al., 2013; Wang et al., 2017). Therefore, this mechanism provides an excellent example of the interaction between genetic and activity-dependent processes that can underlie progenitor-derived differences in synaptic connectivity. The first postnatal weeks are a crucial time for the formation of interneuron circuits (Butt et al., 2007; Chini et al., 2022; Duan et al., 2020; Golshani et al., 2009; Miyoshi and Fishell, 2011; Modol et al., 2020; Stroud et al., 2020; Daw et al., 2007; Pangratz-Fuehrer and Hestrin, 2011). Over the course of the first 2 postnatal weeks, neuronal activity shifts from highly synchronous spontaneous bursts of activity, to being decorrelated (Golshani et al., 2009; Kirkby et al., 2013; Modol et al., 2020; Duan et al., 2020; Alléne et al., 2008) - a process that is thought to be controlled by the onset of inhibitory GABAergic transmission (Chini et al., 2022; Golshani et al., 2009). The exact mechanisms that instruct this decorrelation are not well understood, however, it is possible that some pyramidal neuron types desynchronize more than others. Future studies could explore how pyramidal neurons share inhibitory inputs across development and the impact progenitor type may have on the refinement of inhibitory synaptic circuits.

Activity-dependent mechanisms play a key role in refining synaptic circuitry, such that certain activity patterns can lead to the formation or removal of synapses between specific cell types (Nelson et al., 1990; Saneyoshi et al., 2010). Activity-dependent mechanisms have been implicated in the preferential synaptic connectivity and similar receptive field properties between clonally related neurons, through

the preferential formation of gap junctions that synchronize responses to feedforward inputs (Ko et al., 2014; Li et al., 2012; Ohtsuki et al., 2012; Yu et al., 2009). Whilst it seems unlikely that a similar mechanism involving gap junction formation between interneurons and pyramidal neurons underlies the findings from **Chapters 3** and **4**, reciprocally synaptically connected L2/3 pyramidal neurons and fast-spiking interneurons have been shown to receive more common excitatory inputs than unconnected pairs (Yoshimura and Callaway, 2005). Therefore, it does appear that correlated inputs can lead to the formation of preferentially connected subnetworks of excitatory and inhibitory neurons. There is also evidence to suggest that these subnetworks relate to the receptive field properties of pyramidal neurons. For instance, pyramidal neurons preferentially receive input from interneurons that share receptive field properties (Palagina et al., 2019; Znamenskiy et al., 2018). Therefore, it is possible that there are differences in the receptive field properties of IP-derived and OP-derived L2/3 neurons, which may in turn influence their sampling of local inhibition. For example, one explanation for the results in **Chapters 3** and **4** could be that IP-derived neurons have broader receptive fields, leading to sampling of a larger inhibitory network.

6.3.4 Implications for the preferential recruitment of IP-derived L2/3 neurons by primary motor cortex

Whilst the response properties of neurons in S1 to bottom-up sensory inputs have been extensively studied, it is increasingly recognised that neurons in S1 are strongly recruited by feedback projections from higher order cortical areas, which play an active role in sensory processing (Aronoff et al., 2010; Kwon et al., 2016; Mao et al., 2011; Naskar et al., 2021; Petreanu et al., 2007, 2012; Xu et al., 2012). How feedback projections engage distinct cell types within circuits in S1 is not well understood. **Chapter 5** of this thesis investigated the extent to which neurons derived from different progenitor types are recruited by long-range inputs from S2 and M1. Whilst IP-derived and OP-derived neurons were recruited equally by the activation of S2 afferents, IP-derived neurons received more monosynaptic excitation from M1 afferents than OP-derived neurons. These results represent the first evidence that progenitor type influences the recruitment by feedback projections from higher order cortical

areas. Indeed, whilst there is a range evidence for the role of developmental history on local cortical connections (Cadwell et al., 2020; Ellender et al., 2019; Lin et al., 2023; Ohtsuki et al., 2012; Yu et al., 2009), fewer studies have investigated how pyramidal neuron progenitor type influences the long-range inputs and outputs of cortical circuitry (Buchan et al., 2022; Ellender et al., 2019; Huilgol et al., 2023a). Therefore, my results contribute to the idea that the generation of cortical neurons via distinct progenitor types acts to amplify and diversify specific connectivity patterns in long-range cortical circuits (Huilgol et al., 2023a).

Interestingly, research from the visual system suggests that feedback inputs from cortical motor areas to primary visual cortex convey predictions about how an animal's movements influence their visual field (Heindorf et al., 2018; Leinweber et al., 2017). By controlling an animal's visual and motor environment whilst recording L2/3 pyramidal neuron responses in visual cortex, Jordan and Keller (2020) showed that artificially generated 'mismatches' between movement and visual flow elicits two distinct response types in L2/3 pyramidal neurons, either net excitation or net inhibition. The recruitment of IP-derived L2/3 neurons by M1 may therefore reflect their contribution to the excitatory, or positive, prediction error L2/3 subtype. Interestingly, the fact that prediction errors can generate excitation or inhibition in L2/3 neurons implies that these subtypes are controlled by separate inhibitory subnetworks (Jordan and Keller, 2020; Hertäg and Clopath, 2022). Therefore, a unifying interpretation of the results from my thesis is that the local and long-range connectivity of IP-derived and OP-derived L2/3 pyramidal neurons implicates them in distinct prediction error circuits.

Recent research has shown that L2/3 prediction error neurons map onto distinct transcriptomic cell types (O'Toole et al., 2023). It was found that L2/3 Rrad and Adamts2 transcriptomic subtypes comprise positive and negative prediction error neurons, respectively. IP-derived neurons mainly consist of the Agmat cell type (Ellender et al., 2019), which was not found to encode either prediction error response (O'Toole et al., 2023). The authors propose that the Agmat cell type may encode a different type of prediction error that signals mismatch across different sensory variables, or may function to integrate over both positive and negative prediction errors. It is also important to note that this study was conducted in visual cortex,

and therefore it is unclear how these circuits and cell types might correspond to those in barrel cortex.

It is important to consider that the activation of M1 has broad and diverse effects on a variety of cell types in S1. Notably, M1 strongly recruits VIP interneurons, leading to the inhibition of SST interneurons and disinhibition of pyramidal cell dendrites (Lee et al., 2013; Naskar et al., 2021). The disinhibition of pyramidal neuron dendrites is thought to enable the coincident detection of sensory touch and whisker movements, generating large calcium transients, and leading to supralinear increases in response properties Khateb et al. (2017); Larkum (2013); Petersen (2014); Xu et al. (2012); Zagha et al. (2013). The findings from **Chapter 4** suggest that progenitor type does not influence the level of inhibitory input received by L2/3 pyramidal neurons from VIP or SST interneurons. However, the strength of disinhibitory circuits are difficult to test *in vitro* as they require controlling the activity of multiple cell types simultaneously. Additionally, space clamp errors present challenges of accurately measuring excitation in distal dendrites. It would therefore be interesting to explore the influence of M1 input to dendritic regions of IP-derived neurons *in vivo*, where disinhibitory circuits are intact. One such experiment could use calcium or voltage imaging of the apical dendrites of IP-derived neurons to measure changes in dendritic excitability following M1 activation. To assess the contribution of IP-derived neurons to sensorimotor processing, one could use IUE to express inhibitory opsins in IP-derived neurons and assess the effect of inhibiting IP-derived neuron activity on tasks requiring integration of sensory input and whisker movements.

6.3.5 Functional implications for cortical excitatory and inhibitory subnetworks specified by progenitor type

The findings of this thesis implicate the role of pyramidal neuron progenitor type in the shaping of local inhibitory and long-range excitatory inputs to L2/3 pyramidal neurons (**Figure 6.2a**). This presents the question of the functionality which might be conferred by these IP-derived circuits. Whilst the implications for the preferential sampling of M1 input by IP-derived neurons in predictive processing was discussed

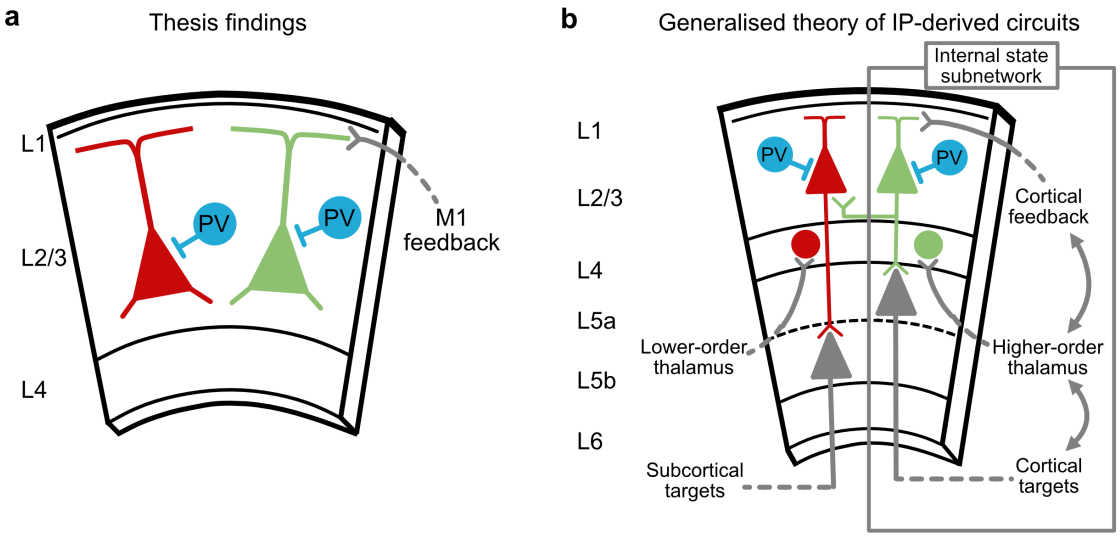


Figure 6.2: IP-derived cortical circuits. (**a**) Schematic summarising the findings of my thesis. OP-derived (red) and IP-derived (green) L2/3 neurons participate in segregated PV subnetworks. IP-derived neurons receive preferential monosynaptic excitatory feedback from M1. (**b**) Schematic summarising the findings of my thesis in addition to those from Buchan et al. (2022) and Ellender et al. (2019). OP-derived L4 neurons receive preferential input from the lower order thalamus, VPM, whereas IP-derived L4 neurons receive preferential input from the higher order thalamus, POm (Buchan et al., 2022). IP-derived L2/3 neurons form intralaminar synaptic connectivity biases with OP-derived L2/3 neurons and translaminar output biases to L5a pyramidal neurons (Ellender et al., 2019). OP-derived L2/3 neurons form translaminar output biases to L5b pyramidal neurons Ellender et al. (2019). IP-derived L2/3 neurons receive preferential feedback from M1. Taken together, these findings suggest that IP-derived neurons preferentially form cortico-cortical subnetworks, potentially serving the role of conveying information about internal state.

in **Chapter 6.3.4**, the following section will explore the functionality of progenitor-dependent subnetworks more generally.

One of the challenges the brain faces during sensory processing is to accurately represent external stimuli whilst simultaneously integrating this information with contextual signals, such as motor, behavioural and arousal cues. The whisker somatosensory system achieves such tasks by separating information into parallel processing streams. The lemniscal pathway is primarily driven by the first-order thalamic nucleus, VPM, whereas the paralemniscal pathway is driven by the higher-order thalamic nucleus, POm. These pathways remain segregated within cortical circuits, primarily targeting distinct cell types across cortical layers (Bureau et al., 2006; Sermet et al., 2019; Shepherd and Svoboda, 2005). Previous research has implicated the preferential involvement of IP-derived neurons in the paralemniscal pathway, suggesting that one function of progenitor-dependent subnetworks is to differen-

tially contribute to parallel streams of sensory processing. Buchan et al. (2022) found that IP-derived neurons in L4 receive preferential input from POm, whereas OP-derived neurons receive more input from VPM. My findings that IP-derived and OP-derived L2/3 neurons sample from different inhibitory subnetworks and that IP-derived neurons receive preferential input from M1, support the idea that these cell types contribute to separate information streams during sensory processing. Both POm and M1 are activated prior to or during whisking (Alloway, 2008; Alloway et al., 2004; Petersen, 2007; Petreanu et al., 2012; Zagha et al., 2013), suggesting that the recruitment of IP-derived neurons in S1 across cortical layers is important for integrating signals encoding whisker movement.

Further evidence implicates IP-derived circuits in differential sensory processing streams. Ellender et al. (2019) found that IP-derived L2/3 pyramidal neurons preferentially synapse onto L5 intratelencephalic (IT) neurons, whereas OP-derived neurons preferentially synapse onto L5 extratelencephalic (ET) neurons. Furthermore, Huilgol et al. (2023a) found that IP-derived neurons specifically contribute to IT projection neuron classes. Taken together, these findings suggest that IP-derived neurons expand and diversify cortico-cortical networks. Computational theories of cortical function suggest that recurrent activity in cortico-cortical networks represents an internal model of the world from which predictions are made about incoming stimuli (Gilbert and Sigman, 2007; Keller and Mrsic-Flogel, 2018; Moberg and Takahashi, 2022). Therefore, the findings from this thesis, together with those previously reported, are consistent with a model whereby IP-derived neurons preferentially form subnetworks that convey information about internal state (Buchan et al., 2022; Ellender et al., 2019; Huilgol et al., 2023a) (**Figure 6.2b**).

Within this framework, several aspects of IP-derived circuits may confer specific functions. For example, the fact that IP-derived and OP-derived neurons are intermixed across cortical layers holds potential significance for the integration of signals about internal state with signals about the external environment. Such integration is necessary in order to generate a comprehensive representation of the outside world. One functionality of this integration may be the prediction error circuits described in **Chapter 6.3.4**. Additionally, the preference for IP-derived neurons to connect to OP-derived neurons (Ellender et al., 2019) may serve as a mechanism to

enable control or modulation of the OP-derived subnetwork by the IP-derived subnetwork. Although speculative, these interpretations help to consolidate the local and long-range observations of IP-derived circuits into a unified theory.

It would be interesting for future research to test predictions which build upon the idea that IP-derived circuits serve to generate subnetworks about internal state. For example, do IP-derived neurons exhibit similar connection biases across cortical areas? This could be tested by using IUE to target labelling of IP-derived neurons to different cortical areas, such as visual or auditory cortex. It would then be possible to test if IP-derived neurons in these areas also receive preferential input from higher-order thalamic nuclei or from motor cortex, which would suggest a general function of IP-derived circuits across primary sensory cortical areas. It would also be interesting to explore the synaptic connectivity of IP-derived neurons in higher-order cortical areas, such as S2 or M1. IP-derived neurons within these areas may help pass information up the cortical hierarchy, towards areas like secondary motor cortex or frontal cortex. Alternatively, they may preferentially participate in feedback circuits, targeting lower-order cortical areas, such as S1. Collectively, these experiments would facilitate our knowledge towards a general theory about the functionality of IP-derived circuits.

The evolutionary expansion of IPs in higher order mammals may enable them to execute more complex behaviour, for example, through integration of external signals with a wider variety of internally generated behavioural states (Dehay and Kennedy, 2023; Kennedy et al., 2021). A major site of neurogenesis in humans and non-human primates (NHPs) is the outer SVZ (oSVZ), which does not exist in rodents. The oSVZ contains additional progenitor types, novel gene expression patterns and more complex lineages compared to the proliferative zones in the mouse (Arcila et al., 2014; Betizeau et al., 2013; Dehay and Kennedy, 2023; Kennedy et al., 2021; Pebworth et al., 2021; Wilsch-Bräuninger et al., 2016). These progenitor types generate neurons that contribute towards the supragranular cortical layers, which exhibit significant expansion as well as diversification in humans and NHPs (Berg et al., 2021; Kennedy et al., 2021; Planert et al., 2023). Elucidating the role of additional progenitor types in the human brain represents a paramount objective in developmental neuroscience. Nevertheless, conducting experiments to examine

the functionality of diverse progenitor-derived circuits in humans and NHPs poses inherent challenges. Consequently, probing the functionality of IP-derived circuits in rodents offers an avenue for inferring the functional significance of these circuits.

6.3.6 Progenitor type as a general mechanism for specifying cortical circuitry

The results of this thesis and that of previous work (Buchan et al., 2022; Ellender et al., 2019; Guillamon-Vivancos et al., 2019; Tyler et al., 2015) prompt an important question: to what extent does the classification of neurons based on their progenitor type offer a meaningful framework for understanding excitatory neuron diversity? Specifically, does awareness of a neuron's progenitor type provide additional insight into its identity and function, beyond what may be inferred from knowing it's transcriptomic cell type or axonal projection target? These ideas will be explored in the following subsection.

A range of studies suggest that progenitor type of origin can bias many aspects of neuronal identity. These include local connectivity (Ellender et al., 2019), inputs from thalamic nuclei (Buchan et al., 2022), morphology (Buchan et al., 2022; Guillamon-Vivancos et al., 2019; Tyler et al., 2015), local and long range excitatory connections (Huilgol et al., 2023a) (**Chapter 5**) and inhibitory inputs (**Chapter 4**). Findings from Ellender et al. (2019) found that IP-derived and OP-derived L2/3 neurons are comprised of different proportions of L2/3 transcriptomic cell types. OP-derived neurons were found to consist of a mix across several L2/3 transcriptomic cell types, whereas IP-derived neurons were found to consist almost exclusively of the Agmat cell type. This extends previous work suggesting that the temporal progression of progenitors during neurogenesis gives rise to different transcriptomic cell types in a sequential manner (Franco and Müller, 2013; Gao et al., 2014; Heavner et al., 2020; Magrinelli et al., 2022; Ruan et al., 2021; Telley et al., 2019). Therefore, one could argue that progenitor type biases in the transcriptomic output of their progeny is sufficient to explain differences in the functional properties of neurons born from distinct progenitor types. This is supported by studies identifying transcriptomic cell types that correspond to their functional properties (Cadwell et al.,

2015; Földy et al., 2016; Gouwens et al., 2020; Kim et al., 2015; Zeng, 2022; Zeng and Sanes, 2017; Zhang et al., 2021; Sorensen et al., 2023). Indeed, one could empirically test whether the intralaminar progenitor-type connection biases identified in Ellender et al. (2019) are a result of transcriptomic cell type, through using recently developed viral tools that specifically label transcriptomic cell types in L2/3 (O'Toole et al., 2023), alongside patch-clamp electrophysiology to test monosynaptic connections between different L2/3 transcriptomic cell types.

If individual progenitors are restricted in their potential to produce certain transcriptomic cell types, this may offer insights into the previously described relationships between clonal and non-clonal neurons (Cadwell et al., 2020; Ohtsuki et al., 2012; Yu et al., 2009). In other words, if a clone encompasses a specific subset of neuronal cell types, the observed biased clonal connectivity might arise as an inherent characteristic of these cell types, rather than being directly attributable to clonality itself. To test this prediction, one could use genetic barcoding to label clonally related neurons in combination with RNA sequencing to investigate their corresponding transcriptomic cell type. Interestingly, the distribution of clonal neurons across layers is non-random (Lin et al., 2021; Llorca et al., 2019), suggesting that individual progenitors may be biased in their output of transcriptomically defined neurons.

Conversely, there is evidence to suggest that transcriptomic cell type alone is insufficient at explaining differences between neurons derived from separate progenitor types (Buchan et al., 2022). L4 neurons have traditionally been thought of as a relatively homogenous population and have been classified as one transcriptomic cell type (Tasic et al., 2018). Despite this, Buchan et al. (2022) revealed differences in the sampling of thalamic nuclei and receptive field properties of L4 neurons derived from IPs compared to those derived from OPs. Interestingly, these differences could be equalised through manipulating the expression level of the transcription factor Lhx2 between the two neuronal populations. Therefore, this study suggests that progenitor type has the potential to confer a finer grain of diversity than may be acknowledged at the level of transcriptomic cell type. It is possible that more in-depth sequencing attempts may reveal transcriptomic differences between IP-derived and OP-derived L4 neurons. Additionally, this study signifies how the differential expression of one or a few key transcription factors can have profound consequences

for neuronal identity, whilst simultaneously not being sufficient to separate neuronal populations into distinct transcriptomic cell types (Huilgol et al., 2023b).

Further support for fine grain diversity that is not recognised at the level of transcriptomic cell types can be seen in Kim et al. (2020). In this study, rabies tracing was used in combination with single-cell RNA sequencing to investigate how the projection targets of L2/3 neurons in visual cortex aligns with their transcriptomic cell type. Despite projecting to different cortical areas, these neurons constituted a genetically continuous population and could not be separated based on their gene expression levels alone. Comparable findings of genetically continuous L2/3 neurons has been reported in motor cortex (Zhang et al., 2021). This questions whether discrete neuronal subtypes really exist, or if transcriptomic cell types lie along a continuum. If the latter is true, it challenges the utility of transcriptomics in delineating meaningful and functionally relevant cell types. It may be the case that progenitor type indicates a discrete fate choice that guides transcriptomic cell type, yet shared environmental factors throughout development may contribute towards the convergence of cell types into a continuum in the mature cortex.

Progenitor type may therefore provide a foundational level of neuronal specification, perhaps orchestrated by the inheritance of a few key genes (Arlotta et al., 2005; Chen et al., 2005; Matho et al., 2021; Molyneaux et al., 2005; Pearson et al., 2020), upon which developmental programs guided by environmental factors further refine neuronal subtypes (Greig et al., 2013; Molyneaux et al., 2007; Nowakowski et al., 2017; Telley et al., 2016). Recent evidence suggests that transcriptomic subtypes of both excitatory and inhibitory neurons can predict their activity in vivo (Bugeon et al., 2022; Condylis et al., 2020; O'Toole et al., 2023; Schneider et al., 2023). Therefore, the embryonic origins of such cell types may represent a developmental mechanism allowing the predisposing of neurons for different information processing streams in mature cortex. Such specification of functionality during neurogenesis is particularly intriguing given the evolutionary expansion of progenitor diversity in higher-order mammals (Kennedy et al., 2021; Martinez-Cerdeno et al., 2006). This expansion may act to amplify and diversify specific information processing streams, enhancing the computational capabilities of cortical circuits.

6.4 Concluding remarks

In this thesis I have examined the inputs from local inhibitory interneurons and long-range feedback to L2/3 pyramidal neurons as a function of their progenitor type. Firstly, I have shown that IP-derived neurons receive inhibition that is less well correlated to local network activity. Secondly, whilst the overall level of synaptic inhibition to neurons derived from IPs is comparable to that of OPs, I show that PV interneurons differentially connect to L2/3 pyramidal neurons based on their progenitor type, determining how inhibition is shared amongst L2/3 pyramidal neurons. Finally, I have demonstrated that IP-derived neurons receive preferential input from M1, but not S2 or L5 of S1, when compared to OP-derived neurons. These data contribute to a growing body of evidence that progenitor type governs local and long-range synaptic circuits in mammalian cortex. This supports the conclusion that the construction of excitatory-inhibitory cortical networks is embedded in embryonic development and that heterogeneity amongst progenitors contributes to diversity within these networks. Therefore, progenitor diversity may have evolved in part to generate specific cortical subnetworks, and progenitor identity may be an effective approach for understanding the origins of inhibitory subnetworks across brain areas and species.

Bibliography

Abe, P., Lavalley, A., Morassut, I., Klingler, E., Santinha, A. J., Platt, R. J., and Jabaudon, D. (2023). Developmental molecular controls over arealization of descending cortical motor pathways. *bioRxiv*, page 2023.06.29.546438.

Abs, E., Poorthuis, R. B., Apelblat, D., Muhammad, K., Pardi, M. B., Enke, L., Kushinsky, D., Pu, D.-L., Eizinger, M. F., Conzelmann, K.-K., Spiegel, I., and Letzkus, J. J. (2018). Learning-related plasticity in dendrite-targeting layer 1 interneurons. *Neuron*, 100:684–699.e6.

Adesnik, H. (2018). Layer-specific excitation/inhibition balances during neuronal synchronization in the visual cortex. *The Journal of Physiology*, 596:1639–1657.

Adesnik, H. and Scanziani, M. (2010). Lateral competition for cortical space by layer-specific horizontal circuits. *Nature*, 464:1155–1160.

Alfonsa, H., Burman, R. J., Brodersen, P. J., Newey, S. E., Mahfooz, K., Yamagata, T., Panayi, M. C., Bannerman, D. M., Vyazovskiy, V. V., and Akerman, C. J. (2023). Intracellular chloride regulation mediates local sleep pressure in the cortex. *Nature Neuroscience*, 26:64–78.

Alléne, C., Cattani, A., Ackman, J. B., Bonifazi, P., Aniksztejn, L., Ben-Ari, Y., and Cossart, R. (2008). Sequential generation of two distinct synapse-driven network patterns in developing neocortex. *The Journal of Neuroscience*, 28:12851–12863.

Alloway, K. D. (2008). Information processing streams in rodent barrel cortex: The differential functions of barrel and septal circuits. *Cerebral Cortex*, 18:979–989.

Alloway, K. D., Zhang, M., and Chakrabakti, S. (2004). Septal columns in rodent barrel cortex: Functional circuits for modulating whisking behavior. *Journal of Comparative Neurology*, 480:299–309.

Anastasiades, P. G., Marques-Smith, A., Lyngholm, D., Lickiss, T., Raffiq, S.,

Katzel, D., Miesenbock, G., and Butt, S. J. (2016). Gabaergic interneurons form transient layer-specific circuits in early postnatal neocortex. *Nature Communications*, 7:1–13.

Anderson, C. T., Sheets, P. L., Kiritani, T., and Shepherd, G. M. (2010). Sublayer-specific microcircuits of corticospinal and corticostriatal neurons in motor cortex. *Nature Neuroscience*, 13:739–744.

Anderson, S. A., Kaznowski, C. E., Horn, C., Rubenstein, J. L., and McConnell, S. K. (2002). Distinct origins of neocortical projection neurons and interneurons in vivo. *Cerebral Cortex*, 12:702–709.

Anthony, T. E., Klein, C., Fishell, G., and Heintz, N. (2004). Radial glia serve as neuronal progenitors in all regions of the central nervous system. *Neuron*, 41:881–890.

Anton-Bolanos, N., Sempere-Ferràndez, A., Guillamón-Vivancos, T., Martini, F. J., Pérez-Saiz, L., Gezelius, H., Filipchuk, A., Valdeolmillos, M., and López-Bendito, G. (2019). Prenatal activity from thalamic neurons governs the emergence of functional cortical maps in mice. *Science*, 364:987.

Antypa, M., Faux, C., Eichele, G., Parnavelas, J. G., and Andrews, W. D. (2011). Differential gene expression in migratory streams of cortical interneurons. *The European journal of neuroscience*, 34:1584–1594.

Arcila, M. L., Betizeau, M., Cambronne, X. A., Guzman, E., Doerflinger, N., Bouhallier, F., Zhou, H., Wu, B., Rani, N., Bassett, D. S., Borello, U., Huissoud, C., Goodman, R. H., Dehay, C., and Kosik, K. S. (2014). Novel primate mirnas coevolved with ancient target genes in germinal zone-specific expression patterns. *Neuron*, 81:1255–1262.

Arlotta, P., Molyneaux, B. J., Chen, J., Inoue, J., Kominami, R., and MacKlis, J. D. (2005). Neuronal subtype-specific genes that control corticospinal motor neuron development in vivo. *Neuron*, 45:207–221.

Aronoff, R., Matyas, F., Mateo, C., Ciron, C., Schneider, B., and Petersen, C. (2010). Long-range connectivity of mouse primary somatosensory barrel cortex. *Eur. J. Neurosci.*, 31:2221–2233.

Ascoli, G. A., Alonso-Nanclares, L., Anderson, S. A., Barrionuevo, G., Benavides-Piccione, R., Burkhalter, A., Buzsáki, G., Cauli, B., DeFelipe, J., Fairén, A., Feldmeyer, D., Fishell, G., Fregnac, Y., Freund, T. F., Gardner, D., Gardner, E. P., Goldberg, J. H., Helmstaedter, M., Hestrin, S., Karube, F., Kisvárday, Z. F., Lambolez, B., Lewis, D. A., Marin, O., Markram, H., uoz, A. M., Packer, A., Petersen, C. C., Rockland, K. S., Rossier, J., Rudy, B., Somogyi, P., Staiger, J. F., Tamas, G., Thomson, A. M., Toledo-Rodriguez, M., Wang, Y., West, D. C., and Yuste, R. (2008). Petilla terminology: nomenclature of features of gabaergic interneurons of the cerebral cortex. *Nature Reviews Neuroscience*, 9:557–568.

Ashby, M. C. and Isaac, J. T. (2011). Maturation of a recurrent excitatory neocortical circuit by experience-dependent unsilencing of newly formed dendritic spines. *Neuron*, 70:510–521.

Atallah, B. V. and Scanziani, M. (2009). Instantaneous modulation of gamma oscillation frequency by balancing excitation with inhibition. *Neuron*, 62:566–577.

Attardo, A., Calegari, F., Haubensak, W., Wilsch-Bräuninger, M., and Huttner, W. B. (2008). Live imaging at the onset of cortical neurogenesis reveals differential appearance of the neuronal phenotype in apical versus basal progenitor progeny. *PLOS ONE*, 3:e2388.

Audette, N. J., Bernhard, S. M., Ray, A., Stewart, L. T., and Barth, A. L. (2019). Rapid plasticity of higher-order thalamocortical inputs during sensory learning. *Neuron*, 103:277–291.e4.

Audette, N. J., Urban-Ciecko, J., Matsushita, M., and Barth, A. L. (2018). Pom thalamocortical input drives layer-specific microcircuits in somatosensory cortex. *Cerebral Cortex*, 28:1312–1328.

Avermann, M., Tomm, C., Mateo, C., Gerstner, W., and Petersen, C. C. (2012). Microcircuits of excitatory and inhibitory neurons in layer 2/3 of mouse barrel cortex. *Journal of neurophysiology*, 107(11):3116–3134.

Baker, A., Kalmbach, B., Morishima, M., Kim, J., Juavinett, A., Li, N., and Dembrow, N. (2018). Specialized subpopulations of deep-layer pyramidal neurons in

the neocortex: Bridging cellular properties to functional consequences. *The Journal of Neuroscience*, 38:5441.

Bandler, R. C., Vitali, I., Delgado, R. N., Ho, M. C., Dvoretskova, E., Molinas, J. S. I., Frazel, P. W., Mohammadkhani, M., Machold, R., Maedler, S., Liddelow, S. A., Nowakowski, T. J., Fishell, G., and Mayer, C. (2021). Single-cell delineation of lineage and genetic identity in the mouse brain. *Nature*, 601:404–409.

Bar-Yehuda, D. and Korngreen, A. (2008). Space-clamp problems when voltage clamping neurons expressing voltage-gated conductances. *Journal of Neurophysiology*, 99:1127–1136.

Barth, A. L. and Poulet, J. F. (2012). Experimental evidence for sparse firing in the neocortex. *Trends in Neurosciences*, 35:345–355.

Bartolini, G., Ciceri, G., and Marín, O. (2013). Integration of gabaergic interneurons into cortical cell assemblies: Lessons from embryos and adults. *Neuron*, 79:849–864.

Bartolini, G., niz, J. A. S.-A., Osório, C., Valiente, M., García-Frigola, C., and Marín, O. (2017). Neuregulin 3 mediates cortical plate invasion and laminar allocation of gabaergic interneurons. *Cell Reports*, 18:1157–1170.

Bartolo, R., Saunders, R. C., Mitz, A. R., and Averbeck, B. B. (2020). Information-limiting correlations in large neural populations. *The Journal of Neuroscience*, 40:1668–1678.

Baruchin, L. J., Ghezzi, F., Kohl, M. M., and Butt, S. J. (2022). Contribution of interneuron subtype-specific gabaergic signaling to emergent sensory processing in mouse somatosensory whisker barrel cortex. *Cerebral Cortex*, 32:2538–2554.

Bastos, A. M., Usrey, W. M., Adams, R. A., Mangun, G. R., Fries, P., and Friston, K. J. (2012). Canonical microcircuits for predictive coding. *Neuron*, 76:695–711.

Basu, R., Taylor, M. R., and Williams, M. E. (2015). The classic cadherins in synaptic specificity. *Cell Adhesion Migration*, 9:193.

Baumgart, J. and Grebe, N. (2015). C57bl/6-specific conditions for efficient *in utero*

electroporation of the central nervous system. *Journal of Neuroscience Methods*, 240:116–124.

Bé, J. V. L., Silberberg, G., Wang, Y., and Markram, H. (2007). Morphological, electrophysiological, and synaptic properties of corticocallosal pyramidal cells in the neonatal rat neocortex. *Cerebral Cortex*, 17:2204–2213.

Beaulieu, C. (1993). Numerical data on neocortical neurons in adult rat, with special reference to the gaba population. *Brain research*, 609:284–292.

Bedogni, F. and Hevner, R. F. (2021). Cell-type-specific gene expression in developing mouse neocortex: Intermediate progenitors implicated in axon development. *Frontiers in Molecular Neuroscience*, 14:686034.

Beierlein, M., Gibson, J. R., and Connors, B. W. (2003). Two dynamically distinct inhibitory networks in layer 4 of the neocortex. *Journal of Neurophysiology*, 90:2987–3000.

Bella, D. J. D., Habibi, E., Stickels, R. R., Scalia, G., Brown, J., Yadollahpour, P., Yang, S. M., Abbate, C., Biancalani, T., Macosko, E. Z., Chen, F., Regev, A., and Arlotta, P. (2021). Molecular logic of cellular diversification in the mouse cerebral cortex. *Nature*, 595:554–559.

Beltramo, R., D'Urso, G., Maschio, M. D., Farisello, P., Bovetti, S., Clovis, Y., Lassi, G., Tucci, V., Tonelli, D. D. P., and Fellin, T. (2013). Layer-specific excitatory circuits differentially control recurrent network dynamics in the neocortex. *Nature Neuroscience 2013 16:2*, 16:227–234.

Bender, K. J., Rangel, J., and Feldman, D. E. (2003). Development of columnar topography in the excitatory layer 4 to layer 2/3 projection in rat barrel cortex. *Journal of Neuroscience*, 23:8759–8770.

Berg, J., Sorensen, S. A., Ting, J. T., Miller, J. A., Chartrand, T., Buchin, A., Bakken, T. E., Budzillo, A., Dee, N., Ding, S. L., Gouwens, N. W., Hodge, R. D., Kalmbach, B., Lee, C., Lee, B. R., Alfiler, L., Baker, K., Barkan, E., Beller, A., Berry, K., Bertagnolli, D., Bickley, K., Bomben, J., Braun, T., Brouner, K., Casper, T., Chong, P., Crichton, K., Dalley, R., de Frates, R., Desta, T., Lee, S. D., DâOrazi, F., Dotson, N., Egdorf, T., Enstrom, R., Farrell, C., Feng, D.,

Fong, O., Furdan, S., Galakhova, A. A., Gamlin, C., Gary, A., Glandon, A., Goldy, J., Gorham, M., Goriounova, N. A., Gratiy, S., Graybuck, L., Gu, H., Hadley, K., Hansen, N., Heistek, T. S., Henry, A. M., Heyer, D. B., Hill, D. J., Hill, C., Hupp, M., Jarsky, T., Kebede, S., Keene, L., Kim, L., Kim, M. H., Kroll, M., Latimer, C., Levi, B. P., Link, K. E., Mallory, M., Mann, R., Marshall, D., Maxwell, M., McGraw, M., McMillen, D., Melief, E., Mertens, E. J., Mezei, L., Mihut, N., Mok, S., Molnar, G., Mukora, A., Ng, L., Ngo, K., Nicovich, P. R., Nyhus, J., Olah, G., Oldre, A., Omstead, V., Ozsvar, A., Park, D., Peng, H., Pham, T., Pom, C. A., Potekhina, L., Rajanbabu, R., Ransford, S., Reid, D., Rimorin, C., Ruiz, A., Sandman, D., Sulc, J., Sunkin, S. M., Szafer, A., Szemenyei, V., Thomsen, E. R., Tieu, M., Torkelson, A., Trinh, J., Tung, H., Wakeman, W., Waleboer, F., Ward, K., Wilbers, R., Williams, G., Yao, Z., Yoon, J. G., Anastassiou, C., Arkhipov, A., Barzo, P., Bernard, A., Cobbs, C., de Witt Hamer, P. C., Ellenbogen, R. G., Esposito, L., Ferreira, M., Gwinn, R. P., Hawrylycz, M. J., Hof, P. R., Idema, S., Jones, A. R., Keene, C. D., Ko, A. L., Murphy, G. J., Ng, L., Ojemann, J. G., Patel, A. P., Phillips, J. W., Silbergeld, D. L., Smith, K., Tasic, B., Yuste, R., Segev, I., de Kock, C. P., Mansvelder, H. D., Tamas, G., Zeng, H., Koch, C., and Lein, E. S. (2021). Human neocortical expansion involves glutamatergic neuron diversification. *Nature*, 598:151–158.

Berger, T. K., Silberberg, G., Perin, R., and Markram, H. (2010). Brief bursts self-inhibit and correlate the pyramidal network. *PLOS Biology*, 8:e1000473.

Bernander, O., Douglas, R. J., Martin, K. A., and Koch, C. (1991). Synaptic background activity influences spatiotemporal integration in single pyramidal cells. *Proceedings of the National Academy of Sciences of the United States of America*, 88:11569–11573.

Betizeau, M., Cortay, V., Patti, D., Pfister, S., Gautier, E., Bellemin-Ménard, A., Afanassieff, M., Huissoud, C., Douglas, R. J., Kennedy, H., and Dehay, C. (2013). Precursor diversity and complexity of lineage relationships in the outer subventricular zone of the primate. *Neuron*, 80:442–457.

Binzegger, T., Douglas, R. J., and Martin, K. A. (2004). A quantitative map of the circuit of cat primary visual cortex. *The Journal of Neuroscience*, 24:8441–8453.

Bishop, K. M., Goudreau, G., and O'Leary, D. D. (2000). Regulation of area identity in the mammalian neocortex by emx2 and pax6. *Science*, 288(5464):344–349.

Bock, D. D., Lee, W. C. A., Kerlin, A. M., Andermann, M. L., Hood, G., Wetzel, A. W., Yurgenson, S., Soucy, E. R., Kim, H. S., and Reid, R. C. (2011). Network anatomy and *in vivo* physiology of visual cortical neurons. *Nature*, 471:177–184.

Borg-Graham, L. J., Monier, C., and Fregnac, Y. (1998). Visual input evokes transient and strong shunting inhibition in visual cortical neurons. *Nature*, 393:369–373.

Bortone, D. S., Olsen, S. R., and Scanziani, M. (2014). Translaminar inhibitory cells recruited by layer 6 corticothalamic neurons suppress visual cortex. *Neuron*, 82:474–485.

Boyden, E. S. (2011). A history of optogenetics: the development of tools for controlling brain circuits with light. *F1000 Biology Reports*, 3:11.

Boyden, E. S., Zhang, F., Bamberg, E., Nagel, G., and Deisseroth, K. (2005). Millisecond-timescale, genetically targeted optical control of neural activity. *Nature Neuroscience*, 8:1263–1268.

Brasch, J., Goodman, K. M., Noble, A. J., Rapp, M., Mannepalli, S., Bahna, F., Dandey, V. P., Bepler, T., Berger, B., Maniatis, T., Potter, C. S., Carragher, B., Honig, B., and Shapiro, L. (2019). Visualization of clustered protocadherin neuronal self-recognition complexes. *Nature*, 569:280–283.

Brecht, M., Roth, A., and Sakmann, B. (2003). Dynamic receptive fields of reconstructed pyramidal cells in layers 3 and 2 of rat somatosensory barrel cortex. *The Journal of Physiology*, 553:243–265.

Brecht, M. and Sakmann, B. (2002). Dynamic representation of whisker deflection by synaptic potentials in spiny stellate and pyramidal cells in the barrels and septa of layer 4 rat somatosensory cortex. *The Journal of Physiology*, 543:49–70.

Briggs, F. (2010). Organizing principles of cortical layer 6. *Frontiers in Neural Circuits*, 4:750.

Brodmann, K. (1909). *Vergleichende Lokalisationslehre der Grosshirnrinde in ihren Prinzipien dargestellt auf Grund des Zellenbaues*. Barth.

Brown, S. P. and Hestrin, S. (2009). Intracortical circuits of pyramidal neurons reflect their long-range axonal targets. *Nature*, 457:1133–1136.

Buchan, M. J., Mahfooz, K., van Rheede, J. J., Gothard, G., Avery, S. V., Ellender, T. J., Newey, S. E., and Akerman, C. J. (2022). Cortical integration of higher-order thalamic inputs is lineage-dependent. *bioRxiv*, page 2022.03.28.486015.

Buchanan, K. A., Blackman, A. V., Moreau, A. W., Elgar, D., Costa, R. P., Lalanne, T., Jones, A. A. T., Oyrer, J., and Sjöström, P. J. (2012). Target-specific expression of presynaptic nmda receptors in neocortical microcircuits. *Neuron*, 75:451.

Bugeon, S., Duffield, J., Dipoppa, M., Ritoux, A., Prankerd, I., Nicoloutsopoulos, D., Orme, D., Shinn, M., Peng, H., Forrest, H., Viduolyte, A., Reddy, C. B., Isogai, Y., Carandini, M., and Harris, K. D. (2022). A transcriptomic axis predicts state modulation of cortical interneurons. *Nature*, 607:330–338.

Bulchand, S., Subramanian, L., and Tole, S. (2003). Dynamic spatiotemporal expression of lim genes and cofactors in the embryonic and postnatal cerebral cortex. *Developmental Dynamics*, 226:460–469.

Bullier, J., Hupé, J. M., James, A. C., and Girard, P. (2001). The role of feedback connections in shaping the responses of visual cortical neurons. *Progress in brain research*, 134:193–204.

Bureau, I., Paul, F. S. V., and Svoboda, K. (2006). Interdigitated paralemniscal and lemniscal pathways in the mouse barrel cortex. *PLoS biology*, 4:2361–2371.

Bureau, I., Shepherd, G. M., and Svoboda, K. (2004). Precise development of functional and anatomical columns in the neocortex. *Neuron*, 42:789–801.

Burman, R. J., Brodersen, P. J., Raimondo, J. V., Sen, A., and Akerman, C. J. (2023). Active cortical networks promote shunting fast synaptic inhibition in vivo. *bioRxiv*, page 2023.03.01.530641.

Bush, P. and Sejnowski, T. (1996). Inhibition synchronizes sparsely connected cor-

tical neurons within and between columns in realistic network models. *Journal of computational neuroscience*, 3:91–110.

Buskila, Y., Breen, P. P., Tapson, J., Schaik, A. V., Barton, M., and Morley, J. W. (2014). Extending the viability of acute brain slices. *Scientific Reports*, 4.

Butt, S. J., Cobos, I., Golden, J., Kessaris, N., Pachnis, V., and Anderson, S. (2007). Transcriptional regulation of cortical interneuron development. *Journal of Neuroscience*, 27:11847–11850.

Butt, S. J., Fuccillo, M., Nery, S., Noctor, S., Kriegstein, A., Corbin, J. G., and Fishell, G. (2005). The temporal and spatial origins of cortical interneurons predict their physiological subtype. *Neuron*, 48:591–604.

Butt, S. J., Sousa, V. H., Fuccillo, M. V., Hjerling-Leffler, J., Miyoshi, G., Kimura, S., and Fishell, G. (2008). The requirement of nkx2-1 in the temporal specification of cortical interneuron subtypes. *Neuron*, 59:722–732.

Buzsáki, G. (2004). Large-scale recording of neuronal ensembles. *Nature Neuroscience*, 7:446–451.

Buzsáki, G., Anastassiou, C. A., and Koch, C. (2012). The origin of extracellular fields and currents–eeg, ecog, lfp and spikes. *Nature Reviews Neuroscience*, 13:407–20.

Buzsáki, G. and Wang, X.-J. (2012). Mechanisms of gamma oscillations. *Annual Review of Neuroscience*, 35:203–225.

Cadwell, C. R., Palasantza, A., Jiang, X., Berens, P., Deng, Q., Yilmaz, M., Reimer, J., Shen, S., Bethge, M., Tolias, K. F., Sandberg, R., and Tolias, A. S. (2015). Electrophysiological, transcriptomic and morphologic profiling of single neurons using patch-seq. *Nature Biotechnology 2015 34:2*, 34:199–203.

Cadwell, C. R., Scala, F., Fahey, P. G., Kobak, D., Mulherkar, S., Sinz, F. H., Papadopoulos, S., Tan, Z. H., Johnsson, P., Hartmanis, L., Li, S., Cotton, R. J., Tolias, K. F., Sandberg, R., Berens, P., Jiang, X., and Tolias, A. S. (2020). Cell type composition and circuit organization of clonally related excitatory neurons in the juvenile mouse neocortex. *eLife*, 9.

Cajal, S. R. (1999). *Texture of the Nervous System of Man and the Vertebrates*, volume 1. Springer Science & Business Media.

Callaway, E. M. and Borrell, V. (2011). Developmental sculpting of dendritic morphology of layer 4 neurons in visual cortex: influence of retinal input. *The Journal of neuroscience : the official journal of the Society for Neuroscience*, 31:7456–7470.

Cárdenas, A., Villalba, A., de Juan Romero, C., Picó, E., Kyrousi, C., Tzika, A. C., Tessier-Lavigne, M., Ma, L., Drukker, M., Cappello, S., and Borrell, V. (2018). Evolution of cortical neurogenesis in amniotes controlled by robo signaling levels. *Cell*, 174:590.

Cardin, J. A. (2018). Inhibitory interneurons regulate temporal precision and correlations in cortical circuits. *Trends in Neurosciences*, 41:689–700.

Cardin, J. A., Carlén, M., Meletis, K., Knoblich, U., Zhang, F., Deisseroth, K., Tsai, L. H., and Moore, C. I. (2009). Driving fast-spiking cells induces gamma rhythm and controls sensory responses. *Nature*, 459:663–667.

Cardin, J. A., Palmer, L. A., and Contreras, D. (2007). Stimulus feature selectivity in excitatory and inhibitory neurons in primary visual cortex. *The Journal of Neuroscience*, 27:10333–10344.

Cavalieri, D., Angelova, A., Islah, A., Lopez, C., Bocchio, M., Bollmann, Y., Baude, A., and Cossart, R. (2021). Ca1 pyramidal cell diversity is rooted in the time of neurogenesis. *eLife*, 10.

Caviness Jr, V. S. (1982). Neocortical histogenesis in normal and reeler mice: a developmental study based upon [3h] thymidine autoradiography. *Developmental Brain Research*, 4(3):293–302.

Chakrabarti, S. and Alloway, K. D. (2006). Differential origin of projections from si barrel cortex to the whisker representations in sii and mi. *Journal of Comparative Neurology*, 498:624–636.

Che, A., Babij, R., Iannone, A. F., Fetcho, R. N., Ferrer, M., Liston, C., Fishell,

G., and García, N. V. D. M. (2018). Layer i interneurons sharpen sensory maps during neonatal development. *Neuron*, 99:98–116.e7.

Chen, B., Schaevitz, L. R., and McConnell, S. K. (2005). Fezl regulates the differentiation and axon targeting of layer 5 subcortical projection neurons in cerebral cortex. *Proceedings of the National Academy of Sciences of the United States of America*, 102:17184–17189.

Chen, J. L., Carta, S., Soldado-Magraner, J., Schneider, B. L., and Helmchen, F. (2013). Behaviour-dependent recruitment of long-range projection neurons in somatosensory cortex. *Nature*, 499:336–340.

Chen, J. L., Margolis, D. J., Stankov, A., Sumanovski, L. T., Schneider, B. L., and Helmchen, F. (2015). Pathway-specific reorganization of projection neurons in somatosensory cortex during learning. *Nature Neuroscience*, 18:1101–1108.

Chevée, M., Robertson, J. D. J., Cannon, G. H., Brown, S. P., and Goff, L. A. (2018). Variation in activity state, axonal projection, and position define the transcriptional identity of individual neocortical projection neurons. *Cell Reports*, 22:441–455.

Chini, M., Pfeffer, T., and Hanganu-Opatz, I. (2022). An increase of inhibition drives the developmental decorrelation of neural activity. *eLife*, 11.

Chiu, C. Q., Lur, G., Morse, T. M., Carnevale, N. T., Ellis-Davies, G. C., and Higley, M. J. (2013). Compartmentalization of gabaergic inhibition by dendritic spines. *Science*, 340:759.

Chmielowska, J., Carvell, G. E., and Simons, D. J. (1989). Spatial organization of thalamocortical and corticothalamic projection systems in the rat smi barrel cortex. *Journal of Comparative Neurology*, 285:325–338.

Colbert, C. M. (2006). Preparation of cortical brain slices for electrophysiological recording. *Methods in Molecular Biology*, 337:117–125.

Condylis, C., Lowet, E., Ni, J., Bistrong, K., Ouellette, T., Josephs, N., and Chen, J. L. (2020). Context-dependent sensory processing across primary and secondary somatosensory cortex. *Neuron*, 106:515–525.e5.

Crochet, S., Poulet, J. F., Kremer, Y., and Petersen, C. C. (2011). Synaptic mechanisms underlying sparse coding of active touch. *Neuron*, 69:1160–1175.

Crossley, P., Martinez, S., Ohkubo, Y., and Rubenstein, J. (2001). Coordinate expression of fgf8, otx2, bmp4, and shh in the rostral prosencephalon during development of the telencephalic and optic vesicles. *Neuroscience*, 108(2):183–206.

Cutts, C. S. and Eglen, X. S. J. (2014). Detecting pairwise correlations in spike trains: an objective comparison of methods and application to the study of retinal waves. *The Journal of Neuroscience*, 34:14288–14303.

Dantzker, J. L. and Callaway, E. M. (2000). Laminar sources of synaptic input to cortical inhibitory interneurons and pyramidal neurons. *Nature Neuroscience*, 3:701–707.

D'Arcy, B. R., Lennox, A. L., Musso, C. M., Bracher, A., Escobar-Tomlienovich, C., Perez-Sanchez, S., and Silver, D. L. (2023). Non-muscle myosins control radial glial basal endfeet to mediate interneuron organization. *PLOS Biology*, 21.

David, S. V., Fritz, J. B., and Shamma, S. A. (2012). Task reward structure shapes rapid receptive field plasticity in auditory cortex. *Proceedings of the National Academy of Sciences of the United States of America*, 109:2144–2149.

Daw, M. I., Ashby, M. C., and Isaac, J. T. (2007). Coordinated developmental recruitment of latent fast spiking interneurons in layer iv barrel cortex. *Nature Neuroscience*, 10:453–461.

de Kock, C. P. J., Bruno, R. M., Spors, H., and Sakmann, B. (2007). Layer- and cell-type-specific suprathreshold stimulus representation in rat primary somatosensory cortex. *The Journal of physiology*, 581:139–54.

Dehay, C. and Kennedy, H. (2023). Area v1 development, a model system to link corticogenesis to adult cortex structure and function. *Neocortical Neurogenesis in Development and Evolution*, pages 63–81.

Denardo, L. A., Berns, D. S., Deloach, K., and Luo, L. (2015). Connectivity of

mouse somatosensory and prefrontal cortex examined with trans-synaptic tracing. *Nature Neuroscience*, 18:1687–1697.

Denaxa, M., Neves, G., Rabinowitz, A., Kemlo, S., Liodis, P., Burrone, J., and Pachnis, V. (2018). Modulation of apoptosis controls inhibitory interneuron number in the cortex. *Cell Reports*, 22:1710–1721.

Desai, A. R. and McConnell, S. K. (2000). Progressive restriction in fate potential by neural progenitors during cerebral cortical development. *Development*, 127:2863–2872.

Deschênes, M., Veinante, P., and Zhang, Z. W. (1998). The organization of corticothalamic projections: reciprocity versus parity. *Brain Research Reviews*, 28:286–308.

Destexhe, A. and Paré, D. (1999). Impact of network activity on the integrative properties of neocortical pyramidal neurons in vivo. *Journal of Neurophysiology*, 81:1531–1547.

Destexhe, A., Rudolph, M., and Paré, D. (2003). The high-conductance state of neocortical neurons in vivo. *Nature Reviews Neuroscience*, 4:739–751.

Deweese, M. R. and Zador, A. M. (2004). Shared and private variability in the auditory cortex. *Journal of Neurophysiology*, 92:1840–1855.

Douglas, R. J., Martin, K. A., and Whitteridge, D. (1989). A canonical microcircuit for neocortex. *Neural Computation*, 1:480–488.

Douglas, R. J. and Martin, K. A. C. (2004). Neuronal circuits of the neocortex. *Annual Review of Neuroscience*, 27:419–51.

D'Souza, R. D., Bista, P., Meier, A. M., Ji, W., and Burkhalter, A. (2019). Spatial clustering of inhibition in mouse primary visual cortex. *Neuron*, 104:588–600.e5.

Duan, X., Krishnaswamy, A., Huerta, I. D. L., and Sanes, J. R. (2014). Type ii cadherins guide assembly of a direction-selective retinal circuit. *Cell*, 158:793–807.

Duan, X., Krishnaswamy, A., Laboulaye, M. A., Liu, J., Peng, Y. R., Yamagata, M., Toma, K., and Sanes, J. R. (2018). Cadherin combinations recruit dendrites

of distinct retinal neurons to a shared interneuronal scaffold. *Neuron*, 99:1145–1154.e6.

Duan, Z. R. S., Che, A., Chu, P., Modol, L., Bollmann, Y., Babij, R., Fetcho, R. N., Otsuka, T., Fuccillo, M. V., Liston, C., Pisapia, D. J., Cossart, R., and García, N. V. D. M. (2020). Gabaergic restriction of network dynamics regulates interneuron survival in the developing cortex. *Neuron*, 105:75–92.e5.

Dupont, E., Hanganu, I. L., Kilb, W., Hirsch, S., and Luhmann, H. J. (2005). Rapid developmental switch in the mechanisms driving early cortical columnar networks. *Nature*, 439:79–83.

Ecker, A. S., Berens, P., Keliris, G. A., Bethge, M., Logothetis, N. K., and Tolias, A. S. (2010). Decorrelated neuronal firing in cortical microcircuits. *Science*, 327:584–587.

Ecker, A. S., Berens, P., Tolias, A. S., and Bethge, M. (2011). The effect of noise correlations in populations of diversely tuned neurons. *The Journal of Neuroscience*, 31:14272–14283.

Einevoll, G. T., Kayser, C., Logothetis, N. K., and Panzeri, S. (2013). Modelling and analysis of local field potentials for studying the function of cortical circuits. *Nature Reviews Neuroscience 2013 14:11*, 14:770–785.

Ellender, T. J., Avery, S. V., Mahfooz, K., Scaber, J., von Klemperer, A., Nixon, S. L., Buchan, M. J., van Rheede, J. J., Gatti, A., Waites, C., Pavlou, H. J., Sims, D., Newey, S. E., and Akerman, C. J. (2019). Embryonic progenitor pools generate diversity in fine-scale excitatory cortical subnetworks. *Nature Communications*, 10:1–16.

Ellender, T. J., Raimondo, J. V., Irkle, A., Lamsa, K. P., and Akerman, C. J. (2014). Excitatory effects of parvalbumin-expressing interneurons maintain hippocampal epileptiform activity via synchronous afterdischarges. *The Journal of Neuroscience*, 34:15208.

Englund, C., Fink, A., Lau, C., Pham, D., Daza, R. A., Bulfone, A., Kowalczyk, T., and Hevner, R. F. (2005). Pax6, tbr2, and tbr1 are expressed sequentially by

radial glia, intermediate progenitor cells, and postmitotic neurons in developing neocortex. *Journal of Neuroscience*, 25:247–251.

Erzurumlu, R. S., Bates, C. A., and Killackey, H. P. (1980). Differential organization of thalamic projection cells in the brain stem trigeminal complex of the rat. *Brain research*, 198(2):427–433.

Erzurumlu, R. S. and Gaspar, P. (2012). Development and critical period plasticity of the barrel cortex. *The European Journal of Neuroscience*, 35:1540.

Feldmeyer, D. (2012). Excitatory neuronal connectivity in the barrel cortex. *Frontiers in Neuroanatomy*, 6.

Feldmeyer, D., Lübke, J., and Sakmann, B. (2006). Efficacy and connectivity of intracolumnar pairs of layer 2/3 pyramidal cells in the barrel cortex of juvenile rats. *The Journal of Physiology*, 575:583–602.

Fenno, L. E., Mattis, J., Ramakrishnan, C., Hyun, M., Lee, S. Y., He, M., Tucciarone, J., Selimbeyoglu, A., Berndt, A., Grosenick, L., Zalocusky, K. A., Bernstein, H., Swanson, H., Perry, C., Diester, I., Boyce, F. M., Bass, C. E., Neve, R., Huang, Z. J., and Deisseroth, K. (2014). Targeting cells with single vectors using multiple-feature boolean logic. *Nature Methods*, 11:763–772.

Fino, E., Packer, A. M., and Yuste, R. (2013). The logic of inhibitory connectivity in the neocortex.

Fino, E. and Yuste, R. (2011). Dense inhibitory connectivity in neocortex. *Neuron*, 69:1188–1203.

Flames, N., Long, J. E., Garratt, A. N., Fischer, T. M., Gassmann, M., Birchmeier, C., Lai, C., Rubenstein, J. L., and Marın, O. (2004). Short-and long-range attraction of cortical gabaergic interneurons by neuregulin-1. *Neuron*, 44(2):251–261.

Flames, N., Pla, R., Gelman, D. M., Rubenstein, J. L., Puelles, L., and Marín, O. (2007). Delineation of multiple subpallial progenitor domains by the combinatorial expression of transcriptional codes. *Journal of Neuroscience*, 27:9682–9695.

Flavell, S. W. and Greenberg, M. E. (2008). Signaling mechanisms linking neuronal

activity to gene expression and plasticity of the nervous system. *Annual review of neuroscience*, 31:563–590.

Florio, M. and Huttner, W. B. (2014). Neural progenitors, neurogenesis and the evolution of the neocortex. *Development*, 141:2182–2194.

Foeller, E. and Feldman, D. E. (2004). Synaptic basis for developmental plasticity in somatosensory cortex. *Current Opinion in Neurobiology*, 14:89–95.

Fogarty, M., Grist, M., Gelman, D., Marín, O., Pachnis, V., and Kessaris, N. (2007). Spatial genetic patterning of the embryonic neuroepithelium generates gabaergic interneuron diversity in the adult cortex. *The Journal of Neuroscience*, 27:10935.

Földy, C., Darmanis, S., Aoto, J., Malenka, R. C., Quake, S. R., and Südhof, T. C. (2016). Single-cell rnaseq reveals cell adhesion molecule profiles in electrophysiologically defined neurons. *Proceedings of the National Academy of Sciences of the United States of America*, 113:E5222–E5231.

Fox, K. (1992). A critical period for experience-dependent synaptic plasticity in rat barrel cortex. *The Journal of Neuroscience*, 12:1826–1838.

Franco, S. J., Gil-Sanz, C., Martinez-Garay, I., Espinosa, A., Harkins-Perry, S. R., Ramos, C., and Müller, U. (2012). Fate-restricted neural progenitors in the mammalian cerebral cortex. *Science*, 337:746.

Franco, S. J. and Müller, U. (2013). Shaping our minds: stem and progenitor cell diversity in the mammalian neocortex. *Neuron*, 77:19–34.

Freeman, M. R. and Rowitch, D. H. (2013). Evolving concepts of gliogenesis: a look way back and ahead to the next 25 years. *Neuron*, 80:613–623.

Fu, Y., Tucciarone, J. M., Espinosa, J. S., Sheng, N., Darcy, D. P., Nicoll, R. A., Huang, Z. J., and Stryker, M. P. (2014). A cortical circuit for gain control by behavioral state. *Cell*, 156:1139.

Fujita, I., Tanaka, K., Ito, M., and Cheng, K. (1992). Columns for visual features of objects in monkey inferotemporal cortex. *Nature 1992 360:6402*, 360:343–346.

Fukuchi-Shimogori, T. and Grove, E. A. (2001). Neocortex patterning by the secreted signaling molecule fgf8. *Science*, 294(5544):1071–1074.

Fuzik, J., Zeisel, A., Mate, Z., Calvigioni, D., Yanagawa, Y., Szabo, G., Linnarsson, S., and Harkany, T. (2015). Integration of electrophysiological recordings with single-cell rna-seq data identifies neuronal subtypes. *Nature Biotechnology 2015 34:2*, 34:175–183.

Gal, J. S., Morozov, Y. M., Ayoub, A. E., Chatterjee, M., Rakic, P., and Haydar, T. F. (2006). Molecular and morphological heterogeneity of neural precursors in the mouse neocortical proliferative zones. *Journal of Neuroscience*, 26:1045–1056.

Galarreta, M. and Hestrin, S. (2001). Spike transmission and synchrony detection in networks of gabaergic interneurons. *Science*, 292:2295–2299.

Gambino, F., Pagès, S., Kehayas, V., Baptista, D., Tatti, R., Carleton, A., and Holtmaat, A. (2014). Sensory-evoked ltp driven by dendritic plateau potentials in vivo. *Nature*, 515:116–119.

Gao, P., Postiglione, M. P., Krieger, T. G., Hernandez, L., Wang, C., Han, Z., Streicher, C., Papusheva, E., Insolera, R., Chugh, K., Kodish, O., Huang, K., Simons, B. D., Luo, L., Hippenmeyer, S., and Shi, S. H. (2014). Deterministic progenitor behavior and unitary production of neurons in the neocortex. *Cell*, 159:775–788.

Garcia, N. V. D. M., Priya, R., Tuncdemir, S. N., Fishell, G., and Karayannis, T. (2015). Sensory inputs control the integration of neurogliaform interneurons into cortical circuits. *Nature Neuroscience*, 18:393–401.

Gelman, D., Griveau, A., Dehorter, N., Teissier, A., Varela, C., Pla, R., Pierani, A., and Marín, O. (2011). A wide diversity of cortical gabaergic interneurons derives from the embryonic preoptic area. *Journal of Neuroscience*, 31:16570–16580.

Gelman, D. M., Martini, F. J., Nóbrega-Pereira, S., Pierani, A., Kessaris, N., and Marín, O. (2009). The embryonic preoptic area is a novel source of cortical gabaergic interneurons. *Journal of Neuroscience*, 29:9380–9389.

Gentet, L. J., Avermann, M., Matyas, F., Staiger, J. F., and Petersen, C. C. (2010). Membrane potential dynamics of gabaergic neurons in the barrel cortex of behaving mice. *Neuron*, 65:422–435.

Gentet, L. J., Kremer, Y., Taniguchi, H., Huang, Z. J., Staiger, J. F., and Petersen, C. C. (2012). Unique functional properties of somatostatin-expressing gabaergic neurons in mouse barrel cortex. *Nature Neuroscience*, 15:607–612.

Gerfen, C. R., Economo, M. N., and Chandrashekar, J. (2018). Long distance projections of cortical pyramidal neurons. *Journal of Neuroscience Research*, 96:1467–1475.

Gerfen, C. R., Paletzki, R., and Heintz, N. (2013). Gensat bac cre-recombinase driver lines to study the functional organization of cerebral cortical and basal ganglia circuits. *Neuron*, 80:1368–1383.

Gil-Sanz, C., Espinosa, A., Fregoso, S. P., Bluske, K. K., Cunningham, C. L., Martinez-Garay, I., Zeng, H., Franco, S. J., and Müller, U. (2015). Lineage tracing using cux2-cre and cux2-creert2 mice. *Neuron*, 86:1091–1099.

Gilbert, C. D. (1983). Microcircuitry of the visual cortex. *Annual review of neuroscience*, 6:217–247.

Gilbert, C. D. and Li, W. (2013). Top-down influences on visual processing. *Nature Reviews Neuroscience*, 14:350–363.

Gilbert, C. D. and Sigman, M. (2007). Brain states: Top-down influences in sensory processing. *Neuron*, 54:677–696.

Gilbert, C. D. and Wiesel, T. N. (1983). Clustered intrinsic connections in cat visual cortex. *Journal of Neuroscience*, 3:1116–1133.

Golshani, P., Gonçalves, J. T., Khoshkhoo, S., Mostany, R., Smirnakis, S., and Portera-Cailliau, C. (2009). Internally mediated developmental desynchronization of neocortical network activity. *Journal of Neuroscience*, 29:10890–10899.

Gouwens, N. W., Sorensen, S. A., Baftizadeh, F., Budzillo, A., Lee, B. R., Jarsky, T., Alfiler, L., Baker, K., Barkan, E., Berry, K., Bertagnolli, D., Bickley, K., Bomben, J., Braun, T., Brouner, K., Casper, T., Crichton, K., Daigle, T. L., Dalley, R., de Frates, R. A., Dee, N., Desta, T., Lee, S. D., Dotson, N., Egdorf, T., Ellingwood, L., Enstrom, R., Esposito, L., Farrell, C., Feng, D., Fong, O., Gala, R., Gamlin, C., Gary, A., Glandon, A., Goldy, J., Gorham, M., Graybuck,

L., Gu, H., Hadley, K., Hawrylycz, M. J., Henry, A. M., Hill, D. J., Hupp, M., Kebede, S., Kim, T. K., Kim, L., Kroll, M., Lee, C., Link, K. E., Mallory, M., Mann, R., Maxwell, M., McGraw, M., McMillen, D., Mukora, A., Ng, L., Ng, L., Ngo, K., Nicovich, P. R., Oldre, A., Park, D., Peng, H., Penn, O., Pham, T., Pom, A., Popović, Z., Potekhina, L., Rajanbabu, R., Ransford, S., Reid, D., Rimorin, C., Robertson, M., Ronellenfitch, K., Ruiz, A., Sandman, D., Smith, K., Sulc, J., Sunkin, S. M., Szafer, A., Tieu, M., Torkelson, A., Trinh, J., Tung, H., Wakeman, W., Ward, K., Williams, G., Zhou, Z., Ting, J. T., Arkhipov, A., Sümbül, U., Lein, E. S., Koch, C., Yao, Z., Tasic, B., Berg, J., Murphy, G. J., and Zeng, H. (2020). Integrated morphoelectric and transcriptomic classification of cortical gabaergic cells. *Cell*, 183:935–953.e19.

Govindan, S. and Jabaudon, D. (2017). Coupling progenitor and neuronal diversity in the developing neocortex. *FEBS letters*, 591(24):3960–3977.

Greenberg, D. S., Houweling, A. R., and Kerr, J. N. (2008). Population imaging of ongoing neuronal activity in the visual cortex of awake rats. *Nature Neuroscience*, 11:749–751.

Greig, L. C., Woodworth, M. B., Galazo, M. J., Padmanabhan, H., and Macklis, J. D. (2013). Molecular logic of neocortical projection neuron specification, development and diversity. *Nature Reviews Neuroscience*, 14:755–769.

Groh, A., Bokor, H., Mease, R. A., Plattner, V. M., Hangya, B., Stroh, A., Deschenes, M., and Acsády, L. (2014). Convergence of cortical and sensory driver inputs on single thalamocortical cells. *Cerebral Cortex*, 24:3167–3179.

Grove, E. A., Tole, S., Limon, J., Yip, L.-w., and Ragsdale, C. W. (1998). The hem of the embryonic cerebral cortex is defined by the expression of multiple wnt genes and is compromised in gli3-deficient mice. *Development*, 125(12):2315–2325.

Guillamon-Vivancos, T., Tyler, W. A., Medalla, M., Chang, W. W. E., Okamoto, M., Haydar, T. F., and Luebke, J. I. (2019). Distinct neocortical progenitor lineages fine-tune neuronal diversity in a layer-specific manner. *Cerebral Cortex*, 29:1121.

Guo, C., Peng, J., Zhang, Y., Li, A., Li, Y., Yuan, J., Xu, X., Ren, M., Gong,

H., and Chen, S. (2017). Single-axon level morphological analysis of corticofugal projection neurons in mouse barrel field. *Scientific Reports*, 7.

Gupta, A., Wang, Y., and Markram, H. (2000). Organizing principles for a diversity of gabaergic interneurons and synapses in the neocortex. *Science*, 287:273–278.

Guy, J. and Staiger, J. F. (2017). The functioning of a cortex without layers. *Frontiers in Neuroanatomy*, 11:253303.

Hage, T. A., Bosma-Moody, A., Baker, C. A., Kratz, M., Campagnola, L., Jarsky, T., Zeng, H., and Murphy, G. J. (2022). Synaptic connectivity to l2/3 of primary visual cortex measured by two-photon optogenetic stimulation. *eLife*, 11.

Hagihara, K. M., Ishikawa, A. W., Yoshimura, Y., Tagawa, Y., and Ohki, K. (2021). Long-range interhemispheric projection neurons show biased response properties and fine-scale local subnetworks in mouse visual cortex. *Cerebral Cortex*, 31:1307–1315.

Haider, B., Duque, A., Hasenstaub, A. R., and McCormick, D. A. (2006). Neocortical network activity *in vivo* is generated through a dynamic balance of excitation and inhibition. *Journal of Neuroscience*, 26:4535–4545.

Haider, B., Häusser, M., and Carandini, M. (2013). Inhibition dominates sensory responses in awake cortex. *Nature*, 493:97.

Haider, B., Schulz, D. P. P., Häusser, M., and Carandini, M. (2016). Millisecond coupling of local field potentials to synaptic currents in the awake visual cortex. *Neuron*, 90:35–42.

Hang, G. B. and Dan, Y. (2011). Asymmetric temporal integration of layer 4 and layer 2/3 inputs in visual cortex. *Journal of Neurophysiology*, 105:347.

Hanganu-Opatz, I. L., Butt, S. J., Hippenmeyer, S., de Marco García, N. V., Cardin, J. A., Voytek, B., and Muotri, A. R. (2021). The logic of developing neocortical circuits in health and disease. *The Journal of Neuroscience*, 41:813.

Harris, K. D. and Mrsic-Flogel, T. D. (2013). Cortical connectivity and sensory coding. *Nature*, 503:51–58.

Harris, K. D. and Shepherd, G. M. (2015). The neocortical circuit: themes and variations. *Nature Neuroscience*, 18:170.

Hartung, J. and Letzkus, J. J. (2021). Inhibitory plasticity in layer 1 - dynamic gatekeeper of neocortical associations. *Current opinion in neurobiology*, 67:26–33.

Hartung, J., Schroeder, A., Péréz, V. R., Poorthuis, R., and Letzkus, J. (2023). Layer 1 ndnf interneurons are specialized top-down master regulators of cortical circuits. *bioRxiv*, page 2023.10.02.560136.

Hasenstaub, A., Shu, Y., Haider, B., Kraushaar, U., Duque, A., and McCormick, D. A. (2005). Inhibitory postsynaptic potentials carry synchronized frequency information in active cortical networks. *Neuron*, 47:423–435.

Hattox, A. M. and Nelson, S. B. (2007). Layer v neurons in mouse cortex projecting to different targets have distinct physiological properties. *Journal of neurophysiology*, 98:3330–3340.

Haubensak, W., Attardo, A., Denk, W., and Huttner, W. B. (2004). Neurons arise in the basal neuroepithelium of the early mammalian telencephalon: a major site of neurogenesis. *Proceedings of the National Academy of Sciences of the United States of America*, 101:3196–3201.

He, M., Tucciarone, J., Lee, S. H., Nigro, M. J., Kim, Y., Levine, J. M., Kelly, S. M., Krugikov, I., Wu, P., Chen, Y., Gong, L., Hou, Y., Osten, P., Rudy, B., and Huang, Z. J. (2016). Strategies and tools for combinatorial targeting of gabaergic neurons in mouse cerebral cortex. *Neuron*, 91:1228–1243.

Heavner, W. E., Ji, S., Notwell, J. H., Dyer, E. S., Tseng, A. M., Birgmeier, J., Yoo, B., Bejerano, G., and McConnell, S. K. (2020). Transcription factor expression defines subclasses of developing projection neurons highly similar to single-cell rna-seq subtypes. *Proceedings of the National Academy of Sciences of the United States of America*, 117:25074–25084.

Heindorf, M., Arber, S., and Keller, G. B. (2018). Mouse motor cortex coordinates the behavioral response to unpredicted sensory feedback. *Neuron*, 99:1040–1054.e5.

Helmchen, F., Gilad, A., and Chen, J. L. (2018). Neocortical dynamics during whisker-based sensory discrimination in head-restrained mice. *Neuroscience*, 368:57–69.

Helmstaedter, M., Sakmann, B., and Feldmeyer, D. (2009a). L2/3 interneuron groups defined by multiparameter analysis of axonal projection, dendritic geometry, and electrical excitability. *Cerebral Cortex*, 19:951–962.

Helmstaedter, M., Sakmann, B., and Feldmeyer, D. (2009b). Neuronal correlates of local, lateral, and translaminar inhibition with reference to cortical columns. *Cerebral Cortex*, 19:926–937.

Hensch, T. K. (2005). Critical period plasticity in local cortical circuits. *Nature Reviews Neuroscience*, 6:877–888.

Hertäg, L. and Clopath, C. (2022). Prediction-error neurons in circuits with multiple neuron types: Formation, refinement, and functional implications. *Proceedings of the National Academy of Sciences of the United States of America*, 119:e2115699119.

Hill, D. N., Curtis, J. C., Moore, J. D., and Kleinfeld, D. (2011). Primary motor cortex reports efferent control of vibrissa motion on multiple timescales. *Neuron*, 72:344–356.

Hioki, H., Okamoto, S., Konno, M., Kameda, H., Sohn, J., Kuramoto, E., Fujiyama, F., and Kaneko, T. (2013). Cell type-specific inhibitory inputs to dendritic and somatic compartments of parvalbumin-expressing neocortical interneuron. *Journal of Neuroscience*, 33:544–555.

Hippenmeyer, S. (2023). Principles of neural stem cell lineage progression: Insights from developing cerebral cortex. *Current Opinion in Neurobiology*, 79:102695.

Hirata, T., Li, P., Lanuza, G. M., Cocas, L. A., Huntsman, M. M., and Corbin, J. G. (2009). Identification of distinct telencephalic progenitor pools for neuronal diversity in the amygdala. *Nature Neuroscience*, 12:141–149.

Hoerder-Suabedissen, A., Hayashi, S., Upton, L., Nolan, Z., Casas-Torremocha, D., Grant, E., Viswanathan, S., Kanold, P. O., Clasca, F., Kim, Y., and Molnár,

Z. (2018). Subset of cortical layer 6b neurons selectively innervates higher order thalamic nuclei in mice. *Cerebral Cortex*, 28:1882–1897.

Hofer, S. B., Ko, H., Pichler, B., Vogelstein, J., Ros, H., Zeng, H., Lein, E., Lesica, N. A., and Mrsic-Flogel, T. D. (2011). Differential connectivity and response dynamics of excitatory and inhibitory neurons in visual cortex. *Nature Neuroscience*, 14:1045–1052.

Hoffer, Z. S., Hoover, J. E., and Alloway, K. D. (2003). Sensorimotor corticocortical projections from rat barrel cortex have an anisotropic organization that facilitates integration of inputs from whiskers in the same row. *The Journal of comparative neurology*, 466:525–544.

Holmes, W. R. and Woody, C. D. (1989). Effects of uniform and non-uniform synaptic 'activation-distributions' on the cable properties of modeled cortical pyramidal neurons. *Brain research*, 505:12–22.

Holmgren, C., Harkany, T., Svennenfors, B., and Zilberter, Y. (2003). Pyramidal cell communication within local networks in layer 2/3 of rat neocortex. *The Journal of Physiology*, 551:139.

Hooks, B. M., Hires, S. A., Zhang, Y. X., Huber, D., Petreanu, L., Svoboda, K., and Shepherd, G. M. (2011). Laminar analysis of excitatory local circuits in vibrissal motor and sensory cortical areas. *PLoS Biology*, 9.

Hooks, B. M., Mao, T., Gutnisky, D. A., Yamawaki, N., Svoboda, K., and Shepherd, G. M. (2013). Organization of cortical and thalamic input to pyramidal neurons in mouse motor cortex. *The Journal of Neuroscience*, 33:748–760.

Howard, A., Tamas, G., and Soltesz, I. (2005). Lighting the chandelier: New vistas for axo-axonic cells. *Trends in Neurosciences*, 28:310–316.

Hu, H. and Jonas, P. (2014). A supercritical density of na+ channels ensures fast signaling in gabaergic interneuron axons. *Nature Neuroscience*, 17:686–693.

Hu, H., Martina, M., and Jonas, P. (2010). Dendritic mechanisms underlying rapid synaptic activation of fast-spiking hippocampal interneurons. *Science*, 327:52–58.

Hu, J. S., Vogt, D., Lindtner, S., Sandberg, M., Silberberg, S. N., and Rubenstein,

J. L. (2017). Coup-tf1 and coup-tf2 control subtype and laminar identity of mge-derived neocortical interneurons. *Development*, 144:2837–2851.

Hu, R., Fan, P., Wang, Y., Shan, J., Jing, L., Xu, W., Mo, F., Wang, M., Luo, Y., Wang, Y., Cai, X., and Luo, J. (2023). Multi-channel microelectrode arrays for detection of single-cell level neural information in the hippocampus ca1 under general anesthesia induced by low-dose isoflurane. *Fundamental Research*.

hua Liu, B., tang Li, Y., pei Ma, W., jie Pan, C., Zhang, L. I., and Tao, H. W. (2011). Broad inhibition sharpens orientation selectivity by expanding input dynamic range in mouse simple cells. *Neuron*, 71:542–554.

Hubel, D. H. and Wiesel, T. N. (1962). Receptive fields, binocular interaction and functional architecture in the cat's visual cortex. *The Journal of physiology*, 160:106–54.

Huilgol, D., Levine, J. M., Galbavy, W., Wang, B.-S., He, M., Suryanarayana, S. M., and Huang, Z. J. (2023a). Direct and indirect neurogenesis generate a mosaic of distinct glutamatergic projection neuron types in cerebral cortex. *Neuron*, 111.

Huilgol, D., Russ, J. B., Srivas, S., and Huang, Z. J. (2023b). The progenitor basis of cortical projection neuron diversity. *Current Opinion in Neurobiology*, 81:102726.

Huszár, R., Zhang, Y., Blockus, H., and Buzsáki, G. (2022). Preconfigured dynamics in the hippocampus are guided by embryonic birthdate and rate of neurogenesis. *Nature Neuroscience*, 25:1201–1212.

Ibrahim, L. A., Huang, S., Fernandez-Otero, M., Sherer, M., Qiu, Y., Vemuri, S., Xu, Q., Machold, R., Pouchelon, G., Rudy, B., and Fishell, G. (2021). Bottom-up inputs are required for establishment of top-down connectivity onto cortical layer 1 neurogliaform cells. *Neuron*, 109:3473–3485.e5.

Inan, M., Welagen, J., and Anderson, S. A. (2012). Spatial and temporal bias in the mitotic origins of somatostatin- and parvalbumin-expressing interneuron subgroups and the chandelier subtype in the medial ganglionic eminence. *Cerebral Cortex*, 22:820–827.

Isaacson, J. S. and Scanziani, M. (2011). How inhibition shapes cortical activity. *Neuron*, 72:231–243.

Ivanov, A. and Zilberter, Y. (2011). Critical state of energy metabolism in brain slices: the principal role of oxygen delivery and energy substrates in shaping neuronal activity. *Frontiers in Neuroenergetics*, 3.

Jabaudon, D. (2017). Fate and freedom in developing neocortical circuits. *Nature Communications*, 8:1–9.

Jabaudon, D., Shnider, S. J., Tischfield, D. J., Galazo, M. J., and MacKlis, J. D. (2012). Rorβ induces barrel-like neuronal clusters in the developing neocortex. *Cerebral Cortex*, 22:996–1006.

Jacob, V., Mitani, A., Toyoizumi, T., and Fox, K. (2017). Whisker row deprivation affects the flow of sensory information through rat barrel cortex. *Journal of Neurophysiology*, 117:4–17.

Jacquin, M. F., Barcia, M., and Rhoades, R. W. (1989). Structure-function relationships in rat brainstem subnucleus interpolaris: Iv. projection neurons. *Journal of Comparative Neurology*, 282(1):45–62.

Jang, H. J., Chung, H., Rowland, J. M., Richards, B. A., Kohl, M. M., and Kwag, J. (2020). Distinct roles of parvalbumin and somatostatin interneurons in gating the synchronization of spike times in the neocortex. *Scientific Advances*, 6:5333–5355.

Jézéquel, J., Condomitti, G., Kroon, T., Hamid, F., Sanalidou, S., Garces, T., Maeso, P., Balia, M., and Rico, B. (2023). Cadherins orchestrate specific patterns of perisomatic inhibition onto distinct pyramidal cell populations. *bioRxiv*, page 2023.09.28.559922.

Jiang, X., Shen, S., Cadwell, C. R., Berens, P., Sinz, F., Ecker, A. S., Patel, S., and Tolias, A. S. (2015). Principles of connectivity among morphologically defined cell types in adult neocortex. *Science*, 350:aac9462.

Jiang, X., Wang, G., Lee, A. J., Stornetta, R. L., and Zhu, J. J. (2013). The organization of two new cortical interneuronal circuits. *Nature Neuroscience*, 16:210–218.

Jiao, Y., Zhang, C., Yanagawa, Y., and Sun, Q. Q. (2006). Major effects of sen-

sory experiences on the neocortical inhibitory circuits. *Journal of Neuroscience*, 26:8691–8701.

Jordan, R. (2021). Optimized protocol for *in vivo* whole-cell recordings in head-fixed, awake behaving mice. *STAR protocols*, 2.

Jordan, R. and Keller, G. B. (2020). Opposing influence of top-down and bottom-up input on excitatory layer 2/3 neurons in mouse primary visual cortex. *Neuron*, 108:1194–1206.e5.

Jouhanneau, J.-S., Ferrarese, L., Estebanez, L., Audette, N., Brecht, M., Barth, A., and Poulet, J. (2014). Cortical fosgfp expression reveals broad receptive field excitatory neurons targeted by pom. *Neuron*, 84:1065–1078.

Jouhanneau, J. S., Kremkow, J., and Poulet, J. F. (2018). Single synaptic inputs drive high-precision action potentials in parvalbumin expressing gaba-ergic cortical neurons in vivo. *Nature Communications 2018 9:1*, 9:1–11.

Jouhanneau, J. S. and Poulet, J. F. (2019). Multiple two-photon targeted whole-cell patch-clamp recordings from monosynaptically connected neurons in vivo. *Frontiers in Synaptic Neuroscience*, 11.

Junghans, D., Heidenreich, M., Hack, I., Taylor, V., Frotscher, M., and Kemler, R. (2008). Postsynaptic and differential localization to neuronal subtypes of protocadherin β16 in the mammalian central nervous system. *European Journal of Neuroscience*, 27:559–571.

Kageyama, R., Ohtsuka, T., Shimojo, H., and Imayoshi, I. (2008). Dynamic notch signaling in neural progenitor cells and a revised view of lateral inhibition. *Nature Neuroscience*, 11:1247–1251.

Kampa, B. M., Letzkus, J. J., and Stuart, G. J. (2006). Cortical feed-forward networks for binding different streams of sensory information. *Nature Neuroscience*, 9:1472–1473.

Kanatani, S., Yozu, M., Tabata, H., and Nakajima, K. (2008). Coup-tfii is preferentially expressed in the caudal ganglionic eminence and is involved in the caudal migratory stream. *The Journal of Neuroscience*, 28:13582–13591.

Kanold, P. O., Nelken, I., and Polley, D. B. (2014). Local versus global scales of organization in auditory cortex. *Trends in neurosciences*, 37:502–510.

Kapfer, C., Glickfeld, L. L., Atallah, B. V., and Scanziani, M. (2007). Supralinear increase of recurrent inhibition during sparse activity in the somatosensory cortex. *Nature neuroscience*, 10:743–753.

Karimi, A., Odenthal, J., Drawitsch, F., Boergens, K. M., and Helmstaedter, M. (2020). Cell-type specific innervation of cortical pyramidal cells at their apical dendrites. *eLife*, 9.

Karnani, M. M., Jackson, J., Ayzenshtat, I., Sichani, X. H., Manoocheri, K., Kim, S., and Yuste, R. (2016). Opening holes in the blanket of inhibition: Localized lateral disinhibition by vip interneurons. *The Journal of Neuroscience*, 36:3471.

Kasper, E. M., Lübke, J., Larkman, A. U., and Blakemore, C. (1994). Pyramidal neurons in layer 5 of the rat visual cortex. iii. differential maturation of axon targeting, dendritic morphology, and electrophysiological properties. *Journal of Comparative Neurology*, 339(4):495–518.

Kätzel, D., Zemelman, B. V., Buetfering, C., Wölfel, M., and Miesenböck, G. (2010). The columnar and laminar organization of inhibitory connections to neocortical excitatory cells. *Nature Neuroscience*, 14:100–107.

Katzner, S., Nauhaus, I., Benucci, A., Bonin, V., Ringach, D. L., and Carandini, M. (2009). Local origin of field potentials in visual cortex. *Neuron*, 61:35–41.

Kawaguchi, A., Ikawa, T., Kasukawa, T., Ueda, H. R., Kurimoto, K., Saitou, M., and Matsuzaki, F. (2008). Single-cell gene profiling defines differential progenitor subclasses in mammalian neurogenesis. *Development*, 135:3113–3124.

Kawaguchi, Y. and Kubota, Y. (1997). Gabaergic cell subtypes and their synaptic connections in rat frontal cortex. *Cerebral Cortex*, 7:476–486.

Keller, A. J., Dipoppa, M., Roth, M. M., Caudill, M. S., Ingrosso, A., Miller, K. D., and Scanziani, M. (2020). A disinhibitory circuit for contextual modulation in primary visual cortex. *Neuron*, 108(6):1181–1193.

Keller, G. B. and Mrsic-Flogel, T. D. (2018). Predictive processing: A canonical cortical computation. *Neuron*, 100:424.

Kennedy, H., Wianny, F., and Dehay, C. (2021). Determinants of primate neurogenesis and the deployment of top-down generative networks in the cortical hierarchy. *Current Opinion in Neurobiology*, 66:69–76.

Kepecs, A. and Fishell, G. (2014). Interneuron cell types are fit to function. *Nature*, 505:318–326.

Kerlin, A. M., Andermann, M. L., Berezovskii, V. K., and Reid, R. C. (2010). Broadly tuned response properties of diverse inhibitory neuron subtypes in mouse visual cortex. *Neuron*, 67:858–871.

Kerr, J. N. and Denk, W. (2008). Imaging in vivo: watching the brain in action. *Nature Reviews Neuroscience*, 9:195–205.

Khalilov, I., Minlebaev, M., Mukhtarov, M., and Khazipov, R. (2015). Dynamic changes from depolarizing to hyperpolarizing gabaergic actions during giant depolarizing potentials in the neonatal rat hippocampus. *The Journal of Neuroscience*, 35:12635–12642.

Khan, A. G., Poort, J., Chadwick, A., Blot, A., Sahani, M., Mrsic-Flogel, T. D., and Hofer, S. B. (2018). Distinct learning-induced changes in stimulus selectivity and interactions of gabaergic interneuron classes in visual cortex. *Nature Neuroscience 2018 21:6*, 21:851–859.

Khateb, M., Schiller, J., and Schiller, Y. (2017). Feedforward motor information enhances somatosensory responses and sharpens angular tuning of rat s1 barrel cortex neurons. *eLife*, 6.

Khurana, S. and Li, W. K. (2013). Baptisms of fire or death knells for acute-slice physiology in the age of 'omics' and light? *Reviews in the Neurosciences*, 24:527–536.

Kim, E. J., Juavinett, A. L., Kyubwa, E. M., Jacobs, M. W., and Callaway, E. M. (2015). Three types of cortical layer 5 neurons that differ in brain-wide connectivity and function. *Neuron*, 88:1253–1267.

Kim, E. J., Zhang, Z., Huang, L., Ito-Cole, T., Jacobs, M. W., Juavinett, A. L., Senturk, G., Hu, M., Ku, M., Ecker, J. R., and Callaway, E. M. (2020). Extraction of distinct neuronal cell types from within a genetically continuous population. *Neuron*, 107:274–282.e6.

Kim, M. H., Znamenskiy, P., Iacaruso, M. F., and Mrsic-Flogel, T. D. (2018). Segregated subnetworks of intracortical projection neurons in primary visual cortex. *Neuron*, 100:1313–1321.e6.

Kinnischtzke, A. K., Simons, D. J., and Fanselow, E. E. (2014). Motor cortex broadly engages excitatory and inhibitory neurons in somatosensory barrel cortex. *Cerebral Cortex*, 24:2237.

Kiritani, T., Wickersham, I. R., Seung, H. S., and Shepherd, G. M. (2012). Hierarchical connectivity and connection-specific dynamics in the corticospinalâcorticostriatal microcircuit in mouse motor cortex. *Journal of Neuroscience*, 32:4992–5001.

Kirkby, L. A., Sack, G. S., Firl, A., and Feller, M. B. (2013). A role for correlated spontaneous activity in the assembly of neural circuits. *Neuron*, 80:1129.

Knoblich, U., Huang, L., Zeng, H., and Li, L. (2019). Neuronal cell-subtype specificity of neural synchronization in mouse primary visual cortex. *Nature Communications*, 10:1–13.

Ko, H., Cossell, L., Baragli, C., Antolik, J., Clopath, C., Hofer, S. B., and Mrsic-Flogel, T. D. (2013). The emergence of functional microcircuits in visual cortex. *Nature*, 496(7443):96–100.

Ko, H., Hofer, S. B., Pichler, B., Buchanan, K. A., Sjöström, P. J., and Mrsic-Flogel, T. D. (2011). Functional specificity of local synaptic connections in neocortical networks. *Nature*, 473:87–91.

Ko, H., Mrsic-Flogel, T. D., and Hofer, S. B. (2014). Emergence of feature-specific connectivity in cortical microcircuits in the absence of visual experience. *The Journal of Neuroscience*, 34:9812–9816.

Kohmura, N., Senzaki, K., Hamada, S., Nobuyuki, K., Yasuda, R., Watanabe, M., Ishii, H., Yasuda, M., Mishina, M., and Yagi, T. (1998). Diversity revealed by a

novel family of cadherins expressed in neurons at a synaptic complex. *Neuron*, 20:1137–1151.

Kostadinov, D. and Sanes, J. R. (2015). Protocadherin-dependent dendritic self-avoidance regulates neural connectivity and circuit function. *eLife*, 4.

Kowalczyk, T., Pontious, A., Englund, C., Daza, R. A., Bedogni, F., Hodge, R., Attardo, A., Bell, C., Huttner, W. B., and Hevner, R. F. (2009). Intermediate neuronal progenitors (basal progenitors) produce pyramidalâprojection neurons for all layers of cerebral cortex. *Cerebral Cortex*, 19:2439–2450.

Kriegstein, A. (2006). [s16]: Neural stem and progenitor cells in cortical development. *International Journal of Developmental Neuroscience*, 24:478–478.

Krook-Magnuson, E., Varga, C., Lee, S. H., and Soltesz, I. (2012). New dimensions of interneuronal specialization unmasked by principal cell heterogeneity. *Trends in Neurosciences*, 35:175.

Kwon, S. E., Yang, H., Minamisawa, G., and O'Connor, D. H. (2016). Sensory and decision-related activity propagate in a cortical feedback loop during touch perception. *Nature Neuroscience*, 19:1243–1249.

Lacefield, C. O., Pnevmatikakis, E. A., Paninski, L., and Bruno, R. M. (2019). Reinforcement learning recruits somata and apical dendrites across layers of primary sensory cortex. *Cell Reports*, 26:2000–2008.e2.

Langevin, L. M., Mattar, P., Scardigli, R., Roussigné, M., Logan, C., Blader, P., and Schuurmans, C. (2007). Validating *in utero* electroporation for the rapid analysis of gene regulatory elements in the murine telencephalon. *Developmental Dynamics*, 236:1273–1286.

Larkum, M. (2013). A cellular mechanism for cortical associations: an organizing principle for the cerebral cortex. *Trends in Neurosciences*, 36:141–151.

Larkum, M. E., Senn, W., and Lüscher, H. R. (2004). Top-down dendritic input increases the gain of layer 5 pyramidal neurons. *Cerebral Cortex*, 14:1059–1070.

Le Bé, J.-V. and Markram, H. (2006). Spontaneous and evoked synaptic rewiring

in the neonatal neocortex. *Proceedings of the National Academy of Sciences*, 103(35):13214–13219.

Lee, A. T., Gee, S. M., Vogt, D., Patel, T., Rubenstein, J. L., and Sohal, V. S. (2014a). Pyramidal neurons in prefrontal cortex receive subtype-specific forms of excitation and inhibition. *Neuron*, 81:61–68.

Lee, L. J., Chen, W. J., Chuang, Y. W., and Wang, Y. C. (2009). Neonatal whisker trimming causes long-lasting changes in structure and function of the somatosensory system. *Experimental neurology*, 219:524–532.

Lee, S., Kruglikov, I., Huang, Z. J., Fishell, G., and Rudy, B. (2013). A disinhibitory circuit mediates motor integration in the somatosensory cortex. *Nature Neuroscience*, 16:1662–1670.

Lee, S. H., Hjerling-Leffler, J., Zagha, E., Fishell, G., and Rudy, B. (2010). The largest group of superficial neocortical gabaergic interneurons expresses ionotropic serotonin receptors. *The Journal of Neuroscience*, 30:16796.

Lee, S. H., Marchionni, I., Bezaire, M., Varga, C., Danielson, N., Lovett-Barron, M., Losonczy, A., and Soltesz, I. (2014b). Parvalbumin-positive basket cells differentiate among hippocampal pyramidal cells. *Neuron*, 82:1129–1144.

Lefebvre, J. L., Kostadinov, D., Chen, W. V., Maniatis, T., and Sanes, J. R. (2012). Protocadherins mediate dendritic self-avoidance in the mammalian nervous system. *Nature*, 488:517–521.

Lefort, S. and Petersen, C. C. (2017). Layer-dependent short-term synaptic plasticity between excitatory neurons in the c2 barrel column of mouse primary somatosensory cortex. *Cerebral Cortex*, 27:3869–3878.

Lefort, S., Tomm, C., Sarria, J. C. F., and Petersen, C. C. (2009). The excitatory neuronal network of the c2 barrel column in mouse primary somatosensory cortex. *Neuron*, 61:301–316.

Leinweber, M., Ward, D. R., Sobczak, J. M., Attinger, A., and Keller, G. B. (2017). A sensorimotor circuit in mouse cortex for visual flow predictions. *Neuron*, 95:1420–1432.e5.

Letzkus, J. J., Kampa, B. M., and Stuart, G. J. (2006). Learning rules for spike timing-dependent plasticity depend on dendritic synapse location. *Journal of Neuroscience*, 26(41):10420–10429.

Letzkus, J. J., Wolff, S. B., and Lüthi, A. (2015). Disinhibition, a circuit mechanism for associative learning and memory. *Neuron*, 88:264–276.

Li, Y., Lu, H., Cheng, P. L., Ge, S., Xu, H., Shi, S. H., and Dan, Y. (2012). Clonally related visual cortical neurons show similar stimulus feature selectivity. *Nature*, 486:118.

Li, Z., Tyler, W. A., Zeldich, E., Baró, G. S., Okamoto, M., Gao, T., Li, M., Sestan, N., and Haydar, T. F. (2020). Transcriptional priming as a conserved mechanism of lineage diversification in the developing mouse and human neocortex. *Science Advances*, 6.

Lim, L., Mi, D., Llorca, A., and Marín, O. (2018a). Development and functional diversification of cortical interneurons. *Neuron*, 100:294–313.

Lim, L., Mi, D., Llorca, A., and Marín, O. (2018b). Development and functional diversification of cortical interneurons. *Neuron*, 100:294.

Lin, Y., Yang, J., Shen, Z., Ma, J., Simons, B. D., and Shi, S. H. (2021). Behavior and lineage progression of neural progenitors in the mammalian cortex. *Current opinion in Neurobiology*, 66:144.

Lin, Y., Zhang, X. J., Yang, J., Li, S., Li, L., Lv, X., Ma, J., and Shi, S. H. (2023). Developmental neuronal origin regulates neocortical map formation. *Cell Reports*, 42.

Lipkin, A. M. and Bender, K. J. (2023). Axon initial segment gaba inhibits action potential generation throughout periadolescent development. *The Journal of neuroscience : the official journal of the Society for Neuroscience*, 43.

Liu, L., Yun, Z., Manubens-Gil, L., Chen, H., Xiong, F., Dong, H., Zeng, H., Hawrylycz, M., Ascoli, G. A., and Peng, H. (2023). Neuronal connectivity as a determinant of cell types and subtypes. *Research square*.

Llorca, A., Ciceri, G., Beattie, R., Wong, F. K., Diana, G., Serafeimidou-Pouliou,

E., Fernández-Otero, M., Streicher, C., Arnold, S. J., Meyer, M., Hippenmeyer, S., Maravall, M., and Marín, O. (2019). A stochastic framework of neurogenesis underlies the assembly of neocortical cytoarchitecture. *eLife*, 8.

Lodato, S., Rouaux, C., Quast, K. B., Jantrachotechatchawan, C., Studer, M., Hensch, T. K., and Arlotta, P. (2011). Excitatory projection neuron subtypes control the distribution of local inhibitory interneurons in the cerebral cortex. *Neuron*, 69:763–779.

Lohse, M., Cooper, M., Sader, E., Langfelder, A., Kahn, M., Baxter, L., Bartram, J., Phillips, J. W., Upton, A. L., and Mann, E. O. (2018). Motor cortex can modulate somatosensory processing via cortico-thalamo-cortical pathway. *bioRxiv*, page 366567.

López-Bendito, G., niz, J. A. S.-A., Pla, R., Borrell, V., Picó, E., Valdeolmillos, M., and Marín, O. (2008). Chemokine signaling controls intracortical migration and final distribution of gabaergic interneurons. *The Journal of Neuroscience*, 28:1613–1624.

Lourenço, J., Koukouli, F., and Bacci, A. (2020). Synaptic inhibition in the neocortex: Orchestration and computation through canonical circuits and variations on the theme. *Cortex*, 132:258–280.

Lu, J., Tucciarone, J., Padilla-Coreano, N., He, M., Gordon, J. A., and Huang, Z. J. (2017). Selective inhibitory control of pyramidal neuron ensembles and cortical subnetworks by chandelier cells. *Nature Neuroscience*, 20:1377–1383.

Lund, J. S. (1988). Anatomical organization of macaque monkey striate visual cortex. *Annual review of neuroscience*, 11(1):253–288.

Lv, X., Li, S., Li, J., Yu, X. Y., Ge, X., Li, B., Hu, S., Lin, Y., Zhang, S., Yang, J., Zhang, X., Yan, J., Joyner, A. L., Shi, H., Wu, Q., and Shi, S. H. (2022). Patterned cpcdh expression regulates the fine organization of the neocortex. *Nature*, 612:503–511.

Lytton, W. W. and Sejnowski, T. J. (1991). Simulations of cortical pyramidal neurons synchronized by inhibitory interneurons. *The Journal of Neurophysiology*, 66:1059–1079.

Ma, P. M. (1991). The barrelettes–architectonic vibrissal representations in the brainstem trigeminal complex of the mouse. i. normal structural organization. *The Journal of Comparative Neurology*, 309:161–199.

Ma, Y., Hu, H., and Agmon, A. (2012). Short-term plasticity of unitary inhibitory-to-inhibitory synapses depends on the presynaptic interneuron subtype. *The Journal of Neuroscience*, 32:983.

Ma, Y., Hu, H., Berrebi, A. S., Mathers, P. H., and Agmon, A. (2006). Distinct subtypes of somatostatin-containing neocortical interneurons revealed in transgenic mice. *Journal of Neuroscience*, 26:5069–5082.

Magrinelli, E., Baumann, N., Wagener, R. J., Glangetas, C., Bellone, C., Jabaudon, D., and Klingler, E. (2022). Heterogeneous fates of simultaneously-born neurons in the cortical ventricular zone. *Scientific Reports*, 12:1–11.

Makino, H. and Komiyama, T. (2015). Learning enhances the relative impact of top-down processing in the visual cortex. *Nature neuroscience*, 18:1116–1122.

Malina, K. C.-K., Tsivourakis, E., Kushinsky, D., Apelblat, D., Shtiglitz, S., Zohar, E., Sokoletsky, M., ichi Tasaka, G., Mizrahi, A., Lampl, I., and Spiegel, I. (2021). Ndnf interneurons in layer 1 gain-modulate whole cortical columns according to an animalâs behavioral state. *Neuron*, 109:2150–2164.e5.

Manita, S., Suzuki, T., Homma, C., Matsumoto, T., Odagawa, M., Yamada, K., Ota, K., Matsubara, C., Inutsuka, A., Sato, M., Ohkura, M., Yamanaka, A., Yanagawa, Y., Nakai, J., Hayashi, Y., Larkum, M. E., and Murayama, M. (2015). A top-down cortical circuit for accurate sensory perception. *Neuron*, 86:1304–1316.

Mao, T., Kusefoglu, D., Hooks, B. M., Huber, D., Petreanu, L., and Svoboda, K. (2011). Long-range neuronal circuits underlying the interaction between sensory and motor cortex. *Neuron*, 72:111–123.

Maravall, M., Stern, E. A., and Svoboda, K. (2004). Development of intrinsic properties and excitability of layer 2/3 pyramidal neurons during a critical period for sensory maps in rat barrel cortex. *Journal of neurophysiology*, 92:144–156.

Margrie, T. W., Brecht, M., and Sakmann, B. (2002). In vivo, low-resistance, whole-cell recordings from neurons in the anaesthetized and awake mammalian brain. *Pflugers Archiv : European journal of physiology*, 444:491–498.

Marín, O., Plump, A. S., Flames, N., Sánchez-Camacho, C., Tessier-Lavigne, M., and Rubenstein, J. L. (2003). Directional guidance of interneuron migration to the cerebral cortex relies on subcortical slit1/2-independent repulsion and cortical attraction. *Development*, 130:1889–1901.

Markram, H., Lübke, J., Frotscher, M., and Sakmann, B. (1997). Regulation of synaptic efficacy by coincidence of postsynaptic aps and epsps. *Science*, 275:213–215.

Markram, H., Toledo-Rodriguez, M., Wang, Y., Gupta, A., Silberberg, G., and Wu, C. (2004). Interneurons of the neocortical inhibitory system.

Marques-Smith, A., Lyngholm, D., Kaufmann, A.-K., Stacey, J. A., Hoerder-Suabedissen, A., Becker, E. B., Wilson, M. C., Molnar, Z., and Butt, S. J. (2016). A transient translaminar gabaergic interneuron circuit connects thalamocortical recipient layers in neonatal somatosensory cortex. *Neuron*, 89(3):536–549.

Martinez-Cerdeno, V., Noctor, S. C., and Kriegstein, A. R. (2006). The role of intermediate progenitor cells in the evolutionary expansion of the cerebral cortex. *Cerebral Cortex*, 16 Suppl 1.

Marx, M. and Feldmeyer, D. (2013). Morphology and physiology of excitatory neurons in layer 6b of the somatosensory rat barrel cortex. *Cerebral Cortex*, 23:2803–2817.

Mateo, C., Avermann, M., Gentet, L. J., Zhang, F., Deisseroth, K., and Petersen, C. C. (2011). *in vivo* optogenetic stimulation of neocortical excitatory neurons drives brain-state-dependent inhibition. *Current Biology*, 21:1593–1602.

Matho, K. S., Huilgol, D., Galbavy, W., He, M., Kim, G., An, X., Lu, J., Wu, P., Bella, D. J. D., Shetty, A. S., Palaniswamy, R., Hatfield, J., Raudales, R., Narasimhan, A., Gamache, E., Levine, J. M., Tucciarone, J., Szelenyi, E., Harris, J. A., Mitra, P. P., Osten, P., Arlotta, P., and Huang, Z. J. (2021). Genetic

dissection of the glutamatergic neuron system in cerebral cortex. *Nature*, 598:182–187.

Matsui, A., Tran, M., Yoshida, A. C., Kikuchi, S. S., Mami, U., Ogawa, M., and Shimogori, T. (2013). Btbd3 controls dendrite orientation toward active axons in mammalian neocortex. *Science*, 342:1114–1118.

McConnell, S. K. (1988). Fates of visual cortical neurons in the ferret after isochronic and heterochronic transplantation. *Journal of Neuroscience*, 8:945–974.

McConnell, S. K. and Kaznowski, C. E. (1991). Cell cycle dependence of laminar determination in developing neocortex. *Science*, 254(5029):282–285.

McCormick, D. A., Connors, B. W., Lighthall, J. W., and Prince, D. A. (1985). Comparative electrophysiology of pyramidal and sparsely spiny stellate neurons of the neocortex. *Journal of Neurophysiology*, 54:782–806.

Medvedeva, Y. V., Lin, B., Shuttleworth, C. W., and Weiss, J. H. (2009). Intracellular zn2+ accumulation contributes to synaptic failure, mitochondrial depolarization, and cell death in an acute slice oxygenâglucose deprivation model of ischemia. *Journal of Neuroscience*, 29:1105–1114.

Mercier, B. E., Legg, C. R., and Glickstein, M. (1990). Basal ganglia and cerebellum receive different somatosensory information in rats. *Proceedings of the National Academy of Sciences of the United States of America*, 87:4388–4392.

Meyer, H. S., Schwarz, D., Wimmer, V. C., Schmitt, A. C., Kerr, J. N., Sakmann, B., and Helmstaedter, M. (2011). Inhibitory interneurons in a cortical column form hot zones of inhibition in layers 2 and 5a. *Proceedings of the National Academy of Sciences of the United States of America*, 108:16807–16812.

Meynert, T. (1872). Chapter xxxi. the brain of mammals. by theodor meynert, of vienna. general account of the structure of the brain. *Manual of human and comparative histology*, 2:367.

Miles, R. (1990). Synaptic excitation of inhibitory cells by single ca3 hippocampal pyramidal cells of the guinea-pig in vitro. *The Journal of Physiology*, 428:61–77.

Miller-Hansen, A. J. and Sherman, S. M. (2022). Conserved patterns of functional

organization between cortex and thalamus in mice. *Proceedings of the National Academy of Sciences of the United States of America*, 119:e2201481119.

Minamisawa, G., Kwon, S. E., Chevée, M., Brown, S. P., and O'Connor, D. H. (2018). A non-canonical feedback circuit for rapid interactions between somatosensory cortices. *Cell Reports*, 23:2718–2731.e6.

Mitchell, B. D. and Cauller, L. J. (2001). Corticocortical and thalamocortical projections to layer i of the frontal neocortex in rats. *Brain research*, 921:68–77.

Mitchell, S. J. and Silver, R. A. (2003). Shunting inhibition modulates neuronal gain during synaptic excitation. *Neuron*, 38:433–445.

Miyashita, E., Keller, A., and Asanuma, H. (1994). Input-output organization of the rat vibrissal motor cortex. *Experimental Brain Research*, 99:223–232.

Miyata, T., Kawaguchi, A., Okano, H., and Ogawa, M. (2001). Asymmetric inheritance of radial glial fibers by cortical neurons. *Neuron*, 31(5):727–741.

Miyata, T., Kawaguchi, A., Saito, K., Kawano, M., Muto, T., and Ogawa, M. (2004). Asymmetric production of surface-dividing and non-surface-dividing cortical progenitor cells. *Development*, 131:3133–3145.

Miyoshi, G., Butt, S. J., Takebayashi, H., and Fishell, G. (2007). Physiologically distinct temporal cohorts of cortical interneurons arise from telencephalic olig2-expressing precursors. *The Journal of Neuroscience*, 27:7786–7798.

Miyoshi, G. and Fishell, G. (2011). Gabaergic interneuron lineages selectively sort into specific cortical layers during early postnatal development. *Cerebral Cortex*, 21:845–852.

Miyoshi, G., Hjerling-Leffler, J., Karayannis, T., Sousa, V. H., Butt, S. J. B., Battiste, J., Johnson, J. E., Machold, R. P., and Fishell, G. (2010). Development/-plasticity/repair genetic fate mapping reveals that the caudal ganglionic eminence produces a large and diverse population of superficial cortical interneurons.

Mizutani, K. I., Yoon, K., Dang, L., Tokunaga, A., and Gaiano, N. (2007). Differential notch signalling distinguishes neural stem cells from intermediate progenitors. *Nature*, 449:351–355.

Mo, C. and Sherman, S. M. (2019). A sensorimotor pathway via higher-order thalamus. *The Journal of Neuroscience*, 39:692.

Moberg, S. and Takahashi, N. (2022). Neocortical layer 5 subclasses: From cellular properties to roles in behavior. *Frontiers in Synaptic Neuroscience*, 14:1006773.

Modol, L., Bollmann, Y., Tressard, T., Baude, A., Che, A., Duan, Z. R. S., Babij, R., García, N. V. D. M., and Cossart, R. (2020). Assemblies of perisomatic gabaergic neurons in the developing barrel cortex. *Neuron*, 105:93–105.e4.

Molyneaux, B. J., Arlotta, P., Hirata, T., Hibi, M., and Macklis, J. D. (2005). Fezl is required for the birth and specification of corticospinal motor neurons. *Neuron*, 47:817–831.

Molyneaux, B. J., Arlotta, P., Menezes, J. R., and Macklis, J. D. (2007). Neuronal subtype specification in the cerebral cortex. *Nature Reviews Neuroscience*, 8:427–437.

Morgenstern, N. A., Bourg, J., and Petreanu, L. (2016). Multilaminar networks of cortical neurons integrate common inputs from sensory thalamus. *Nature Neuroscience*, 19:1034–1040.

Morishima, M. and Kawaguchi, Y. (2006). Recurrent connection patterns of corticostriatal pyramidal cells in frontal cortex. *The Journal of Neuroscience*, 26:4394–4405.

Morishima, M., Morita, K., Kubota, Y., and Kawaguchi, Y. (2011). Highly differentiated projection-specific cortical subnetworks. *The Journal of Neuroscience*, 31:10380–10391.

Mountcastle, V., Berman, A., and Davies, P. (1955). Topographic organization and modality representation in first somatic area of catâs cerebral cortex by method of single unit analysis. *Am J Physiol*, 183.

Muldal, A. M., Lillicrap, T. P., Richards, B. A., and Akerman, C. J. (2014). Clonal relationships impact neuronal tuning within a phylogenetically ancient vertebrate brain structure. *Current Biology*, 24:1929–1933.

Müller-Komorowska, D., Opitz, T., Elzoheiry, S., Schweizer, M., Giovannetti, E. A.,

and Beck, H. (2020). Nonspecific expression in limited excitatory cell populations in interneuron-targeting cre-driver lines can have large functional effects. *Frontiers in Neural Circuits*, 14.

Nadarajah, B., Brunstrom, J. E., Grutzendler, J., Wong, R. O., and Pearlman, A. L. (2001). Two modes of radial migration in early development of the cerebral cortex. *Nature Neuroscience*, 4:143–150.

Najafi, F., Elsayed, G. F., Cao, R., Pnevmatikakis, E., Latham, P. E., Cunningham, J. P., and Churchland, A. K. (2020). Excitatory and inhibitory subnetworks are equally selective during decision-making and emerge simultaneously during learning. *Neuron*, 105:165–179.e8.

Naka, A. (2015). Cell-type-specific manipulation reveals new specificity in the neocortical microcircuit. *Journal of Neuroscience*, 35:8976–8978.

Naka, A., Veit, J., Shababo, B., Chance, R. K., Risso, D., Stafford, D., Snyder, B., Egladyous, A., Chu, D., Sridharan, S., Mossing, D. P., Paninski, L., Ngai, J., and Adesnik, H. (2019). Complementary networks of cortical somatostatin interneurons enforce layer specific control. *eLife*, 8.

Narboux-Nême, N., Evrard, A., Ferezou, I., Erzurumlu, R. S., Kaeser, P. S., Lainé, J., Rossier, J., Ropert, N., Südhof, T. C., and Gaspar, P. (2012). Neurotransmitter release at the thalamocortical synapse instructs barrel formation but not axon patterning in the somatosensory cortex. *The Journal of Neuroscience*, 32:6183.

Naskar, S., Qi, J., Pereira, F., Gerfen, C. R., and Lee, S. (2021). Cell-type-specific recruitment of gabaergic interneurons in the primary somatosensory cortex by long-range inputs. *Cell Reports*, 34:108774.

Negrón, A., Getz, M. P., Handy, G., and Doiron, B. (2023). The mechanics of correlated variability in segregated cortical excitatory subnetworks. *bioRxiv*, page 2023.04.25.538323.

Nelson, P. G., Fields, R. D., Yu, C., and Neale, E. A. (1990). Mechanisms involved in activity-dependent synapse formation in mammalian central nervous system cell cultures. *Journal of Neurobiology*, 21:138–156.

Nery, S., Fishell, G., and Corbin, J. G. (2002). The caudal ganglionic eminence is a source of distinct cortical and subcortical cell populations. *Nature Neuroscience*, 5:1279–1287.

Niell, C. M. and Stryker, M. P. (2008). Highly selective receptive fields in mouse visual cortex. *Journal of Neuroscience*, 28:7520–7536.

Nieto, M., Monuki, E. S., Tang, H., Imitola, J., Haubst, N., Khoury, S. J., Cunningham, J., Gotz, M., and Walsh, C. A. (2004). Expression of cux-1 and cux-2 in the subventricular zone and upper layers ii-iv of the cerebral cortex. *The Journal of comparative neurology*, 479:168–180.

Nigro, M. J., Hashikawa-Yamasaki, Y., and Rudy, B. (2018). Diversity and connectivity of layer 5 somatostatin-expressing interneurons in the mouse barrel cortex. *Journal of Neuroscience*, 38:1622–1633.

Niquille, M., Limoni, G., Markopoulos, F., Cadilhac, C., Prados, J., Holtmaat, A., and Dayer, A. (2018). Neurogliaform cortical interneurons derive from cells in the preoptic area. *eLife*, 7.

Noctor, S. C., Flint, A. C., Weissman, T. A., Dammerman, R. S., and Kriegstein, A. R. (2001). Neurons derived from radial glial cells establish radial units in neocortex. *Nature*, 409:714–720.

Noctor, S. C., Martinez-Cerdeno, V., Ivic, L., and Kriegstein, A. R. (2004). Cortical neurons arise in symmetric and asymmetric division zones and migrate through specific phases. *Nature Neuroscience*, 7:136–144.

Noctor, S. C., Martinez-Cerdeno, V., and Kriegstein, A. R. (2008). Distinct behaviors of neural stem and progenitor cells underlie cortical neurogenesis. *The Journal of comparative neurology*, 508:28–44.

Nogueira, R., Rodgers, C. C., Bruno, R. M., and Fusi, S. (2023). The geometry of cortical representations of touch in rodents. *Nature Neuroscience*, 26:239–250.

Nowakowski, T. J., Bhaduri, A., Pollen, A. A., Alvarado, B., Mostajo-Radji, M. A., Lullo, E. D., Haeussler, M., Sandoval-Espinosa, C., Liu, S. J., Velmeshev, D., Ounadjela, J. R., Shuga, J., Wang, X., Lim, D. A., West, J. A., Leyrat, A. A.,

Kent, W. J., and Kriegstein, A. R. (2017). Spatiotemporal gene expression trajectories reveal developmental hierarchies of the human cortex. *Science*, 358:1318–1323.

Oberlaender, M., Kock, C. P. D., Bruno, R. M., Ramirez, A., Meyer, H. S., Dercksen, V. J., Helmstaedter, M., and Sakmann, B. (2012). Cell typeâspecific three-dimensional structure of thalamocortical circuits in a column of rat vibrissal cortex. *Cerebral Cortex*, 22:2375.

Oberst, P., Fièvre, S., Baumann, N., Concetti, C., Bartolini, G., and Jabaudon, D. (2019). Temporal plasticity of apical progenitors in the developing mouse neocortex. *Nature*, 573:370–374.

O'Connor, D. H., Peron, S. P., Huber, D., and Svoboda, K. (2010). Neural activity in barrel cortex underlying vibrissa-based object localization in mice. *Neuron*, 67:1048–1061.

Ohtaka-Maruyama, C., Okamoto, M., Endo, K., Oshima, M., Kaneko, N., Yura, K., Okado, H., Miyata, T., and Maeda, N. (2018). Synaptic transmission from subplate neurons controls radial migration of neocortical neurons. *Science*, 360(6386):313–317.

Ohtsuki, G., Nishiyama, M., Yoshida, T., Murakami, T., Histed, M., Lois, C., and Ohki, K. (2012). Similarity of visual selectivity among clonally related neurons in visual cortex. *Neuron*, 75:65–72.

Okun, M. and Lampl, I. (2008). Instantaneous correlation of excitation and inhibition during ongoing and sensory-evoked activities. *Nature Neuroscience*, 11:535–537.

Okun, M., Naim, A., and Lampl, I. (2010). The subthreshold relation between cortical local field potential and neuronal firing unveiled by intracellular recordings in awake rats. *Journal of Neuroscience*, 30:4440–4448.

Okun, M., Steinmetz, N. A., Cossell, L., Iacaruso, M. F., Ko, H., Barthó, P., Moore, T., Hofer, S. B., Mrsic-Flogel, T. D., Carandini, M., and Harris, K. D. (2015). Diverse coupling of neurons to populations in sensory cortex. *Nature*, 521:511–515.

Oláh, S., Füle, M., Komlósi, G., Varga, C., Báldi, R., Barzó, P., and Tamás, G. (2009). Regulation of cortical microcircuits by unitary gaba-mediated volume transmission. *Nature*, 461:1278–1281.

Onodera, K. and Kato, H. K. (2022). Translaminar recurrence from layer 5 suppresses superficial cortical layers. *Nature Communications*, 13.

O'Rourke, N. A., Dailey, M. E., Smith, S. J., and McConnell, S. K. (1992). Diverse migratory pathways in the developing cerebral cortex. *Science*, 258:299–302.

Oswald, M., Tantirigama, M., Sonntag, I., Hughes, S., and Empson, R. (2013). Diversity of layer 5 projection neurons in the mouse motor cortex. *Frontiers in Cellular Neuroscience*, 7.

O'Toole, S. M., Oyibo, H. K., and Keller, G. B. (2023). Molecularly targetable cell types in mouse visual cortex have distinguishable prediction error responses. *Neuron*, 111:2918–2928.e8.

Otsuka, T. and Kawaguchi, Y. (2008). Firing-pattern-dependent specificity of cortical excitatory feed-forward subnetworks. *Journal of Neuroscience*, 28:11186–11195.

Otsuka, T. and Kawaguchi, Y. (2009). Cortical inhibitory cell types differentially form intralaminar and interlaminar subnetworks with excitatory neurons. *The Journal of Neuroscience*, 29:10533–10540.

Otsuka, T. and Kawaguchi, Y. (2011). Cell diversity and connection specificity between callosal projection neurons in the frontal cortex. *The Journal of Neuroscience*, 31:3862–3870.

Pachitariu, M., Lyamzin, D. R., Sahani, M., and Lesica, N. A. (2015). State-dependent population coding in primary auditory cortex. *The Journal of Neuroscience*, 35:2058–2073.

Packer, A. M. and Yuste, R. (2011). Dense, unspecific connectivity of neocortical parvalbumin-positive interneurons: A canonical microcircuit for inhibition? *Journal of Neuroscience*, 31:13260–13271.

Pagès, S., Chenouard, N., Chéreau, R., Kouskoff, V., Gambino, F., and Holtmaat, A.

(2021). An increase in dendritic plateau potentials is associated with experience-dependent cortical map reorganization. *Proceedings of the National Academy of Sciences of the United States of America*, 118:e2024920118.

Pala, A. and Petersen, C. C. (2015). *in vivo* measurement of cell-type-specific synaptic connectivity and synaptic transmission in layer 2/3 mouse barrel cortex. *Neuron*, 85:68.

Palagina, G., Meyer, J. F., and Smirnakis, S. M. (2019). Inhibitory units: An organizing nidus for feature-selective subnetworks in area v1. *The Journal of Neuroscience*, 39:4931–4944.

Palmer, L. M., Shai, A. S., Reeve, J. E., Anderson, H. L., Paulsen, O., and Larkum, M. E. (2014). Nmda spikes enhance action potential generation during sensory input. *Nature Neuroscience*, 17:383–390.

Pangratz-Fuehrer, S. and Hestrin, S. (2011). Synaptogenesis of electrical and gabaergic synapses of fast-spiking inhibitory neurons in the neocortex. *Journal of Neuroscience*, 31:10767–10775.

Panzeri, S., Moroni, M., Safaai, H., and Harvey, C. D. (2022). The structures and functions of correlations in neural population codes. *Nature Reviews Neuroscience 2022 23:9*, 23:551–567.

Pardi, M. B., Schroeder, A., and Letzkus, J. J. (2023). Probing top-down information in neocortical layer 1. *Trends in Neurosciences*, 46:20–31.

Pearson, C. A., Moore, D. M., Tucker, H. O., Dekker, J. D., Hu, H., Miquelajáuregui, A., and Novitch, B. G. (2020). Foxp1 regulates neural stem cell self-renewal and bias toward deep layer cortical fates. *Cell Reports*, 30:1964–1981.e3.

Pebworth, M. P., Ross, J., Andrews, M., Bhaduri, A., and Kriegstein, A. R. (2021). Human intermediate progenitor diversity during cortical development. *Proceedings of the National Academy of Sciences of the United States of America*, 118.

Perin, R., Berger, T. K., and Markram, H. (2011). A synaptic organizing principle for cortical neuronal groups. *Proceedings of the National Academy of Sciences of the United States of America*, 108:5419–5424.

Petersen, C. C. (2007). The functional organization of the barrel cortex. *Neuron*, 56:339–355.

Petersen, C. C. (2014). Cortical control of whisker movement. *Annual review of neuroscience*, 37:183–203.

Petersen, C. C. and Crochet, S. (2013). Synaptic computation and sensory processing in neocortical layer 2/3.

Petersen, C. C., Grinvald, A., and Sakmann, B. (2003). Spatiotemporal dynamics of sensory responses in layer 2/3 of rat barrel cortex measured *in vivo* by voltage-sensitive dye imaging combined with whole-cell voltage recordings and neuron reconstructions. *Journal of Neuroscience*, 23:1298–1309.

Petersen, C. C. and Sakmann, B. (2001). Functionally independent columns of rat somatosensory barrel cortex revealed with voltage-sensitive dye imaging. *The Journal of neuroscience : the official journal of the Society for Neuroscience*, 21:8435–46.

Petreanu, L., Gutnisky, D. A., Huber, D., Xu, N. L., Oconnor, D. H., Tian, L., Looger, L., and Svoboda, K. (2012). Activity in motorâsensory projections reveals distributed coding in somatosensation. *Nature*, 489:299–303.

Petreanu, L., Huber, D., Sobczyk, A., and Svoboda, K. (2007). Channelrhodopsin-2-assisted circuit mapping of long-range callosal projections. *Nature Neuroscience*, 10:663–668.

Petreanu, L., Mao, T., Sternson, S. M., and Svoboda, K. (2009). The subcellular organization of neocortical excitatory connections. *Nature*, 457:1142–1145.

Petros, T. J., Bultje, R. S., Ross, M. E., Fishell, G., and Anderson, S. A. (2015). Apical versus basal neurogenesis directs cortical interneuron subclass fate. *Cell Reports*, 13:1090–1095.

Pfeffer, C. K., Xue, M., He, M., Huang, Z. J., and Scanziani, M. (2013). Inhibition of inhibition in visual cortex: the logic of connections between molecularly distinct interneurons. *Nature Neuroscience*, 16:1068–1076.

Phillips, G. R., Tanaka, H., Frank, M., Elste, A., Fidler, L., Benson, D. L., and

Colman, D. R. (2003). γ-protocadherins are targeted to subsets of synapses and intracellular organelles in neurons. *The Journal of Neuroscience*, 23:5096.

Pierret, T., Lavallée, P., and Deschênes, M. (2000). Parallel streams for the relay of vibrissal information through thalamic barreloids. *Journal of Neuroscience*, 20(19):7455–7462.

Pilz, G. A., Shitamukai, A., Reillo, I., Pacary, E., Schwausch, J., Stahl, R., Ninkovic, J., Snippert, H. J., Clevers, H., Godinho, L., Guillemot, F., Borrell, V., Matsuzaki, F., and tz, M. G. (2013). Amplification of progenitors in the mammalian telencephalon includes a new radial glial cell type. *Nature Communications*, 4:1–11.

Pizzorusso, T., Medini, P., Berardi, N., Chierzi, S., Fawcett, J. W., and Maffei, L. (2002). Reactivation of ocular dominance plasticity in the adult visual cortex. *Science*, 298:1248–1251.

Pla, R., Borrell, V., Flames, N., and Marín, O. (2006). Layer acquisition by cortical gabaergic interneurons is independent of reelin signaling. *The Journal of Neuroscience*, 26:6924–6934.

Planert, H., Mittermaier, F. X., Grosser, S., Fidzinski, P., Schneider, U. C., Radbruch, H., Onken, J., Holtkamp, M., Schmitz, D., Alle, H., 2, V., Rolf, J., Geiger, P., and Peng, Y. (2023). Cellular and synaptic diversity of layer 2-3 pyramidal neurons in human individuals. *bioRxiv*, page 2021.11.08.467668.

Poleg-Polsky, A. and Diamond, J. S. (2011). Imperfect space clamp permits electrotonic interactions between inhibitory and excitatory synaptic conductances, distorting voltage clamp recordings. *PLOS ONE*, 6:e19463.

Poort, J., Khan, A. G., Pachitariu, M., Keller, G. B., Mrsic-Flogel, T. D., Correspondence, S. B. H., Nemri, A., Orsolic, I., Krupic, J., Bauza, M., Sahani, M., and Hofer, S. B. (2015). Learning enhances sensory and multiple non-sensory representations in primary visual cortex article learning enhances sensory and multiple non-sensory representations in primary visual cortex. *Neuron*, 86.

Porter, L. L. and White, E. L. (1983). Afferent and efferent pathways of the vibrissal region of primary motor cortex in the mouse. *The Journal of comparative neurology*, 214:279–289.

Pouille, F., Marin-Burgin, A., Adesnik, H., Atallah, B. V., and Scanziani, M. (2009). Input normalization by global feedforward inhibition expands cortical dynamic range. *Nature Neuroscience*, 12:1577–1585.

Pouille, F. and Scanziani, M. (2001). Enforcement of temporal fidelity in pyramidal cells by somatic feed-forward inhibition. *Science*, 293:1159–63.

Poulet, J. F. and Crochet, S. (2019). The cortical states of wakefulness. *Frontiers in Systems Neuroscience*, 12:428018.

Poulet, J. F. and Petersen, C. C. (2008). Internal brain state regulates membrane potential synchrony in barrel cortex of behaving mice. *Nature*, 454:881–885.

Price, S. R., Garcia, N. V. D. M., Ranscht, B., and Jessell, T. M. (2002). Regulation of motor neuron pool sorting by differential expression of type ii cadherins. *Cell*, 109:205–216.

Priya, R., Paredes, M. F., Karayannis, T., Yusuf, N., Liu, X., Jaglin, X., Graef, I., Alvarez-Buylla, A., and Fishell, G. (2018). Activity regulates cell death within cortical interneurons through a calcineurin-dependent mechanism. *Cell Reports*, 22:1695–1709.

Rabinovich, R. J., Kato, D. D., and Bruno, R. M. (2022). Learning enhances encoding of time and temporal surprise in mouse primary sensory cortex. *Nature Communications 2022 13:1*, 13:1–15.

Rakic, P. (1972). Mode of cell migration to the superficial layers of fetal monkey neocortex. *The Journal of comparative neurology*, 145:61–83.

Rakic, P. (1988). Specification of cerebral cortical areas. *Science*, 241:170–176.

Ramamurthy, D. L., Chen, A., Zhou, J., Park, C., Huang, P. C., Bharghavan, P., Krishna, G., Liu, J., Casale, K., and Feldman, D. E. (2023). Vip interneurons in sensory cortex encode sensory and action signals but not direct reward signals. *Current biology : CB*, 33:3398–3408.e7.

Ramirez, A., Pnevmatikakis, E. A., Merel, J., Paninski, L., Miller, K. D., and Bruno, R. M. (2014). Spatiotemporal receptive fields of barrel cortex revealed by reverse correlation of synaptic input. *Nature Neuroscience*, 17:866–875.

Ramos, S. I., Makeyev, E. V., Salierno, M., Kodama, T., Kawakami, Y., and Sahara, S. (2020). Tuba8 drives differentiation of cortical radial glia into apical intermediate progenitors by tuning modifications of tubulin c termini. *Developmental Cell*, 52:477–491.e8.

Rancz, E. A., Franks, K. M., Schwarz, M. K., Pichler, B., Schaefer, A. T., and Margrie, T. W. (2011). Transfection via whole-cell recording in vivo: bridging single-cell physiology, genetics and connectomics. *Nature Neuroscience*, 14:527–532.

Ranjbar-Slamloo, Y. and Arabzadeh, E. (2019). Diverse tuning underlies sparse activity in layer 2/3 vibrissal cortex of awake mice. *The Journal of Physiology*, 597:2803–2817.

Ratz, M., von Berlin, L., Larsson, L., Martin, M., Westholm, J. O., Manno, G. L., Lundeberg, J., and Frisén, J. (2022). Clonal relations in the mouse brain revealed by single-cell and spatial transcriptomics. *Nature Neuroscience*, 25:285–294.

Reik, W., Dean, W., and Walter, J. (2001). Epigenetic reprogramming in mammalian development. *Science*, 293:1089–1093.

Reiner, A., Jiao, Y., Mar, N. D., Laverghetta, A. V., and Lei, W. L. (2003). Differential morphology of pyramidal tract-type and intratelencephalically projecting-type corticostriatal neurons and their intrastriatal terminals in rats. *Journal of Comparative Neurology*, 457:420–440.

Reyes, A., Lujan, R., Rozov, A., Burnashev, N., Somogyi, P., and Sakmann, B. (1998). Target-cell-specific facilitation and depression in neocortical circuits. *Nature Neuroscience*, 1:279–284.

Rocco, M. M. and Brumberg, J. C. (2007). The sensorimotor slice. *Journal of Neuroscience Methods*, 162:139–147.

Rodgers, C. C., Nogueira, R., Pil, B. C., Greeman, E. A., Park, J. M., Hong, Y. K., Fusi, S., and Bruno, R. M. (2021). Sensorimotor strategies and neuronal representations for shape discrimination. *Neuron*, 109:2308–2325.e10.

Rojas-Piloni, G., Guest, J. M., Egger, R., Johnson, A. S., Sakmann, B., and Ober-

laender, M. (2017). Relationships between structure, *in vivo* function and long-range axonal target of cortical pyramidal tract neurons. *Nature Communications*, 8:1–11.

Roux, L. and Buzsáki, G. (2015). Tasks for inhibitory interneurons in intact brain circuits. *Neuropharmacology*, 88:10–23.

Ruan, X., Kang, B., Qi, C., Lin, W., Wang, J., and Zhang, X. (2021). Progenitor cell diversity in the developing mouse neocortex. *Proceedings of the National Academy of Sciences of the United States of America*, 118:e2018866118.

Rubinstein, R., Thu, C. A., Goodman, K. M., Wolcott, H. N., Bahna, F., Mannepalli, S., Ahlsen, G., Chevee, M., Halim, A., Clausen, H., Maniatis, T., Shapiro, L., and Honig, B. (2015). Molecular logic of neuronal self-recognition through protocadherin domain interactions. *Cell*, 163:629–642.

Rudy, B., Fishell, G., Lee, S. H., and Hjerling-Leffler, J. (2011). Three groups of interneurons account for nearly 100gabaergic neurons. *Developmental Neurobiology*, 71:45–61.

Rudy, B. and McBain, C. J. (2001). Kv3 channels: Voltage-gated k+ channels designed for high-frequency repetitive firing. *Trends in Neurosciences*, 24:517–526.

Runyan, C. A. and Sur, M. (2013). Response selectivity is correlated to dendritic structure in parvalbumin-expressing inhibitory neurons in visual cortex. *The Journal of Neuroscience*, 33:11724–11733.

Ryan, L., Sun-Yan, A., Laughton, M., and Peron, S. (2023). Cortical circuitry mediating inter-areal touch signal amplification. *bioRxiv*.

Rymar, V. V. and Sadikot, A. F. (2007). Laminar fate of cortical gabaergic interneurons is dependent on both birthdate and phenotype. *The Journal of Comparative Neurology*, 501:369–380.

Safari, M. S., Mirnajafi-Zadeh, J., Hioki, H., and Tsumoto, T. (2017). Parvalbumin-expressing interneurons can act solo while somatostatin-expressing interneurons act in chorus in most cases on cortical pyramidal cells. *Scientific Reports*, 7:1–14.

Saito, T. (2006). *in vivo* electroporation in the embryonic mouse central nervous system. *Nature Protocols*, 1:1552–1558.

Saito, T. and Nakatsuji, N. (2001). Efficient gene transfer into the embryonic mouse brain using *in vivo* electroporation. *Developmental Biology*, 240:237–246.

Sakata, S. and Harris, K. D. (2009). Laminar structure of spontaneous and sensory-evoked population activity in auditory cortex. *Neuron*, 64:404–418.

Salkoff, D. B., Zagha, E., özge Yüzgeç, and McCormick, D. A. (2015). Synaptic mechanisms of tight spike synchrony at gamma frequency in cerebral cortex. *Journal of Neuroscience*, 35:10236–10251.

Sampathkumar, V., Miller-Hansen, A., Sherman, S. M., and Kasthuri, N. (2021). Integration of signals from different cortical areas in higher order thalamic neurons. *Proceedings of the National Academy of Sciences of the United States of America*, 118.

Saneyoshi, T., Fortin, D. A., and Soderling, T. R. (2010). Regulation of spine and synapse formation by activity-dependent intracellular signaling pathways. *Current Opinion in Neurobiology*, 20:108–115.

Sato, T. R. and Svoboda, K. (2010). The functional properties of barrel cortex neurons projecting to the primary motor cortex. *The Journal of Neuroscience*, 30:4256–4260.

Save, L., Baude, A., and Cossart, R. (2019). Temporal embryonic origin critically determines cellular physiology in the dentate gyrus. *Cerebral Cortex*, 29:2639–2652.

Scala, F., Kobak, D., Bernabucci, M., Bernaerts, Y., Cadwell, C. R., Castro, J. R., Hartmanis, L., Jiang, X., Laturnus, S., Miranda, E., et al. (2021). Phenotypic variation of transcriptomic cell types in mouse motor cortex. *Nature*, 598(7879):144–150.

Schneider, A., Azabou, M., McDougall-Vigier, L., Parks, D. F., Ensley, S., Bhaskaran-Nair, K., Nowakowski, T., Dyer, E. L., and Hengen, K. B. (2023). Tran-

scriptomic cell type structures *in vivo* neuronal activity across multiple timescales. *Cell Reports*, 42:112318.

Schnütgen, F., Doerflinger, N., Calléja, C., Wendling, O., Chambon, P., and Ghyselinck, N. B. (2003). A directional strategy for monitoring cre-mediated recombination at the cellular level in the mouse. *Nature Biotechnology*, 21:562–565.

Schreiner, D. and Weiner, J. A. (2010). Combinatorial homophilic interaction between γ-protocadherin multimers greatly expands the molecular diversity of cell adhesion. *Proceedings of the National Academy of Sciences of the United States of America*, 107:14893–14898.

Schuman, B., Machold, R. P., Hashikawa, Y., Fuzik, J., Fishell, G. J., and Rudy, B. (2019). Four unique interneuron populations reside in neocortical layer 1. *Journal of Neuroscience*, 39:125–139.

Schwarz, M. K. and Remy, S. (2019). Rabies virus-mediated connectivity tracing from single neurons. *Journal of neuroscience methods*, 325.

Seeman, S. C., Campagnola, L., Davoudian, P. A., Hoggarth, A., Hage, T. A., Bosma-Moody, A., Baker, C. A., Lee, J. H., Mihalas, S., Teeter, C., Ko, A. L., Ojemann, J. G., Gwinn, R. P., Silbergeld, D. L., Cobbs, C., Phillips, J., Lein, E., Murphy, G., Koch, C., Zeng, H., and Jarsky, T. (2018). Sparse recurrent excitatory connectivity in the microcircuit of the adult mouse and human cortex. *eLife*, 7.

Sermet, B. S., Truschow, P., Feyerabend, M., Mayrhofer, J. M., Oram, T. B., Yizhar, O., Staiger, J. F., and Petersen, C. C. (2019). Pathway-, layer-and cell-type-specific thalamic input to mouse barrel cortex. *eLife*, 8.

Sessa, A., Mao, C. A., Colasante, G., Nini, A., Klein, W. H., and Broccoli, V. (2010). Tbr2-positive intermediate (basal) neuronal progenitors safeguard cerebral cortex expansion by controlling amplification of pallial glutamatergic neurons and attraction of subpallial gabaergic interneurons. *Genes Development*, 24:1816–1826.

Shamir, M. and Sompolinsky, H. (2006). Implications of neuronal diversity on population coding. *Neural Computation*, 18:1951–1986.

Shepherd, G. M. (2013). Corticostriatal connectivity and its role in disease. *Nature Reviews Neuroscience*, 14:278–291.

Shepherd, G. M., Morse, T. M., Marenco, L., Cheung, K., Carnevale, T., Migliore, M., Mcdougal, R. A., Hines, M., and Miller, P. (2015). Spike triggered average. *Encyclopedia of Computational Neuroscience*, pages 2832–2835.

Shepherd, G. M., Stepanyants, A., Bureau, I., Chklovskii, D., and Svoboda, K. (2005). Geometric and functional organization of cortical circuits. *Nature Neuroscience*, 8:782–790.

Shepherd, G. M. and Svoboda, K. (2005). Laminar and columnar organization of ascending excitatory projections to layer 2/3 pyramidal neurons in rat barrel cortex. *The Journal of Neuroscience*, 25:5670–5679.

Sherman, S. M. and Guillery, R. W. (1996). Functional organization of thalamocortical relays. *Journal of neurophysiology*, 76:1367–1395.

Shetty, A. S., Godbole, G., Maheshwari, U., Padmanabhan, H., Chaudhary, R., Muralidharan, B., Hou, P. S., Monuki, E. S., Kuo, H. C., Rema, V., and Tole, S. (2013). Lhx2 regulates a cortex-specific mechanism for barrel formation. *Proceedings of the National Academy of Sciences of the United States of America*, 110:E4913–E4921.

Shimogori, T. and Ogawa, M. (2008). Gene application with *in utero* electroporation in mouse embryonic brain. *Development, growth differentiation*, 50:499–506.

Shimojo, H., Ohtsuka, T., and Kageyama, R. (2008). Oscillations in notch signaling regulate maintenance of neural progenitors. *Neuron*, 58:52–64.

Shitamukai, A., Konno, D., and Matsuzaki, F. (2011). Oblique radial glial divisions in the developing mouse neocortex induce self-renewing progenitors outside the germinal zone that resemble primate outer subventricular zone progenitors. *The Journal of Neuroscience*, 31:3683–3695.

Shohayeb, B., Muzar, Z., and Cooper, H. M. (2021). Conservation of neural progenitor identity and the emergence of neocortical neuronal diversity. *Seminars in Cell Developmental Biology*, 118:4–13.

Sidman, R. L. and Rakic, P. (1973). Neuronal migration, with special reference to developing human brain: a review. *Brain research*, 62:1–35.

Sigworth, F. J. (1995). Electronic design of the patch clamp. *Single-Channel Recording*, pages 95–127.

Silberberg, G. and Markram, H. (2007). Disynaptic inhibition between neocortical pyramidal cells mediated by martinotti cells. *Neuron*, 53:735–746.

Sippy, T. and Yuste, R. (2013). Decorrelating action of inhibition in neocortical networks. *The Journal of Neuroscience*, 33:9813–9830.

Smith, G. B. and Fitzpatrick, D. (2012). Specifying cortical circuits: a role for cell lineage. *Neuron*, 75:4–5.

Smith, S. L., Smith, I. T., Branco, T., and Häusser, M. (2013). Dendritic spikes enhance stimulus selectivity in cortical neurons in vivo. *Nature*, 503:115–120.

Sohal, V. S., Zhang, F., Yizhar, O., and Deisseroth, K. (2009). Parvalbumin neurons and gamma rhythms enhance cortical circuit performance. *Nature*, 459:698–702.

Song, S., Miller, K. D., and Abbott, L. F. (2000). Competitive hebbian learning through spike-timing-dependent synaptic plasticity. *Nature neuroscience*, 3(9):919–926.

Song, S., Sjöström, P. J., Reigl, M., Nelson, S., and Chklovskii, D. B. (2005). Highly nonrandom features of synaptic connectivity in local cortical circuits. *PLoS biology*, 3:0507–0519.

Sorensen, S. A., Gouwens, N. W., Wang, Y., Mallory, M., Budzillo, A., Dalley, R., Lee, B., Gliko, O., chi Kuo, H., Kuang, X., Mann, R., Ahmadinia, L., Alfiler, L., Baftizadeh, F., Baker, K., Bannick, S., Bertagnolli, D., Bickley, K., Bohn, P., Brown, D., Bomben, J., Brouner, K., Chen, C., Chen, K., Chvilicek, M., Collman, F., Daigle, T., Dawes, T., de Frates, R., Dee, N., DePartee, M., Egdorf, T., El-Hifnawi, L., Enstrom, R., Esposito, L., Farrell, C., Gala, R., Glomb, A., Gamlin, C., Gary, A., Goldy, J., Gu, H., Hadley, K., Hawrylycz, M., Henry, A., Hill, D., Hirokawa, K. E., Huang, Z., Johnson, K., Juneau, Z., Kebede, S., Kim, L., Lee, C., Lesnar, P., Li, A., Glomb, A., Li, Y., Liang, E., Link, K., Maxwell,

M., McGraw, M., McMillen, D. A., Mukora, A., Ng, L., Ochoa, T., Oldre, A., Park, D., Pom, C. A., Popovich, Z., Potekhina, L., Rajanbabu, R., Ransford, S., Reding, M., Ruiz, A., Sandman, D., Siverts, L., Smith, K. A., Stoecklin, M., Sulc, J., Tieu, M., Ting, J., Trinh, J., Vargas, S., Vumbaco, D., Walker, M., Wang, M., Wanner, A., Waters, J., Williams, G., Wilson, J., Xiong, W., Lein, E., Berg, J., Kalmbach, B., Yao, S., Gong, H., Luo, Q., Ng, L., Sümbül, U., Jarsky, T., Yao, Z., Tasic, B., and Zeng, H. (2023). Connecting single-cell transcriptomes to projectomes in mouse visual cortex. *bioRxiv*, page 2023.11.25.568393.

Southwell, D. G., Paredes, M. F., Galvao, R. P., Jones, D. L., Froemke, R. C., Sebe, J. Y., Alfaro-Cervello, C., Tang, Y., Garcia-Verdugo, J. M., Rubenstein, J. L., Baraban, S. C., and Alvarez-Buylla, A. (2012). Intrinsically determined cell death of developing cortical interneurons. *Nature*, 491:109–113.

Spruston, N., Jaffe, D. B., Williams, S. H., and Johnston, D. (1993). Voltage- and space-clamp errors associated with the measurement of electrotonically remote synaptic events. *Journal of Neurophysiology*, 70:781–802.

Staley, K. J. and Mody, I. (1992). Shunting of excitatory input to dentate gyrus granule cells by a depolarizing gabaa receptor-mediated postsynaptic conductance. *Journal of Neurophysiology*, 68:197–212.

Stancik, E. K., Navarro-Quiroga, I., Sellke, R., and Haydar, T. F. (2010). Heterogeneity in ventricular zone neural precursors contributes to neuronal fate diversity in the postnatal neocortex. *Journal of Neuroscience*, 30:7028–7036.

Stepanyants, A., Hof, P. R., and Chklovskii, D. B. (2002a). Geometry and structural plasticity of synaptic connectivity. *Neuron*, 34(2):275–288.

Stepanyants, A., Hof, P. R., and Chklovskii, D. B. (2002b). Information storage capacity of synaptic connectivity patterns. *Neurocomputing*, 44:661–665.

Stern, E. A., Maravall, M., and Svoboda, K. (2001). Rapid development and plasticity of layer 2/3 maps in rat barrel cortex in vivo. *Neuron*, 31:305–315.

Stringer, C., Pachitariu, M., Steinmetz, N. A., Okun, M., Bartho, P., Harris, K. D., Sahani, M., and Lesica, N. A. (2016). Inhibitory control of correlated intrinsic variability in cortical networks. *eLife*, 5.

Stroud, H., Yang, M. G., Tsitohay, Y. N., Davis, C. P., Sherman, M. A., Hrvatin, S., Ling, E., and Greenberg, M. E. (2020). An activity-mediated transition in transcription in early postnatal neurons. *Neuron*, 107.

Sun, Q. Q. and Zhang, Z. (2011). Whisker experience modulates long-term depression in neocortical Î^3 – $aminobutyricacidergicinterneuronsinbarrelcortex.JournalofNeuroscienceResearch$, 89 : 73 – −85.

Sun, Y. C., Chen, X., Fischer, S., Lu, S., Zhan, H., Gillis, J., and Zador, A. M. (2021). Integrating barcoded neuroanatomy with spatial transcriptional profiling enables identification of gene correlates of projections. *Nature Neuroscience*, 24:873–885.

Tabata, H., of Neuroscience, K. N. J., and undefined 2003 (2003). Multipolar migration: the third mode of radial neuronal migration in the developing cerebral cortex. *Soc Neuroscience*.

Takeichi, M. (2006). The cadherin superfamily in neuronal connections and interactions. *Nature Reviews Neuroscience*, 8:11–20.

Tamamaki, N., Nakamura, K., Okamoto, K., and Kaneko, T. (2001). Radial glia is a progenitor of neocortical neurons in the developing cerebral cortex. *Neuroscience Research*, 41:51–60.

Tan, X. and Shi, S. H. (2013). Neocortical neurogenesis and neuronal migration. *Wiley interdisciplinary reviews. Developmental biology*, 2:443–459.

Tanaka, D. H. and Nakajima, K. (2012). Migratory pathways of gabaergic interneurons when they enter the neocortex. *European Journal of Neuroscience*, 35:1655–1660.

Taniguchi, H., Lu, J., and Huang, Z. J. (2013). The spatial and temporal origin of chandelier cells in mouse neocortex. *Science*, 339:70.

Tarusawa, E., Sanbo, M., Okayama, A., Miyashita, T., Kitsukawa, T., Hirayama, T., Hirabayashi, T., Hasegawa, S., Kaneko, R., Toyoda, S., Kobayashi, T., Kato-Itoh, M., Nakauchi, H., Hirabayashi, M., Yagi, T., and Yoshimura, Y. (2016).

Establishment of high reciprocal connectivity between clonal cortical neurons is regulated by the dnmt3b dna methyltransferase and clustered protocadherins. *BMC Biology*, 14:1–19.

Tasic, B., Menon, V., Nguyen, T. N., Kim, T. K., Jarsky, T., Yao, Z., Levi, B., Gray, L. T., Sorensen, S. A., Dolbeare, T., et al. (2016). Adult mouse cortical cell taxonomy revealed by single cell transcriptomics. *Nature neuroscience*, 19(2):335–346.

Tasic, B., Yao, Z., Graybuck, L. T., Smith, K. A., Nguyen, T. N., Bertagnolli, D., Goldy, J., Garren, E., Economo, M. N., Viswanathan, S., Penn, O., Bakken, T., Menon, V., Miller, J., Fong, O., Hirokawa, K. E., Lathia, K., Rimorin, C., Tieu, M., Larsen, R., Casper, T., Barkan, E., Kroll, M., Parry, S., Shapovalova, N. V., Hirschstein, D., Pendergraft, J., Sullivan, H. A., Kim, T. K., Szafer, A., Dee, N., Groblewski, P., Wickersham, I., Cetin, A., Harris, J. A., Levi, B. P., Sunkin, S. M., Madisen, L., Daigle, T. L., Looger, L., Bernard, A., Phillips, J., Lein, E., Hawrylycz, M., Svoboda, K., Jones, A. R., Koch, C., and Zeng, H. (2018). Shared and distinct transcriptomic cell types across neocortical areas. *Nature*, 563:72–78.

Taub, A. H., Lampl, I., and Okun, M. (2015). Local field potential, relationship to membrane synaptic potentials. *Encyclopedia of Computational Neuroscience*, pages 1572–1579.

Telley, L., Agirman, G., Prados, J., Amberg, N., Fièvre, S., Oberst, P., Bartolini, G., Vitali, I., Cadilhac, C., Hippenmeyer, S., Nguyen, L., Dayer, A., and Jabaudon, D. (2019). Temporal patterning of apical progenitors and their daughter neurons in the developing neocortex. *Science*, 364.

Telley, L., Govindan, S., Prados, J., Stevant, I., Nef, S., Dermitzakis, E., Dayer, A., and Jabaudon, D. (2016). Sequential transcriptional waves direct the differentiation of newborn neurons in the mouse neocortex. *Science*, 351:1443–1446.

Thomson, A. M. and Lamy, C. (2007). Functional maps of neocortical local circuitry. *Frontiers in Neuroscience*, 1:19.

Thu, C. A., Chen, W. V., Rubinstein, R., Chevee, M., Wolcott, H. N., Felsovalyi, K. O., Tapia, J. C., Shapiro, L., Honig, B., and Maniatis, T. (2014). Single-cell

identity generated by combinatorial homophilic interactions between α, β, and γ protocadherins. *Cell*, 158:1045–1059.

Tiveron, M. C., Rossel, M., Moepps, B., Yong, L. Z., Seidenfaden, R., Favor, J., König, N., and Cremer, H. (2006). Molecular interaction between projection neuron precursors and invading interneurons via stromal-derived factor 1 (cxcl12)/cxcr4 signaling in the cortical subventricular zone/intermediate zone. *The Journal of Neuroscience*, 26:13273–13278.

To, M. S., Honnuraiah, S., and Stuart, G. J. (2022). Voltage clamp errors during estimation of concurrent excitatory and inhibitory synaptic input to neurons with dendrites. *Neuroscience*, 489:98–110.

Torigoe, M., Yamauchi, K., Kimura, T., Uemura, Y., and Murakami, F. (2016). Evidence that the laminar fate of lge/cge-derived neocortical interneurons is dependent on their progenitor domains. *The Journal of Neuroscience*, 36:2044.

Toyoda, S., Kawaguchi, M., Kobayashi, T., Tarusawa, E., Toyama, T., Okano, M., Oda, M., Nakauchi, H., Yoshimura, Y., Sanbo, M., Hirabayashi, M., Hirayama, T., Hirabayashi, T., and Yagi, T. (2014). Developmental epigenetic modification regulates stochastic expression of clustered protocadherin genes, generating single neuron diversity. *Neuron*, 82:94–108.

Traynelis, S. F. (1998). Software-based correction of single compartment series resistance errors. *Journal of Neuroscience Methods*, 86:25–34.

Tremblay, R., Lee, S., and Rudy, B. (2016). Gabaergic interneurons in the neocortex: From cellular properties to circuits. *Neuron*, 91:260–292.

Tyler, W. A. and Haydar, T. F. (2010). A new contribution to brain convolution: progenitor cell logistics during cortex development. *Nature Neuroscience*, 13:656–657.

Tyler, W. A. and Haydar, T. F. (2013). Multiplex genetic fate mapping reveals a novel route of neocortical neurogenesis, which is altered in the ts65dn mouse model of down syndrome. *The Journal of Neuroscience*, 33:5106–5119.

Tyler, W. A., Medalla, M., Guillamon-Vivancos, T., Luebke, J. I., and Haydar, T. F.

(2015). Neural precursor lineages specify distinct neocortical pyramidal neuron types. *Journal of Neuroscience*, 35:6142–6152.

Tyson, J. A., Goldberg, E. M., Maroof, A. M., Xu, Q., Petros, T. J., and Anderson, S. A. (2015). Duration of culture and sonic hedgehog signaling differentially specify pv versus sst cortical interneuron fates from embryonic stem cells. *Development*, 142:1267–1278.

Urban-Ciecko, J. and Barth, A. L. (2016). Somatostatin-expressing neurons in cortical networks. *Nature Reviews Neuroscience*, 17:401.

Valcanis, H. and Tan, S. S. (2003). Layer specification of transplanted interneurons in developing mouse neocortex. *The Journal of Neuroscience*, 23:5113–5122.

Valero, M., Cid, E., Averkin, R. G., Aguilar, J., Sanchez-Aguilera, A., Viney, T. J., Gomez-Dominguez, D., Bellistri, E., and Prida, L. M. D. L. (2015). Determinants of different deep and superficial ca1 pyramidal cell dynamics during sharp-wave ripples. *Nature Neuroscience*, 18:1281–1290.

Van der Loos, H. and Woolsey, T. A. (1973). Somatosensory cortex: structural alterations following early injury to sense organs. *Science*, 179(4071):395–398.

van Heusden, F., Macey-Dare, A., Gordon, J., Krajeski, R., Sharott, A., and Ellender, T. (2021). Diversity in striatal synaptic circuits arises from distinct embryonic progenitor pools in the ventral telencephalon. *Cell Reports*, 35.

Varga, C., Lee, S. Y., and Soltesz, I. (2010). Target-selective gabaergic control of entorhinal cortex output. *Nature Neuroscience*, 13:822–824.

Vavladeli, A., Daigle, T., Zeng, H., Crochet, S., and Petersen, C. C. (2020). Projection-specific activity of layer 2/3 neurons imaged in mouse primary somatosensory barrel cortex during a whisker detection task. *Function*, 1:8.

Vecchia, D., Beltramo, R., Vallone, F., Chéreau, R., Forli, A., Molano-Mazón, M., Bawa, T., Binini, N., Moretti, C., Holtmaat, A., Panzeri, S., and Fellin, T. (2020). Temporal sharpening of sensory responses by layer v in the mouse primary somatosensory cortex. *Current biology*, 30:1589–1599.e10.

Veinante, P. and Deschênes, M. (1999). Single- and multi-whisker channels in the

ascending projections from the principal trigeminal nucleus in the rat. *Journal of Neuroscience*, 19:5085–5095.

Veinante, P., Jacquin, M. F., and Deschênes, M. (2000). Thalamic projections from the whisker-sensitive regions of the spinal trigeminal complex in the rat. *Journal of Comparative Neurology*, 420(2):233–243.

Vélez-Fort, M., Rousseau, C. V., Niedworok, C. J., Wickersham, I. R., Rancz, E. A., Brown, A. P., Strom, M., and Margrie, T. W. (2014). The stimulus selectivity and connectivity of layer six principal cells reveals cortical microcircuits underlying visual processing. *Neuron*, 83:1431–1443.

Viaene, A. N., Petrof, I., and Sherman, S. M. (2011a). Properties of the thalamic projection from the posterior medial nucleus to primary and secondary somatosensory cortices in the mouse. *Proceedings of the National Academy of Sciences of the United States of America*, 108:18156–18161.

Viaene, A. N., Petrof, I., and Sherman, S. M. (2011b). Synaptic properties of thalamic input to layers 2/3 and 4 of primary somatosensory and auditory cortices. *Journal of Neurophysiology*, 105:279–292.

Voelcker, B., Pancholi, R., and Peron, S. (2022). Transformation of primary sensory cortical representations from layer 4 to layer 2. *Nature Communications 2022 13:1*, 13:1–13.

von Klemperer, A. (2021). *Investigating Translaminar Signalling from Layer 5 Pyramidal Subpopulations to Layer 2/3 in Somatosensory Cortex*. PhD thesis, University of Oxford.

Voss, L. J. (2020). Relationship between artificial cerebrospinal fluid oxygenation, slice depth and tissue performance in submerged brain slice experiments. *Neuroscience Letters*, 736:135275.

Vreeswijk, C. V., Abbott, L. F., and Ermentrout, G. B. (1994). When inhibition not excitation synchronizes neural firing. *Journal of Computational Neuroscience*, 1:313–321.

Vucurovic, K., Gallopin, T., Ferezou, I., Rancillac, A., Chameau, P., Hooft, J. A. V.,

Geoffroy, H., Monyer, H., Rossier, J., and Vitalis, T. (2010). Serotonin 3a receptor subtype as an early and protracted marker of cortical interneuron subpopulations. *Cerebral Cortex*, 20:2333–2347.

Wall, N. R., Parra, M. D. L., Sorokin, J. M., Taniguchi, H., Huang, Z. J., and Callaway, E. M. (2016). Brain-wide maps of synaptic input to cortical interneurons. *The Journal of Neuroscience*, 36:4000–4009.

Wamsley, B. and Fishell, G. (2017). Genetic and activity-dependent mechanisms underlying interneuron diversity. *Nature Reviews Neuroscience*, 18:299–309.

Wang, C.-F., Hsing, H.-W., Zhuang, Z.-H., Nieto, M., Shyu, B. C., and Correspondence, S.-J. C. (2017). Lhx2 expression in postmitotic cortical neurons initiates assembly of the thalamocortical somatosensory circuit. *Cell Reports*, 18:849–856.

Wang, X., Tsai, J. W., Lamonica, B., and Kriegstein, A. R. (2011). A new subtype of progenitor cell in the mouse embryonic neocortex. *Nature Neuroscience*, 14:555–562.

Wang, Y., Gupta, A., Toledo-Rodriguez, M., Wu, C. Z., and Markram, H. (2002). Anatomical, physiological, molecular and circuit properties of nest basket cells in the developing somatosensory cortex. *Cerebral Cortex*, 12:395–410.

Wang, Y., Liu, Y. Z., Wang, S. Y., and Wang, Z. (2016). *in vivo* whole-cell recording with high success rate in anaesthetized and awake mammalian brains. *Molecular Brain*, 9:1–14.

Wang, Y., Toledo-Rodriguez, M., Gupta, A., Wu, C., Silberberg, G., Luo, J., and Markram, H. (2004). Anatomical, physiological and molecular properties of martinotti cells in the somatosensory cortex of the juvenile rat. *The Journal of Physiology*, 561:65–90.

Wehr, M. and Zador, A. M. (2003). Balanced inhibition underlies tuning and sharpens spike timing in auditory cortex. *Nature*, 426:442–446.

Weiler, S., Nilo, D. G., Bonhoeffer, T., Hübener, M., Rose, T., and Scheuss, V. (2023). Functional and structural features of l2/3 pyramidal cells continuously covary with pial depth in mouse visual cortex. *Cerebral Cortex*, 33:3715–3733.

Wen, J. A. and Barth, A. L. (2011). Input-specific critical periods for experience-dependent plasticity in layer 2/3 pyramidal neurons. *The Journal of Neuroscience*, 31:4456–4465.

White, E. L. and DeAmicis, R. A. (1977). Afferent and efferent projections of the region in mouse sml cortex which contains the posteromedial barrel subfield. *Journal of Comparative Neurology*, 175:455–481.

Wichterle, H., Alvarez-Dolado, M., Erskine, L., and Alvarez-Buylla, A. (2003). Permissive corridor and diffusible gradients direct medial ganglionic eminence cell migration to the neocortex. *Proceedings of the National Academy of Sciences of the United States of America*, 100:727–732.

Wichterle, H., Turnbull, D. H., Nery, S., Fishell, G., and Alvarez-Buylla, A. (2001). *in utero* fate mapping reveals distinct migratory pathways and fates of neurons born in the mammalian basal forebrain. *Development*, 128:3759–3771.

Wilent, W. B. and Contreras, D. (2005). Dynamics of excitation and inhibition underlying stimulus selectivity in rat somatosensory cortex. *Nature Neuroscience*, 8:1364–1370.

Wilke, S. D. and Eurich, C. W. (2002). Representational accuracy of stochastic neural populations. *Neural Computation*, 14:155–189.

Williams, L. E. and Holtmaat, A. (2019). Higher-order thalamocortical inputs gate synaptic long-term potentiation via disinhibition. *Neuron*, 101:91–102.e4.

Williams, M. N., Zahm, D. S., and Jacquin, M. F. (1994). Differential foci and synaptic organization of the principal and spinal trigeminal projections to the thalamus in the rat. *European Journal of Neuroscience*, 6(3):429–453.

Williams, S. R. and Mitchell, S. J. (2008). Direct measurement of somatic voltage clamp errors in central neurons. *Nature Neuroscience*, 11:790–798.

Wilsch-Bräuninger, M., Florio, M., and Huttner, W. B. (2016). Neocortex expansion in development and evolution - from cell biology to single genes. *Current Opinion in Neurobiology*, 39:122–132.

Wonders, C. P. and Anderson, S. A. (2006). The origin and specification of cortical interneurons. *Nature Reviews Neuroscience*, 7:687–696.

Wonders, C. P., Taylor, L., Welagen, J., Mbata, I. C., Xiang, J. Z., and Anderson, S. A. (2008). A spatial bias for the origins of interneuron subgroups within the medial ganglionic eminence. *Developmental Biology*, 314:127–136.

Wong, F. K., Bercsenyi, K., Sreenivasan, V., Portalés, A., Fernández-Otero, M., and Marín, O. (2018). Pyramidal cell regulation of interneuron survival sculpts cortical networks. *Nature*, 557:668–673.

Woolsey, T. A. and der Loos, H. V. (1970). The structural organization of layer iv in the somatosensory region (si) of mouse cerebral cortex. the description of a cortical field composed of discrete cytoarchitectonic units. *Brain research*, 17:205–42.

Wu, P. R., Cho, K. K., Vogt, D., Sohal, V. S., and Rubenstein, J. L. (2017). The cytokine cxcl12 promotes basket interneuron inhibitory synapses in the medial prefrontal cortex. *Cerebral Cortex*, 27:4303–4313.

Wu, Q. and Maniatis, T. (1999). A striking organization of a large family of human neural cadherin-like cell adhesion genes. *Cell*, 97:779–790.

Wu, S. J., Sevier, E., Dwivedi, D., Saldi, G. A., Hairston, A., Yu, S., Abbott, L., Choi, D. H., Sherer, M., Qiu, Y., Shinde, A., Lenahan, M., Rizzo, D., Xu, Q., Barrera, I., Kumar, V., Marrero, G., Prönneke, A., Huang, S., Kullander, K., Stafford, D. A., Macosko, E., Chen, F., Rudy, B., and Fishell, G. (2023). Cortical somatostatin interneuron subtypes form cell-type-specific circuits. *Neuron*, 111:2675–2692.e9.

Xu, H., Jeong, H. Y., Tremblay, R., and Rudy, B. (2013). Neocortical somatostatin-expressing gabaergic interneurons disinhibit the thalamorecipient layer 4. *Neuron*, 77:155–167.

Xu, H. T., Han, Z., Gao, P., He, S., Li, Z., Shi, W., Kodish, O., Shao, W., Brown, K. N., Huang, K., and Shi, S. H. (2014). Distinct lineage-dependent structural and functional organization of the hippocampus. *Cell*, 157:1552–1564.

Xu, N. L., Harnett, M. T., Williams, S. R., Huber, D., O'Connor, D. H., Svoboda,

K., and Magee, J. C. (2012). Nonlinear dendritic integration of sensory and motor input during an active sensing task. *Nature*, 492:247–251.

Xu, Q., Cobos, I., Cruz, E. D. D. L., Rubenstein, J. L., and Anderson, S. A. (2004). Origins of cortical interneuron subtypes. *The Journal of Neuroscience*, 24:2612.

Xue, M., Atallah, B. V., and Scanziani, M. (2014). Equalizing excitation-inhibition ratios across visual cortical neurons. *Nature*, 511:596–600.

Yagi, T. (2012). Molecular codes for neuronal individuality and cell assembly in the brain. *Frontiers in Molecular Neuroscience*, 5:1–31.

Yamashita, T., Pala, A., Pedrido, L., Kremer, Y., Welker, E., and Petersen, C. C. (2013). Membrane potential dynamics of neocortical projection neurons driving target-specific signals. *Neuron*, 80(6):1477–1490.

Yamashita, T. and Petersen, C. C. (2016). Target-specific membrane potential dynamics of neocortical projection neurons during goal-directed behavior. *elife*, 5:e15798.

Yamashita, T., Vavladeli, A., Pala, A., Galan, K., Crochet, S., Petersen, S. S., and Petersen, C. C. (2018). Diverse long-range axonal projections of excitatory layer 2/3 neurons in mouse barrel cortex. *Frontiers in Neuroanatomy*, 12:369199.

Yamawaki, N. and Shepherd, G. M. (2015). Synaptic circuit organization of motor corticothalamic neurons. *The Journal of Neuroscience*, 35:2293–2307.

Yang, H., Kwon, S. E., Severson, K. S., and O'Connor, D. H. (2015). Origins of choice-related activity in mouse somatosensory cortex. *Nature Neuroscience*, 19:127–134.

Yang, W., Chini, M., Pöpplau, J. A., Formozov, A., Dieter, A., Piechocinski, P., Rais, C., Morellini, F., Sporns, O., Hanganu-Opatz, I. L., and Wiegert, J. S. (2021). Anesthetics fragment hippocampal network activity, alter spine dynamics, and affect memory consolidation. *PLOS Biology*, 19:e3001146.

Yang, W. and Sun, Q. Q. (2018). Circuit-specific and neuronal subcellular-wide e-i balance in cortical pyramidal cells. *Scientific Reports 2018 8:1*, 8:1–15.

Yassin, L., Benedetti, B. L., Jouhanneau, J. S., Wen, J. A., Poulet, J. F., and Barth,

A. L. (2010). An embedded subnetwork of highly active neurons in the neocortex. *Neuron*, 68:1043–1050.

Yetman, M. J., Washburn, E., Hyun, J. H., Osakada, F., Hayano, Y., Zeng, H., Callaway, E. M., Kwon, H. B., and Taniguchi, H. (2019). Intersectional monosynaptic tracing for dissecting subtype-specific organization of gabaergic interneuron inputs. *Nature Neuroscience*, 22:492–502.

Yin, Y. Q., Wang, L. F., Chen, C., Gao, T., Zhao, Z. F., and Li, C. H. (2016). *in vivo* field recordings effectively monitor the mouse cortex and hippocampus under isoflurane anesthesia. *Neural Regeneration Research*, 11:1951.

Yoon, K. J., Koo, B. K., Im, S. K., Jeong, H. W., Ghim, J., chul Kwon, M., Moon, J. S., Miyata, T., and Kong, Y. Y. (2008). Mind bomb 1-expressing intermediate progenitors generate notch signaling to maintain radial glial cells. *Neuron*, 58:519–531.

Yoshimura, Y. and Callaway, E. M. (2005). Fine-scale specificity of cortical networks depends on inhibitory cell type and connectivity. *Nature Neuroscience*, 8:1552–1559.

Yoshimura, Y., Dantzker, J. L., and Callaway, E. M. (2005). Excitatory cortical neurons form fine-scale functional networks. *Nature*, 433:868–873.

Young, H., Belbut, B., Baeta, M., and Petreanu, L. (2021). Laminar-specific cortico-cortical loops in mouse visual cortex. *eLife*, 10:1–25.

Yu, Y. C., Bultje, R. S., Wang, X., and Shi, S. H. (2009). Specific synapses develop preferentially among sister excitatory neurons in the neocortex. *Nature*, 458:501–504.

Yu, Y. C., He, S., Chen, S., Fu, Y., Brown, K. N., Yao, X. H., Ma, J., Gao, K. P., Sosinsky, G. E., Huang, K., and Shi, S. H. (2012). Preferential electrical coupling regulates neocortical lineage-dependent microcircuit assembly. *Nature*, 486:113–117.

Zador, A. M. (2019). A critique of pure learning and what artificial neural networks can learn from animal brains. *Nature Communications*, 10:1–7.

Zagha, E., Casale, A. E., Sachdev, R. N., McGinley, M. J., and McCormick, D. A. (2013). Motor cortex feedback influences sensory processing by modulating network state. *Neuron*, 79:567–578.

Zaitsev, A. V., Povysheva, N. V., Lewis, D. A., and Krimer, L. S. (2007). P/q-type, but not n-type, calcium channels mediate gaba release from fast-spiking interneurons to pyramidal cells in rat prefrontal cortex. *Journal of Neurophysiology*, 97:3567–3573.

Zeisel, A., Muñoz-Manchado, A. B., Codeluppi, S., Lönnerberg, P., La Manno, G., Juréus, A., Marques, S., Munguba, H., He, L., Betsholtz, C., et al. (2015). Cell types in the mouse cortex and hippocampus revealed by single-cell rna-seq. *Science*, 347(6226):1138–1142.

Zeng, H. (2022). What is a cell type and how to define it? *Cell*, 185:2739–2755.

Zeng, H. and Sanes, J. R. (2017). Neuronal cell-type classification: challenges, opportunities and the path forward. *Nature Reviews Neuroscience*, 18:530–546.

Zhang, W. and Bruno, R. M. (2019). High-order thalamic inputs to primary somatosensory cortex are stronger and longer lasting than cortical inputs. *eLife*, 8.

Zhang, Z. and Zagha, E. (2023). Motor cortex gates distractor stimulus encoding in sensory cortex. *Nature Communications*, 14:1–17.

Zhang, Z., Zhou, J., Tan, P., Pang, Y., Rivkin, A. C., Kirchgessner, M. A., Williams, E., Lee, C. T., Liu, H., Franklin, A. D., Miyazaki, P. A., Bartlett, A., Aldridge, A. I., Vu, M., Boggeman, L., Fitzpatrick, C., Nery, J. R., Castanon, R. G., Rashid, M., Jacobs, M. W., Ito-Cole, T., OâConnor, C., Pinto-Duartec, A., Dominguez, B., Smith, J. B., Niu, S. Y., Lee, K. F., Jin, X., Mukamel, E. A., Behrens, M. M., Ecker, J. R., and Callaway, E. M. (2021). Epigenomic diversity of cortical projection neurons in the mouse brain. *Nature*, 598:167–173.

Zimmer, G., Rudolph, J., Landmann, J., Gerstmann, K., Steinecke, A., Gampe, C., and Bolz, J. (2011). Bidirectional ephrinb3/epha4 signaling mediates the segregation of medial ganglionic eminence- and preoptic area-derived interneurons in the deep and superficial migratory stream. *The Journal of Neuroscience*, 31:18364.

Zliang, Z. W. and Deschênes, M. (1998). Projections to layer vi of the posteromedial barrel field in the rat: a reappraisal of the role of corticothalamic pathways. *Cerebral Cortex*, 8:428–436.

Zmarz, P. and Keller, G. B. (2016). Mismatch receptive fields in mouse visual cortex. *Neuron*, 92(4):766–772.

Znamenskiy, P., Kim, M.-H., Muir, D. R., Iacaruso, M. F., Hofer, S. B., and Mrsic-Flogel, T. D. (2018). Functional selectivity and specific connectivity of inhibitory neurons in primary visual cortex. *bioRxiv*, page 294835.